# Analytical and finite element buckling solutions of anisotropic laminated composite columns/plates under axial compression with various boundary conditions

by

Rund Ahmad Al-Masri

B.S., Jordan University of Science and Technology, 2012
M.S., Jordan University of Science and Technology, 2014

AN ABSTRACT OF A DISSERTATION

submitted in partial fulfillment of the requirements for the degree

DOCTOR OF PHILOSOPHY

Department of Civil Engineering
College of Engineering

KANSAS STATE UNIVERSITY
Manhattan, Kansas

2017

# Abstract

The use of laminated composites in aerospace, automotive, and civil engineering applications is ever growing due to their distinguished properties (High stiffness-to-weight ratio, high strength-to-weight ratio, fatigue and corrosion resistance). This growth has resulted in increasing the demand for better understanding the mechanics of laminated composites. Composite columns and wide plates, like any traditional members subjected to axial compression, undergo stability issues prior to failure. Limited amount of research studies has focused on the buckling of laminated anisotropic composite members. Analytical formula for the buckling load of generally anisotropic laminated composite simply supported thin columns and wide plates is derived using the Rayleigh Ritz approximation and bifurcation approach. The effective axial, coupling and flexural stiffness coefficients of the anisotropic layup is determined from the generalized constitutive relationship using dimensional reduction by static condensation of the 6x6 composite stiffness matrix. The resulting explicit formula is expressed in terms of the generally anisotropic material properties as well as the member geometry. The developed formula may be considered an extension to Euler buckling formula using Rayleigh-Ritz approximation and the first of its kind since Euler. This formula reduces down to Euler buckling formula once the effective coupling stiffness term vanishes for isotropic and certain classes of laminated composites. The analytical results are verified against finite element Eigen value solutions for a wide range of anisotropic laminated layups yielding high accuracy. Comparisons with experiments; conducted at Kansas State University for the simply supported case, are also performed showing good correspondence. A brief parametric study is then conducted to examine the effect of ply orientations and material properties including hybrid carbon/glass fiber composites, element thickness, and element type in FE analysis. Relevance of the numerical and analytical results is discussed for all these cases.

# Analytical and finite element buckling solutions of anisotropic laminated composite columns/plates under axial compression with various boundary conditions

by

Rund Ahmad Al-Masri

B.S., Jordan University of Science and Technology, 2012
M.S., Jordan University of Science and Technology, 2014

A DISSERTATION

submitted in partial fulfillment of the requirements for the degree

DOCTOR OF PHILOSOPHY

Department of Civil Engineering
College of Engineering

KANSAS STATE UNIVERSITY
Manhattan, Kansas

2017

Approved by:

Major Professor
Prof. Hayder Rasheed

# Copyright

# Abstract

The use of laminated composites in aerospace, automotive, and civil engineering applications is ever growing due to their distinguished properties (High stiffness-to-weight ratio, high strength-to-weight ratio, fatigue and corrosion resistance). This growth has resulted in increasing the demand for better understanding the mechanics of laminated composites. Composite columns and wide plates, like any traditional members subjected to axial compression, undergo stability issues prior to failure. Limited amount of research studies has focused on the buckling of laminated anisotropic composite members. Analytical formula for the buckling load of generally anisotropic laminated composite simply supported thin columns and wide plates is derived using the Rayleigh Ritz approximation and bifurcation approach. The effective axial, coupling and flexural stiffness coefficients of the anisotropic layup is determined from the generalized constitutive relationship using dimensional reduction by static condensation of the 6x6 composite stiffness matrix. The resulting explicit formula is expressed in terms of the generally anisotropic material properties as well as the member geometry. The developed formula may be considered an extension to Euler buckling formula using Rayleigh-Ritz approximation and the first of its kind since Euler. This formula reduces down to Euler buckling formula once the effective coupling stiffness term vanishes for isotropic and certain classes of laminated composites. The analytical results are verified against finite element Eigen value solutions for a wide range of anisotropic laminated layups yielding high accuracy. Comparisons with experiments; conducted at Kansas State University for the simply supported case, are also performed showing good correspondence. A brief parametric study is then conducted to examine the effect of ply orientations and material properties including hybrid carbon/glass fiber composites, element thickness, and element type in FE analysis. Relevance of the numerical and analytical results is discussed for all these cases.

# Table of Contents

# List of Figures

# List of Tables

# Acknowledgements

This study is supported in part by the Department of Civil Engineering at Kansas State University. The E-glass fibers and epoxy used in the experimental part was provided by Structural Technologies, Inc.

Moreover, I would like to thank and express my gratitude to Professor Hayder Rasheed whose expertise, guidance, advice, as well as support made it possible for me to conduct this research that was of a great interest for me. I am thankful for the committee members Professor Hani Melhem, Professor Asad Esmaeily, Professor Bacim Alali, and Professor Donghai Wang for taking the time to go through my dissertation.

I would like to thank Mohammad Rasheed, Yu-Szu Chen, and Cody Delany for their help in conducting the experimental work for this research. I am thankful for my family who supported me during my study.

# Dedication

To my parents, the reason of what I become today. Thanks for your great support and continuous care. I also dedicate this dissertation to Dr. Hayder Rasheed who was like a second family for me.

I would like to dedicate this work to my friends; Tasneem Shakeeb, Yu-Szu Chen, Cale Armstrong, James Scott, and Robert Schweiger, who have always supported throughout the entire program. I will always appreciate all what they have done.

# Chapter 1 - Introduction

## 1.1 Background

Composites are defined as a composition of two or more constituents combined at a macroscopic scale to form a new material with enhanced properties. Laminated composite consists of two main constituent, fiber and matrix. Fibers are defined as the reinforcement agent that has the major contribution to strength and stiffness in composites. On the other hand, matrix can be described as the binder that bonds the fibers together, distributes the load, as well as protects the fibers from chemical and environmental attacks. Composite materials are known for their high strength-to-weight ratio, high stiffness-to-weight ratio, electromagnetically inert characteristic, as well as fatigue and corrosion resistance. Laminated composite material is a stack of laminas in different orientations in which each lamina is described as flat or curved thin layer of unidirectional fibers or woven fabric in a matrix that behaves as an orthotropic material. As a result, the laminated composite material will generally have anisotropic behavior where the material properties are different in each direction.

In the past few decades, a growth in the use of laminated composite materials in various industrial applications such as aerospace engineering, marine, automotive, and civil engineering has been noticed. Accordingly, an increase in the demand to understand the mechanical behavior of laminated composite has been realized. Stability (i.e. buckling) issues prior to failure are some of the problems that needed to be investigated. Limited amount of research has focused on the buckling of anisotropic laminated composite members. However, sufficient amount of research has been performed to predict the stability response of plates, shells, cylinders and beams. This research investigates the stability of anisotropic laminated composite columns and wide plates under axial compression with various boundary conditions. Rayleigh-Ritz displacement field

approximation and bifurcation approaches are attempted to develop closed form buckling solutions. Furthermore, finite element analysis is conducted to validate the derived formulas. A parametric study is performed to investigate the effect of changing material properties including hybrid (steel-composite) material, ply orientations, element thickness, and element type in FE analysis. In relation to the simply supported anisotropic and hybrid columns, experimental work is additionally performed. Furthermore, different definitions are used to describe the results in which excellent agreement refers to error values less than 5 %. Results with error values less than 10 % are listed in the very good agreement category. Moreover, a good agreement reflects error with values less than 15 %.

## 1.2 Objectives

The present research is aimed at developing generalized analytical buckling solutions for anisotropic laminated composite columns and wide plates under axial compression with various boundary conditions. Furthermore, parametric studies are conducted to assess the effect of different aspects such as material properties including hybrid material, ply orientations, element thickness, and element type in finite element analysis.

## 1.3 Scope of Dissertation

This dissertation consists of thirteen chapters. The first chapter presents introduction of the topic, objectives of this work and dissertation scope. Chapter two includes the literature review undertaken on the topics related to the dissertation scope. Chapter three introduces the work conducted on simply supported anisotropic laminated composite columns in which a closed form buckling solution is developed using Rayleigh-Ritz method. Finite element analysis is performed to verify the analytical results for different stacking sequences. Moreover, the effect of various

parameters on the buckling load is studied. Experimental technique is performed to predict the buckling load of four-layer E-Glass/Epoxy composite simply supported columns. In chapter four, a generalized analytical buckling formula is presented for simply supported anisotropic laminated wide plates utilizing Rayleigh-Ritz approximation. Additionally, the proposed formula is confirmed against numerical analysis. Different aspects are taken into account while predicting the stability response.

Chapter five addresses Rayleigh-Ritz methods for developing the analytical buckling formula of fixed-fixed anisotropic laminated composite columns based on the energy approach. The presented formula is expressed in terms of the flexural stiffness and the column geometry. In order to decrease some of the discrepancy between the analytical and finite element analysis results, the bifurcation approach of the pre-buckling deformation is attempted yielding a new formula with an additional term that includes the coupling and axial coefficients. A parametric study is then conducted to examine the effect of different parameters. In chapter six, a similar procedure to the one in chapter five is presented for the anisotropic laminated composite wide plates.

Chapter seven reports on buckling solutions of fixed-free anisotropic laminated composite columns under axial compression using Rayleigh-Ritz formulation and finite element analysis. The developed formula is expressed in terms of flexural, extensional, and coupling stiffness along with the column geometry. The effect of ply orientations, element thickness, and material properties including hybrid carbon/glass fiber composites. In chapter eight, Rayleigh-Ritz solution is addressed for anisotropic laminated composite wide plates with clamped-free boundary conditions under uniaxial compression loading. Finite element solution is also attempted to validate the proposed buckling formula.

In chapter nine, pre-buckling deformation is substituted into the bifurcation approach to derive a generalized closed form buckling solution for clamped-pinned anisotropic laminated composite columns under axial compression. The presented analytical explicit formula reproduces Euler buckling expression while it furnishes extra two terms which are functions of the effective coupling, flexural and axial stiffness. Eigenvalue and nonlinear geometry analysis is conducted to predict critical buckling load values and the stability response of the composite columns for a wide range of stacking sequences, respectively. Moreover, the analytical and numerical results are compared with previous work. Chapter ten presents closed form stability solution of clamped-pinned anisotropic laminated composite wide plates under uniaxial compression compared with numerical (FE) analysis. A study is also performed to assess the effect of material properties, element thickness, and element type in FE analysis on the stability response. In chapter eleven, buckling of simply supported anisotropic Steel-FRP hybrid columns using Rayleigh-Ritz formulation with numerical and experimental verification is introduced. Two categories of anisotropic steel-glass fiber reinforced polymer (GFRP) columns are tested under axial compression loading in which category A has steel sandwiched in-between the composite layers and category B has steel on the side of the composite layup. Conclusions, recommendations, and future work are discussed in chapter twelve.

# Chapter 2 - Literature Review

## 2.1 Overview

A brief overview regarding the work conducted on the stability of laminated composite structures is introduced in this chapter. Section 2.2 presents work performed to develop analytical formulations of the buckling of laminated composite members. Numerical solutions and finite element analysis-based papers are presented in section 2.3. Furthermore, section 2.4 introduces experimental work performed on the composite laminated structures.

## 2.2 Analytical Studies

Rasheed and Yousif [1] studied the buckling of thin laminated orthotropic composite rings and long cylinders under external pressure. A generalized analytical buckling formula was developed for a multi-angle laminated orthotropic rings and long cylinders. The developed formula is expressed in terms of the generally orthotropic extensional, flexural, and coupling stiffness coefficients. The following equation represents the critical buckling formula:

$$\boldsymbol{P_{cr} = 3\left(\frac{A_{orth}D_{orth}-B_{orth}^2}{A_{orth}R^3+2B_{orth}R^2+D_{orth}R}\right)} \qquad \textbf{(1)}$$

In which $A_{orth}$, $B_{orth}$, and $D_{orth}$ are simply the extensional, coupling, and flexural stiffness coefficients, respectively, obtained from the dimensional reduction of orthotropic behavior. The developed formula yielded improved results compared to some design codes. Rasheed and Yousif [2] derived a generalized closed form buckling formula of anisotropic laminated thin rings and long cylinders subjected to external hydrostatic pressure. The formula is presented in terms of the generally anisotropic material and the member geometry. The developed formula was confirmed against finite element solutions and the results showed that the buckling modes are symmetric with respect to rotated axes of the twisted section of the pre-buckling solution in case of anisotropy.

Silva et al. [3] presented a formulation of a generalized beam theory (GBT) to predict the local and global buckling behavior of fiber reinforced polymer (FRP) composite open-section thin-walled columns. The solution for buckling using GBT included solving the following eigenvalue problem:

$$(\boldsymbol{K} + \boldsymbol{\gamma G})\boldsymbol{d} = \boldsymbol{0} \qquad \textbf{(2)}$$

Where K is the global linear stiffness matrix; G is the geometric stiffness matrix; and d is the eigenvector. The paper presented finite element beam to solve the generalized beam theory (GBT).

Silvestre and Camotim [4] studied the buckling behavior of thin walled arbitrary orthotropic members by developing a second order generalized beam theory (GBT). The second order GBT formulation was also compared with Bauld and Lih-Shyng theory [5]. The results showed that the critical load exists for all isotropic or cross-ply orthotropic members. Furthermore, non-linear primary path is exhibited and no specific bifurcation is detected for asymmetric orthotropic lay-ups. Xu et al. [6] presented an approximate analytical method based on the equivalent anisotropic plate approach to study the buckling of tri-axial woven fabric composite structures subjected to bi-axial loading. The presented method was verified against non-linear finite element analysis. It was observed that the analytical solution gives upper bound results for buckling loads and can be used to predict the buckling behavior for real world problems subjected to bi-axial loading. Shukla et al. [7] presented an analytical formulation to predict the stability of cross-ply and angle-ply laminated composite rectangular plates under in-plane uniaxial and biaxial loading based on the Reissner-Mindlin first order shear deformation theory and von-Karaman type nonlinearity for various combinations of boundary conditions. The non-dimensional critical load parameter $\lambda_{cr}$ is expressed in the following:

$$\boldsymbol{\lambda_{cr}} = \frac{(N_{\delta b})_{cr}\, b^2}{E_2 h^3} \qquad \textbf{(3)}$$

In which $N_{\delta b}$ is the uniform in-plane mechanical loading, b is the width of the plate, $E_2$ is the modulus of elasticity in transverse direction, and h is the plate thickness. Span to thickness ratio, plate aspect ratio, lamination scheme, number of layers and modulus ratio effects were considered in estimating the buckling behavior. The analytical formulation results showed a good agreement with the numerical analysis results.

Herencia et al. [8] presented a closed form solutions for buckling of long anisotropic plates with various boundary conditions under axial compression using Rayleigh-Ritz approximation method. The following equation defines the closed from solution:

$$\boldsymbol{N_x^{cr}} = \boldsymbol{\kappa_x} \frac{\pi^2}{b^2} \sqrt{D_{11} D_{22}} \qquad \textbf{(4)}$$

Where $D_{ij}$ is the bending stiffness; b is the width of the plate; and $\kappa_x$ is the non-dimensional buckling coefficient related to the boundary conditions. The results showed an excellent agreement with existing solutions (Weaver [9] [10], Qiao and Shan [11]) and finite element results. Sun and Harik [12] studied the buckling of stiffened antisymmetric laminated composite plates with bending-extension coupling by extending the analytical strip method (ASM) developed by Harik and Salamoun [13] to analyze bending of thin orthotropic and stiffened rectangular plates. The results showed that plates with free boundary conditions contribute the weakest stiffening effect. Moreover, the number of layers of ply orientations equal to 0 and 90 had no effect on the critical buckling load since the coupling stiffness matrix vanishes. Shufrin et al. [14] presented a semi-analytical solution for buckling of symmetrically laminated rectangular plates with general boundary conditions under combined tension, compression, and shear depending on multi term

Kantorovich method developed by Kerr [15]. The results showed that the stability of angle-ply laminated plates improved under biaxial compression/tension, shear and additional in-plane forces were created due to the in-plane restrains.

Weaver and Nemeth [16] developed non-dimensional parameters and governing equations to study the buckling behavior of rectangular symmetrically laminated composite plates with different boundary conditions under uniform axial compression, uniform shear, or pure in-plane bending loading. Furthermore, bounds for non-dimensional parameters were presented as an indication of percentage gained in the buckling resistance for laminated plates. The results exhibited 26-36% increase in the buckling resistance for tailored simply supported orthotropic plates; with respect to isotropic plates. Moreover, clamped laminated plates exhibited 9-12% increase in the buckling resistance. Using polar representation of the fourth-order flexural stiffness tensor, Kazemi [17] presented a new exact semi-analytical approach to predict the buckling of laminated composite plates under biaxial compression. The developed formula can be used easily to predict buckling problems, optimization and design of laminated plates under in-plane loading. Thai and Kim [18] proposed a closed form solution for buckling of orthotropic plates with two opposite simply supported edges using two variable refined plate theories. State space concept was used based on Levy type solution to solve the governing equations. The results showed more accurate solutions than the higher order shear deformation theory. Ovesy et al. [19] investigated the stability of laminated composite plates under uniaxial uniform compression. Based on the higher order plate theory (HOPT), a semi-analytical finite strip formulation was presented. A parametric study was conducted to study the effect of plate aspect ratio ($a/b$), width to thickness ratio ($b/h$), material properties, boundary conditions, and number of layers. The results showed that the critical buckling load increases as the plate width to thickness ratio increases and plate aspect ratio

decreases. Moreover, the results obtained from the presented formulation exhibited a good agreement with the 3-D elasticity theory.

Abramovich and Livshits [20] studied the free vibrations of non-symmetric cross ply laminated composite beams based on the first order shear deformation theory. Longitudinal, transverse displacement, rotary inertia, and shear deformation were taken into account in the analysis. The following equation of motion of cross ply laminated composite beams was solved for different boundary conditions:

$$[\mathbf{M}]\{\ddot{\boldsymbol{q}}\} + [\mathbf{C}]\{\boldsymbol{q}\} = \{\mathbf{0}\} \qquad \textbf{(5)}$$

Where [M] is the generalized mass matrix, [C] is the matrix differential operator; and {q} is the vector of the generalized displacements. The new approach and Bernoulli-Euler theory were verified against numerical solutions. Abramovich et al. [21] used the exact method based on Timoshenko equation to study the vibrations and buckling of cross-ply non-symmetric rectangular laminated composite beams. The effects of material properties, number of layers, and boundary conditions were considered. Analytical results showed a good agreement with the numerical results. Moreover, the non-symmetric layup showed a coupling effect between the axial and lateral motion of the beam. Based on Hellinger-Reissner principal, Cortinez and Piovan [22] proposed a theoretical model to investigate the buckling of composite thin-walled beams with shear deformability using nonlinear displacement field. The governing equations were solved using finite elements with fourteen degrees of freedom per element. Based on the results, shear flexibility had a significant effect on the stability of the composite beams. Using Ritz method, Aydogdu [23] studied the stability of cross-ply laminated beams with general boundary conditions depending on the unified three degrees of freedom shear deformable beam theory. The results were verified with

previous work for various length-to-thickness ratios and various layups. Pandey and Sherbourne [24] proposed a general formulation to predict the buckling of rectangular anisotropic symmetric angle ply composite plates under linearly varying uniaxial compressive loading with clamped and simply supported boundary conditions based on energy method and orthogonal polynomial sequences obtained by Gram-Schmidt. Ghaheri et al. [25] studied the bucking and vibration of symmetrically laminated composite elliptical plates on a Winkler-type elastic foundation under uniform in-plane force for various boundary conditions based on the variational approach and Ritz method. The effect of having different layup stacking sequences, aspect ratio, in-plane load, and foundation parameter was also considered. The results showed that as the foundation parameter increases and the aspect ratio decreases, the critical buckling load increases. Heidari-Rarani et al. [26] investigated the effect of angle-ply and cross-ply layups on the stability of E-glass/epoxy square composite laminated plates under axial compression with SFSF (S: simply supported, F: Free) boundary conditions analytically, numerically, and experimentally. Using Rayleigh-Ritz approach based on energy method, a semi-analytical solution was developed to predict the buckling load values. Eigenvalue and nonlinear analysis (Riks Analysis) were conducted to predict buckling load values and the stability response of the laminates using finite element software Abaqus. Eight node quadratic shell element (S8R) was assumed with mesh size equal to 2.5 mm and line load in the y-direction of value 1 N/m was assigned to the edge of the laminates. Moreover, Hashin, Tsai-Wu, and Tsai-Hill failure criteria were attempted in the numerical analysis to study the layer failure of the laminated composites. E-glass/epoxy plates of four layers were made with angle-ply ($[\mp 30]_s$, $[\mp 45]_s$) and cross-ply ($[0/90]_s$) stacking sequences using hand layup method. V-shape fixture was assembled to implement the simply supported boundary conditions and placed in the universal testing machine. The test was conducted under displacement control with rate

equal to 0.5 mm/min. The analytical results showed an excellent agreement with the numerical (FE) results. On the other hand, the semi-analytical and numerical buckling load values were overestimated compared to the experimental ones. Furthermore, Hashine failure criteria were not able to predict the failure of the laminated composite plates efficiently. However, Tsai-Wu and Tsai-Hill failure criteria had the same failure mode as the tested plates in which the failure started from the plate edge then developed along the plate. Lopatin and Morozov [27] proposed an analytical formula to predict the buckling of composite cantilever circular cylindrical shell under uniform external lateral pressure based on the generalized Galerkin method. Finite element software COSMOS/M was used to perform the eigenvalue and eigenvector computations with SHELL4L element and was verified against the analytical results yielding an accurate estimate of the buckling load values.

## 2.3 Numerical Studies

Debski [28] presented numerical analysis of buckling and post-buckling of thin-walled simply supported laminated composite columns with channel section under axial compression. Eight symmetrical layered Carbon/Epoxy columns were analyzed using finite element software Abaqus and Ansys, which was verified with analytical-numerical method [29]. Linear four node shell element with reduced integration schemes (S4R) and eight node shell element (Shell99) were utilized in Abaqus and Ansys, respectively. A good agreement was observed between the finite element results and results obtained from the analytical-numerical method. Kumar and Mukhopadhyay [30] presented a new finite element to predict the buckling of laminated stiffened plate for different boundary conditions based on the first order shear deformation theory. The presented element eliminated any addition of extra nodes in the mesh assignment step at the

stiffener locations. Moreover, the transverse shear deformation was taken into account in the plate and stiffener element. The new finite element captured the critical buckling behavior of thin and thick plate without shear locking. The results showed a good agreement of the developed finite element compared with previous work conducted by Loughlan [31]. Rikards et al. [32] developed a triangular finite element to investigate the buckling and vibration of laminated composite stiffened plates and shells. Equivalent layer shell theory with six degrees of freedom based on the first order shear deformation theory with transverse shear stiffness correction was used. The critical buckling load results obtained from the new triangular element were verified against existence solutions (Jaunky et al. [33]) yielding a good agreement. Depending on full three dimensional elasticity formulation and layer-wise finite element, Setoodeh and Karami [34] proposed a refined layer-wise finite element formulation and computer code named L3WD to predict static, free vibration, and buckling of anisotropic thick laminated composite plates resting on Winkler and Pasternak elastic foundation, elastic line and point support. The results were confirmed against classical laminated plate theory (CLPT), first order shear deformation theory (FSDT), and higher order shear deformation theory (HSDT) yielding a good agreement. The computer code L3WD yielded accurate results for thick composite plates with different boundary conditions, in-plane and out-of- plane deformation. Based on the refined Reddy's higher order theory, Nayak et al. [35] developed nine node shear deformable plate bending element to study buckling and vibration of initially stressed composite sandwich plate with various boundary conditions under different in-plane loading conditions. To prevent shear locking phenomena, assumed strain concept was used with full integration schemes. The effect of loading conditions, stacking sequence, boundary conditions, and thickness ratio was studied. The results observed a good agreement compared to exact results conducted by Noor et al. ([36] and [37]), higher order

shear deformation theory (HSDT), and classical laminated plate theory (CLPT). Grover et al. [38] presented a new inverse hyperbolic shear deformation theory (IHSDT) to study static and buckling of laminated composite and sandwich plates depending on the shear strain shape function to ensure a nonlinear distribution of transverse shear stresses and satisfies traction at free boundary conditions. Principal of virtual work with linear kinematics was used to derive the governing differential equations. Analytical solution was solved using Navier type solution of simply supported composite sandwich plate. Several numerical examples were solved using the presented theory. The developed theory accurately predicted the critical buckling load for simply supported thick plates with minimal numerical error and computational cost. Kidane et al. [39] investigated the stability of grid stiffened composite cylinders. Depending on smeared method, analytical model was developed where the equivalent material properties were determined of grid stiffened composite cylindrical shells. The moment and force effects due to stiffeners were considered for a unit cell in the analysis procedure. Ritz method was performed to calculate the buckling load analysis of simply supported composite cylinders [40] using Matlab code. Experimental work was conducted to verify the developed analytical model results. The results showed that the buckling load decreases as the stiffener spacing increases. Furthermore, stiffener orientation, cylindrical shell thickness, and shell winding angle had a significant effect on the buckling load values of symmetrical and unsymmetrical composite layups in the cylinders.

Based on three dimensional elasticity considerations, Jianqiao Ye and Soldatos [41] studied the stability of simply supported thick laminated cross-ply composite hollow cylinders and open cylindrical panels under combined external loading. Initial zero shear stresses were assumed in the pre-buckling solution. Three dimensional sets of linearized buckling equations were solved using recursive method of a successive approximation approach. The results of the forty-layer laminated

composite cylinder under axial compression were compared with previous work conducted by Noor and Peters [42] yielding an excellent agreement. Moreover, the results showed that Ref. [42] formulation is computationally expensive for problems with high number of degrees of freedom compared to the presented method. Additionally, the buckling analysis was conducted for symmetric and antisymmetric cross-ply layups.

## 2.4 Experimental Studies

Debski et al. [43] investigated the buckling and post-buckling behavior of simply supported thin-walled composite channel column sections under axial compression loading experimentally. Carbon/Epoxy thin walled channel section columns with cross sectional dimensions equal to 80 x 40 x 1.048 mm and length of 300 mm were tested using Zwick Z100/SN3A universal testing machine, moreover, columns were composed of eight symmetrical plies $[0/-45/45/90]_s$. The results were compared with numerical solutions obtained from finite element software Abaqus and ANSYS using 4-node linear shell element (S4R) with reduced integration schemes and 8-node shell element, respectively. Additionally, the experimental results were confirmed against the analytical-numerical method (ANM) based on Koiter theory [44-47]. Meyer-Piening et al. [48] presented a project performed by Institute of Structural Mechanics, Braunschweig (DLR), former Institute of Lightweight Structures and Ropeways (ETH Zurich), and Department of Polymers/Composites (EMPA Dubendorf) to study the stability of thin-walled carbon fiber reinforced polymer (CFRP) laminated cylinders under combined axial compression and torsional loading experimentally and numerically. Carbon/Epoxy cylindrical shells were tested at DLR buckling test facility under axial compression and at EMPA universal testing machine under combined loading. The experimental results were compared with two analytical solutions, shallow shell theory [49] and deep shell theory (using BACCUS program). Furthermore, experimental

results were confirmed against finite element results obtained with MARC K7 yielding accurate results. Isoparametric shell element No. 75 was used in the finite element analysis with element size equal to 60 x 180 mm. The results showed that the analytical solutions predicted accurate buckling load compared with experimental ones for eccentrically laminated circular cylinders with small initial imperfection. Moreover, the stacking sequences of the laminated cylinder had a significant effect on imperfection. Aslan and Sahin [50] studied the buckling of E-glass/Epoxy cross-ply laminated composite rectangular plates with multiple delamination under axial compression. Experimental work was conducted to test fixed-fixed composite plates of stacking sequence $[0/90/0/90]_s$ with and without delamination. The following dimensions were attempted for length, width, and thickness: 100 mm x 30 mm x 2.4 mm, respectively. Axial compression test was performed using Shimazdu AG-X testing machine under displacement control with rate equal to 0.1 mm/min. Finite element analysis was carried out to verify the experimental results using Ansys 11.0. Solid elements with six degrees of freedom (SOLID46) were assumed in FE analysis. A parametric study was conducted to study the effect of having different stacking sequences. The numerical (FE) results exhibited a good agreement against the experimental results. In general, it was observed that increasing the number of delamination defects led to a decrease in the buckling load values. For composite plates without delamination, buckling load values of antisymmetric stacking sequences were lower than symmetric ones. On the other hand, antisymmetric stacking sequences observed higher buckling load for composite plates with multiple delamination. Baba and Baltaci [51] investigated the buckling characteristics of symmetrically and anti-symmetrically laminated composite rectangular plates made of E-glass/Epoxy with central cutout using experimental and numerical techniques. Different laminate configurations, cutout shape, boundary conditions, and length to thickness ratio were taken into consideration. Composite plates were

analyzed using finite element software Ansys. Eight nodded multilayered shell element (SHELL91) was assumed and axial compression loading was attempted. The experimental results were confirmed against finite element analysis yielding a higher buckling load values than the numerical ones. Moreover, the buckling load decreased as the length to thickness ratio increased. For symmetric and antisymmetric laminated composite plates, the buckling load values decreased due to the existence of cutouts. The antisymmetric stacking sequences and clamped boundary conditions showed a higher buckling loads compared to symmetric and simply supported boundary conditions, respectively.

# Chapter 3 - Analytical and Finite Element Buckling Solutions of Simply Supported Anisotropic Laminated Composite Columns under Axial Compression Compared with Experiments

**Hayder A. Rasheed[1] and Rund Al-Masri[2]**

## 3.1 Abstract

**Analytical formula for the buckling load of generally anisotropic laminated composite simply supported thin columns is derived using the Rayleigh Ritz displacement field approximation. The effective axial, coupling and flexural stiffness coefficients of the anisotropic layup is determined from the generalized constitutive relationship using dimensional reduction by static condensation of the 6x6 composite stiffness matrix. The resulting explicit formula has an additional term which is a function of the effective coupling and axial stiffness. This formula reduces down to Euler buckling formula once the effective coupling stiffness term vanishes for isotropic and certain classes of laminated composites. The analytical results are verified against finite element Eigen value solutions for a wide range of anisotropic laminated layups yielding high accuracy. Comparisons with experiments are also performed showing good correspondence. A brief parametric study is then conducted to examine the effect of ply orientations and material properties including hybrid carbon/glass fiber composites. Relevance of the numerical and analytical results is discussed for all these cases.**

Keywords: Buckling of Composite Columns, Simply Supported Boundary Conditions, Anisotropic Laminated Composites, Axial Compression.

[1] Professor, Department of Civil Engineering, Kansas State University, Manhattan, KS 66506

[2] Ph.D. Candidate, Department of Civil Engineering, Kansas State University, Manhattan, KS 66506

## 3.2 Introduction

The use of laminated composites in aerospace, automotive, marine and civil engineering applications is ever growing due to their distinguished properties (High stiffness-to-weight ratio, high strength-to-weight ratio, fatigue and corrosion resistance). This growth has resulted in increasing the demand for better understanding the mechanics of laminated composites. Composite columns, like any traditional members subjected to axial compression, undergo stability issues prior to failure. Not many research studies have focused on the buckling of columns, however, a significant amount of research has been performed to study the buckling behavior of composite members, plates and shells in the recent years [1-13]. Silva et al. [1] developed a formulation of a generalized beam theory (GBT) to study local and global buckling behavior of fiber reinforced polymer composite open section thin-walled columns. The solution for buckling using GBT included solving the following eigenvalue problem:

$$(\boldsymbol{K} + \boldsymbol{\gamma G})\boldsymbol{d} = \boldsymbol{0} \qquad \textbf{(1)}$$

Where K is the global linear stiffness matrix; G is the geometric stiffness matrix; and d is the eigenvector. Silvestre and Camotim [2] developed a second order generalized beam theory (GBT) to predict buckling behavior for thin walled arbitrary orthotropic thin-walled members. The second order GBT formulation was also compared with Bauld and Lih-Shyng theory [3]. The results showed that the critical load exists for all isotropic or cross-ply orthotropic members. On the other hand, non-linear primary path is exhibited and no specific bifurcation is detected for asymmetric orthotropic lay-ups. Rasheed and Yousif [4] used the energy approach to develop a closed form solution to predict buckling of thin laminated orthotropic composite rings/long cylinder under external pressure:

$$\boldsymbol{P_{cr}} = \boldsymbol{3}\left(\frac{\boldsymbol{A_{orth}D_{orth} - B_{orth}^2}}{\boldsymbol{A_{orth}R^3 + 2B_{orth}R^2 + D_{orth}R}}\right) \qquad \textbf{(2)}$$

Where $A_{orth}, B_{orth}, and\ D_{orth}$ constants are simply the extensional, coupling, and bending stiffness coefficients obtained from dimensional reduction of orthotropic behavior. The developed formula yielded improved results compared to some design codes. Rasheed and Yousif [5], developed a closed form solution for buckling of anisotropic laminated composite rings and long cylinders subjected to external hydrostatic pressure. They confirmed their analytical results against finite element solutions and also concluded that the buckling modes are symmetric with respect to rotated axes of the twisted section of the pre-buckling solution in case of anisotropy. Xu et al. [6] developed an approximate analytical solution to predict buckling of a tri-axial woven fabric composite structure under bi-axial loading based on the equivalent anisotropic plate method. They concluded that the analytical solution gives an upper bound solution for buckling load and it can be used to predict buckling behavior for real world problems subjected to bi-axial loading. Using first order shear deformation and von-Karman type nonlinearity, Shukla et al. [7] estimated critical buckling loads for laminated composite plates with various boundary conditions under in-plane uniaxial and biaxial loading. Span to thickness ratio, plate aspect ratio, lamination scheme, number of layers and modulus ratio effects were considered in estimating the buckling behavior. Sun and Harik [8] developed analytical buckling solution of stiffened antisymmetric laminated composite plates with bending-extension coupling using analytical strip method (ASM) which was first developed by Harik and Salamoun [9] to analyze bending of thin orthotropic and stiffened rectangular plates. The results showed that plates with free boundary conditions contribute the weakest stiffening effect. Moreover, the number of layers of ply orientations equal to 0 and 90 had no effect on the critical buckling load since the coupling stiffness matrix vanishes. Debski et al. [10] studied buckling and post-buckling behavior of thin-walled composite channel column

sections experimentally. The results were compared with numerical solutions obtained from finite element models (Abaqus and ANSYS) and analytical-numerical method (ANM). Based on multi term Kantorovich method developed by Kerr [11], Shufrin et al. [12] developed a semi-analytical solution for buckling of symmetrically laminated rectangular plates with general boundary conditions under combined tension, compression, and shear. The results showed that the stability of angle-ply laminated plates improved under biaxial compression/tension and shear. Moreover, additional in-plane forces were created due to the in-plane restrains. Thai and Kim [13] proposed a closed form solution for buckling of orthotropic plates with two opposite simply supported edge using two variable refined plate theories. State space concept was used on Levy type solution to solve the governing equations. The results showed more accurate solutions than the higher order shear deformation theory.

In this work, a generalized analytical formula for buckling of simply supported laminated composite columns subjected to axial compression is developed. The Rayleigh–Ritz approximation was used to obtain the buckling formula. Axial, coupling and flexural rigidities in 1D are determined using dimensional reduction by the static condensation approach starting with the 3D rigidity matrix. Moreover, finite element models for the columns are established using the commercial software Abaqus. Furthermore, glass fiber-epoxy columns were made and tested in the laboratory. The finite element numerical solution was compared to the analytical solution resulting in excellent agreement. The experimental results also showed reasonable comparison with the newly developed analytical results. A good agreement between all three types of results was observed, regardless of the complexity of the composite lay-ups used.

## 3.3 Analytical Formulation

A generalized closed form buckling formula for simply supported anisotropic laminated composite columns under axial compression is derived using Rayleigh-Ritz approximation.

1.1 Assumptions:

1. Buckling takes place in the x-y plane about the weak axis (z-axis).
2. The y-axis runs through the thickness of the column where the composite lamination takes place, Figure 3.1
3. The lamination angle ( $\alpha$ ) is measured with respect to the x-axis (i.e. 0° fibers run parallel to the x-axis and 90° fibers run parallel to the z-axis). Accordingly, the angle ( $\alpha$ ) is rotated about the y-axis.
4. Plane sections before bending remain plane after bending and perpendicular to the mid surface (i.e. simple beam theory holds).
5. Classical lamination theory is applicable with shear deformations ignored.

### 3.3.1 Kinematics

Figure 3.1 illustrates geometry and the Cartesian coordinates of the simply supported column used. The z-axis is the weak axis of the column about which bending takes place. The following displacement relations were assumed based on the isotopic Euler first buckling mode:

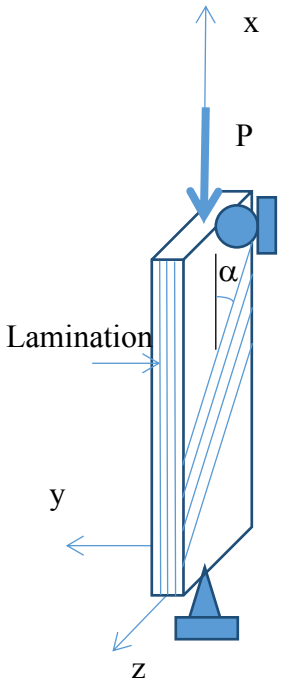


Figure 3.1 The column geometry.

$$\boldsymbol{u}(\boldsymbol{x}) = \boldsymbol{B_1 x} + \boldsymbol{B_2 \theta_z(x) y}\,; \quad \boldsymbol{v}(\boldsymbol{x}) = \boldsymbol{C_1} \sin\frac{\pi x}{L} \tag{3}$$

Where $u(x)$, and $v(x)$ is the axial, and lateral displacements; $B_1$, $B_2$ and $C_1$ are constants to be solved; and x is the distance along the axis of the column. The second term in the axial displacement expression is neglected since the % variation in cross section axial displacement is found from the finite element analysis below to be very small. More specifically, this percentage varies between 0.07 - 4.00% for materials with high stiffness ratio ($E_{11}/E_{22}$) (e.g. Graphite/Epoxy) and between 0.05 - 2.00% for materials with lower stiffness ratio ($E_{11}/E_{22}$) (e.g. S Glass/Epoxy). For an intermediate class of deformation, the axial strain $\varepsilon_x$ and curvature $\kappa_x$ are defined as follow.

$$\boldsymbol{\varepsilon_x} = \frac{\boldsymbol{du}}{\boldsymbol{dx}} + \frac{\boldsymbol{1}}{\boldsymbol{2}}\left(\frac{\boldsymbol{dv}}{\boldsymbol{dx}}\right)^{\boldsymbol{2}} = \boldsymbol{u'} + \frac{\boldsymbol{1}}{\boldsymbol{2}}\boldsymbol{v'^2}; \qquad \boldsymbol{\kappa_x} = \frac{\boldsymbol{d^2 v}}{\boldsymbol{d^2 x}} = \boldsymbol{v''} \tag{4}$$

### 3.3.2 Constitutive equations

The principal material directions were transformed into the column coordinate system, the stresses and strains are then related in the following equation

$$\begin{Bmatrix} \boldsymbol{\sigma_x} \\ \boldsymbol{\sigma_z} \\ \boldsymbol{\tau_{xz}} \end{Bmatrix} = \begin{bmatrix} \boldsymbol{\bar{Q}_{11}} & \boldsymbol{\bar{Q}_{12}} & \boldsymbol{\bar{Q}_{16}} \\ \boldsymbol{\bar{Q}_{12}} & \boldsymbol{\bar{Q}_{22}} & \boldsymbol{\bar{Q}_{26}} \\ \boldsymbol{\bar{Q}_{16}} & \boldsymbol{\bar{Q}_{26}} & \boldsymbol{\bar{Q}_{66}} \end{bmatrix} \begin{Bmatrix} \boldsymbol{\varepsilon_x} \\ \boldsymbol{\varepsilon_z} \\ \boldsymbol{\gamma_{xz}} \end{Bmatrix} \quad \textbf{(5)}$$

Where $\bar{Q}_{ij}$ matrix represents the transformed reduced stiffness matrix as defined in standard composite textbooks [14]. Accordingly, the coupled force-strain relationship is established as follows:

$$\begin{Bmatrix} \boldsymbol{N_x} \\ \boldsymbol{N_z} \\ \boldsymbol{N_{xz}} \\ \boldsymbol{M_x} \\ \boldsymbol{M_z} \\ \boldsymbol{M_{xz}} \end{Bmatrix} = \begin{bmatrix} \boldsymbol{A_{11}} & \boldsymbol{A_{12}} & \boldsymbol{A_{16}} & \boldsymbol{B_{11}} & \boldsymbol{B_{12}} & \boldsymbol{B_{16}} \\ \boldsymbol{A_{12}} & \boldsymbol{A_{22}} & \boldsymbol{A_{26}} & \boldsymbol{B_{12}} & \boldsymbol{B_{22}} & \boldsymbol{B_{26}} \\ \boldsymbol{A_{16}} & \boldsymbol{A_{26}} & \boldsymbol{A_{66}} & \boldsymbol{B_{16}} & \boldsymbol{B_{26}} & \boldsymbol{B_{66}} \\ \boldsymbol{B_{11}} & \boldsymbol{B_{12}} & \boldsymbol{B_{16}} & \boldsymbol{D_{11}} & \boldsymbol{D_{12}} & \boldsymbol{D_{16}} \\ \boldsymbol{B_{12}} & \boldsymbol{B_{22}} & \boldsymbol{B_{26}} & \boldsymbol{D_{12}} & \boldsymbol{D_{22}} & \boldsymbol{D_{26}} \\ \boldsymbol{B_{16}} & \boldsymbol{B_{26}} & \boldsymbol{B_{66}} & \boldsymbol{D_{16}} & \boldsymbol{D_{26}} & \boldsymbol{D_{66}} \end{bmatrix} \begin{Bmatrix} \boldsymbol{\varepsilon_x} \\ \boldsymbol{\varepsilon_z} \\ \boldsymbol{\gamma_{xz}} \\ \boldsymbol{\kappa_x} \\ \boldsymbol{\kappa_z} \\ \boldsymbol{\kappa_{xz}} \end{Bmatrix} \quad \textbf{(6)}$$

Where:

$$\boldsymbol{A_{ij}} = \sum_{\boldsymbol{k=1}}^{\boldsymbol{N}} \boldsymbol{\bar{Q}_{ij} t_k}$$

$$\boldsymbol{B_{ij}} = \sum_{\boldsymbol{k=1}}^{\boldsymbol{N}} \boldsymbol{\bar{Q}_{ij} t_k \bar{y}_k}$$

$$\boldsymbol{D_{ij}} = \sum_{\boldsymbol{k=1}}^{\boldsymbol{N}} \boldsymbol{\bar{Q}_{ij} t_k} \left( \boldsymbol{\bar{y}_k^2} + \frac{\boldsymbol{t_k^2}}{\boldsymbol{12}} \right) \quad \textbf{(7)}$$

$$\boldsymbol{t_k} = \boldsymbol{y_k} - \boldsymbol{y_{k-1}}$$

$$\boldsymbol{\bar{y}_k} = \frac{\boldsymbol{y_k} + \boldsymbol{y_{k-1}}}{\boldsymbol{2}}$$

In which $A_{ij}$,$B_{ij}$ and $D_{ij}$ are the axial, coupling, and flexural rigidity coefficients. $t_k$ = thickness of the k-th ply; and N = number of different plies in the stacking sequence.

The three dimensional (3D) rigidity matrix is established first using the material properties and the fiber orientations into equation (7). Then the dimension is reduced to 1D anisotropic axial, coupling and flexural rigidities using static condensation approach after applying the zero forces and moments.

$$\begin{Bmatrix} N_x \\ N_z = 0 \\ N_{xz} = 0 \\ M_x \\ M_z = 0 \\ M_{xz} = 0 \end{Bmatrix} = \begin{bmatrix} A_{11} & A_{12} & A_{16} & B_{11} & B_{12} & B_{16} \\ A_{12} & A_{22} & A_{26} & B_{12} & B_{22} & B_{26} \\ A_{16} & A_{26} & A_{66} & B_{16} & B_{26} & B_{66} \\ B_{11} & B_{12} & B_{16} & D_{11} & D_{12} & D_{16} \\ B_{12} & B_{22} & B_{26} & D_{12} & D_{22} & D_{26} \\ B_{16} & B_{26} & B_{66} & D_{16} & D_{26} & D_{66} \end{bmatrix} \begin{Bmatrix} \varepsilon_x \\ \varepsilon_z \\ \gamma_{xz} \\ \kappa_x \\ \kappa_z \\ \kappa_{xz} \end{Bmatrix} \tag{8}$$

Equation (8) is solved first for the axial strain and axial curvature ($\varepsilon_x$ ,$\kappa_x$) in terms of the rest of the deformation components by extracting the second, third, fifth and sixth linear equations from the matrix.

$$-\begin{bmatrix} A_{12} & B_{12} \\ A_{16} & B_{16} \\ B_{12} & D_{12} \\ B_{16} & D_{16} \end{bmatrix} \begin{Bmatrix} \varepsilon_x \\ \kappa_x \end{Bmatrix} = \begin{bmatrix} A_{22} & A_{26} & B_{22} & B_{26} \\ A_{26} & A_{66} & B_{26} & B_{66} \\ B_{22} & B_{26} & D_{22} & D_{26} \\ B_{26} & B_{66} & D_{26} & D_{66} \end{bmatrix} \begin{Bmatrix} \varepsilon_z \\ \gamma_{xz} \\ \kappa_{yz} \\ \kappa_{xz} \end{Bmatrix}$$

$$-R \begin{Bmatrix} \varepsilon_x \\ \kappa_x \end{Bmatrix} = Q \begin{Bmatrix} \varepsilon_z \\ \gamma_{xz} \\ \kappa_z \\ \kappa_{xz} \end{Bmatrix} \tag{9}$$

Inverting the matrix Q to the other side of equation (9), the condensed deformation components are obtained in terms of the axial strain and curvature:

$$\begin{Bmatrix} \varepsilon_z \\ \gamma_{xz} \\ \kappa_z \\ \kappa_{xz} \end{Bmatrix} = -[Q]^{-1}[R] \begin{Bmatrix} \varepsilon_x \\ \kappa_x \end{Bmatrix} \tag{10}$$

Substituting equation (10) into the first and fourth linear equation of the matrix (8); the axial force and in-plane moment vs. the axial strain and in-plane curvature relationship can be expressed in terms of the generally anisotropic material properties

$$\begin{bmatrix} N_x \\ M_x \end{bmatrix} = \begin{bmatrix} A_{ani} & B_{ani} \\ B_{ani} & D_{ani} \end{bmatrix} \begin{Bmatrix} \varepsilon_x \\ \kappa_x \end{Bmatrix} \tag{11}$$

Where

$$\begin{bmatrix} A_{ani} & B_{ani} \\ B_{ani} & D_{ani} \end{bmatrix} = \begin{bmatrix} A_{11} & B_{11} \\ B_{11} & D_{11} \end{bmatrix} - [R]^T [Q]^{-1} [R] \tag{12}$$

### 3.3.3 Energy Formulation

A generalized buckling formula was derived using Rayleigh-Ritz approximation based on the energy approach. Strain energy can be expressed in terms of the integration of the applied loads multiplying the corresponding deformations.

$$U = \int_0^L \left( \frac{1}{2} N_x \varepsilon_x + \frac{1}{2} M_x \kappa_x \right) dx$$

$$= \int_0^L \frac{1}{2} (A_{ani} \varepsilon_x^2 + B_{ani} \varepsilon_x \kappa_x)\, dx + \int_0^L \frac{1}{2} (B_{ani} \varepsilon_x \kappa_x + D_{ani} \kappa_x^2)\, dx \tag{13}$$

The potential of external loads can be expressed as shown in equation (14)

$$W = -P\, u(L) \tag{14}$$

Taking the total potential energy function and substituting equations (13) and (14) into equation (15)

$$\Pi = U - W$$

$$\Pi = \int_0^L \frac{1}{2} (A_{ani} \varepsilon_x^2 + 2B_{ani} \varepsilon_x \kappa_x + D_{ani} \kappa_x^2)\, dx + P\, u(L) \tag{15}$$

Minimizing the total potential energy function with respect to $B_1$ and $C_1$ and setting the resulting expressions to zero, performing the integration by parts and manipulating the equations to give:

$$\frac{\partial \Pi}{\partial B_1} = A_{ani} B_1 L + \frac{A_{ani} C_1^2 L}{4}\left(\frac{\pi}{L}\right)^2 - 2B_{ani} C_1 \left(\frac{\pi}{L}\right) + PL = 0 \tag{16}$$

$$\frac{\partial \Pi}{\partial C_1} = \frac{A_{ani} B_1 C_1 L}{2}\left(\frac{\pi}{L}\right)^2 + \frac{3A_{ani} C_1^3 L}{16}\left(\frac{\pi}{L}\right)^4 - 2B_{ani} B_1 \left(\frac{\pi}{L}\right) - B_{ani} C_1^2 \left(\frac{\pi}{L}\right)^3 + \frac{D_{ani} C_1 L}{2}\left(\frac{\pi}{L}\right)^4 = 0 \tag{17}$$

Solving equation (16) for $B_1$ then substituting the resulting expression in equation (17), the following cubic equation is formulated in terms of $C_1$ value

$$B_1 = \frac{2B_{ani} C_1}{A_{ani} L}\frac{\pi}{L} - \frac{C_1^2}{4}\left(\frac{\pi}{L}\right)^2 - \frac{P}{A_{ani}} \tag{18}$$

$$q_1 C_1^3 + q_2 C_1^2 + q_3 C_1 + q_4 = 0 \tag{19}$$

Where

$$q_1 = \frac{A_{ani} L}{16}\left(\frac{\pi}{L}\right)^2,\ q_2 = \frac{B_{ani}}{2}\frac{\pi}{L},\ q_3 = \left[\frac{D_{ani} L}{2}\left(\frac{\pi}{L}\right)^2 - \frac{4B_{ani}^2}{A_{ani} L} - \frac{L}{2}P\right], q_4 = \frac{2B_{ani}}{A_{ani}}\frac{PL}{\pi}$$

Equation (19) does not lend itself to a closed form solution. Therefore, considering the critical stability matrix:

$$\begin{bmatrix} \frac{\partial^2 \Pi}{\partial^2 B_1} & \frac{\partial^2 \Pi}{\partial B_1 \partial C_1} \\ \frac{\partial^2 \Pi}{\partial C_1 \partial B_1} & \frac{\partial^2 \Pi}{\partial^2 C_1} \end{bmatrix} \tag{20}$$

Where

$$\frac{\partial^2 \Pi}{\partial B_1^2} = A_{ani} L$$

$$\frac{\partial^2 \Pi}{\partial B_1 \partial C_1} = A_{ani} C_1 \left(\frac{\pi}{L}\right)^2 \frac{L}{2} - 2B_{ani} \frac{\pi}{L}$$

$$\frac{\partial^2 \Pi}{\partial C_1 \partial B_1} = A_{ani} C_1 \left(\frac{\pi}{L}\right)^2 \frac{L}{2} - 2B_{ani} \frac{\pi}{L} \tag{21}$$

$$\frac{\partial^2 \Pi}{\partial C_1^2} = \frac{A_{ani} B_1 L}{2} \left(\frac{\pi}{L}\right)^2 + \frac{9 A_{ani} C_1^2 L}{16} \left(\frac{\pi}{L}\right)^4 - 2B_{ani} C_1 \left(\frac{\pi}{L}\right)^3 + \frac{D_{ani} L}{2} \left(\frac{\pi}{L}\right)^4$$

Setting the determinant of the matrix in Equation (20) to zero, substituting $B_1$ expression from equation (18) and solving for $C_1$ using the general solution of a quadratic equation:

$$C_1 = \frac{-A_{ani} L B_{ani} \left(\frac{\pi}{L}\right) \mp \sqrt{A_{ani}^2 L^2 B_{ani}^2 \left(\frac{\pi}{L}\right)^2 - 4\left(\frac{3}{16}\right) A_{ani}^2 L^2 \left(\frac{\pi}{L}\right)^2 \left[\frac{A_{ani} D_{ani} L^2}{2} \left(\frac{\pi}{L}\right)^2 - 4B_{ani}^2 - \frac{A_{ani}^2 L^2}{2} P\right.}}{2\left(\frac{3}{16}\right) A_{ani}^2 L^2 \left(\frac{\pi}{L}\right)^2} \tag{22}$$

In order for the $C_1$ value to be real, the discriminant must be at least zero. By setting the discriminant to zero and manipulating its expression, a closed form solution for the critical buckling load is derived:

$$P_{cr} = \frac{D_{ani} \pi^2}{L^2} - \frac{32}{3} \frac{B_{ani}^2}{A_{ani} L^2} \tag{23}$$

In the case of isotropic or specially-orthotropic materials, the coupling term vanishes reducing the equation to that of Euler buckling.

## 3.4 Numerical Formulation

Finite element buckling analysis was used to verify the analytical solution, derived in the previous section, using the commercial software package Abaqus for laminated anisotropic columns. Columns composed of four layers of composites were modeled with simply supported ends, in

which roller and pin supports were introduced on the top and bottom of the column, respectively. Moreover, a concentrated load was applied at the top of the column. Linear elastic laminated material was used for orthotropic and anisotropic layups, respectively. Moreover, graphite/epoxy material was mainly used to simulate the composite columns. Quadrilateral eight-node doubly curved thick shell element (S8R) and 3D solid 20-node quadratic brick element (C3D20R) were utilized for modeling the columns in 3D-space. Element size equal to 0.5 x 0.5 mm with total number of elements equal to 400 were used for a column size of 100 mm x 1 mm x 0.4 mm after conducting a convergence study to select the appropriate mesh size. Figure 3.2 illustrates the model's boundary conditions and mesh for the shell elements.

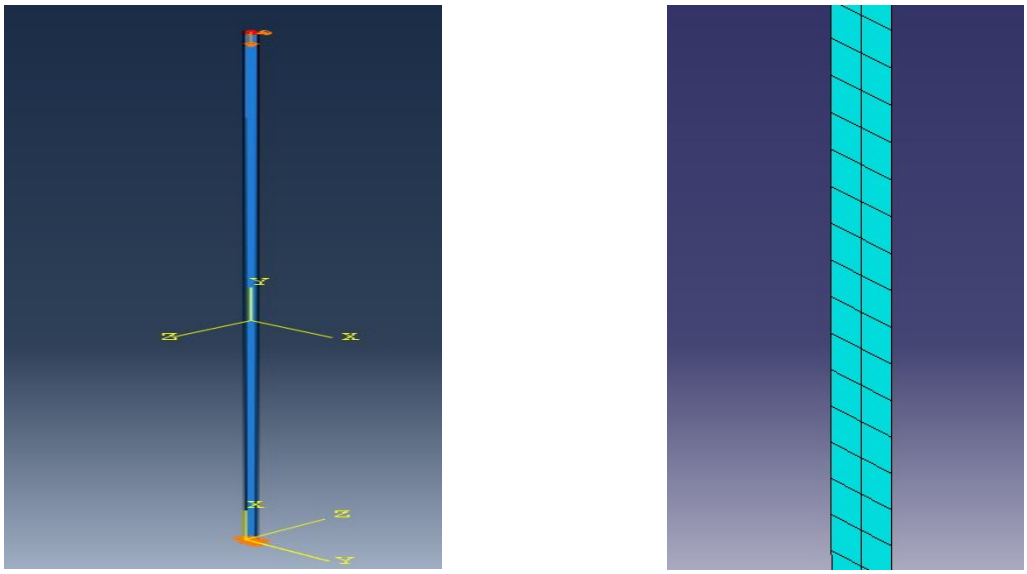

Figure 3.2 Left: Boundary conditions and applied load. Right: Meshed Model.

Two types of analyses were undertaken in this study. First, a buckling analysis using Lanczos solver to simulate eigenvalue computation was undertaken. Lanczos method is one of the methods used to solve for eigenvalues and eigenvectors for complex Hermitian matrix using power methods. Lanczos method reduces $m \times m$ symmetric matrix using recurrence relations (multidimensional array values) to a tridiagonal matrix [15].

Secondly, a nonlinear geometry analysis using the modified Riks formulation was performed to predict the nonlinear stability response (pre-buckling and buckling) of the composite column. The modified Riks analysis uses the Arc length method to follow the equilibrium path, representing either the bifurcation points or the limit points. Load increments are applied during the analysis in which equilibrium iterations converge along the arc length, forcing the constraint equation to be satisfied at every arc length increment [16].

## 3.5 Experimental Program

### 3.5.1 Specimen Preparation

Twelve E-glass fiber/epoxy columns were made in the laboratory with four different sequences. V-Wrap EG50 unidirectional fabric was cut at different angles (30, -30, 0, and 90) as shown in Figure 3.3. Properties of V-Wrap EG50 fabric are shown in Table 3.1 [17].

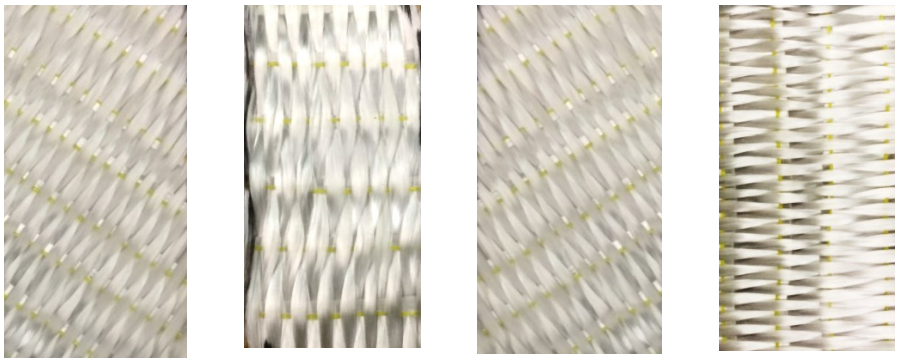


Figure 3.3 Glass fiber orientations

Table 3.1 Dry fiber properties [17].

| | |
|---|---|
| **Tensile Strength** | 3240 MPa (470,000 psi) |
| **Tensile Modulus** | 72,400 MPa (10.5 x $10^6$ psi) |
| **Elongation** | 4.5 % |

| | |
|---|---|
| **Density** | 2.55 g/cm$^3$ (0.092 lbs/in$^3$) |

Epoxy resin and hardener were mixed together to make the matrix material with 100 to 34.5 ratio by volume, respectively, using a mechanical rotary mixer as shown in Figure 3.4. The epoxy resin was first applied to the non-stick preparation sheet then a ply of fiber is laid by a paint roller against the resin. A second layer of resin was applied with the roller on top of the fiber ply and the process is repeated as many times as the number of fiber plies in the stacking sequence, Figure 3.5.

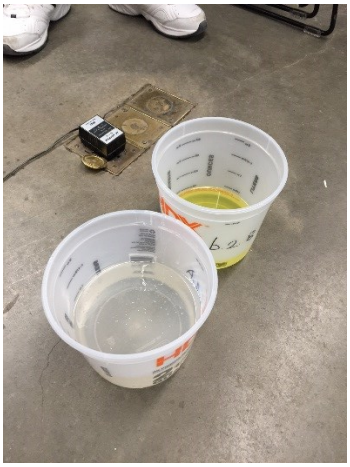

Figure 3.4 Resin preparation

Figure 3.5 Specimen preparation

Four different stacking sequences were constructed by the wet layup process. The strips were then left to harden for one week at room temperature then were cut to column final sizes using a table saw, see Figure 3.6.

Figure 3.6 Composite strip after the wet layup process.

Thickness and width of the hardened specimens were measured using a digital caliper at three locations to take the average. Layer thickness ($t_i$) is assumed equal to one quarter of the average specimen's thickness since each laminate was composed of four plies. Fiber and matrix volume fractions ($V_f$ and $V_m$) were calculated using equation (22). Using rule of mixtures and the Halpin-Tsai equation, elastic properties in the fiber, transverse and in-plane shear directions were obtained.

$$V_f = \frac{thickness\ of\ uncured\ fiber\ (t_f)}{thickness\ of\ cured\ layer\ (t_i)}$$

$$V_m = 1 - V_f \tag{22}$$

Where the thickness $t_f$ was measured to be 0.305 mm, the thickness $t_i$ varied based on the different laminates as shown in Table 6 below.

$$Rule\ of\ mixtures\colon\ E_1 = E_f V_f + E_m V_m$$

$$\nu_{12} = \nu_f V_f + \nu_m V_m$$

$$Halpin - Tsai\ equation\colon\ \frac{E_2}{E_m} = \frac{1 + \xi\eta V_f}{1 - \eta V_f}$$

$$\eta = \frac{E_f/E_m - 1}{E_f/E_m + \xi}$$

$$\frac{G_{12}}{G_m} = \frac{1 + \xi\eta V_f}{1 - \eta V_f} \tag{23}$$

$$\eta = \frac{G_f/G_m - 1}{G_f/G_m + \xi}$$

In which $E_f$, and $E_m$ are fiber and matrix modulus, $G_f$, and $G_m$ are fiber and matrix shear modulus, $\xi$ value was taken equal to one to provide more accurate results [18]. Equation (24) determines the minor Poisson's ratio:

$$\frac{\nu_{12}}{E_1} = \frac{\nu_{21}}{E_2} \quad \textbf{(24)}$$

### 3.5.2 Test Setup

After one week of curing, the four different stacking sequences, shown in Table 3.2, were tested. Columns were tested under axial compression using the Shimadzu AG-IC 50 kN testing machine, operating with Trapezium X software following a displacement control protocol with a displacement rate of 1 mm/minute.

Table 3.2 Samples of the four different stacking sequences

| Sample Number | Stacking Sequence |
|---|---|
| **1** | 30/-30/0/90 |
| **2** | 30/-30/90/0 |
| **3** | 0/30/-30/90 |
| **4** | 30/0/90/-30 |

Simply supported boundary conditions were applied at the ends of the composite columns, see Figure 3.7. Columns were loaded in axial compressive displacement until the load dropped indicating the attainment of a limit load.

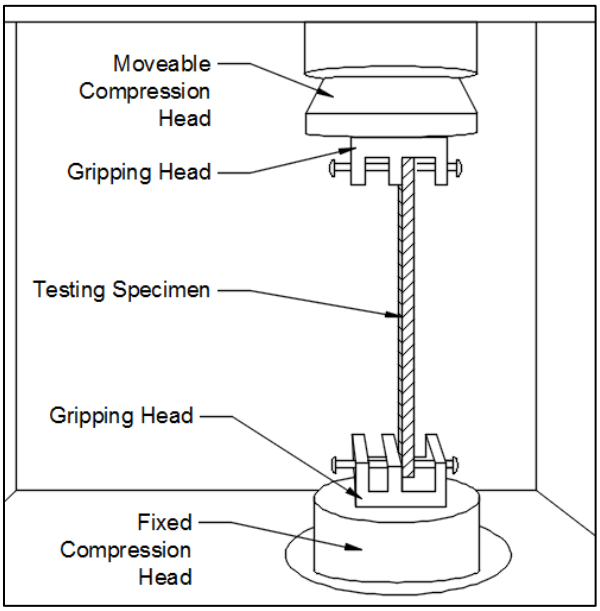


Figure 3.7 Axial Compression Test Setup

## 3.6 Results and Applications:

### 3.6.1 Numerical Validation

Table 3.3 presents the material properties of High Strength Graphite/Epoxy; obtained from typical values in an FRP textbook [18], that was used to simulate the analytical and numerical results for different stacking sequences of composite columns with the following dimension: 100 mm x 1.0 mm x 0.4 mm for length, width, and thickness, respectively with length to thickness ratio equal to 250. The comparison between the analytical and numerical buckling loads is reported in Table 3.4 for various layup stacking sequences. The results match reasonably with a minimum error equal to 0.0038% for the single specially orthotropic layer (90/90/90/90) and a maximum error equal to

11.2121% for the symmetric angle ply laminate (30/-30/-30/30). It is important to note that the layup with the maximum error yields the analytical buckling load on the conservative side.

Table 3.3 High Strength Graphite/Epoxy Material Properties [18].

| **Material** | $E_{11}$ | $E_{22}$ | $G_{12}$ | $\nu_{12}$ |
|---|---|---|---|---|
| **High Strength Graphite/Epoxy** | 145.0 GPa | 10.0 GPa | 4.8 GPa | 0.25 |

Table 3.4 Comparison of analytical and numerical buckling load for various layup sequences of Graphite/Epoxy Composite Column.

| **Ply Orientation** | **Analytical Results, N** | **Numerical Results, N** | **% Error** | **Layup Type** |
|---|---|---|---|---|
| **0/0/0/0** | 0.76325 | 0.76289 | 0.0472 | Single Specially Orthotropic |
| **90/90/90/90** | 0.052638 | 0.05264 | 0.0038 | Single Specially Orthotropic |
| **0/90/90/0** | 0.67612 | 0.67573 | 0.0577 | Symmetric Cross Ply |
| **0/90/0/90** | 0.34631 | 0.35089 | 1.3226 | Antisymmetric Cross Ply |
| **90/0/0/90** | 0.14182 | 0.1418 | 0.0142 | Symmetric Cross Ply |
| **30/-30/30/-30** | 0.23915 | 0.23909 | 0.0251 | Antisymmetric Angle Ply |
| **45/-45/45/-45** | 0.088707 | 0.08871 | 0.0034 | Antisymmetric Laminates |
| **60/-60/60/-60** | 0.05689 | 0.05688 | 0.0176 | Antisymmetric Laminates |
| **30/-30/60/-60** | 0.09435 | 0.10161 | 7.6948 | Balanced Angle Ply |
| **60/-60/45/-45** | 0.06968 | 0.07126 | 2.2676 | Balanced Angle Ply |
| **30/-30/45/-45** | 0.13098 | 0.13452 | 2.7028 | Balanced Angle Ply |
| **30/-30/0/0** | 0.36506 | 0.39188 | 7.3468 | Anisotropic |
| **30/-30/-30/30** | 0.19256 | 0.21415 | 11.2121 | Symmetric Angle Ply |

| | | | | |
|---|---|---|---|---|
| **-45/30/-30/45** | 0.11408 | 0.11407 | 0.0088 | Antisymmetric Angle Ply |
| **30/30/-30/-30** | 0.16171 | 0.1615 | 0.1299 | Antisymmetric Angle Ply |
| **30/-30/0/90** | 0.17569 | 0.18431 | 4.9064 | Anisotropic |

Figure **3.8** shows the load versus mid height displacement curve for three different stacking sequences obtained from the finite element Abaqus Riks analysis along with the analytical buckling load marked for comparison. An excellent agreement between the results is seen in which the antisymmetric cross ply stacking sequence exhibit higher buckling load than the two other sequences. On the other hand, the balanced anisotropic angle ply layup showed the lowest buckling load. Single specially-orthotropic layer (0/0/0/0) exhibits the highest buckling load due to having all fibers aligned with the loading axis while the coupling coefficient $\boldsymbol{B_{ani}}$ vanishes.

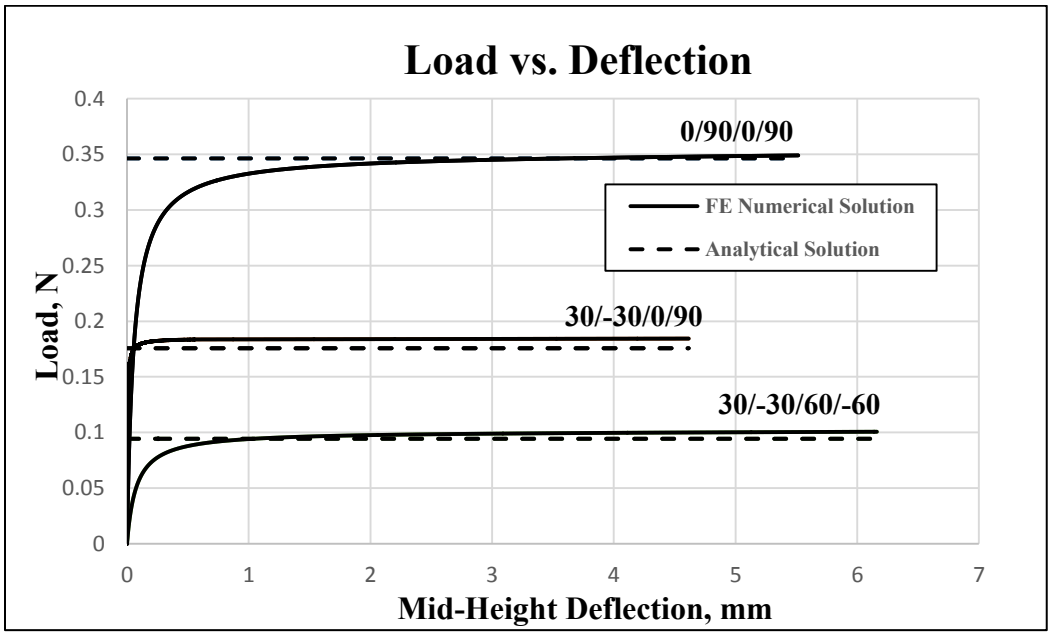


Figure 3.8 Analytical versus numerical solutions.

### 3.6.2 Experimental Results

Table **3.5** lists the average thickness and width of the tested specimens in four different stacking sequences in which the difference in the columns sizes is due to the wet layup procedure that has

a limited control over the amount of epoxy applied for each layer. Composite mechanical properties are illustrated in Table **3.6**.

Table 3.5 Geometry of column specimen

| | Average | | |
|---|---|---|---|
| | **Thickness, mm** | **Width, mm** | **Length, mm** |
| **1_2** | 5.7997 | 10.4733 | 295 |
| **1_3** | 5.7277 | 8.145 | 292.5 |
| **2_1** | 6.3458 | 10.6342 | 294 |
| **2_2** | 6.1976 | 10.5537 | 294.5 |
| **3_1** | 5.7997 | 10.0288 | 293.3 |
| **4_1** | 5.2959 | 8.6022 | 284 |
| **4_2** | 5.6812 | 10.4013 | 287 |

Table 3.6 Composite properties of E-glass/epoxy used in experiments.

| | **$V_f$** | **$V_m$** | **$E_1$,MPa** | **$E_2$,MPa** | **$G_{12}$,MPa** | **$\nu_{12}$** | **$\nu_{21}$** |
|---|---|---|---|---|---|---|---|
| **1_2** | 0.5344 | 0.4657 | 40546.569 | 11336.196 | 4175.05 | 0.322 | 0.0901 |
| **1_3** | 0.5411 | 0.459 | 41005.765 | 11514.961 | 4241.67 | 0.3214 | 0.0903 |
| **2_1** | 0.4884 | 0.5117 | 37401.468 | 10214.439 | 3757.51 | 0.3261 | 0.0891 |
| **2_2** | 0.5 | 0.5 | 38200 | 10483.413 | 3857.55 | 0.325 | 0.0892 |
| **3_1** | 0.5344 | 0.4657 | 40546.569 | 11336.196 | 4175.05 | 0.322 | 0.0901 |
| **4_1** | 0.5852 | 0.4149 | 44023.022 | 12801.836 | 4721.9 | 0.3174 | 0.0923 |
| **4_2** | 0.5455 | 0.4546 | 41309.091 | 11635.349 | 4286.55 | 0.321 | 0.0904 |

The column limit loads of the four stacking sequences, listed in Table 3.2, were compared with analytical and numerical buckling loads as shown in Table 3.7. The highest buckling load was observed in (30/-30/90/0) layup stacking sequence with a value equal to 562.5 N and the lowest value equal to 242.2 N for the (30/-30/0/90) columns. Generally speaking, a good correspondence between experimental, analytical and numerical results was observed. The experimental buckling loads for columns with layups (30/-30/0/90) and (30/-30/90/0) were consistently lower than the analytical and numerical results which is to be expected due the inherent initial imperfections in the tested columns. Nevertheless, experimental results for columns with layups (0/30/-30/90) and (30/0/90/-30) were slightly higher than the analytical and numerical values. This can only be attributed to variations in thickness and width for which the average value of a prismatic column may not render accurate estimates of the buckling load. For example, column 4_2 had a non-prismatic section with thickness values at the top, bottom, and middle of the column equal to: 5.4356, 5.8674, and 5.7404 mm, respectively.

Table 3.7 Comparison of experimental results with analytical and numerical results for E glass/epoxy composite column.

| **Ply-Orientation** | | **$P_{cr}$ Experimental, N** | **$P_{cr}$ Analytical, N** | **$P_{cr}$ Numerical, N** |
|---|---|---|---|---|
| **30/-30/0/90** | **1_1** | 300 | 337.004 | 342.927 |
| | **1_3** | 242.1875 | 264.665 | 268.583 |
| **30/-30/90/0** | **2_1** | 553.125 | 647.82 | 659.35 |
| | **2_2** | 562.5 | 610.518 | 621.479 |
| **0/30/-30/90** | **3_1** | 424.219 | 407.132 | 412.208 |
| **30/0/90/-30** | **4_1** | 303.125 | 280.202 | 279.743 |
| | **4_2** | 471.094 | 408.572 | 376.057 |

Out of the twelve columns cut from the four strips of various stacking sequences, five had evident thickness imperfections at the ends and were accordingly excluded from testing. End imperfections in these five columns were noticed due to personal errors during the cutting process as shown in Figure 3.9. Moreover, local delamination between layers was observed after testing the columns due to the rise of interlaminar shear stresses during the testing of columns with out of straightness imperfection, see Figure 3.10.

Figure 3.9 Initial Imperfection in column specimen.

Figure 3.10 Local delamination after testing

Figure 3.11 and Figure 3.12 illustrates the critical buckling mode shape obtained from numerical analysis and experimental work.

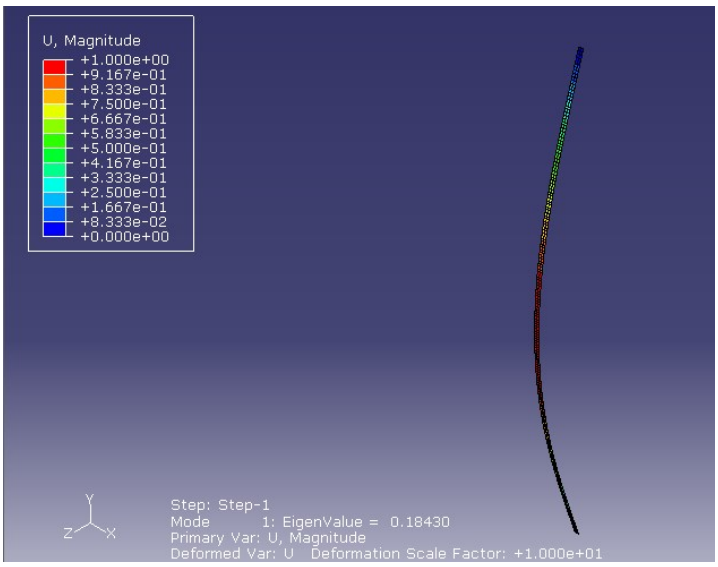


Figure 3.11 Numerical critical buckling mode shape.

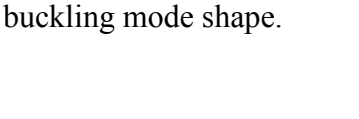

Figure 3.12 Experimental critical buckling mode shape.

### 3.6.3 Parametric Study

#### 3.6.3.1 Effect of Ply Orientation

Parametric study was done to study the effect of having different stacking sequences with the following dimensions for length, width and thickness: 100 mm x 1 mm x 0.4 mm, respectively. Table 4.4 in the previous section shows buckling load values for different stacking sequences with values range between 0.05264 N and 0.763 N.

#### 3.6.3.2 Effect of Material Properties

Two types of materials were used to study the effect of changing material properties on the stability of the composite columns. High Strength Graphite/Epoxy and S-Glass/Epoxy were used to conduct this study and their properties were implemented from typical values reported by an FRP textbook are illustrated in Table 3.3 and Table 3.8 [18].

Table 3.8 S-Glass/Epoxy material properties [18].

| **Material** | $E_{11}$ | $E_{22}$ | $G_{12}$ | $\nu_{12}$ |
|---|---|---|---|---|
| **S-Glass/Epoxy** | 55.0 GPa | 16.0 GPa | 7.6 GPa | 0.28 |

Table 3.4 and Table 3.9 presents results of High Strength Graphite/ Epoxy and S-Glass/Epoxy for different stacking sequences. In general, it was observed that S-Glass/Epoxy exhibits much lower buckling loads than High Strength Graphite/Epoxy since it has lower stiffness values along the fiber direction.

Table 3.9 Analytical and numerical results for various layup sequences for S-Glass/Epoxy.

| Ply Orientation | Analytical Results, N | Numerical Results, N | % Error | Layup Type |
|---|---|---|---|---|
| **0/0/0/0** | 0.28951 | 0.28948 | 0.0104 | Single Specially Orthotropic |
| **90/90/90/90** | 0.08423 | 0.08422 | 0.0119 | Single Specially Orthotropic |
| **0/90/90/0** | 0.26483 | 0.26477 | 0.0227 | Symmetric Cross Ply |
| **0/90/0/90** | 0.17651 | 0.17734 | 0.4703 | Antisymmetric Cross Ply |
| **90/0/0/90** | 0.11029 | 0.110283 | 0.0064 | Symmetric Cross Ply |
| **30/-30/30/-30** | 0.1741 | 0.17408 | 0.0115 | Antisymmetric Angle Ply |
| **45/-45/45/-45** | 0.11478 | 0.11477 | 0.0088 | Antisymmetric Angle Ply |
| **60/-60/60/-60** | 0.09054 | 0.09053 | 0.0111 | Antisymmetric Angle Ply |
| **30/-30/60/-60** | 0.11953 | 0.12148 | 1.6314 | Balanced Angle Ply |
| **60/-60/45/-45** | 0.10108 | 0.1015 | 0.416 | Balanced Angle Ply |
| **30/-30/45/-45** | 0.13887 | 0.13947 | 0.433 | Balanced Angle Ply |
| **30/-30/0/0** | 0.21601 | 0.22062 | 2.135 | Anisotropic |
| **30/-30/-30/30** | 0.16021 | 0.17015 | 6.205 | Symmetric Angle Ply |
| **-45/30/-30/45** | 0.12408 | 0.12407 | 0.009 | Antisymmetric Angle Ply |
| **30/30/-30/-30** | 0.15288 | 0.15285 | 0.02 | Antisymmetric Angle Ply |
| **30/-30/0/90** | 0.13764 | 0.14035 | 1.969 | Anisotropic |

Table 3.10 presents the buckling results when S-Glass and High Strength Graphite/Epoxy hybrid material properties were used for the composite column in which Graphite/Epoxy properties were

used for layers with $0^o$ and $\pm 30^o$ orientation and S-Glass/Epoxy for the other orientations. Combining two materials showed a higher error values between numerical and analytical results than using one material therefore more terms might need to be added to the Rayleigh-Ritz approximation to capture the complexity in behavior. This was beyond the scope of the present paper.

Table 3.10 Analytical vs. numerical buckling loads for various layup sequences of hybrid Graphite and S-Glass/Epoxy composites.

| Orientation | Analytical Results, N | Numerical Results, N | % Error |
|---|---|---|---|
| **30/-30/60/-60** | 0.12748 | 0.1341 | 5.193 |
| **30/-30/0/90** | 0.19 | 0.19643 | 3.3843 |
| **0/90/90/0** | 0.67942 | 0.67856 | 0.1266 |
| **0/90/0/90** | 0.3704 | 0.3732 | 0.756 |
| **90/0/0/90** | 0.16905 | 0.16926 | 0.1243 |

#### 3.6.3.3 Effect of Element Type in FE Analysis

As mentioned earlier, two types of elements were utilized in the analysis of High Strength Graphite/Epoxy columns discussed earlier. Table 3.11 presents the comparison between the analytical and numerical results using the quadratic shell element (S8R) and quadratic solid element (C3D20R) both with reduced integration schemes having element mesh size equal to 0.5 x 0.5 mm. An excellent agreement between analytical and shell element results is observed for all stacking sequences. On the other hand, solid element results showed excellent agreements with the analytical and shell element results for single specially orthotropic and antisymmetric angle ply.

However, solid elements results were off for the antisymmetric cross ply and anisotropic layups, Table 3.11.

Table 3.11 Analytical and numerical results with shell and solid elements.

| Ply Orientation | Analytical Results, N | Shell Element S8R, N | Solid Element C3D20R, N |
|---|---|---|---|
| **0/0/0/0** | 0.763 | 0.76289 | 0.76289 |
| **90/90/90/90** | 0.05264 | 0.05264 | 0.0526358 |
| **0/90/90/0** | 0.676 | 0.67573 | 0.409173 |
| **0/90/0/90** | 0.346 | 0.35089 | 0.409124 |
| **90/0/0/90** | 0.14182 | 0.1418 | 0.409175 |
| **30/-30/30/-30** | 0.239 | 0.23909 | 0.238503 |
| **45/-45/45/-45** | 0.08871 | 0.08871 | 0.0886286 |
| **60/-60/60/-60** | 0.05688 | 0.05688 | 0.0568754 |
| **30/-30/60/-60** | 0.0943 | 0.10161 | 0.154953 |
| **30/-30/0/90** | 0.1757 | 0.18431 | 0.329724 |

## 3.7 Conclusions

A generalized closed form buckling formula for anisotropic laminated composite columns with simply supported end condition under axial compression was derived which may be considered an extension to the Euler buckling formula of isotropic columns. The buckling load formula was expressed with respect to the composite material axial, coupling, and flexural rigidities as well as the column geometry. An excellent agreement between the analytical formula and the finite element analysis results is observed. Limit Loads of buckled laminated composite columns gave generally good correspondence with the analytical and numerical results. On the other hand, some

of the experimental results differed from the analytical and numerical solutions due to imperfections or dimension variations in the composite column which reduced or increased the buckling load, respectively. The parametric study showed that using a single composite material type per column yielded less deviation of the analytical solution from the numerical results compared to using a two-material hybrid composite. Also, the use of shell finite elements was found to yield very accurate buckling loads for all stacking sequences compared to the use of solid finite elements when benchmarked against the present analytical solution.

## 3.8 Acknowledgements

This study is supported in part by the Department of Civil Engineering at Kansas State University. The E-glass fibers and epoxy used in the experimental part was provided by Structural Technologies, Inc.

## 3.9 References

[1] Silva, N.M.F., Silvestre, N., and Camotim, D., "GBT formulation to analyse the buckling behaviour of FRP composite open-section thin-walled columns," *Composite Structures*, vol. 93, no. 1, pp. 79-92, 2010.

[2] Silvestre, N., and Camotim, D., "Second-order generalised beam theory for arbitrary orthotropic materials," *Thin-Walled Structures*, vol. 40, no. 9, pp. 791-820, 2002.

[3] Bauld, R.B., and Tzeng, L.A., "Vlasov theory for fiber-reinforced beams with thin-walled open cross-section," Int. J. Solids Struct., vol. 20, no. 3, pp. 277-94, 1984.

[4] Rasheed, H.A., and Yousif, O.H., "Buckling of thin laminated orthotropic rings/long cylinders under external pressure," *International Journal of Structural Stability and Dynamics*, vol. 1, no. 4, pp. 485-507, 2002.

[5] Rasheed, H.A., and Yousif, O.H., "Stability of anisotropic laminated rings and long cylinders subjected to external hydrostatic pressure," *Journal of Aerospace Engineering* , vol. 18, no. 3, pp. 129-138, 2005.

[6] Xu, D., Ganesan, R. and Hoa, S.V., "Buckling analysis of tri-axial woven fabric composite structures subjected to bi-axial loading," *Composite Structures*, vol. 21, no. 3, pp. 140-152, 2007.

[7] Shukla, K.K., Nath, Y., Kreuzer, E., and Kumar, K.V.S., "Buckling of laminated composite rectangular plates," *Journal of Aerospace Engineering*, vol. 18, no. 4, pp. 215-223, 2005.

[8] Sun, L., and Harik, I.E., "Buckling of stiffened antisymmetric laminated plates," *Journal of Engineering Mechanics*, vol. 139, no. 8, 2013.

[9] Harik, I.E., and Salamoun, G.L., "The analytical strip method of solution for stiffened rectangular plates," *Computers & Structures*, vol. 29, no. 2, pp. 283-291, 1988.

[10] Debski, H., Kubiak, T., and Teter, A., "Buckling and postbuckling behaviour of thin-walled composite channel section column," *Composite Structures*, vol. 100, pp. 195-204, 2013.

[11] Kerr, A.D., "An extended Kantorovich method for solution of eigenvalue problem," *Int. J. Solid Struct*, vol. 5, no. 6, pp. 559-572, 1969.

[12] Shufrin, I., Rabinovitch, O., and Eisenberger M., "Buckling of laminated plates with general boundary conditions under combined compression, tension, and shear- A semi-analytical solution," *Thin-Walled Structures*, vol. 46, pp. 925-938, 2008.

[13] Thai, H.T., and Kim S.E., "Levy-type solution for buckling analysis of orthotropic plates based on two variable refined plate theory," *Composite Structures*, vol.93, no. 7, pp. 1738-1746, 2011.

[14] Jones, R.M, Mechanics of composite materials, New York: Hemisphere Publishing Corporation, 1975.

[15] Hernandez, V., Roman, J.E., Tomas, A., and Vidal, V., "Lanczos methods in SLEPc," Polytechnic University of Valencia, Province of Valencia, 2006.

[16] Memon, B.A., Su, X.S., "Arc-length technique for nonlinear finite element analysis," Journal of Zhejiang University SCI, vol. 5, no. 5, pp. 618-628, 2004.

[17] Structural Technologies, "Strengthening Solutions, V-WrapTM EG50, High Strength Glass Fiber Fabric". structuraltechnologies.com. 2011.

[18] Rasheed, H.A., Strengthening Design of Reinforced Concrete with FRP, New York: CRC Press, 2015.

# Chapter 4 - Analytical and Finite Element Buckling Solutions of Simply Supported Anisotropic Laminated Composite Wide Plates under Axial Compression

**Rund Al-Masri[1], Hayder A. Rasheed[2]**

## 4.1 Abstract

**Rayleigh-Ritz approximation was used to derive analytical buckling formula of generally anisotropic laminated composite simply supported thin plates. Effective axial, coupling, and flexural stiffness coefficients of the anisotropic layup are determined from the generalized constitutive relationship using dimensional reduction of the 6x6 composite stiffness matrix. The resulting explicit formula has an additional term which is a function of the effective coupling and axial stiffness. For isotropic and certain classes of laminated composite, the analytical buckling formula reduces down to isotropic buckling formula once the effective coupling stiffness term vanishes. The analytical results are verified against finite element Eigen value solutions for a wide range of anisotropic laminated layups yielding high accuracy. A parametric study is then performed to examine the effect of ply orientations and material properties including hybrid carbon/glass fiber composites. Relevance of the numerical and analytical results is discussed for all these cases.**

Keywords: Buckling of Composite Plates, Simply Supported Boundary Conditions, Anisotropic Laminated Material, Axial Compression.

[1] Ph.D. Candidate, Department of Civil Engineering, Kansas State University, Manhattan, KS 66506

[2] Professor, Department of Civil Engineering, Kansas State University, Manhattan, KS 66506

## 4.2 Introduction

The use of laminated composite is increasingly growing in different applications in industry because of their distinguished properties (High strength-to-weight ratio, high stiffness-to-weight ratio, corrosion resistance, and fatigue). Due to this growth, an increase in demand for better understanding the mechanics of laminated composites has resulted. Wide plates undergo stability (i.e. buckling) issues prior to failure. In recent years, a significant amount of research has been conducted to study the buckling behavior of plates and shells [1-17]. Herenica et al. [1] developed a closed form solution for buckling of long anisotropic plates under axial compression ($N_x$) with various boundary conditions. The closed form solution can be expressed as:

$$N_x^{cr} = \kappa_x \frac{\pi^2}{b^2} \sqrt{D_{11} D_{22}} \qquad (1)$$

Where $D_{ij}$ is the bending stiffness; b is the width of the plate; and $\kappa_x$ is the non-dimensional buckling coefficient related to the boundary conditions. The results were validated with existing solutions (Weaver [2] [3], Qiao and Shan [4]), finite element solutions and showed an excellent agreement. Mahesh et al. [5] presented a general buckling formulation of plates under linearly varying uniaxial compressive load with general out-of-plane boundary conditions. Rayleigh-Ritz method based on the energy approach was used to present this formula along with orthogonal polynomials generated by a Gram-Schmidt process. Results exhibit a good agreement with differential quadrature (DQ) models [6]. Silva et al. [7] studied local and global buckling of fiber reinforced polymer composite open section thin-walled columns by presenting a formulation of generalized beam theory (GBT). Silvestre and Camotim [8] predicted buckling behavior for thin walled arbitrary orthotropic thin-walled members by developing a second order generalized beam theory (GBT). The second order theory was compared with Bauld and Lih-Shyng theory [9].

According to results, the critical buckling load exists for all isotropic or cross-ply orthotropic members. Moreover, no specific bifurcation is detected for a symmetric orthotropic layups along with non-linear path. Using Rayleigh-Ritz method, Ghaheri et al. [10] studied the stability of symmetrically laminated composite elliptical plates on elastic foundation under uniform in-plane loading with various boundary conditions. Weaver and Nemeth [11] presented non-dimensional parameters and governing equations to predict buckling behavior of rectangular symmetrically laminated composite plates with different boundary conditions under uniform axial compression, uniform shear, or pure in-plane bending loading. Bounds for non-dimensional parameters were also presented to indicate percentage gained in the buckling resistance for laminated plates. The results showed 26-36% increase in the buckling resistance for tailored simply supported orthotropic plates; with respect to isotropic plates. On the other hand, clamped laminated plates exhibited 9-12% increase in the buckling resistance. Xu et al. [12] presented an approximate analytical solution to investigate the buckling of a tri-axial woven fabric composite structure under bi-axial loading using equivalent anisotropic plate method. The results showed that the analytical solution provides an upper bound solution for buckling; moreover, the solution can be used to predict buckling behavior for real life problem under bi-axial loading. Sun and Harik [13] presented analytical solution to predict buckling of stiffened antisymmetric laminated composite plates with bending-extension coupling. Analytical strip method (ASM); developed by Harik and Salamoun [14], was used to present the analytical solution. Based on the results, plates with free ends contribute to the weakest stiffening effects. Furthermore, since the coupling stiffness matrix vanishes, layers with ply orientation $0^o$ and $90^o$ had no effect on the buckling load. Shufrin et al. [15] proposed a semi-analytical solution for buckling of symmetrically laminated rectangular plates with various boundary conditions under combined tension, compression, and shear based

on multi term Kantorovich method [16]. Stability of the angle-ply laminated plates improved compared to free in-plane restraint plates under biaxial compression/tension, and shear. Also extra in-plane forces were created because of the in-plane restraint. Using state space concept on Levy type solution, Thai and Kim [17] presented a closed form solution for buckling of orthotropic plates with two opposite simply supported edges using two variable refined plate theories. The results showed more accurate solutions than the higher order shear deformation theory.

In this work, a generalized closed form solution of simply supported laminated composite wide plates subjected to axial compression was developed. The Rayleigh-Ritz approximation was used to obtain the buckling formula. Extensional, coupling, and flexural rigidities in 1D are determined using dimensional reduction starting with 3D rigidity matrix. Furthermore, finite element models for the plates are established using commercial software Abaqus. The finite element numerical solution was compared to the analytical solution resulting in excellent agreement regardless of the complexity of the composite lay-ups used.

## 4.3 Analytical Formulation

A generalized closed form buckling solution for simply supported anisotropic laminated composite wide plates under axial compression is derived using Rayleigh-Ritz approximation.

### 4.3.1 Assumptions:

6. Buckling takes place in the x-y plane about the weak axis (z-axis).
7. The y-axis runs through the thickness of the plate where the composite lamination takes place, Figure 4.1

8. The lamination angle ( α ) is measured with respect to the x-axis (i.e. 0° fibers run parallel to the x-axis and 90° fibers run parallel to the z-axis). Accordingly, the angle ( α ) is rotated about the y-axis.
9. Plane sections before bending remain plane after bending and perpendicular to the mid surface (i.e. simple beam theory holds).
10. Classical lamination theory is applicable with shear deformations ignored.

### 4.3.2 Kinematics

Geometry and Cartesian coordinates are presented in Figure 4.1 for simply supported wide plates. The z-axis is the weak axis of the plate about which bending takes place. The following displacement relations were assumed based on the isotopic Euler first buckling mode:

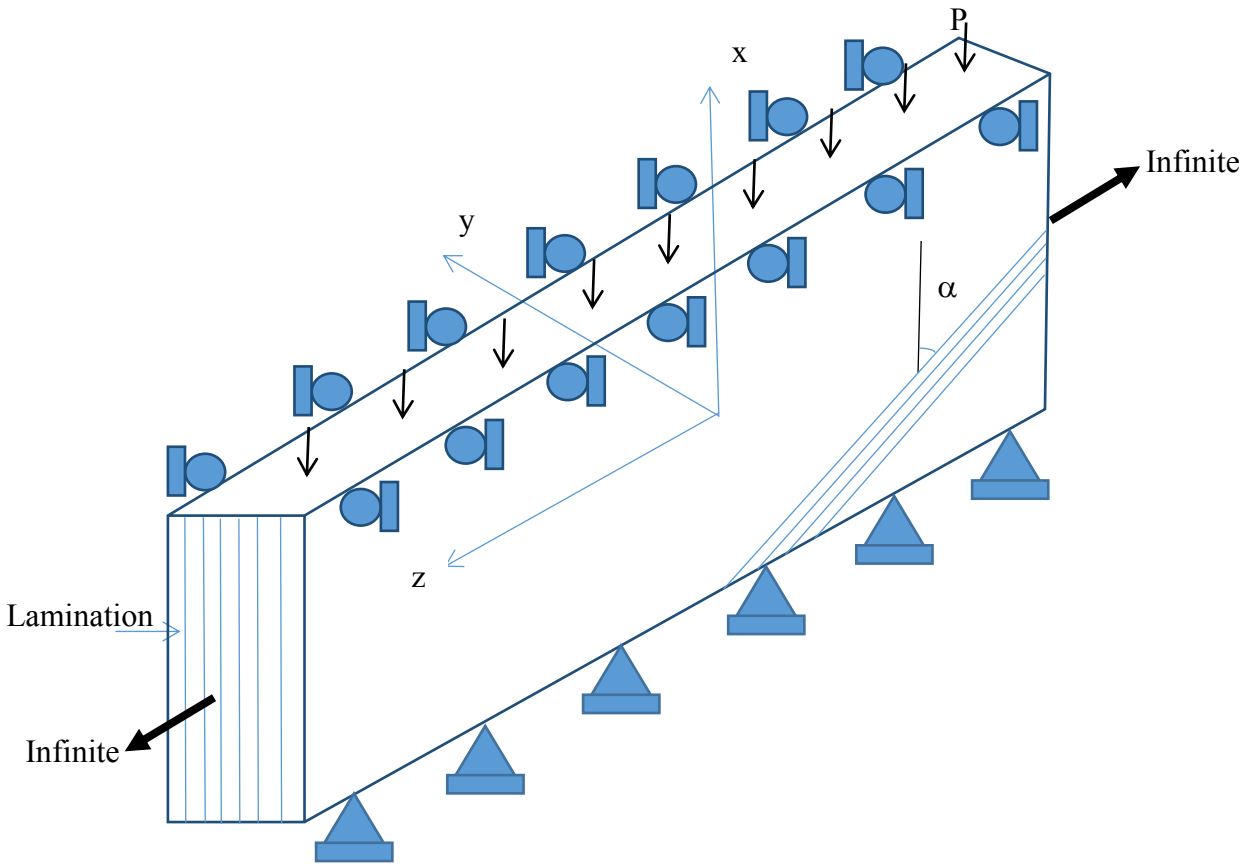


**Figure 4.1The wide plate geometry.**

$$\boldsymbol{u}(\boldsymbol{x}) = \boldsymbol{B_1 x}; \quad \boldsymbol{v}(\boldsymbol{x}) = \boldsymbol{C_1} \sin\frac{\pi x}{L} \tag{2}$$

Where $u(x)$, and $v(x)$ is the axial, and lateral displacements; $B_1$, and $C_1$ are constants to be solved; and x is the distance along the axis of the plate. For an intermediate class of deformation, the axial strain $\varepsilon_x$ and curvature $\kappa_x$are defined as follow.

$$\boldsymbol{\varepsilon_x} = \frac{\boldsymbol{du}}{\boldsymbol{dx}} + \frac{\boldsymbol{1}}{\boldsymbol{2}}\left(\frac{\boldsymbol{dv}}{\boldsymbol{dx}}\right)^{\boldsymbol{2}} = \boldsymbol{u'} + \frac{\boldsymbol{1}}{\boldsymbol{2}}\boldsymbol{v'^2}; \qquad \boldsymbol{\kappa_x} = \frac{\boldsymbol{d^2v}}{\boldsymbol{d^2x}} = \boldsymbol{v''} \tag{3}$$

### 4.3.3 Constitutive equations

The principal material directions were transformed into the plate coordinate system, the stresses and strains are then related in the following equation

$$\begin{Bmatrix} \boldsymbol{\sigma_x} \\ \boldsymbol{\sigma_z} \\ \boldsymbol{\tau_{xz}} \end{Bmatrix} = \begin{bmatrix} \boldsymbol{\bar{Q}_{11}} & \boldsymbol{\bar{Q}_{12}} & \boldsymbol{\bar{Q}_{16}} \\ \boldsymbol{\bar{Q}_{12}} & \boldsymbol{\bar{Q}_{22}} & \boldsymbol{\bar{Q}_{26}} \\ \boldsymbol{\bar{Q}_{16}} & \boldsymbol{\bar{Q}_{26}} & \boldsymbol{\bar{Q}_{66}} \end{bmatrix} \begin{Bmatrix} \boldsymbol{\varepsilon_x} \\ \boldsymbol{\varepsilon_z} \\ \boldsymbol{\gamma_{xz}} \end{Bmatrix} \tag{4}$$

Where $\bar{Q}_{ij}$ matrix represents the transformed reduced stiffness matrix as defined in standard composite textbooks [18]. Accordingly, the coupled force-strain relationship is established as follows:

$$\begin{Bmatrix} \boldsymbol{N_x} \\ \boldsymbol{N_z} \\ \boldsymbol{N_{xz}} \\ \boldsymbol{M_x} \\ \boldsymbol{M_z} \\ \boldsymbol{M_{xz}} \end{Bmatrix} = \begin{bmatrix} \boldsymbol{A_{11}} & \boldsymbol{A_{12}} & \boldsymbol{A_{16}} & \boldsymbol{B_{11}} & \boldsymbol{B_{12}} & \boldsymbol{B_{16}} \\ \boldsymbol{A_{12}} & \boldsymbol{A_{22}} & \boldsymbol{A_{26}} & \boldsymbol{B_{12}} & \boldsymbol{B_{22}} & \boldsymbol{B_{26}} \\ \boldsymbol{A_{16}} & \boldsymbol{A_{26}} & \boldsymbol{A_{66}} & \boldsymbol{B_{16}} & \boldsymbol{B_{26}} & \boldsymbol{B_{66}} \\ \boldsymbol{B_{11}} & \boldsymbol{B_{12}} & \boldsymbol{B_{16}} & \boldsymbol{D_{11}} & \boldsymbol{D_{12}} & \boldsymbol{D_{16}} \\ \boldsymbol{B_{12}} & \boldsymbol{B_{22}} & \boldsymbol{B_{26}} & \boldsymbol{D_{12}} & \boldsymbol{D_{22}} & \boldsymbol{D_{26}} \\ \boldsymbol{B_{16}} & \boldsymbol{B_{26}} & \boldsymbol{B_{66}} & \boldsymbol{D_{16}} & \boldsymbol{D_{26}} & \boldsymbol{D_{66}} \end{bmatrix} \begin{Bmatrix} \boldsymbol{\varepsilon_x} \\ \boldsymbol{\varepsilon_z} \\ \boldsymbol{\gamma_{xz}} \\ \boldsymbol{\kappa_x} \\ \boldsymbol{\kappa_z} \\ \boldsymbol{\kappa_{xz}} \end{Bmatrix} \tag{5}$$

Where:

$$\boldsymbol{A_{ij}} = \sum_{\boldsymbol{k=1}}^{\boldsymbol{N}} \boldsymbol{\bar{Q}_{ij} t_k}$$

$$\boldsymbol{B_{ij}} = \sum_{\boldsymbol{k=1}}^{\boldsymbol{N}} \boldsymbol{\bar{Q}_{ij} t_k \bar{y}_k}$$

$$\boldsymbol{D_{ij}} = \sum_{\boldsymbol{k=1}}^{\boldsymbol{N}} \boldsymbol{\bar{Q}_{ij} t_k}\left(\boldsymbol{\bar{y}_k^2} + \frac{\boldsymbol{t_k^2}}{\boldsymbol{12}}\right) \tag{6}$$

$$t_k = y_k - y_{k-1}$$

$$\bar{y}_k = \frac{y_k + y_{k-1}}{2}$$

In which $A_{ij}$,$B_{ij}$, and $D_{ij}$ are the axial, coupling, and flexural rigidity coefficients. $t_k$ = thickness of the k-th ply; and N = number of different plies in the stacking sequence.

The three dimensional (3D) rigidity matrix is established first using the material properties and the fiber orientations into equation (5). Then the dimension is reduced to 1D anisotropic axial, coupling and flexural rigidities using static condensation approach after applying the zero forces and moments.

$$\begin{Bmatrix} N_x \\ N_z \\ N_{xz} \\ M_x \\ M_z \\ M_{xz} \end{Bmatrix} = \begin{bmatrix} A_{11} & A_{12} & A_{16} & B_{11} & B_{12} & B_{16} \\ A_{12} & A_{22} & A_{26} & B_{12} & B_{22} & B_{26} \\ A_{16} & A_{26} & A_{66} & B_{16} & B_{26} & B_{66} \\ B_{11} & B_{12} & B_{16} & D_{11} & D_{12} & D_{16} \\ B_{12} & B_{22} & B_{26} & D_{12} & D_{22} & D_{26} \\ B_{16} & B_{26} & B_{66} & D_{16} & D_{26} & D_{66} \end{bmatrix} \begin{Bmatrix} \varepsilon_x \\ \varepsilon_z = 0 \\ \gamma_{xz} = 0 \\ \kappa_x \\ \kappa_z = 0 \\ \kappa_{xz} = 0 \end{Bmatrix} \quad \textbf{(7)}$$

Equation (7) is solved first for the axial strain and axial curvature ($\varepsilon_x$ ,$\kappa_x$) in terms of the rest of the deformation components by extracting the second, third, fifth and sixth linear equations from the matrix. Since the rest of the deformation components for wide plate are equal zero resulting in equation (8):

$$\begin{bmatrix} N_x \\ M_x \end{bmatrix} = \begin{bmatrix} A_{11} & B_{11} \\ B_{11} & D_{11} \end{bmatrix} \begin{Bmatrix} \varepsilon_x \\ \kappa_x \end{Bmatrix} \quad \textbf{(8)}$$

The axial force and in-plane moment vs. the axial strain and in-plane curvature relationship can be expressed in terms of the generally anisotropic material properties

$$\begin{bmatrix} N_x \\ M_x \end{bmatrix} = \begin{bmatrix} A_{11} & B_{11} \\ B_{11} & D_{11} \end{bmatrix} \begin{Bmatrix} \varepsilon_x \\ \kappa_x \end{Bmatrix} \quad \textbf{(9)}$$

It may be observed that equation 9 the material properties for wide plate is expressed in terms extensional, coupling, and bending stiffness in the principal directions.

### 4.3.4 Energy Formulation

Rayleigh-Ritz approximation method was used to develop a generalized buckling solution based on the energy approach. . Strain energy can be expressed in terms of the integration of the applied loads multiplying the corresponding deformations.

$$\boldsymbol{U = \int_0^L \left(\frac{1}{2} N_x \varepsilon_x + \frac{1}{2} M_x \kappa_x\right) dx}$$

$$\boldsymbol{= \int_0^L \frac{1}{2} (A_{11}\varepsilon_x^2 + B_{11}\varepsilon_x\kappa_x)\, dx + \int_0^L \frac{1}{2} (B_{11}\varepsilon_x\kappa_x + D_{11}\kappa_x^2)\, dx} \quad \textbf{(10)}$$

The potential of external loads can be expressed as shown in equation (11)

$$\boldsymbol{W = -P\, u(L)} \quad \textbf{(11)}$$

Taking the total potential energy function and substituting equations (10) and (11) into equation (12)

$$\boldsymbol{\Pi = U - W}$$

$$\boldsymbol{\Pi = \int_0^L \frac{1}{2} (A_{11}\varepsilon_x^2 + 2B_{11}\varepsilon_x\kappa_x + D_{11}\kappa_x^2)\, dx + P\, u(L)} \quad \textbf{(12)}$$

Minimizing the total potential energy function with respect to $B_1$ and $C_1$ and setting the resulting expressions to zero, performing the integration by parts and manipulating the equations to give:

$$\boldsymbol{\frac{\partial \Pi}{\partial B_1} = A_{11}B_1L + \frac{A_{11}C_1^2L}{4}\left(\frac{\pi}{L}\right)^2 - 2B_{11}C_1\left(\frac{\pi}{L}\right) + PL = 0} \quad \textbf{(13)}$$

$$\boldsymbol{\frac{\partial \Pi}{\partial C_1} = \frac{A_{11}B_1C_1L}{2}\left(\frac{\pi}{L}\right)^2 + \frac{3A_{11}C_1^3L}{16}\left(\frac{\pi}{L}\right)^4 - 2B_{11}B_1\left(\frac{\pi}{L}\right) - B_{11}C_1^2\left(\frac{\pi}{L}\right)^3 + \frac{D_{11}C_1L}{2}\left(\frac{\pi}{L}\right)^4 = 0} \quad \textbf{(14)}$$

Solving equation (13) for $B_1$ then substituting the resulting expression in equation (14), the following cubic equation is formulated in terms of $C_1$ value

$$\boldsymbol{B_1 = \frac{2B_{11}C_1}{A_{11}L}\frac{\pi}{L} - \frac{C_1^2}{4}\left(\frac{\pi}{L}\right)^2 - \frac{P}{A_{11}}} \tag{15}$$

$$\boldsymbol{q_1C_1^3 + q_2C_1^2 + q_3C_1 + q_4 = 0} \tag{16}$$

Where

$$\boldsymbol{q_1 = \frac{A_{11}L}{16}\left(\frac{\pi}{L}\right)^2,\ q_2 = \frac{B_{11}}{2}\frac{\pi}{L},\ q_3 = \left[\frac{D_{11}L}{2}\left(\frac{\pi}{L}\right)^2 - \frac{4B_{11}^2}{A_{11}L} - \frac{L}{2}P\right], q_4 = \frac{2B_{11}}{A_{11}}\frac{PL}{\pi}}$$

Considering the critical stability matrix since equation (16) does not lend itself to a closed form solution:

$$\begin{bmatrix} \frac{\partial^2\Pi}{\partial^2 B_1} & \frac{\partial^2\Pi}{\partial B_1 \partial C_1} \\ \frac{\partial^2\Pi}{\partial C_1 \partial B_1} & \frac{\partial^2\Pi}{\partial^2 C_1} \end{bmatrix} \tag{17}$$

Where

$$\boldsymbol{\frac{\partial^2\Pi}{\partial B_1^2} = A_{11}L}$$

$$\boldsymbol{\frac{\partial^2\Pi}{\partial B_1 \partial C_1} = A_{11}C_1\left(\frac{\pi}{L}\right)^2\frac{L}{2} - 2B_{11}\frac{\pi}{L}}$$

$$\boldsymbol{\frac{\partial^2\Pi}{\partial C_1 \partial B_1} = A_{11}C_1\left(\frac{\pi}{L}\right)^2\frac{L}{2} - 2B_{11}\frac{\pi}{L}} \tag{18}$$

$$\boldsymbol{\frac{\partial^2\Pi}{\partial C_1^2} = \frac{A_{11}B_1L}{2}\left(\frac{\pi}{L}\right)^2 + \frac{9A_{11}C_1^2L}{16}\left(\frac{\pi}{L}\right)^4 - 2B_{11}C_1\left(\frac{\pi}{L}\right)^3 + \frac{D_{11}L}{2}\left(\frac{\pi}{L}\right)^4}$$

Setting the determinant of the matrix in Equation (18) to zero, substituting $B_1$ expression from equation (15) and solving for $C_1$ using the general solution of a quadratic equation:

$$C_1 = \frac{-A_{11}LB_{11}(\frac{\pi}{L}) \mp \sqrt{A_{11}^2L^2B_{11}^2(\frac{\pi}{L})^2 - 4(\frac{3}{16})A_{11}^2L^2\left(\frac{\pi}{L}\right)^2\left[\frac{A_{11}D_{11}L^2}{2}\left(\frac{\pi}{L}\right)^2 - 4B_{11}^2 - \frac{A_{11}^2L^2}{2}P\right.}}{2(\frac{3}{16})A_{11}^2L^2(\frac{\pi}{L})^2} \quad \textbf{(19)}$$

In order for the $C_1$ value to be real, the discriminant must be at least zero. By setting the discriminant to zero and manipulating its expression, a closed form solution for the critical buckling load is derived:

$$P_{cr} = \frac{D_{11}\pi^2}{L^2} - \frac{32}{3}\frac{B_{11}^2}{A_{11}L^2} \quad \textbf{(20)}$$

The equation is reduced to Euler buckling in the case of isotropic or specially-orthotropic materials since the coupling term vanishes.

## 4.4 Numerical Formulation

Analytical buckling results were verified with finite element buckling analysis for laminated anisotropic plates using software package Abaqus. Plates of four layers were constructed with simply supported ends, in which roller and pin supports were introduced on the top and bottom edge of the plate, respectively. Additionally, translation in x-direction and rotation in y direction is prevented, moreover, a shell edge load was applied at the top of the plate as shown in Figure 4.2.

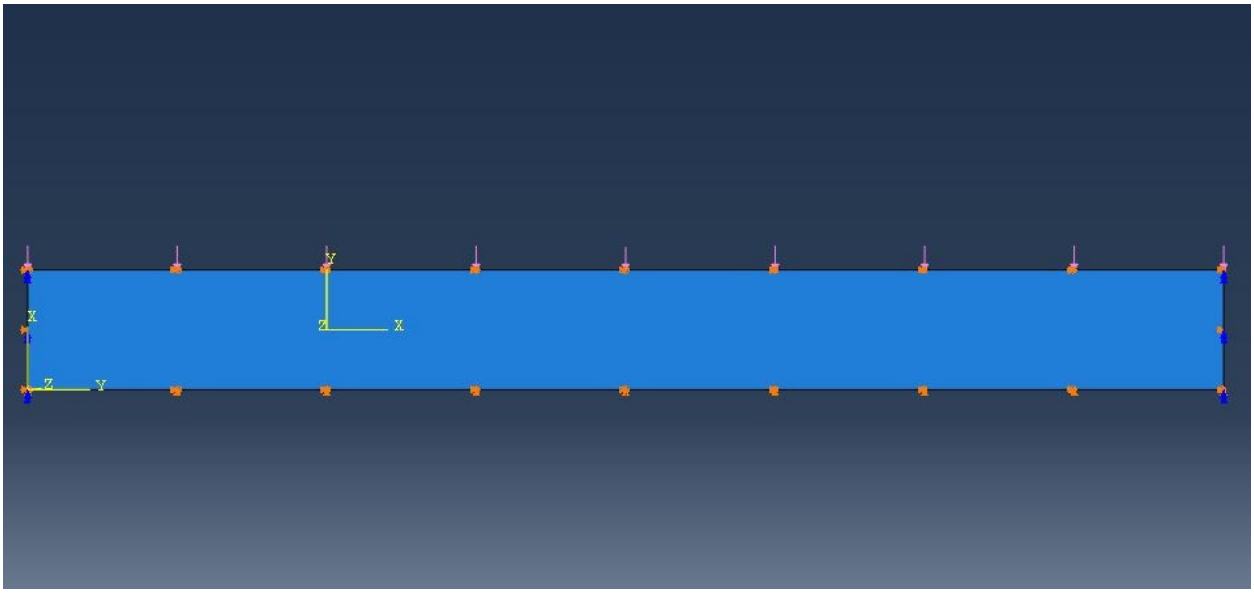


Figure 4.2Boundary conditions and applied load.

Figure 4.3 illustrates model's mesh. Linear elastic laminated material was used for orthotropic and anisotropic layups, respectively where s-glass/epoxy material was assumed to simulate the composite plates. Quadrilateral eight node doubly curved thick shell element (S8R) was used for modeling the plates in 3D-space. Additionally, 3D solid 20-node quadratic brick element (C3D20R) was also attempted. Mesh size of 10.0 mm was attempted with total number of elements equal to 1000 for plate size of 1000 mm x 100 mm x 0.4 mm after performing a convergence study to select the appropriate mesh size.

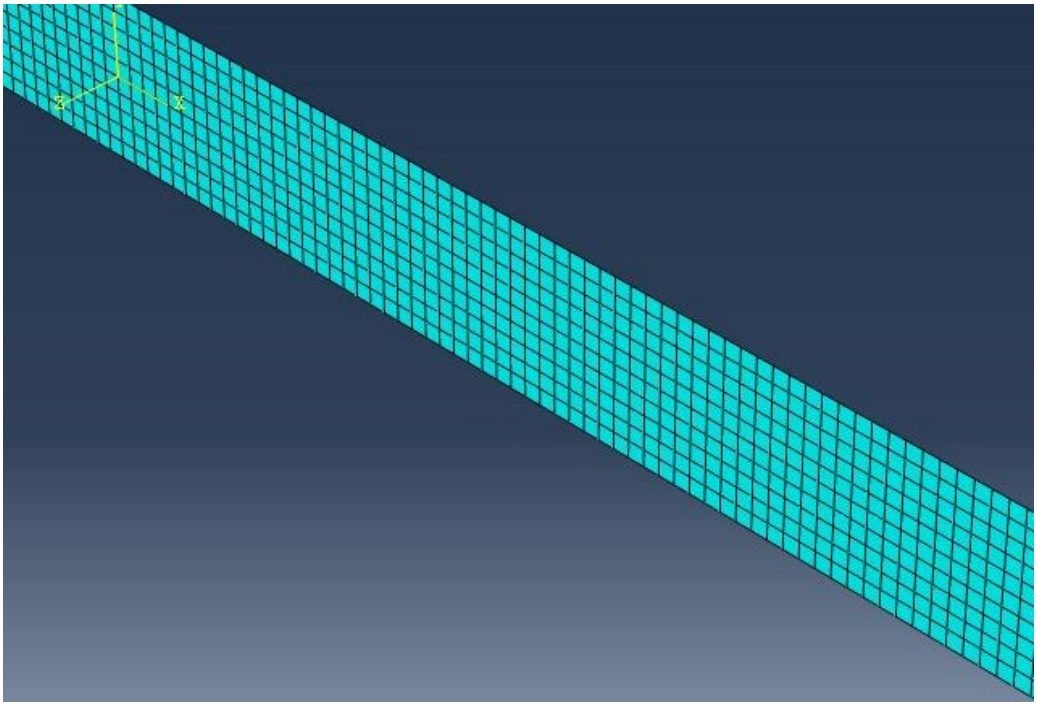

Figure 4.3 Meshed Model.

Two types of analyses were attempted in this study. Buckling analysis using Lanczos solver was performed to simulate eigenvalue computation. Lanczos method is one of the methods used to solve for eigenvalues and eigenvectors for complex Hermitian matrix using power methods. Lanczos method reduces $m \times m$ symmetric matrix to a tridiagonal matrix using recurrence relations (multidimensional array values) [19].

Additionally, nonlinear geometry analysis was conducted using the modified Riks analysis to predict the nonlinear stability response (pre-buckling and buckling) of the composite plates. The modified Riks analysis follows the equilibrium path, representing either the bifurcation points or the limit points using the Arc length method. Load increments are applied during the analysis in which equilibrium iterations converge along the arc length, forcing the constraint equation to be satisfied at every iteration [20].

## 4.5 Results and Applications:

### 4.5.1 Numerical Validation

S-Glass/Epoxy material properties; obtained from typical values in FRP textbook [21], were used to simulate the analytical and numerical results for different stacking sequences of composite plates; see Table 4.1, with the following dimensions for width, length, and thickness: 1000 mm x 100 mm x 0.4 mm, respectively. The comparison between the analytical and numerical buckling loads is reported in Table 4.2 for different layup stacking sequences. The results match closely with a minimum error equal to 0.0102% for single specially orthotropic layer (0/0/0/0) and a maximum error equal to 4.6853% for the antisymmetric angle ply (30/-30/30/-30). It is important to note that the layup with maximum error yield the analytical buckling load on the un-conservative side.

Table 4.1 S-Glass/Epoxy material properties [21].

| **Material** | $E_{11}$ | $E_{22}$ | $G_{12}$ | $\nu_{12}$ |
|---|---|---|---|---|
| **S-Glass/Epoxy** | 55.0 GPa | 16.0 GPa | 7.6 GPa | 0.28 |

Table 4.2 Analytical and numerical results for different layup sequences for S-Glass/Epoxy.

| **Ply Orientation** | **Analytical Results, N** | **Numerical Results, N** | **% Error** | **Layup Type** |
|---|---|---|---|---|
| **0/0/0/0** | 0.29627 | 0.2963 | 0.0102 | Single Specially Orthotropic |
| **90/90/90/90** | 0.08619 | 0.0862 | 0.0117 | Single Specially Orthotropic |
| **30/-30/30/-30** | 0.21109 | 0.2012 | 4.6853 | Antisymmetric Angle Ply |
| **45/-45/45/-45** | 0.14769 | 0.142 | 3.8527 | Antisymmetric Angle Ply |
| **60/-60/60/-60** | 0.10605 | 0.1045 | 1.4616 | Antisymmetric Angle Ply |
| **60/-60/45/-45** | 0.1241 | 0.1209 | 2.5786 | Balanced Angle Ply |
| **30/-30/45/-45** | 0.17485 | 0.1676 | 4.1465 | Balanced Angle Ply |
| **30/-30/60/-60** | 0.14447 | 0.1407 | 2.6096 | Balanced Angle Ply |

| | | | | |
|---|---|---|---|---|
| **30/-30/0/0** | 0.24789 | 0.2451 | 1.1255 | Anisotropic |
| **30/-30/0/90** | 0.15649 | 0.1539 | 1.6551 | Anisotropic |
| **30/30/30/30** | 0.21109 | 0.2099 | 0.5638 | Single anisotropic layer |
| **30/-30/-30/30** | 0.21109 | 0.2109 | 0.0901 | Symmetric angle Ply |
| **0/90/90/0** | 0.27001 | 0.27 | 0.0038 | Symmetric Cross Ply |
| **30/-60/-60/30** | 0.19796 | 0.1976 | 0.1819 | Symmetric Multiple Angle Ply |
| **0/90/0/90** | 0.17954 | 0.1804 | 0.4791 | Antisymmetric Cross Ply |
| **-45/30/-30/45** | 0.15561 | 0.1508 | 3.0911 | Antisymmetric Multiple Angle Ply |
| **90/0/0/90** | 0.11245 | 0.1125 | 0.0445 | Symmetric Cross Ply |

Load versus mid height deflection curve for three different stacking sequences obtained from the finite element nonlinear Riks analysis along with the analytical solution are illustrated in Figure 4.4 for comparison. Results show excellent agreement between analytical and numerical (FE) solutions. Antisymmetric cross ply (0/90/0/90) exhibit higher buckling load with minimal error between the analytical and numerical results as well. On the other hand, balanced angle ply (60/-60/45/-45) show the maximum error between results. Single specially-orthotropic layer (0/0/0/0) exhibits the highest buckling load due to having all fibers aligned with the loading axis while the coupling coefficient $\boldsymbol{B_{ani}}$. Vanishes.

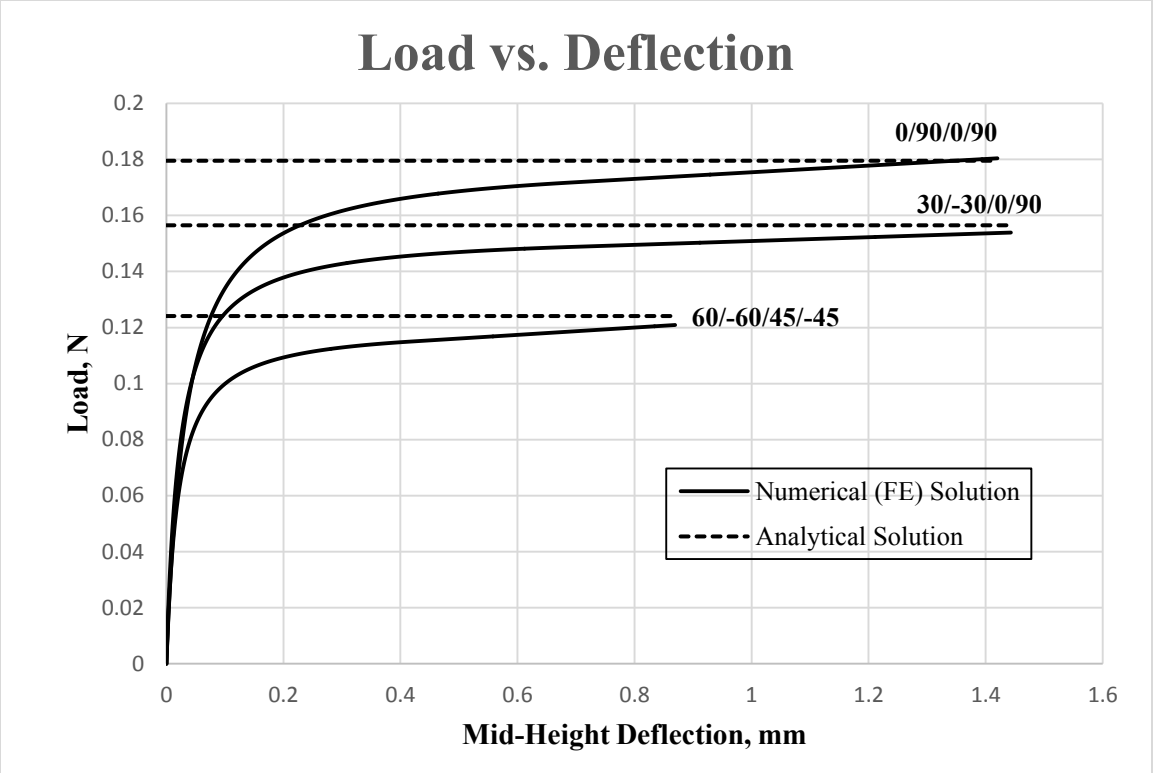


Figure 4.4 Analytical versus numerical solutions.

### 4.5.2 Parametric Study

#### 4.5.2.1 Effect of Ply Orientation

The effect of having different stacking sequences was studied for plates with the following dimensions for width, length, and thickness: 1000 mm x 100 mm x 0.4 mm, respectively. Buckling load values for different stacking sequences are shown in Table 4.2with values range between 0.0862 N and 0.2963 N. Figure 4.5 presents buckling shape of the simply supported plate obtained from the numerical analysis.

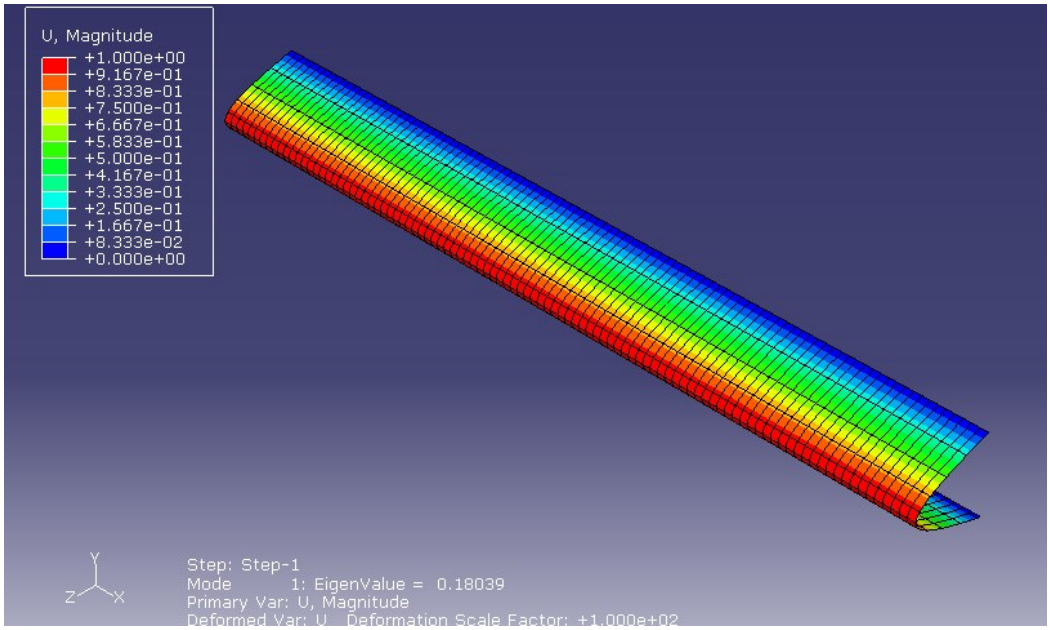

Figure 4.5 Buckling shape of simply supported plate.

#### 4.5.2.2 Effect of Material Properties

A parametric study was conducted to study the effect of changing material properties on the stability of the composite plate using two types of materials. S-Glass/Epoxy and High Strength Graphite/Epoxy were used to conduct this study and their properties are presented in Table 4.1and Table 4.3 obtained from typical values reported by FRP textbook [21].

Table 4.3 High Strength Graphite/Epoxy Material Properties [21].

| **Material** | $E_{11}$ | $E_{22}$ | $G_{12}$ | $\nu_{12}$ |
|---|---|---|---|---|
| **High Strength Graphite/Epoxy** | 145.0 GPa | 10.0 GPa | 4.8 GPa | 0.25 |

S-Glass/Epoxy and High Strength Graphite/Epoxy buckling load results for different stacking sequences are presented in Table 4.2 and Table 4.4. In general, High Strength Graphite/Epoxy exhibits higher buckling loads than S-Glass/Epoxy since it has higher stiffness values along the fiber direction. Furthermore, the error value between the numerical and analytical results reduces for the S-Glass/Epoxy since it has lower $E_{11}/E_{22}$ ratio compared to that of High Strength Graphite/Epoxy.

Table 4.4 Comparison of analytical and numerical buckling load for different layup sequences.

| Ply Orientation | Analytical Results, N | Numerical Results, N | % Error | Layup Type |
|---|---|---|---|---|
| **0/0/0/0** | 0.76656 | 0.7663 | 0.034 | Single Specially Orthotropic |
| **90/90/90/90** | 0.05287 | 0.0529 | 0.0568 | Single Specially Orthotropic |
| **30/-30/30/-30** | 0.4584 | 0.3966 | 13.4817 | Antisymmetric Angle Ply |
| **45/-45/45/-45** | 0.23673 | 0.2076 | 12.3052 | Antisymmetric Angle Ply |
| **60/-60/60/-60** | 0.10156 | 0.0945 | 6.9516 | Antisymmetric Angle Ply |
| **60/-60/45/-45** | 0.14725 | 0.1319 | 10.4245 | Balanced Angle Ply |
| **30/-30/45/-45** | 0.31892 | 0.277 | 13.1444 | Balanced Angle Ply |
| **30/-30/60/-60** | 0.18781 | 0.1658 | 11.7193 | Balanced Angle Ply |
| **30/-30/0/0** | 0.58106 | 0.55 | 5.3455 | Anisotropic |
| **30/-30/0/90** | 0.27616 | 0.2527 | 8.4951 | Anisotropic |
| **30/30/30/30** | 0.4584 | 0.4186 | 8.6824 | Single anisotropic layer |
| **30/-30/-30/30** | 0.4584 | 0.4564 | 0.4364 | Symmetric angle Ply |
| **0/90/90/0** | 0.67735 | 0.677 | 0.0517 | Symmetric Cross Ply |
| **30/-60/-60/30** | 0.4138 | 0.4001 | 3.3108 | Symmetric Multiple Angle Ply |
| **0/90/0/90** | 0.34673 | 0.3514 | 1.3469 | Antisymmetric Cross Ply |
| **-45/30/-30/45** | 0.26444 | 0.2406 | 9.0153 | Antisymmetric Multiple Angle Ply |
| **90/0/0/90** | 0.14208 | 0.1421 | 0.0141 | Symmetric Cross Ply |

Buckling results for hybrid plates using S-Glass and High Strength Graphite/Epoxy material properties are illustrated in Table 4.5. Graphite/Epoxy properties were used for layers with $0^o$ and $\pm 30^o$ orientation and S-Glass/Epoxy for the other orientations. Combining two materials showed a lower error values between analytical and numerical solution than using High Strength Graphite/Epoxy material properties since the overall $E_{11}/E_{22}$ ratio is reduced when combining two material therefore more terms might need to be added to the Rayleigh-Ritz approximation to capture the complexity in behavior which was beyond the scope of the present paper.

Table 4.5 Analytical vs. numerical buckling loads for different layup sequences for hybrid Graphite and S-Glass/Epoxy composites.

| Ply Orientation | Analytical Results, N | Numerical Results, N | % Error |
|---|---|---|---|
| **30/-30/60/-60** | 0.18829 | 0.1741 | 7.5363 |
| **30/-30/0/90** | 0.29611 | 0.2723 | 8.041 |
| **0/90/90/0** | 0.68151 | 0.6812 | 0.0455 |
| **0/90/0/90** | 0.37137 | 0.3754 | 1.0852 |

| | | | |
|---|---|---|---|
| **90/0/0/90** | 0.17124 | 0.1713 | 0.0351 |

#### 4.5.2.3 Effect of Element Type in FE Analysis

A parametric study was performed to study the effect of using different element types in the finite element analysis of S-Glass/Epoxy plates. Using quadratic shell element (S8R) and quadratic solid element (C3D20R) both with reduced integration schemes and element size equal to 10.0 mm x 10.0 mm, comparison between analytical and numerical solution is presented in Table 4.6. An excellent agreement between analytical and shell element results is observed for all stacking sequences. On the other hand, solid element results were off in most of the different stacking sequences. Accordingly, it might be argued that the solid element (C3D20R) is less reliable than the shell element (S8R) for this type of analysis.

Table 4.6 Analytical and numerical results with shell and solid element

| Ply Orientation | Analytical Results, N | Shell Element S8R, N | Solid Element C3D20R, N |
|---|---|---|---|
| **0/0/0/0** | 0.29627 | 0.2963 | 0.295798 |
| **90/90/90/90** | 0.08619 | 0.0862 | 0.0859608 |
| **30/-30/30/-30** | 0.21109 | 0.2012 | 0.208625 |
| **45/-45/45/-45** | 0.14769 | 0.142 | 0.145028 |
| **60/-60/60/-60** | 0.10605 | 0.1045 | 0.104616 |
| **60/-60/45/-45** | 0.1241 | 0.1209 | 0.124857 |
| **30/-30/45/-45** | 0.17485 | 0.1676 | 0.176787 |
| **30/-30/60/-60** | 0.14447 | 0.1407 | 0.156566 |
| **30/-30/0/0** | 0.24789 | 0.2451 | 0.252257 |
| **30/-30/0/90** | 0.15649 | 0.1539 | 0.199848 |

| | | | |
|---|---|---|---|
| **30/30/30/30** | 0.21109 | 0.2099 | 0.204145 |
| **30/-30/-30/30** | 0.21109 | 0.2109 | 0.208886 |
| **0/90/90/0** | 0.27001 | 0.27 | 0.190941 |
| **30/-60/-60/30** | 0.19796 | 0.1976 | 0.156534 |
| **0/90/0/90** | 0.17954 | 0.1804 | 0.19082 |
| **-45/30/-30/45** | 0.15561 | 0.1508 | 0.176957 |
| **90/0/0/90** | 0.11245 | 0.1125 | 0.190942 |

## 4.6 Conclusion

Rayleigh-Ritz approximation was used to derive a generalized analytical buckling formula for anisotropic laminated composite plates with simply supported conditions under axial compression.. The buckling formula was expressed in terms of the composite material axial, coupling, and flexural rigidities as well as the plate geometry. The analytical formula exhibited an excellent agreement with the numerical results. It was observed from the parametric study that using single composite material type with high stiffness ratio ($E_{11}/E_{22}$) per plate generally yielded more deviation of the analytical solution from the numerical results compared to using a two-material hybrid composite. Therefore, more terms need to be added to the Rayleigh-Ritz approximation in the case of composite material with high stiffness ratio. Additionally, the use of shell finite elements was found to be more reliable compared to the use of solid finite elements in the buckling predictions.

## 4.7 References


[1] Herencia, J.E., Weaver, P.M., and Friswell, M.I., "Closed-form solutions for buckling of long anisotropic plates with various boundary conditions under axial compression," *Journal of Engineering Mechanics*, vol. 136, no. 9, pp. 1105-1114, 2010.

[2] Weaver, P.M., "Approximate analysis for buckling of compression loaded long rectangular plates with flexural/twist anisotropy," Proc. R. Soc. London, vol. 462, no. 2065 pp. 59-73, 2006.

[3] Weaver, P.D., "Buckling of long clamped anisotropic plates under compression," in American Society of Composites, 22nd Technical Conf., Lancaster, 2007

[4] Qiao, P., and Shan, L., "Explicit local buckling analysis and design of fiber-reinforced plastic composite structural shapes," *Composite Structures*, vol. 70, no. 4, pp. 468-483, 2005.

[5] Mahesh, P.E., and Archibald, S.N., "Buckling od anisotropic composite plates under stress gradient," *Journal of Engineering Mechanics*, vol. 117, no. 2, pp. 260-275, 1991.

[6] Bellman, R.E., and Casti, J., "Differential quadrature and long-term integration," *J. Math. Anal. Appl.*, vol. 34, no. 2, pp. 235-238, 1971.

[7] Silva, N.M.F., Silvestre, N., and Camotim, D., "GBT formulation to analyse the buckling behaviour of FRP composite open-section thin-walled columns," *Composite Structures*, pp. 79-92, 2010.

[8] Silvestre, N., and Camotim, D., "Second-order generalised beam theory for arbitrary orthotropic materials," *Thin-Walled Structures*, pp. 791-820, 2002.

[9] Bauld, R.B., and Tzeng, L.A., "Vlasov theory for fiber-reinforced beams with thin-walled open cross-section," *Int. J. Solids Struct.*, vol. 20, no. 3, pp. 277-94, 1984.

[10] Ghaheri, A., Keshmiri, A., and Taheri-Behrooz, F., "Buckling and vibration of symmetrically laminated composite elliptical plates on an elastic foundation subjected to uniform in-plane force," *Journal of Engineering Mechanics*, vol. 140, no. 7, pp. 1-10, 2014.

[11] Weaver, P.M., Nemeth, M.P., and Taheri-Behrooz, F., "Bounds on flexural properties and buckling response for symmetrically laminated composite plates" *Journal of Engineering Mechanics*, vol. 133, no. 11, pp. 1-10, 2007.

[12] Xu, D., Ganesan, R. and Hoa, S.V., "Buckling analysis of tri-axial woven fabric composite structures subjected to bi-axial loading," *Composite Structures*, pp. 140-152, 2007.

[13] Sun, L., and Harik, I.E., "Buckling of stiffened antisymmetric laminated plates," *Journal of Engineering Mechanics*, vol. 139, no. 8, 2013.

[14] Harik, I.E., and Salamoun, G.L., "The analytical strip method of solution for stiffened rectangular plates," *Computers & Structures*, vol. 29, no. 2, pp. 283-291, 1988.

[15] Shufrin, I., Rabinovitch, O., and Eisenberger M., "Buckling of laminated plates with general boundary conditions under combined compression, tension, and shear- A semi-analytical solution," *Thin-Walled Structures*, vol. 46, pp. 925-938, 2008.

[16] Kerr, A.D., "An extended Kantorovich method for solution of eigenvalue problem," *Int. J. Solid Struct*, vol. 5, no. 6, pp. 559-572, 1969.

[17] Thai, H.T., and Kim S.E., "Levy-type solution for buckling analysis of orthotropic plates based on two variable refined plate theory," *Composite Structures*, vol.93, no. 7, pp. 1738-1746, 2011.

[18] Jones, R.M, Mechanics of composite materials, New York: Hemisphere Publishing Corporation, 1975.

[19] Hernandez, V., Roman, J.E., Tomas, A., and Vidal, V., "Lanczos methods in SLEPc," Polytechnic University of Valencia, Province of Valencia, 2006.

[20] Memon, B.A., Su, X.S., "Arc-length technique for nonlinear finite element analysis," Journal of Zhejiang University SCI, vol. 5, no. 5, pp. 618-628, 2004.

[21] Rasheed, H.A., Strengthening Design of Reinforced Concrete with FRP, New York: CRC Press, 2015.

# Chapter 5 - Analytical and Finite Element Buckling Solutions of Fixed-Fixed Anisotropic Laminated Composite Columns under Axial Compression

**Rund Al-Masri[1] and Hayder A. Rasheed[2]**

**[International Journal of Structural Stability and Dynamics, Vol.17, Issue 9, 2017, 17]**

**[DOI: 10.1142/S0219455417501036]**

**[http://www.worldscientific.com/worldscinet/ijssd]**

## 5.1 Abstract

**A generalized analytical formula is developed to predict buckling of anisotropic laminated composite fixed-fixed thin columns by using the Rayleigh-Ritz displacement field approximation. Based on the generalized constitutive relationship, the effective extensional, coupling and flexural stiffness coefficients of the anisotropic layup are determined using dimensional reduction by static condensation of the 6x6 composite stiffness matrix. The resulting explicit formula is expressed in terms of the flexural stiffness since the coupling and extensional stiffness coefficients drop out of the formulation for this boundary condition when following the standard Rayleigh-Ritz formulation steps. This formula is similar to the Euler buckling formula in which the flexural rigidity is expressed in terms of the flexural stiffness coefficient of laminated composites. Motivated by reducing some of the discrepancy with the finite element results, the pre-buckling solution was substituted into the bifurcation expression to yield an updated formula that includes the coupling and extensional stiffness coefficients. The analytical results are verified against finite element Eigen value solutions for a wide range of anisotropic laminated layups yielding high accuracy. A parametric study is then conducted to examine the effect of ply orientation and material properties including hybrid carbon/glass fiber composites. Relevance of the numerical and analytical results is discussed for all these cases. In addition, comparisons with an earlier buckling solution for cross-ply laminated columns are made.**

Keywords: buckling of composite columns, fixed-fixed boundary conditions, anisotropic laminated material, axial compression.

---

[1] Ph.D. Candidate

[2] Professor

## 5.2 Introduction

Laminated composite applications in aerospace, automotive, marine, and civil engineering are ever growing due to their excellent properties such as high stiffness-to-weight ratio, high strength-to-weight ratio, fatigue and corrosion resistance. Accordingly, an increase in demand for better understanding of the mechanics of laminated composites has been realized due to this growth. Composite columns, like any traditional members subjected to axial compression, undergo stability issues prior to failure. Not many research studies have focused on the buckling of composite columns. However, in recent years an extensive amount of research has been performed to study the buckling behavior of other composite members, like plates and shells [1-15]. Silva et al. [1] established a formulation of a generalized beam theory (GBT) to study local and global buckling behavior of fiber reinforced polymer composite open section thin-walled columns. The solution for buckling using GBT included solving the following eigenvalue problem:

$$(\mathrm{K} + \gamma \mathrm{G})d = 0 \quad \textbf{(1)}$$

where K is the linear stiffness matrix, G is the geometric stiffness matrix and *d* is the eigenvector. Silvestre and Camotim [2] developed a second order generalized beam theory (GBT) to predict buckling behavior for thin walled arbitrary orthotropic members. The developed theory was compared with Bauld and Lih-Shyng theory [3]. Based on the results, the critical buckling load exists for all isotropic or cross-ply orthotropic members. Additionally, non-linear primary path is showed and no specific bifurcation is detected for symmetric orthotropic lay-ups. Rasheed and Yousif [4] developed a closed form solution to predict buckling of thin laminated orthotropic composite rings/long cylinders under external pressure based on the energy approach:

$$P_{cr} = 3\left(\frac{A_{orth}D_{orth} - B_{orth}^2}{A_{orth}R^3 + 2B_{orth}R^2 + D_{orth}R}\right) \quad \textbf{(2)}$$

where $A_{orth}, B_{orth}, and\ D_{orth}$ constants are the effective extensional, coupling, and bending stiffness coefficients obtained from the dimensional reduction of orthotropic behavior. The developed formula yielded improved results compared to some design codes. Rasheed and Yousif [5] generated a closed form solution to predict buckling of anisotropic laminated composite rings/long cylinders under external hydrostatic pressure. The analytical solution was verified with finite element solutions and concluded that the buckling modes are symmetric with respect to rotated axes of the twisted section of the pre-buckling solution in case of anisotropy. Xu et al. [6] used equivalent anisotropic plate method to develop an approximate analytical solution to predict buckling of tri-axial woven fabric composite structure under bi-axial loading. The results showed that the analytical solution gives an upper bound buckling load and it can be used to predict buckling behavior for real world problems under bi-axial loading. Shukla et al. [7] used first order shear deformation and von-Karman type nonlinearity to estimate the critical buckling loads for laminated composite plates with various boundary conditions subjected to in-plane uniaxial and biaxial loading. The effects of span to thickness ratio, plate aspect ratio, lamination scheme, number of layers and modulus ratio were considered in estimating buckling load. Using analytical strip method (ASM) which was first developed by Harik and Salamoun [8], Sun and Harik [9] developed analytical buckling solution of stiffened antisymmetric laminated composite plates with bending-extension coupling to analyze bending of thin orthotropic and stiffened rectangular plates. Plates with free boundary conditions contribute the weakest stiffening effect. Additionally, the number of layers of ply orientations equal to 0 and 90 had no effect on the critical buckling load since the coupling stiffness matrix vanishes.

Debski et al. [10] studied buckling and post-buckling behavior of thin-walled composite channel column sections experimentally. The experimental results were verified with the numerical

solutions obtained from finite element models (Abaqus and ANSYS) and analytical-numerical method (ANM). Shufrin et al. [11] used multi term Kantorovich method [12] to develop a semi-analytical solution for buckling of symmetrically laminated rectangular plates with general boundary conditions under combined tension, compression, and shear. They concluded that the stability of angle-ply laminated plates improved under biaxial compression/tension and shear compared to free in-plane restraint. Furthermore, due to the in-plane restrains, additional in-plane forces were created. Thai and Kim [13] suggested a closed form solution for buckling of orthotropic plates with two opposite simply supported edges using two-variable refined plate theories. Using state space concept on Levy type solution to solve the governing equations, their results showed more accurate solutions than the higher order shear deformation theory. Using first order shear deformation theory, Abramovich and Livshits [14] studied the free vibrations of non-symmetric cross ply laminated composite beams. Longitudinal, transverse displacement, rotary inertia, and shear deformation were taken into account in the analysis. The following equation of motion of cross ply laminated composite beams was solved for different boundary conditions:

$$[\mathrm{M}]\{\bar{q}\} + [\mathrm{C}]\{q\} = \{0\} \quad \textbf{(3)}$$

where $[\mathrm{M}]$ is the generalized mass matrix, $[\mathrm{C}]$ is the matrix differential operator; and $\{q\}$ is the vector of the generalized displacements. The new approach and Bernoulli-Euler theory were verified against numerical solutions. Abramovich et al. [15] used the exact method based on Timoshenko equation to study the vibrations and buckling of cross-ply non-symmetric rectangular laminated composite beams. The effects of material properties, number of layers, and boundary conditions are considered. Analytical results showed a good agreement with the numerical results. Moreover, the non-symmetric layup showed a coupling effect between the axial and lateral motion of the beam.

In this work, a generalized analytical formula for buckling of fixed-fixed laminated composite columns subjected to axial compression is developed. The Rayleigh–Ritz approximation was used to obtain the buckling formula. Extensional, coupling and flexural rigidities in 1D are determined using dimensional reduction by the static condensation approach starting with the 3D rigidity matrix. Moreover, finite element models for the columns are established using the commercial software Abaqus. The finite element numerical solution was compared to the analytical solution resulting in excellent agreement regardless of the complexity of the composite lay-ups used.

## 5.3 Analytical Formulation

Rayleigh-Ritz approximation is used to derive a generalized closed form buckling solution for fixed-fixed anisotropic laminated composite columns under axial compression

### 5.3.1 Assumptions:

11. Buckling occurs in the x-y plane about the weak axis (z-axis).

    The y-axis is perpendicular to the composite lamination surface,
12. Figure 5.1
13. The lamination angle ( $\alpha$ ) is measured with respect to the x-axis (i.e. 0° fibers run parallel to the x-axis and 90° fibers run parallel to the z-axis). Accordingly, the angle ( $\alpha$ ) is rotated about the y-axis.
14. Plane sections before bending remain plane after bending and perpendicular to the mid surface (i.e. simple beam theory holds).
15. Classical lamination theory is applicable with effect of transverse shear deformation ignored.

### 5.3.2 Kinematics

Geometry and the Cartesian coordinates of the fixed-fixed column are presented in Figure 5.1. Bending occurs about the weak axis of the column which is the z-axis. Depending on the isotropic buckling mode, the following displacement relations were assumed:

$$\boldsymbol{u}\,(\boldsymbol{x}) = \boldsymbol{B_1 x}\,; \quad \boldsymbol{v}\,(\boldsymbol{x}) = \boldsymbol{C_1}(\mathbf{1} - \mathbf{cos}\,\tfrac{\boldsymbol{2\pi x}}{\boldsymbol{L}}) \tag{4}$$

where $u(x)$ is the axial displacement, $v(x)$ the lateral displacement, $B_1$ and $C_1$ are constants to be solved for and $x$ is the distance along the axis of the column,
Figure 5.1. For intermediate class of deformation, the axial strain $\varepsilon_x$ and curvature $\kappa_x$ are presented given by

$$\boldsymbol{\varepsilon_x} = \tfrac{\boldsymbol{du}}{\boldsymbol{dx}} + \tfrac{\mathbf{1}}{\mathbf{2}}(\tfrac{\boldsymbol{dv}}{\boldsymbol{dx}})^{\mathbf{2}} = \boldsymbol{u'} + \tfrac{\mathbf{1}}{\mathbf{2}}\boldsymbol{v'^2}; \qquad \boldsymbol{\kappa_x} = \tfrac{\boldsymbol{d^2v}}{\boldsymbol{d^2x}} = \boldsymbol{v''} \tag{5}$$

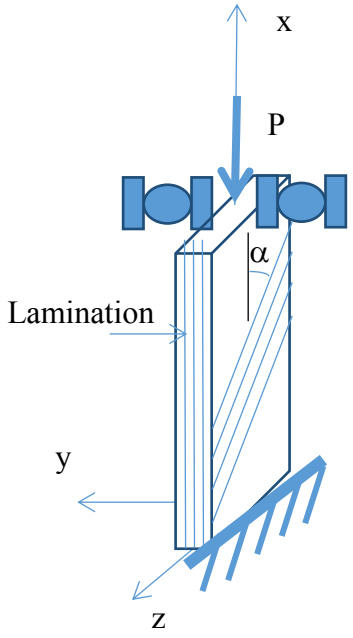


Figure 5.1Column geometry.

### 5.3.3 Constitutive equations

The principal material directions were transformed into the column coordinate system. The stresses and strains are then related in the following equation

$$\begin{Bmatrix} \boldsymbol{\sigma_x} \\ \boldsymbol{\sigma_z} \\ \boldsymbol{\tau_{xz}} \end{Bmatrix} = \begin{bmatrix} \boldsymbol{\bar{Q}_{11}} & \boldsymbol{\bar{Q}_{12}} & \boldsymbol{\bar{Q}_{16}} \\ \boldsymbol{\bar{Q}_{12}} & \boldsymbol{\bar{Q}_{22}} & \boldsymbol{\bar{Q}_{26}} \\ \boldsymbol{\bar{Q}_{16}} & \boldsymbol{\bar{Q}_{26}} & \boldsymbol{\bar{Q}_{66}} \end{bmatrix} \begin{Bmatrix} \boldsymbol{\varepsilon_x} \\ \boldsymbol{\varepsilon_z} \\ \boldsymbol{\gamma_{xz}} \end{Bmatrix} \tag{6}$$

where $\bar{Q}_{ij}$ matrix represents the transformed reduced stiffness matrix as defined in standard composite textbooks [16]. Accordingly, the coupled force-strain relationship is established as

$$\begin{Bmatrix} \boldsymbol{N_x} \\ \boldsymbol{N_z} \\ \boldsymbol{N_{xz}} \\ \boldsymbol{M_x} \\ \boldsymbol{M_z} \\ \boldsymbol{M_{xz}} \end{Bmatrix} = \begin{bmatrix} \boldsymbol{A_{11}} & \boldsymbol{A_{12}} & \boldsymbol{A_{16}} & \boldsymbol{B_{11}} & \boldsymbol{B_{12}} & \boldsymbol{B_{16}} \\ \boldsymbol{A_{12}} & \boldsymbol{A_{22}} & \boldsymbol{A_{26}} & \boldsymbol{B_{12}} & \boldsymbol{B_{22}} & \boldsymbol{B_{26}} \\ \boldsymbol{A_{16}} & \boldsymbol{A_{26}} & \boldsymbol{A_{66}} & \boldsymbol{B_{16}} & \boldsymbol{B_{26}} & \boldsymbol{B_{66}} \\ \boldsymbol{B_{11}} & \boldsymbol{B_{12}} & \boldsymbol{B_{16}} & \boldsymbol{D_{11}} & \boldsymbol{D_{12}} & \boldsymbol{D_{16}} \\ \boldsymbol{B_{12}} & \boldsymbol{B_{22}} & \boldsymbol{B_{26}} & \boldsymbol{D_{12}} & \boldsymbol{D_{22}} & \boldsymbol{D_{26}} \\ \boldsymbol{B_{16}} & \boldsymbol{B_{26}} & \boldsymbol{B_{66}} & \boldsymbol{D_{16}} & \boldsymbol{D_{26}} & \boldsymbol{D_{66}} \end{bmatrix} \begin{Bmatrix} \boldsymbol{\varepsilon_x} \\ \boldsymbol{\varepsilon_z} \\ \boldsymbol{\gamma_{xz}} \\ \boldsymbol{\kappa_x} \\ \boldsymbol{\kappa_z} \\ \boldsymbol{\kappa_{xz}} \end{Bmatrix} \tag{7}$$

where

$$\boldsymbol{A_{ij}} = \sum_{\boldsymbol{k=1}}^{\boldsymbol{N}} \boldsymbol{\bar{Q}_{ij} t_k}$$

$$\boldsymbol{B_{ij}} = \sum_{\boldsymbol{k=1}}^{\boldsymbol{N}} \boldsymbol{\bar{Q}_{ij} t_k \bar{y}_k}$$

$$\boldsymbol{D_{ij}} = \sum_{\boldsymbol{k=1}}^{\boldsymbol{N}} \boldsymbol{\bar{Q}_{ij} t_k} \left( \boldsymbol{\bar{y}_k^2} + \frac{\boldsymbol{t_k^2}}{\boldsymbol{12}} \right) \tag{8}$$

$$\boldsymbol{t_k} = \boldsymbol{y_k} - \boldsymbol{y_{k-1}}$$

$$\boldsymbol{\bar{y}_k} = \frac{\boldsymbol{y_k} + \boldsymbol{y_{k-1}}}{\boldsymbol{2}}$$

In which $A_{ij}$, $B_{ij}$, and $D_{ij}$ are the extensional, coupling, and flexural rigidity coefficients. $t_k$ = thickness of the k-th ply; and $N$ = number of different plies in the stacking sequence.

Material properties and the fiber orientations are used in Eq. (7) to generate the three dimensional (3D) constitutive matrix. Applying the zero forces and moments then by using static condensation, the 3D classical lamination matrix is reduced into 1D anisotropic extensional, coupling and flexural stiffness coefficients.

$$\begin{Bmatrix} N_x \\ N_z = 0 \\ N_{xz} = 0 \\ M_x \\ M_z = 0 \\ M_{xz} = 0 \end{Bmatrix} = \begin{bmatrix} A_{11} & A_{12} & A_{16} & B_{11} & B_{12} & B_{16} \\ A_{12} & A_{22} & A_{26} & B_{12} & B_{22} & B_{26} \\ A_{16} & A_{26} & A_{66} & B_{16} & B_{26} & B_{66} \\ B_{11} & B_{12} & B_{16} & D_{11} & D_{12} & D_{16} \\ B_{12} & B_{22} & B_{26} & D_{12} & D_{22} & D_{26} \\ B_{16} & B_{26} & B_{66} & D_{16} & D_{26} & D_{66} \end{bmatrix} \begin{Bmatrix} \varepsilon_x \\ \varepsilon_z \\ \gamma_{xz} \\ \kappa_x \\ \kappa_z \\ \kappa_{xz} \end{Bmatrix} \tag{9}$$

Extracting the second, third, fifth, and sixth linear equations from matrix (9) to solve the axial strain and axial curvature ($\varepsilon_x$ ,$\kappa_x$) with respect to the other deformation components.

$$-\begin{bmatrix} A_{12} & B_{12} \\ A_{16} & B_{16} \\ B_{12} & D_{12} \\ B_{16} & D_{16} \end{bmatrix} \begin{Bmatrix} \varepsilon_x \\ \kappa_x \end{Bmatrix} = \begin{bmatrix} A_{22} & A_{26} & B_{22} & B_{26} \\ A_{26} & A_{66} & B_{26} & B_{66} \\ B_{22} & B_{26} & D_{22} & D_{26} \\ B_{26} & B_{66} & D_{26} & D_{66} \end{bmatrix} \begin{Bmatrix} \varepsilon_y \\ \gamma_{xz} \\ \kappa_{yz} \\ \kappa_{xz} \end{Bmatrix}$$

$$-R \begin{Bmatrix} \varepsilon_x \\ \kappa_x \end{Bmatrix} = Q \begin{Bmatrix} \varepsilon_z \\ \gamma_{xz} \\ \kappa_z \\ \kappa_{xz} \end{Bmatrix} \tag{10}$$

Inverting the matrix Q to the other side of Eq. (10), the condensed deformation components are obtained in terms of the axial strain and curvature:

$$\begin{Bmatrix} \varepsilon_z \\ \gamma_{xz} \\ \kappa_z \\ \kappa_{xz} \end{Bmatrix} = -[Q]^{-1}[R] \begin{Bmatrix} \varepsilon_x \\ \kappa_x \end{Bmatrix} \tag{11}$$

By substituting Eq. (11) into the first and fourth linear equation of the matrix (9); the axial force and in-plane moment versus the axial strain and in-plane curvature relationship can be expressed in terms of the generally anisotropic material properties

$$\begin{bmatrix} N_x \\ M_x \end{bmatrix} = \begin{bmatrix} A_{ani} & B_{ani} \\ B_{ani} & D_{ani} \end{bmatrix} \begin{Bmatrix} \varepsilon_x \\ \kappa_x \end{Bmatrix} \tag{12}$$

where

$$\begin{bmatrix} A_{ani} & B_{ani} \\ B_{ani} & D_{ani} \end{bmatrix} = \begin{bmatrix} A_{11} & B_{11} \\ B_{11} & D_{11} \end{bmatrix} - [R]^T[Q]^{-1}[R] \tag{13}$$

### 5.3.4 Energy Formulation

Rayleigh-Ritz approximation was used to derive a general buckling formula based on the energy approach. Strain energy can be expressed in terms of the integration of the applied loads multiplying the corresponding deformations.

$$\boldsymbol{U = \int_0^L \left(\frac{1}{2} N_x \varepsilon_x + \frac{1}{2} M_x \kappa_x\right) dx}$$

$$\boldsymbol{= \int_0^L \frac{1}{2} (A_{ani} \varepsilon_x^2 + B_{ani} \varepsilon_x \kappa_x)\, dx + \int_0^L \frac{1}{2} (B_{ani} \varepsilon_x \kappa_x + D_{ani} \kappa_x^2)\, dx} \quad \textbf{(14)}$$

The potential of external loads can be expressed as

$$\boldsymbol{W = -P\, u(L)} \quad \textbf{(15)}$$

In view of Eqs. (14) and (15) , the total potential energy function is given by

$$\boldsymbol{\Pi = U - W = \int_0^L \frac{1}{2} (A_{ani} \varepsilon_x^2 + 2B_{ani} \varepsilon_x \kappa_x + D_{ani} \kappa_x^2)\, dx + P\, u(L)} \quad \textbf{(16)}$$

$$\boldsymbol{\Pi = \frac{1}{2} A_{ani} B_1^2 L + \frac{1}{4} A_{ani} B_1 C_1^2 \left(\frac{2\pi}{L}\right)^2 + \frac{3}{32} A_{ani} C_1^4 L \left(\frac{2\pi}{L}\right)^4 + \frac{1}{4} D_{ani} C_1^2 L \left(\frac{2\pi}{L}\right)^4 + P B_1 L} \quad \textbf{(17)}$$

By minimizing the total potential energy function with respect to $B_1$ and $C_1$ and setting the resulting expressions to zero, performing the integration by parts and manipulating the equations, one obtains

$$\boldsymbol{\frac{\partial \Pi}{\partial B_1} = A_{ani} B_1 L + \frac{A_{ani} C_1^2 L}{4} \left(\frac{2\pi}{L}\right)^2 + PL = 0} \quad \textbf{(18)}$$

$$\boldsymbol{\frac{\partial \Pi}{\partial C_1} = \frac{A_{ani} B_1 C_1 L}{2} \left(\frac{2\pi}{L}\right)^2 + \frac{3 A_{ani} C_1^3 L}{8} \left(\frac{2\pi}{L}\right)^4 + \frac{D_{ani} C_1 L}{2} \left(\frac{2\pi}{L}\right)^4 = 0} \quad \textbf{(19)}$$

In view of Eqs. (18) and (19), we have

$$B_1 = -\frac{C_1^2}{4}\left(\frac{2\pi}{L}\right)^2 - \frac{P}{A_{ani}} \tag{20}$$

$$[\frac{1}{4}A_{ani}LC_1^2\left(\frac{2\pi}{L}\right)^4 - \frac{PL}{2}\left(\frac{2\pi}{L}\right)^2 + \frac{1}{2}D_{ani}L\left(\frac{2\pi}{L}\right)^4]C_1 = 0 \tag{21}$$

and solving Eq. (21), we get $C_1$ as

$$C_1 = 0 \qquad \textbf{which is a trivial solution}$$

$$\textbf{or} \quad C_1 = \sqrt{\frac{P/2 - 1/2\, D_{ani}(2\pi/L)^2}{1/4\, A_{ani}(2\pi/L)^2}} \tag{22}$$

In order for the $C_1$ value to be real, the discriminant must be at least zero. By setting the discriminant to zero, a closed form solution for the critical buckling load is derived:

$$P_{cr} = \frac{4D_{ani}\pi^2}{L^2} \tag{23}$$

It may be observed that Eq. (23) reduces to the Euler buckling formula of the fixed-fixed isotropic column with an effective length factor of 0.5 when $D_{ani}$ is replaced with *EI* of the column.

### 5.3.5 Pre-buckling Solution

All the terms having the coupling effect ($B_{ani}$) in the previous derivation lent to zero, therefore to produce the effect of the coupling on the stability of the laminated composite column, the pre-buckling solution is considered. The in-plane moment ($M_x$) is set to zero during pre-buckling and before reaching the buckling load.

$$M_x = B_{ani}\epsilon_x + D_{ani}\kappa_x \tag{24}$$

$$0 = B_{ani}\epsilon_x + D_{ani}\kappa_x$$

$$\kappa_x = -\frac{B_{ani}}{D_{ani}}\epsilon_x \tag{25}$$

By substituting Eq. (25) into the axial force equation, the axial force versus the axial strain can be expressed in terms of the generally anisotropic material properties

$$\boldsymbol{P_x = A_{ani}\epsilon_x + B_{ani}\kappa_x} \tag{26}$$

$$\boldsymbol{P_x = A_{ani}\epsilon_x - \frac{B_{ani}^2}{D_{ani}}\epsilon_x}$$

$$\boldsymbol{P_x = A_{eff}\epsilon_x} \tag{27}$$

where

$$\boldsymbol{A_{eff} = A_{ani} - \frac{B_{ani}^2}{D_{ani}}} \tag{28}$$

The axial force ($P_x$) is positive and in compression based on the assumed sign convention. However, the axial strain ($\epsilon_x$) is negative although it is in compression as follow:

$$\boldsymbol{u = -B_1 x} \tag{29}$$

Using the axial strain in Eq. (5), setting the lateral displacement term to zero, and substituting equation (29), the axial strain can be expressed as

$$\boldsymbol{\epsilon_x = -B_1} \tag{30}$$

By substituting Eq. (30) into Eq. (27), a relationship between the axial force and the unknown constant ($B_1$) is obtained, i.e.

$$\boldsymbol{-B_1 = \frac{P_x}{A_{eff}}} \tag{31}$$

### 5.3.6 Bifurcation Solution in terms of Pre-buckling Deformation

By substituting Eq. (31) into the total potential energy function given by Eq. (17), one obtains

$$\boldsymbol{\Pi = \frac{1}{2}A_{ani}\left(\frac{P}{A_{eff}}\right)^2 L - \frac{1}{4}A_{ani}\left(\frac{P}{A_{eff}}\right)C_1^2\left(\frac{2\pi}{L}\right)^2 + \frac{3}{32}A_{ani}C_1^4 L\left(\frac{2\pi}{L}\right)^4 + \frac{1}{4}D_{ani}C_1^2 L\left(\frac{2\pi}{L}\right)^4 - PL\frac{P}{A_{eff}}} \tag{32}$$

Minimizing the total potential energy with respect to the unknown $C_1$, setting the resulting expression to zero, and manipulating the equation, one gets

$$\frac{\partial \Pi}{\partial C_1} = -\frac{A_{ani} P_1 C_1 L}{2A_{eff}} \left(\frac{2\pi}{L}\right)^2 + \frac{12 A_{ani} C_1^3 L}{32} \left(\frac{2\pi}{L}\right)^4 + \frac{D_{ani} C_1 L}{2} \left(\frac{2\pi}{L}\right)^4 = 0 \tag{33}$$

By solving Eq. (33), one gets

$$C_1 = 0 \quad \textbf{which is a trivial solution}$$

$$\textbf{or} \quad C_1 = \sqrt{\frac{32}{12A_{ani}} \left(\frac{L}{2\pi}\right)^2 \left[\frac{1}{2} D_{ani} \left(\frac{2\pi}{L}\right)^2 - \frac{P A_{ani}}{2A_{eff}}\right]} \tag{34}$$

In order for the $C_1$ value to be real, the discriminant must be at least zero. By setting the discriminant to zero and substituting Eq. (28), a new closed form solution for the critical buckling load is derived considering the coupling effect:

$$P_{cr} = \frac{D_{ani} \pi^2}{(L/2)^2} - \frac{B_{ani}^2 \pi^2}{A_{ani} (L/2)^2} \tag{35}$$

$$P_{cr} = \frac{\pi^2}{(L/2)^2} \left(D_{ani} - \frac{B_{ani}^2}{A_{ani}}\right) \tag{36}$$

$$P_{cr} = \frac{\pi^2}{(L/2)^2} D_{eff} \tag{37}$$

where

$$D_{eff} = \left(D_{ani} - \frac{B_{ani}^2}{A_{ani}}\right) \tag{38}$$

It is observed that Eq. (36) reduces down to Euler buckling formula of the fixed-fixed isotropic column in the case of isotropic or specially-orthotropic materials.

## 5.4 Numerical Formulation

The derived analytical solution was verified by applying finite element buckling analysis using the commercial software package Abaqus for laminated anisotropic columns. Fixed-fixed columns were assembled with a fixed support at the bottom and fixed-roller support on top of the column, Figure 5.2. Moreover, columns were subjected to axial compression load applied at the top of the columns. Linear elastic laminated material was used for orthotropic and anisotropic layups, respectively. Columns were modeled in 3D space using quadrilateral eight node doubly curved thick shell element (S8R). The Model's boundary conditions and mesh are presented in Figure 5.2. In addition, 3D 6-node quadratic triangular thin shell element (STRI65) was also attempted. Furthermore, a graphite/epoxy material was mainly used to simulate the composite columns.

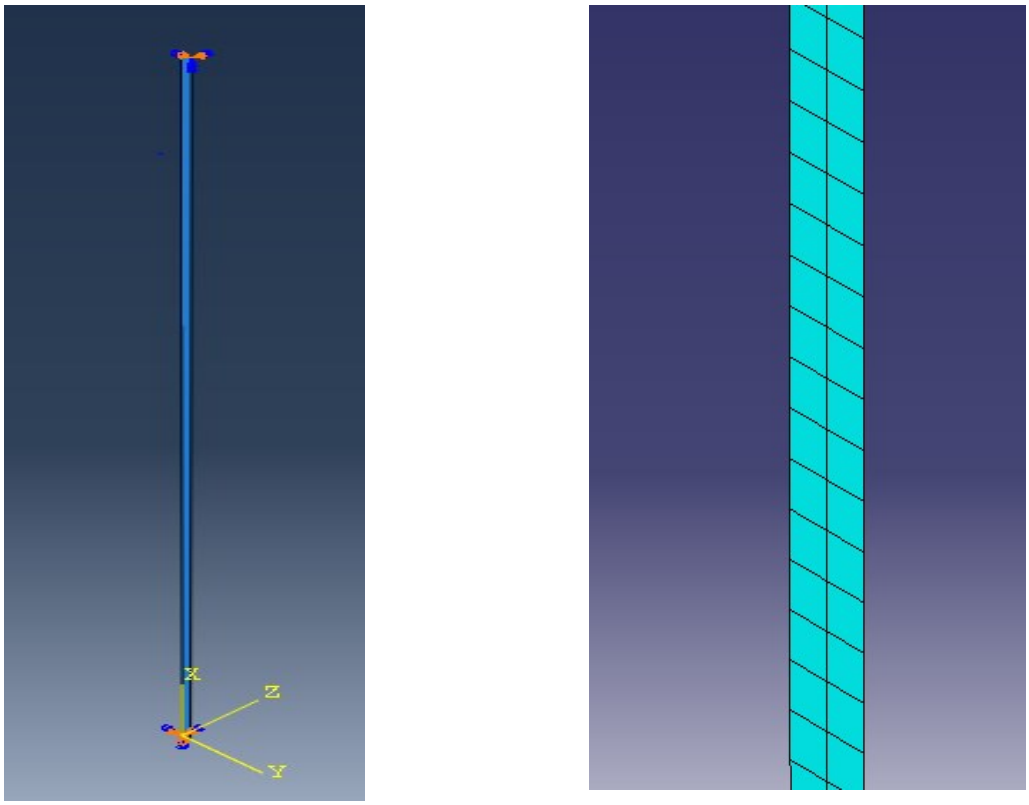


Figure 5.2 Left: Boundary conditions. Right: Meshed Model.

In this study, two types of analyses were attempted. Buckling analysis was done at the beginning to simulate eigenvalue computation. Lanczos method is used to solve for eigenvalues and eigenvectors for complex Hermitian matrix using power method. By adopting recurrence relations (multidimensional array values), $m\ x\ m$ symmetric matrix is reduced to a tridiagonal matrix [17]. Secondly, a nonlinear stability analysis (pre-buckling and buckling) of the composite column was predicted by performing nonlinear geometry analysis using the modified Riks computations. The modified Riks analysis uses the Arc length method to follow the equilibrium path, representing either the bifurcation points or the limit points. Load increments are applied during the analysis in which equilibrium iterations converge along the arc length, forcing the constraint equation to be satisfied at every iteration [18].

## 5.5 Results and Applications:

### 5.5.1 Numerical Validation

To simulate the analytical and numerical results for different stacking sequences of composite columns; High Strength Graphite/Epoxy material properties was used, Table 5.1 [19]. Composite columns were simulated with the following dimensions for length, width, and thickness: 100 mm x 1.0 mm x 0.4 mm, respectively.

Table 5.1 High Strength Graphite/Epoxy Material Properties [19].

| **Material** | $E_{11}$ | $E_{22}$ | $G_{12}$ | $v_{12}$ |
|---|---|---|---|---|
| **High Strength Graphite/Epoxy** | 145.0 GPa | 10.0 GPa | 4.8 GPa | 0.25 |

The comparison between the analytical and numerical buckling loads is reported in Table 5.2 for different layup stacking sequences. The results of Eq. (23) match closely with a minimum error

equal to 0.01995% for the single specially-orthotropic layer (90/90/90/90) and a maximum error equal to 14.345% for the antisymmetric cross ply laminate (0/90/0/90). On the other hand, the analytical results of Eq. (36) showed an excellent agreement with the numerical results with minimum error equal to 0.02375% for the single specially-orthotropic layup (90/90/90/90) and a maximum error equal to 1.109% for the single anisotropic laminate (30/30/30/30). Moreover, it is observed that the error significantly reduced down using Eq. (36) since the coupling and extensional effects are considered.

The load versus mid height deflection curves are plotted for three different stacking sequences obtained from finite element nonlinear Riks analysis along with the analytical solution for comparison. Riks analysis is useful to indicate the existence of pre-buckling deformation in the transverse direction. Isotropic columns buckle through bifurcation where there is no transverse deformation prior to buckling, see Figure 5.3. Results for symmetric angle ply (30/-30/-30/30) and anisotropic layup (30/-30/0/90) show excellent agreement. On the other hand, the antisymmetric angle ply (30/-30/30/-30) exhibits higher buckling load with minimal error between the analytical and numerical results as well.

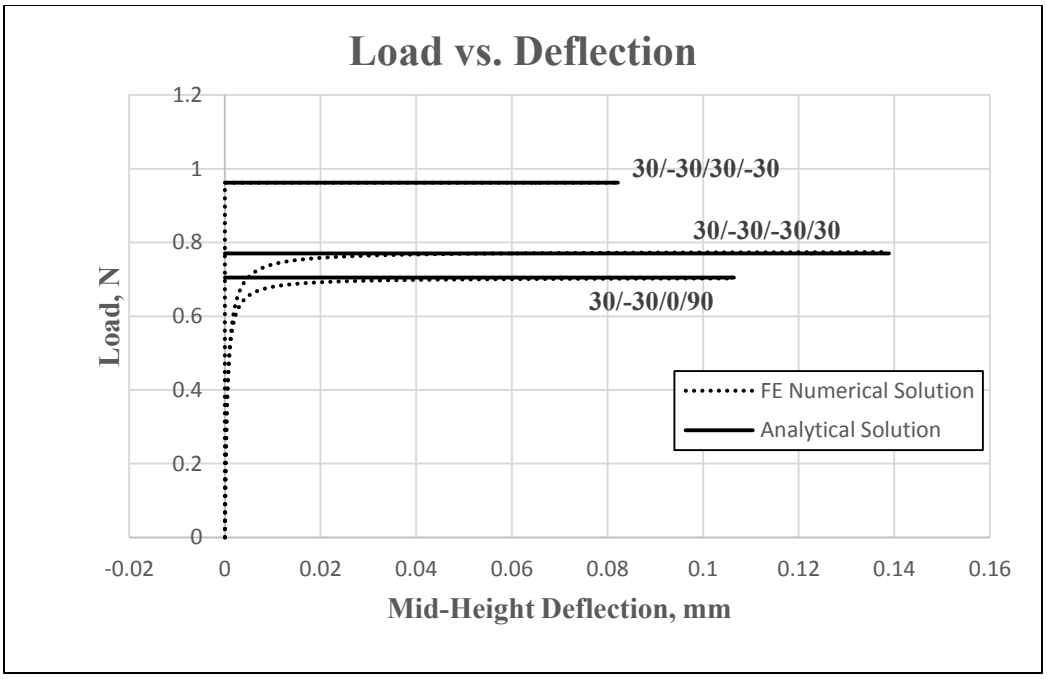


Figure 5.3 Analytical versus numerical solutions.

Table 5.2 Comparison of analytical and numerical buckling load for different layup sequences.

| Ply Orientation | Analytical Results, N, Equation (23) | Analytical Results, N, Equation (36) | Numerical Results, N | % Error, Equation (23) | % Error, Equation (36) | Layup Type |
|---|---|---|---|---|---|---|
| **0/0/0/0** | 3.053 | 3.053 | 3.04733 | 0.18572 | 0.18572 | Single Specially Orthotropic |
| **90/90/90/90** | 0.210552 | 0.21056 | 0.21051 | 0.01995 | 0.02375 | Single Specially Orthotropic |
| **0/90/90/0** | 2.70446 | 2.70446 | 2.69824 | 0.23 | 0.23 | Symmetric Cross ply |
| **90/0/0/90** | 0.56728 | 0.56728 | 0.56698 | 0.05289 | 0.05289 | Symmetric Cross ply |
| **0/90/0/90** | 1.63686 | 1.40404 | 1.40209 | 14.34271 | 0.13889 | Antisymmetric Cross Ply |
| **60/-60/45/-45** | 0.29002 | 0.27956 | 0.28093 | 3.13427 | 0.49006 | Balanced Multiple Angle Ply |
| **30/-30/30/-30** | 0.9566 | 0.9566 | 0.9613 | 0.49133 | 0.49133 | Antisymmetric Angle Ply |
| **45/-45/45/-45** | 0.35483 | 0.35483 | 0.3574 | 0.7243 | 0.7243 | Antisymmetric Laminates |
| **60/-60/60/-60** | 0.22753 | 0.22753 | 0.22822 | 0.30326 | 0.30326 | Antisymmetric Laminates |
| **30/30/30/30** | 0.43373 | 0.43373 | 0.43854 | 1.10899 | 1.10899 | Single anisotropic layer |
| **30/-60/-60/30** | 0.46286 | 0.46286 | 0.46777 | 1.0608 | 1.0608 | Symmetric Multiple Angle Layers |
| **30/-30/-30/30** | 0.77024 | 0.77024 | 0.77585 | 0.72835 | 0.72835 | Symmetric angle Ply |
| **-45/30/-30/45** | 0.4563 | 0.4563 | 0.45972 | 0.74951 | 0.74951 | Antisymmetric Multiple Angle Ply |
| **30/30/-30/-30** | 0.64682 | 0.64682 | 0.64489 | 0.29839 | 0.29839 | Antisymmetric Angle Ply |
| **30/-30/0/90** | 0.70276 | 0.70273 | 0.70451 | 0.24902 | 0.2533 | Anisotropic |

### 5.5.2 Parametric Study

#### 5.5.2.1 Effect of Ply Orientation

The effect of having different stacking sequences was studied for columns with the following dimensions: 100 mm x 1.0 mm x 0.4 mm for length, width, and thickness, respectively. Results for buckling load values for different stacking sequences are presented in Table 5.2 in the previous section with a range values between 0.2106 N and 3.053 N.

#### 5.5.2.2 Effect of Material Properties

A parametric study was performed to investigate the effect of changing material properties on the stability of the composite column using two types of materials. High Strength Graphite/Epoxy and S-Glass/Epoxy material were used to conduct this study and their properties are illustrated in Table 5.1 and Table 5.3 [19].

Table 5.3 S-Glass/Epoxy material properties [19].

| **Material** | $E_{11}$ | $E_{22}$ | $G_{12}$ | $\nu_{12}$ |
|---|---|---|---|---|
| **S-Glass/Epoxy** | 55.0 GPa | 16.0 GPa | 7.6 GPa | 0.28 |

Table 5.2 and Table 5.4 illustrate results of High Strength Graphite/ Epoxy and S-Glass/Epoxy for different stacking sequences. In general, it was observed that High Strength Graphite/Epoxy exhibits much higher buckling loads than S-Glass/Epoxy since it has higher stiffness values along the fiber direction. It is also observed that the amount of error between the analytical and numerical results reduces for the S-Glass/Epoxy since it has lower $E_{11}/E_{22}$ ratio compared to that of the High Strength Graphite/Epoxy. Moreover, it was observed that Eq. (36) decreased the amount of error compared to the error value using Eq. (23).

Table 5.4 Analytical and numerical results for different layup sequences for S-Glass/Epoxy.

| Ply Orientation | Analytical Results, N, Eq. (23) | Analytical Results, N, Eq. (36) | Numerical Results, N | % Error, Eq. (23) | % Error, Eq. (36) | Layup Type |
|---|---|---|---|---|---|---|
| **0/0/0/0** | 1.15804 | 1.15804 | 1.15778 | 0.0225 | 0.02246 | Single Specially Orthotropic |
| **90/90/90/90** | 0.33689 | 0.33689 | 0.33681 | 0.0238 | 0.02375 | Single Specially Orthotropic |
| **0/90/90/0** | 1.05931 | 1.05931 | 1.05857 | 0.0699 | 0.06986 | Symmetric Cross ply |
| **90/0/0/90** | 0.44116 | 0.44116 | 0.44111 | 0.0114 | 0.01134 | Symmetric Cross ply |
| **0/90/0/90** | 0.752 | 0.70945 | 0.70915 | 5.6982 | 0.04229 | Antisymmetric Cross Ply |
| **60/-60/45/-45** | 0.40891 | 0.40463 | 0.40508 | 0.9367 | 0.11122 | Balanced Multiple Angle Ply |
| **30/-30/30/-30** | 0.69638 | 0.69638 | 0.69709 | 0.102 | 0.10196 | Antisymmetric Angle Ply |
| **45/-45/45/-45** | 0.45911 | 0.45911 | 0.45982 | 0.1547 | 0.15465 | Antisymmetric Laminates |
| **60/-60/60/-60** | 0.36215 | 0.36215 | 0.36241 | 0.0718 | 0.0718 | Antisymmetric Laminates |
| **30/30/30/30** | 0.57068 | 0.57068 | 0.57243 | 0.3067 | 0.30666 | Single anisotropic layer |
| **30/-60/-60/30** | 0.56547 | 0.56547 | 0.56685 | 0.2441 | 0.24405 | Symmetric Multiple Angle Layers |

| | | | | | | |
|---|---|---|---|---|---|---|
| **30/-30/-30/30** | 0.64083 | 0.64083 | 0.64219 | 0.2123 | 0.21223 | Symmetric angle Ply |
| **45/30/-30/45** | 0.49629 | 0.49629 | 0.49706 | 0.1552 | 0.15516 | Antisymmetric Multiple Angle Ply |
| **30/30/-30/-30** | 0.6115 | 0.6115 | 0.61163 | 0.0213 | 0.02126 | Antisymmetric Angle Ply |
| **30/-30/0/90** | 0.55642 | 0.55097 | 0.5513 | 0.9202 | 0.0599 | Anisotropic |

Buckling load results using S-Glass and High Strength Graphite/Epoxy hybrid material properties for the composite columns are presented in Table 5.5. High Strength Graphite/Epoxy material was used for layers with $0^o$ and $\pm 30^o$ and S-Glass/Epoxy for the rest of the orientations. Higher error values between the analytical and numerical results were exhibited when combining two materials using Eq. (23). Considering the coupling and extensional effect in Eq. (36) to capture the complexity in behavior of hybrid carbon/glass fiber composites, the error values are decreased and the analytical results showed an excellent agreement with the numerical results.

Table 5.5 Analytical vs. numerical buckling loads for different layup sequences for hybrid Graphite and S-Glass/Epoxy composites.

| **Ply Orientation** | **Analytical Results, N, Eq. (23)** | **Analytical Results, N, Eq. (36)** | **Numerical Results, N** | **% Error, Eq. (23)** | **% Error, Eq. (36)** |
|---|---|---|---|---|---|
| **30/-30/60/-60** | 0.61347 | 0.51765 | 0.5222 | 14.8777 | 0.87898 |
| **30/-30/0/90** | 0.76152 | 0.76011 | 0.75809 | 0.4505 | 0.26576 |
| **0/90/90/0** | 2.71765 | 2.71765 | 2.7096 | 0.2963 | 0.29622 |
| **0/90/0/90** | 1.70108 | 1.49791 | 1.49092 | 12.3546 | 0.46666 |
| **90/0/0/90** | 0.67617 | 0.67617 | 0.67678 | 0.0903 | 0.09022 |

#### 5.5.2.3 Effect of Element Type in FE Analysis

The effect of using different element types in the finite element analysis was also studied. Comparisons between the analytical and numerical results using the quadratic shell element (S8R) and 6-node quadratic triangular thin shell element (STRI65) both with reduced integration schemes having element size equal to 2.5 x 2.5 mm are presented in Table 5.6. Results of the quadrilateral

shell element showed an excellent agreement with the analytical solution for all stacking sequences. On the other hand, the triangular element results showed a good agreement but slightly less accurate comparison with the analytical results.

Table 5.6 Analytical and numerical results with shell and triangular element

| **Ply Orientation** | Analytical Results, N | Shell Element S8R, N | Triangular Thin Shell Element STRI65, N |
|---|---|---|---|
| **0/0/0/0** | 3.053 | 3.04733 | 3.0408 |
| **90/90/90/90** | 0.2106 | 0.21051 | 0.2105 |
| **0/90/90/0** | 2.7045 | 2.69824 | 2.6939 |
| **90/0/0/90** | 0.5673 | 0.56698 | 0.56681 |
| **60/-60/45/-45** | 0.2901 | 0.28093 | 0.2809 |
| **30/-30/30/-30** | 0.9566 | 0.9613 | 0.96156 |
| **45/-45/45/-45** | 0.3549 | 0.3574 | 0.35746 |
| **60/-60/60/-60** | 0.2276 | 0.22822 | 0.22822 |
| **30/30/30/30** | 0.4338 | 0.43854 | 0.43859 |
| **30/-60/-60/30** | 0.4629 | 0.46777 | 0.4681 |
| **30/-30/-30/30** | 0.7703 | 0.77585 | 0.77609 |
| **_45/30/-30/45** | 0.4563 | 0.45972 | 0.4595 |
| **30/30/-30/-30** | 0.6469 | 0.64489 | 0.64742 |
| **30/-30/0/90** | 0.7028 | 0.70451 | 0.70503 |

#### 5.5.2.4 Comparison with Other Solutions

The results of the analytical formula (Equation 36) were compared with previous work conducted by Abramovich et al. [15] for non-symmetric cross ply rectangular laminated composite beams. Table 5.7 presents the results for Ref. [15] and the present analytical solution compared with numerical solution for three different material properties (Glass-Epoxy, and Carbon Epoxy, Kevlar-Epoxy). It was observed that the present analytical formula yields generally more accurate results when compared to finite element results for different material properties and number of layers.

Table 5.7 Comparison of the analytical formula with previous work.

| Glass-epoxy | | | | | | | |
|---|---|---|---|---|---|---|---|
| **Layup orientation** | **$D_{11}$, MPa** | **Non-dimensional buckling parameter, λ** | **Ref. [15], N** | **Analytical solution, N** | **Numerical solution, N** | **Error % Ref. [15]** | **Error %, Analytical solution** |
| **0/90/0/90** | 19.94326 | 37.601 | 0.224966139 | 0.221430227 | 0.22146 | 1.558518 | 0.013445608 |
| **0/90/90/0** | 27.42504 | 39.44 | 0.324493412 | 0.318907912 | 0.31896 | 1.705246 | 0.016333131 |
| **0/90** | 2.492907 | 32.052 | 0.095883283 | 0.094093783 | 0.0941201 | 1.838885 | 0.02796915 |
| **0/90/0** | 12.31033 | 39.438 | 0.258945644 | 0.254059007 | 0.25404 | 1.894469 | 0.00748125 |
| **Carbon-epoxy** | | | | | | | |
| **Layup orientation** | **$D_{11}$, MPa** | **Non-dimensional buckling parameter, λ** | **Ref. [15], N** | **Analytical solution, N** | **Numerical solution, N** | **Error % Ref. [15]** | **Error %, Analytical solution** |
| **0/90/0/90** | 36.48873 | 33.211 | 0.363548532 | 0.364464655 | 0.36401 | 0.126934 | 0.124745968 |
| **0/90/90/0** | 61.44029 | 39.21 | 0.722722825 | 0.726620906 | 0.72557 | 0.393951 | 0.144629146 |
| **0/90** | 4.561092 | 14.842 | 0.081234942 | 0.081193574 | 0.0810311 | 0.250929 | 0.200107074 |
| **0/90/0** | 28.38929 | 39.185 | 0.59333307 | 0.596178399 | 0.59492 | 0.26746 | 0.211077582 |
| **Kevlar-epoxy** | | | | | | | |
| **Layup orientation** | **$D_{11}$, MPa** | **Non-dimensional buckling parameter, λ** | **Ref. [15], N** | **Analytical solution, N** | **Numerical solution, N** | **Error % Ref. [15]** | **Error %, Analytical solution** |
| **0/90/0/90** | 15.85597 | 33.666 | 0.160142295 | 0.160517136 | 0.16004 | 0.063878 | 0.297249221 |
| **0/90/90/0** | 26.25641 | 39.14 | 0.308303108 | 0.309976261 | 0.30912 | 0.264964 | 0.276234448 |

| | | | | | | | |
|---|---|---|---|---|---|---|---|
| **0/90** | 1.981996 | 16.794 | 0.039942816 | 0.039860353 | 0.0397581 | 0.462452 | 0.256527868 |
| **0/90/0** | 12.10614 | 39.109 | 0.252526201 | 0.253564886 | 0.25233 | 0.077695 | 0.487009836 |

L/r = 500, k = 5/6, c = 1 mm.

## 5.6 Conclusions

Rayleigh-Ritz approximation was used to derive a generalized closed form buckling formula for anisotropic laminated composite columns with fixed-fixed end conditions under axial compression which may be considered an extension to the buckling formula of isotropic columns. The buckling load formula was expressed in terms of the composite material effective flexural stiffness coefficient as well as the column geometry. In order to decrease some of the discrepancies in the results with the numerical analysis, the pre-buckling solution was substituted into the bifurcation expression to yield a new formula that includes the coupling and extensional stiffness coefficients. This new analytical formula exhibited an excellent agreement with the finite element analysis results. The parametric study showed that using a single composite material type per column generally yielded less deviation of the analytical solution from the numerical results compared to using a two-material hybrid composite while both cases yielded minimal levels of error when Eq. (36) is used. Additionally, the use of thin triangular and thick quadrilateral shell finite elements was found to be reliable in the buckling predictions. Finally, the present analytical formula yielded excellent correspondence to earlier buckling solutions of cross-ply laminated columns.

## 5.7 References


[1] Silva, N.M.F., Silvestre, N., and Camotim, D., "GBT formulation to analyse the buckling behaviour of FRP composite open-section thin-walled columns," *Composite Structure*s, 93(1) (2010) 79-92.

[2] Silvestre, N., and Camotim, D., "Second-order generalised beam theory for arbitrary orthotropic materials," *Thin-Walled Structures*, 40(9) (2002) 791-820.

[3] Bauld, R.B., and Tzeng, L.A., "Vlasov theory for fiber-reinforced beams with thin-walled open cross-section," *Int. J. Solids Struct*., 20(3) (1984) 277-294.

[4] Rasheed, H.A., and Yousif, O.H., "Buckling of thin laminated orthotropic rings/long cylinders under external pressure," *International Journal of Structural Stability and Dynamics*, 1(4) (2002) 485-507.

[5] Rasheed, H.A., and Yousif, O.H., "Stability of anisotropic laminated rings and long cylinders subjected to external hydrostatic pressure," *Journal of Aerospace Engineering* , 18(3) (2005) 129-138.

[6] Xu, D., Ganesan, R. and Hoa, S.V., "Buckling analysis of tri-axial woven fabric composite structures subjected to bi-axial loading," *Composite Structures*, 21(3) (2007) 140-152.

[7] Shukla, K.K., Nath, Y., Kreuzer, E., and Kumar, K.V.S., "Buckling of laminated composite rectangular plates," *Journal of Aerospace Engineering*, 18(4) (2005) 215-223.

[8] Harik, I.E., and Salamoun, G.L., "The analytical strip method of solution for stiffened rectangular plates," *Computers & Structures*, 29(2) (1988) 283-291.

[9] Sun, L., and Harik, I.E., "Buckling of stiffened antisymmetric laminated plates," *Journal of Engineering Mechanics*, 139(8) (2013) 1110-1123.

[10] Debski, H., Kubiak, T., and Teter, A., "Buckling and postbuckling behaviour of thin-walled composite channel section column," *Composite Structures*, 100 (2013) 195-204.

[11] Shufrin, I., Rabinovitch, O., and Eisenberger M., "Buckling of laminated plates with general boundary conditions under combined compression, tension, and shear- A semi-analytical solution," *Thin-Walled Structures*, 46 (2008) 925-938.

[12] Kerr, A.D., "An extended Kantorovich method for solution of eigenvalue problem," *Int. J. Solid Struct*, 5(6) (1969) 559-572.

[13] Thai, H.T., and Kim, S.E., "Levy-type solution for buckling analysis of orthotropic plates based on two variable refined plate theory," *Composite Structures*, 93(7) (2011) 1738-1746.

[14] Abramovich, H., and Livshits, A., "Free vibrations of non-symmetric cross-ply laminated composite beams", *Journal of Sound and Vibration* , 176 (1994) 597-612.

[15] Abramovich, H., Eisenberger, M., and Shulepov, O., "Vibrations and buckling of cross-ply non-symmetric laminated composite beams", *AIAA Journal* , (34) (1996) 1064-1069.

[16] Jones, R.M, Mechanics of Composite Materials, New York: Hemisphere Publishing Corporation, 1975.

[17] Hernandez, V., Roman, J.E., Tomas, A., and Vidal, V., "Lanczos methods in SLEPc," Polytechnic University of Valencia, Province of Valencia, 2006.

[18] Memon, B.A., Su, X.S., "Arc-length technique for nonlinear finite element analysis," Journal of Zhejiang University SCI, 5(5) (2004) 618-628.

[19] Rasheed, H.A., Strengthening Design of Reinforced Concrete with FRP, New York: CRC Press, 2015.

# Chapter 6 - Analytical and Finite Element Buckling Solutions of Fixed-Fixed Anisotropic Laminated Composite Wide Plates under Axial Compression

**Hayder A. Rasheed[1], Rund Al-Masri[2]**

## 6.1 Abstract

**Using Rayleigh-Ritz approximation, a generalized analytical buckling formula was developed of generally anisotropic laminated fixed-fixed composite plates. Using the generalized constitutive equation, the effective extensional, coupling, and flexural stiffness coefficients of the anisotropic layup are determined using dimensional reduction of 6x6 composite stiffness matrix. The resulting explicit formula is expressed in terms of the flexural stiffness coefficients as well as the plate geometry. In order to decrease some of the discrepancy in some of the results, the coupling and extensional effect was considered through the substitution of the pre-buckling solution into the bifurcation expression to yield a new formula. The analytical results are verified against finite element Eigen value solutions for a wide range of anisotropic laminated layups yielding high accuracy. A parametric study is then conducted to examine the effect of ply orientations, material properties and type of element in FE analysis. Relevance of the numerical and analytical results is discussed for all these cases.**

Keywords: Buckling of Composite Plates, Fixed-Fixed Boundary Conditions, Anisotropic Laminated Material, Axial Compression.

[1] Professor, Department of Civil Engineering, Kansas State University, Manhattan, KS 66506

[2] Ph.D. Candidate, Department of Civil Engineering, Kansas State University, Manhattan, KS 66506

## 6.2 Introduction

Laminated composite material use is ever growing in industrial applications such as aerospace, automotive, and civil engineering due to their distinguished properties (High strength-to-weight ratio, high stiffness-to-weight ratio, fatigue, and corrosion resistance). Accordingly, this growth has resulted in increasing the demand for better understanding the mechanics of laminated composites. Wide plates undergo stability (i.e. buckling) issues prior to failure. An extensive amount of research has been conducted to study buckling behavior of plates and shells in recent years [1-17]. Herenica et al. [1] presented a closed form solution for buckling of long anisotropic plates under axial compression ($N_x$) with various boundary conditions. The closed form solution was expressed as:

$$N_x^{cr} = \kappa_x \frac{\pi^2}{b^2} \sqrt{D_{11} D_{22}} \quad \textbf{(1)}$$

Where $D_{ij}$ is the bending stiffness; b is the width of the plate; and $\kappa_x$ is the non-dimensional buckling coefficient related to the boundary conditions. Results validation with existing solutions (Weaver [2] [3], Qiao and Shan [4]) and finite element solutions was conducted, the results showed an excellent agreement. Mahesh et al. [5] developed a general buckling formulation for plates under linearly varying uniaxial compressive load with general out-of-plane boundary conditions. Formula was presented using Rayleigh-Ritz method based on the energy approach along with orthogonal polynomials generated by a Gram-Schmidt process. Results showed a good agreement with differential quadrature (DQ) models [6]. Silva et al. [7] presented a formulation of generalized beam theory (GBT) to study local and global buckling of fiber reinforced polymer composite open section thin-walled columns. Silvestre and Camotim [8] presented a second order

generalized beam theory (GBT) to predict buckling behavior of thin walled arbitrary orthotropic thin-walled members. The second order theory was compared with Bauld and Lih-Shyng theory [9]. The critical buckling load exists for all isotropic or cross-ply orthotropic members according to results. Moreover, no specific bifurcation is detected for a symmetric orthotropic layups along with non-linear path. Ghaheri et al. [10] used Rayleigh-Ritz method to conduct a study on the buckling behavior of symmetrically laminated composite elliptical plates on elastic foundation under uniform in-plane loading with various boundary conditions. Weaver and Nemeth [11] developed a non-dimensional parameters and governing equations to study buckling behavior of rectangular symmetrically laminated composite plates with different boundary conditions under uniform axial compression, uniform shear, or pure in-plane bending loading. Furthermore, bounds for non-dimensional parameters were presented as an indication of percentage gained in the buckling resistance for laminated plates. The results exhibited 26-36% increase in the buckling resistance for tailored simply supported orthotropic plates; with respect to isotropic plates. Moreover, clamped laminated plates exhibited 9-12% increase in the buckling resistance. Xu et al. [12] developed an approximate analytical solution to predict buckling behavior of a tri-axial woven fabric composite structure under bi-axial loading using equivalent anisotropic plate method. The results showed that the analytical solution provides an upper bound solution for buckling; moreover, the solution can be used to predict buckling behavior for real life problem under bi-axial loading. Using analytical strip method (ASM) developed by Harik and Salamoun [13], Sun and Harik [14] developed analytical solution to predict buckling of stiffened antisymmetric laminated composite plates with bending-extension coupling. According to results, plates with free ends contribute to the weakest stiffening effects. Moreover, since the coupling stiffness matrix vanishes, layers with ply orientation $0^o$ and $90^o$ had no effect on the buckling load.

Shufrin et al. [15] presented a semi-analytical solution for buckling of symmetrically laminated rectangular plates under combined tension, compression, and shear with various boundary conditions using multi term Kantorovich method [16]. Stability of the angle-ply laminated plates improved compared to free in-plane restraint plates under biaxial compression/tension, and shear. Additionally, extra in-plane forces were generated because of the in-plane restraint. Using state space concept on Levy type solution, Thai and Kim [17] developed a closed form solution for buckling of orthotropic plates with two opposite simply supported edges using two variable refined plate theories. The results exhibited more accurate solutions than the higher order shear deformation theory.

In this work, a generalized analytical buckling formula for fixed-fixed laminated composite wide plates subjected to axial compression is developed using Rayleigh-Ritz approximation method. Starting with 3D rigidity matrix and using dimensional reduction approach, extensional, coupling, and flexural rigidities in 1D are determined. Moreover, finite element models for the plates are generated using commercial software Abaqus. The finite element numerical solution was compared to the analytical solution resulting in excellent agreement regardless of the complexity of the composite lay-ups used.

## 6.3 Analytical Formulation

A generalized analytical buckling formula for fixed-fixed anisotropic laminated composite wide plates under axial compression is derived using Rayleigh-Ritz approximation.

### 6.3.1 Assumptions

- Buckling occurs in the x-y plane about the z-axis (weak axis).

- The y-axis runs through the thickness of the plate where the composite lamination takes place, Figure 6.1
- The lamination angle ( α ) is measured with respect to the x-axis (i.e. 0° fibers run parallel to the x-axis and 90° fibers run parallel to the z-axis). Accordingly, the angle ( α ) is rotated about the y-axis.
- Plane sections before bending remain plane after bending and perpendicular to the mid surface (i.e. simple beam theory holds).
- Classical lamination theory is applicable with shear deformations ignored.

### 6.3.2 Kinematics

Figure 6.1 presents geometry and the Cartesian coordinates of the fixed-fixed plate. Bending takes place around the z-axis which is the weak axis. The following displacement relations were assumed based on the isotopic Euler first buckling mode:

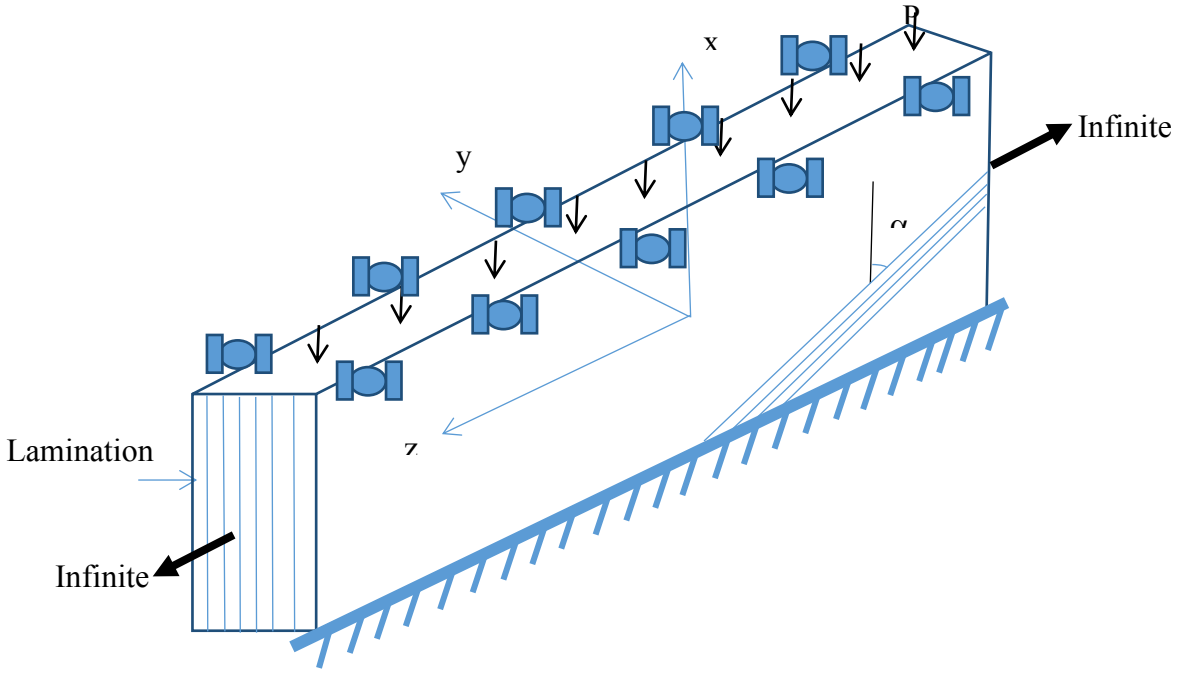


Figure 6.1The wide plate geometry.

$$\boldsymbol{u}\,(\boldsymbol{x}) = \boldsymbol{B_1 x}\,; \quad \boldsymbol{v}\,(\boldsymbol{x}) = \boldsymbol{C_1}(\mathbf{1} - \mathbf{cos}\,\tfrac{\mathbf{2\pi x}}{\boldsymbol{L}}) \tag{2}$$

Where $u(x)$, and $v(x)$ is the axial, and lateral displacements; $B_1$ and $C_1$ are constants to be solved; and x is the distance along the axis of the plate. For an intermediate class of deformation, the axial strain $\varepsilon_x$ and curvature $\kappa_x$are defined as follow.

$$\boldsymbol{\varepsilon_x} = \tfrac{\boldsymbol{du}}{\boldsymbol{dx}} + \tfrac{\mathbf{1}}{\mathbf{2}}(\tfrac{\boldsymbol{dv}}{\boldsymbol{dx}})^{\mathbf{2}} = \boldsymbol{u'} + \tfrac{\mathbf{1}}{\mathbf{2}}\boldsymbol{v'^2}; \qquad \boldsymbol{\kappa_x} = \tfrac{\boldsymbol{d^2 v}}{\boldsymbol{d^2 x}} = \boldsymbol{v''} \tag{3}$$

### 6.3.3 Constitutive equations

Transforming the principle material directions into the plate coordinate system, the stresses and strains are then related in the following equation

$$\begin{Bmatrix} \boldsymbol{\sigma_x} \\ \boldsymbol{\sigma_z} \\ \boldsymbol{\tau_{xz}} \end{Bmatrix} = \begin{bmatrix} \boldsymbol{\bar{Q}_{11}} & \boldsymbol{\bar{Q}_{12}} & \boldsymbol{\bar{Q}_{16}} \\ \boldsymbol{\bar{Q}_{12}} & \boldsymbol{\bar{Q}_{22}} & \boldsymbol{\bar{Q}_{26}} \\ \boldsymbol{\bar{Q}_{16}} & \boldsymbol{\bar{Q}_{26}} & \boldsymbol{\bar{Q}_{66}} \end{bmatrix} \begin{Bmatrix} \boldsymbol{\varepsilon_x} \\ \boldsymbol{\varepsilon_z} \\ \boldsymbol{\gamma_{xz}} \end{Bmatrix} \tag{4}$$

Where $\bar{Q}_{ij}$ matrix represents the transformed reduced stiffness matrix as defined in standard composite textbooks [18]. Accordingly, the coupled force-strain relationship is established as follows:

$$\begin{Bmatrix} \boldsymbol{N_x} \\ \boldsymbol{N_z} \\ \boldsymbol{N_{xz}} \\ \boldsymbol{M_x} \\ \boldsymbol{M_z} \\ \boldsymbol{M_{xz}} \end{Bmatrix} = \begin{bmatrix} \boldsymbol{A_{11}} & \boldsymbol{A_{12}} & \boldsymbol{A_{16}} & \boldsymbol{B_{11}} & \boldsymbol{B_{12}} & \boldsymbol{B_{16}} \\ \boldsymbol{A_{12}} & \boldsymbol{A_{22}} & \boldsymbol{A_{26}} & \boldsymbol{B_{12}} & \boldsymbol{B_{22}} & \boldsymbol{B_{26}} \\ \boldsymbol{A_{16}} & \boldsymbol{A_{26}} & \boldsymbol{A_{66}} & \boldsymbol{B_{16}} & \boldsymbol{B_{26}} & \boldsymbol{B_{66}} \\ \boldsymbol{B_{11}} & \boldsymbol{B_{12}} & \boldsymbol{B_{16}} & \boldsymbol{D_{11}} & \boldsymbol{D_{12}} & \boldsymbol{D_{16}} \\ \boldsymbol{B_{12}} & \boldsymbol{B_{22}} & \boldsymbol{B_{26}} & \boldsymbol{D_{12}} & \boldsymbol{D_{22}} & \boldsymbol{D_{26}} \\ \boldsymbol{B_{16}} & \boldsymbol{B_{26}} & \boldsymbol{B_{66}} & \boldsymbol{D_{16}} & \boldsymbol{D_{26}} & \boldsymbol{D_{66}} \end{bmatrix} \begin{Bmatrix} \boldsymbol{\varepsilon_x} \\ \boldsymbol{\varepsilon_z} \\ \boldsymbol{\gamma_{xz}} \\ \boldsymbol{\kappa_x} \\ \boldsymbol{\kappa_z} \\ \boldsymbol{\kappa_{xz}} \end{Bmatrix} \tag{5}$$

Where:

$$\boldsymbol{A_{ij}} = \sum_{\boldsymbol{k=1}}^{\boldsymbol{N}} \boldsymbol{\bar{Q}_{ij} t_k}$$

$$\boldsymbol{B_{ij}} = \sum_{\boldsymbol{k=1}}^{\boldsymbol{N}} \boldsymbol{\bar{Q}_{ij} t_k \bar{y}_k}$$

$$\boldsymbol{D_{ij}} = \sum_{k=1}^{N} \boldsymbol{\bar{Q}_{ij} t_k} (\boldsymbol{\bar{y}_k^2} + \frac{\boldsymbol{t_k^2}}{\boldsymbol{12}}) \quad \textbf{(6)}$$

$$\boldsymbol{t_k} = \boldsymbol{y_k} - \boldsymbol{y_{k-1}}$$

$$\boldsymbol{\bar{y}_k} = \frac{\boldsymbol{y_k} + \boldsymbol{y_{k-1}}}{\boldsymbol{2}}$$

In which $A_{ij}$,$B_{ij}$, and $D_{ij}$ are the axial, coupling, and flexural rigidity coefficients. $t_k$ = thickness of the k-th ply; and N = number of different plies in the stacking sequence.

To generate the three dimensional (3D) rigidity matrix, material properties and the fiber orientations are used in equation (5). After dimensional reduction approach and applying the zero forces and moments, the dimension is reduced to 1D anisotropic axial, coupling and flexural rigidities.

$$\begin{Bmatrix} \boldsymbol{N_x} \\ \boldsymbol{N_z} \\ \boldsymbol{N_{xz}} \\ \boldsymbol{M_x} \\ \boldsymbol{M_z} \\ \boldsymbol{M_{xz}} \end{Bmatrix} = \begin{bmatrix} \boldsymbol{A_{11}} & \boldsymbol{A_{12}} & \boldsymbol{A_{16}} & \boldsymbol{B_{11}} & \boldsymbol{B_{12}} & \boldsymbol{B_{16}} \\ \boldsymbol{A_{12}} & \boldsymbol{A_{22}} & \boldsymbol{A_{26}} & \boldsymbol{B_{12}} & \boldsymbol{B_{22}} & \boldsymbol{B_{26}} \\ \boldsymbol{A_{16}} & \boldsymbol{A_{26}} & \boldsymbol{A_{66}} & \boldsymbol{B_{16}} & \boldsymbol{B_{26}} & \boldsymbol{B_{66}} \\ \boldsymbol{B_{11}} & \boldsymbol{B_{12}} & \boldsymbol{B_{16}} & \boldsymbol{D_{11}} & \boldsymbol{D_{12}} & \boldsymbol{D_{16}} \\ \boldsymbol{B_{12}} & \boldsymbol{B_{22}} & \boldsymbol{B_{26}} & \boldsymbol{D_{12}} & \boldsymbol{D_{22}} & \boldsymbol{D_{26}} \\ \boldsymbol{B_{16}} & \boldsymbol{B_{26}} & \boldsymbol{B_{66}} & \boldsymbol{D_{16}} & \boldsymbol{D_{26}} & \boldsymbol{D_{66}} \end{bmatrix} \begin{Bmatrix} \boldsymbol{\varepsilon_x} \\ \boldsymbol{\varepsilon_z = 0} \\ \boldsymbol{\gamma_{xz} = 0} \\ \boldsymbol{\kappa_x} \\ \boldsymbol{\kappa_z = 0} \\ \boldsymbol{\kappa_{xz} = 0} \end{Bmatrix} \quad \textbf{(7)}$$

Extracting the second, third, fifth, and sixth linear equations from equation (7), the axial strain and axial curvature ($\boldsymbol{\varepsilon_x}$ ,$\boldsymbol{\kappa_x}$) is solved in terms of the rest of the deformation components. Since the rest of the deformation components for wide plate are equal zero resulting in equation (8):

$$\begin{bmatrix} \boldsymbol{N_x} \\ \boldsymbol{M_x} \end{bmatrix} = \begin{bmatrix} \boldsymbol{A_{11}} & \boldsymbol{B_{11}} \\ \boldsymbol{B_{11}} & \boldsymbol{D_{11}} \end{bmatrix} \begin{Bmatrix} \boldsymbol{\varepsilon_x} \\ \boldsymbol{\kappa_x} \end{Bmatrix} \quad \textbf{(8)}$$

The axial force and in-plane moment vs. the axial strain and in-plane curvature relationship can be expressed in terms of the generally anisotropic material properties

$$\begin{bmatrix} \boldsymbol{N_x} \\ \boldsymbol{M_x} \end{bmatrix} = \begin{bmatrix} \boldsymbol{A_{11}} & \boldsymbol{B_{11}} \\ \boldsymbol{B_{11}} & \boldsymbol{D_{11}} \end{bmatrix} \begin{Bmatrix} \boldsymbol{\varepsilon_x} \\ \boldsymbol{\kappa_x} \end{Bmatrix} \quad \textbf{(9)}$$

It may be observed that equation 9 the material properties for wide plate is expressed in terms extensional, coupling, and bending stiffnesses in the principal directions.

### 6.3.4 Energy Formulation

A generalized analytical buckling formula was derived using Rayleigh-Ritz approximation based on the energy approach. Strain energy can be expressed in terms of the integration of the applied loads multiplying the corresponding deformations.

$$\boldsymbol{U = \int_0^L \left(\frac{1}{2} N_x \varepsilon_x + \frac{1}{2} M_x \kappa_x\right) dx}$$

$$\boldsymbol{= \int_0^L \frac{1}{2} (A_{11} \varepsilon_x^2 + B_{11} \varepsilon_x \kappa_x)\, dx + \int_0^L \frac{1}{2} (B_{11} \varepsilon_x \kappa_x + D_{11} \kappa_x^2)\, dx} \quad \textbf{(10)}$$

Equation (11) expresses the potential of external loads

$$\boldsymbol{W = -P\, u(L)} \quad \textbf{(11)}$$

Taking the total potential energy function and substituting equations (10) and (11) into equation (12)

$$\boldsymbol{\Pi = U - W = \int_0^L \frac{1}{2} (A_{11} \varepsilon_x^2 + 2B_{11} \varepsilon_x \kappa_x + D_{11} \kappa_x^2)\, dx + P\, u(L)} \quad \textbf{(12)}$$

$$\boldsymbol{\Pi = \frac{1}{2} A_{11} B_1^2 L + \frac{1}{4} A_{11} B_1 C_1^2 \left(\frac{2\pi}{L}\right)^2 + \frac{3}{32} A_{11} C_1^4 L \left(\frac{2\pi}{L}\right)^4 + \frac{1}{4} D_{11} C_1^2 L \left(\frac{2\pi}{L}\right)^4 + P B_1 L} \quad \textbf{(13)}$$

Minimizing the total potential energy function with respect to $B_1$ and $C_1$, setting the resulting expressions to zero, performing the integration by parts and manipulating the equations to give:

$$\boldsymbol{\frac{\partial \Pi}{\partial B_1} = A_{11} B_1 L + \frac{A_{11} C_1^2 L}{4} \left(\frac{2\pi}{L}\right)^2 + PL = 0} \quad \textbf{(14)}$$

$$\frac{\partial \Pi}{\partial C_1} = \frac{A_{11}B_1C_1L}{2}\left(\frac{2\pi}{L}\right)^2 + \frac{3A_{11}C_1^3L}{8}\left(\frac{2\pi}{L}\right)^4 + \frac{D_{a11}C_1L}{2}\left(\frac{2\pi}{L}\right)^4 = 0 \quad (15)$$

Solving equation (14) for $B_1$ then substituting the resulting expression into equation (15), equation (17) is formulated in terms of $C_1$.

$$B_1 = -\frac{C_1^2}{4}\left(\frac{2\pi}{L}\right)^2 - \frac{P}{A_{11}} \quad (16)$$

$$\left[\frac{1}{4}A_{11}LC_1^2\left(\frac{2\pi}{L}\right)^4 - \frac{PL}{2}\left(\frac{2\pi}{L}\right)^2 + \frac{1}{2}D_{11}L\left(\frac{2\pi}{L}\right)^4\right]C_1 = 0 \quad (17)$$

Solving Equation 17 for $C_1$:

$$C_1 = zero, \qquad Trivial\ solution$$

$$C_1 = \sqrt{\frac{P/2 - 1/2\, D_{11}(2\pi/L)^2}{1/4\, A_{11}(2\pi/L)^2}} \quad (18)$$

In order for the $C_1$ value to be real, the discriminant must be at least zero. By setting the discriminant to zero, a closed form solution for the critical buckling load is derived:

$$P_{cr} = \frac{4D_{11}\pi^2}{L^2} \quad (19)$$

Euler buckling formula for the fixed-fixed isotropic plate is reduced down with an effective length factor of 0.5 when $D_{ani}$ is replaced with $E'I$ (where $E' = E/(1-\nu)$) of the plate in equation (19).

### 6.3.5 Pre-buckling Solution

In order to decrease some discrepancy between the analytical and numerical results, the pre-buckling solution of the laminated composite plate is considered since the coupling effect ($B_{ani}$)

in all terms in the standard Rayleigh-Ritz approximation lent to zero. During pre-buckling and prior reaching the buckling load, the in-plane moment is set to zero

$$\boldsymbol{M_x = B_{11}\epsilon_x + D_{11}\kappa_x} \tag{20}$$

$$\boldsymbol{0 = B_{11}\epsilon_x + D_{11}\kappa_x}$$

$$\boldsymbol{\kappa_x = -\frac{B_{11}}{D_{11}}\epsilon_x} \tag{21}$$

The axial force versus the axial strain is expressed in terms of the generally anisotropic material properties when substituting Eq. (21) into the axial force equation (22)

$$\boldsymbol{P_x = A_{11}\epsilon_x + B_{11}\kappa_x} \tag{22}$$

$$\boldsymbol{P_x = A_{11}\epsilon_x - \frac{B_{11}^2}{D_{11}}\epsilon_x}$$

$$\boldsymbol{P_x = A_{eff}\epsilon_x} \tag{23}$$

Where

$$\boldsymbol{A_{eff} = A_{11} - \frac{B_{11}^2}{D_{11}}} \tag{24}$$

Based on the assumed sign convention, the axial force ($P_x$) is positive and in compression. On the other hand, the axial strain ($\epsilon_x$) is negative even though it is in compression as illustrated in Eq. (25)

$$\boldsymbol{u = -B_1 x} \tag{25}$$

Using the axial strain in Eq. (3), setting the lateral displacement term to zero, and substituting equation (25), the axial strain can be expressed as

$$\boldsymbol{\epsilon_x = -B_1} \tag{26}$$

A relationship between the axial force and the unknown constant ($B_1$) is obtained by substituting Eq. (26) into Eq. (23), i.e.

$$-\boldsymbol{B_1} = \frac{\boldsymbol{P_x}}{\boldsymbol{A_{eff}}} \tag{27}$$

### 6.3.6 Bifurcation Solution in terms of Pre-buckling Deformation

By substituting Eq. (27) into the total potential energy function given by Eq. (13), one obtains

$$\boldsymbol{\Pi} = \frac{1}{2}\boldsymbol{A_{11}}(\frac{\boldsymbol{P}}{\boldsymbol{A_{eff}}})^2\boldsymbol{L} - \frac{1}{4}\boldsymbol{A_{11}}(\frac{\boldsymbol{P}}{\boldsymbol{A_{eff}}})\boldsymbol{C_1^2}\left(\frac{2\pi}{L}\right)^2 + \frac{3}{32}\boldsymbol{A_{11}C_1^4L}\left(\frac{2\pi}{L}\right)^4 + \frac{1}{4}\boldsymbol{D_{11}C_1^2L}\left(\frac{2\pi}{L}\right)^4 - \boldsymbol{PL}\frac{\boldsymbol{P}}{\boldsymbol{A_{eff}}} \tag{28}$$

Minimizing the total potential energy with respect to $C_1$, setting the resulting expression to zero, and manipulating the equation, one gets

$$\frac{\boldsymbol{\partial\Pi}}{\boldsymbol{\partial C_1}} = -\frac{\boldsymbol{A_{11}P_1C_1L}}{\boldsymbol{2A_{eff}}}\left(\frac{2\pi}{L}\right)^2 + \frac{\boldsymbol{12A_{11}C_1^3L}}{\boldsymbol{32}}\left(\frac{2\pi}{L}\right)^4 + \frac{\boldsymbol{D_{11}C_1L}}{\boldsymbol{2}}\left(\frac{2\pi}{L}\right)^4 = \boldsymbol{0} \tag{29}$$

By solving Eq. (29), one gets

$$\boldsymbol{C_1 = 0} \quad \textbf{which is a trivial solution}$$

$$\textbf{or} \quad \boldsymbol{C_1} = \sqrt{\frac{\boldsymbol{32}}{\boldsymbol{12A_{11}}}(\frac{\boldsymbol{L}}{\boldsymbol{2\pi}})^2\left[\frac{\boldsymbol{1}}{\boldsymbol{2}}\boldsymbol{D_{11}}(\frac{\boldsymbol{2\pi}}{\boldsymbol{L}})^2 - \frac{\boldsymbol{PA_{11}}}{\boldsymbol{2A_{eff}}}\right]} \tag{30}$$

The discriminant must be at least zero to have a real value for $C_1$. By setting the discriminant to zero and substituting Eq. (24), a new analytical critical buckling formula is developed considering the coupling effect:

$$\boldsymbol{P_{cr}} = \frac{\boldsymbol{D_{11}\pi^2}}{(\boldsymbol{L}/\boldsymbol{2})^2} - \frac{\boldsymbol{B_{11}^2\pi^2}}{\boldsymbol{A_{11}}(\boldsymbol{L}/\boldsymbol{2})^2} \tag{31}$$

$$\boldsymbol{P_{cr}} = \frac{\boldsymbol{\pi^2}}{\left(\boldsymbol{L}/\boldsymbol{2}\right)^2}\left(\boldsymbol{D_{11}} - \frac{\boldsymbol{B_{11}^2}}{\boldsymbol{A_{11}}}\right) \tag{32}$$

$$\boldsymbol{P_{cr} = \frac{\pi^2}{\left(L/2\right)^2} D_{eff}} \quad \textbf{(33)}$$

Where

$$\boldsymbol{D_{eff} = \left(D_{11} - \frac{B_{11}^2}{A_{11}}\right)} \quad \textbf{(34)}$$

The new formula reduces down to Euler buckling formula of the fixed-fixed isotropic plate in the case of isotropic or specially-orthotropic materials.

## 6.4 Numerical Formulation

Using commercial software package Abaqus, analytical buckling formula was verified with finite element buckling analysis for laminated anisotropic plates. Plates with four layers were assembled with fixed supports at the bottom and fixed-roller support at the top of the plate. Moreover, translation in x-direction and rotation in y direction is prevented. Figure 6.2 presents the boundary conditions and shell edge load which was applied at the top of the plate.

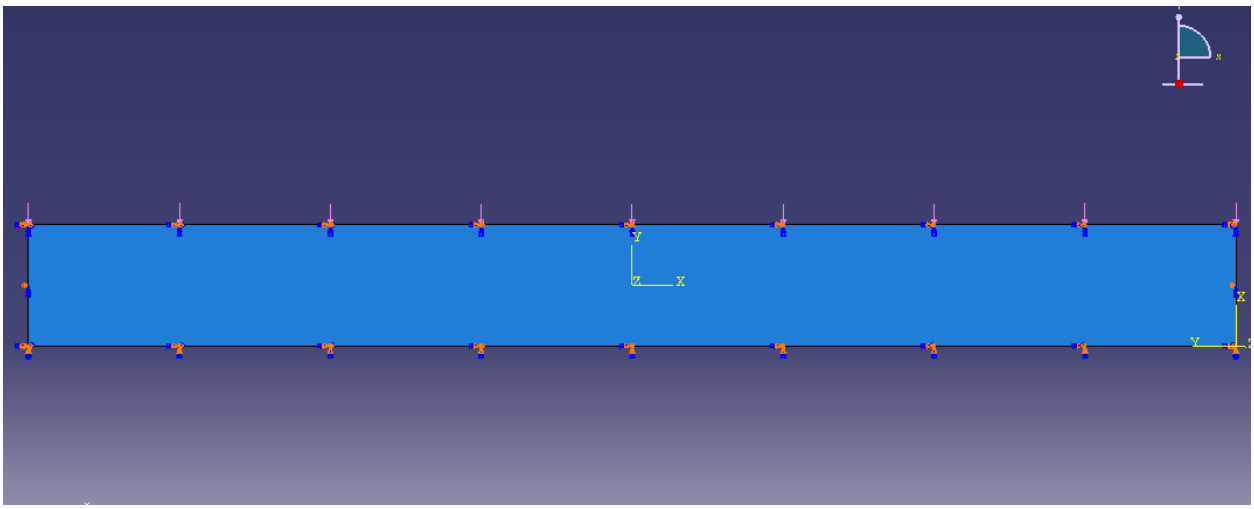

Figure 6.2 Boundary conditions and applied load.

Linear elastic laminated material was used for orthotropic and anisotropic layups, respectively. Additionally, S-Glass/epoxy material was mainly used to simulate the composite plates Quadrilateral eight node doubly curved thick shell element (S8R) was used for modeling the plates in 3D-space as shown in Figure 6.3. Moreover, 3D solid 20-node quadratic brick element (C3D20R) was also attempted. Mesh size equal to 10 mm x 10 mm with total number element equal to 1000 was used after conducting convergence study to select the appropriate size for plates with dimension for width, length, and thickness equal to: 1000 mm x 100 mm x 0.4 mm, respectively.

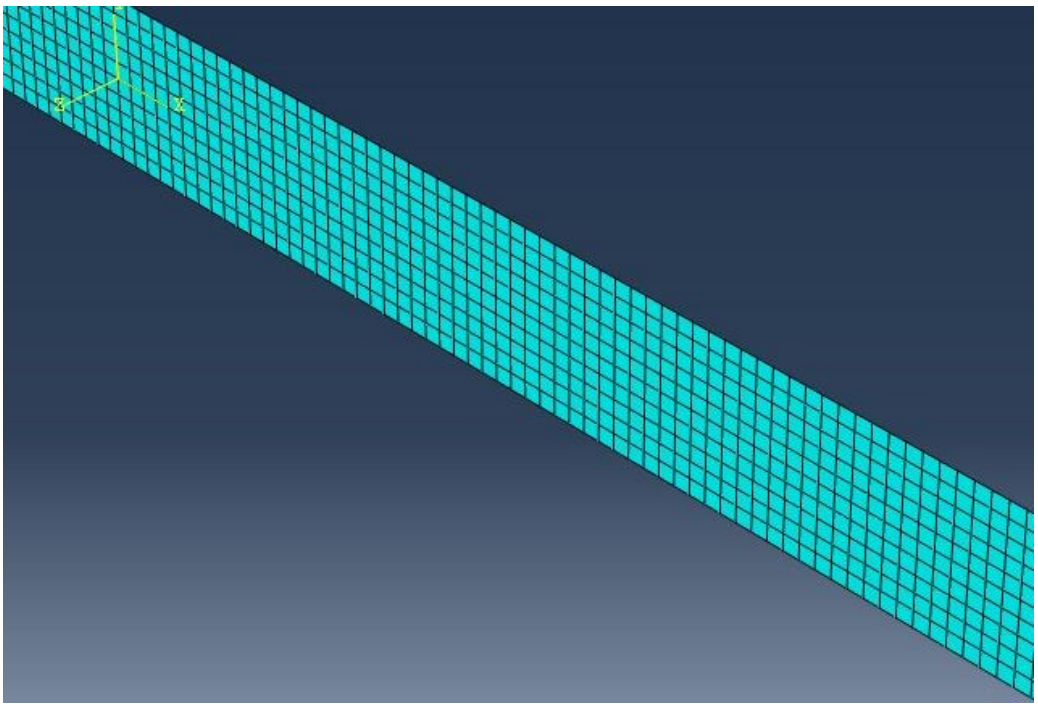

Figure 6.3 Meshed Model.

In this study, two types of analyses were undertaken. To simulate eigenvalue computation, buckling analysis using Lanczos solver was conducted. Eigenvalues and eigenvectors are solved using Lanczos method for complex Hermitian matrix using power methods. Using recurrence relations (multidimensional array values), Lanczos method reduces $m \times m$ symmetric matrix to a tridiagonal matrix [19].

To predict the nonlinear stability response (pre-buckling and buckling) and indicate the existence of pre-buckling deformation in the transverse direction, nonlinear geometry analysis was conducted using the modified Riks analysis of the composite plates. Arc length method which is used in the modified Riks analysis follows the equilibrium path, representing either the bifurcation points or the limit points. During the analysis, load increments are applied in which equilibrium

iterations converge along the arc length, forcing the constraint equation to be satisfied at every iteration [20].

## 6.5 Results and Applications:

### 6.5.1 Numerical Validation

Table 6.1 illustrates S-Glass/Epoxy material properties; obtained from typical values in an FRP textbook [21], used to simulate the analytical and numerical results for different stacking sequences of composite plates with the following dimensions for width, length, and thickness: 1000 mm x 100 mm x 0.4 mm, respectively. Table 6.2 presents the comparison between the analytical and numerical buckling results for different layup stacking sequences using equations (19) and (31). In general, it was observed that results from Eq. (19) showed a good agreement with numerical results with a minimum error equal to 0.0026% for single specially orthotropic layer (0/0/0/0) and a maximum error equal to 11.4776% for the balanced angle ply (60/60/30/-30). Furthermore, results from Eq. (31) yielded an excellent agreement with numerical results with maximum error equal to 4.8984% for the antisymmetric angle ply (30/-30/30/-30). In general, considering the coupling and extensional effect in Eq. (31) reduced the error value significantly. It is important to note that the layup with maximum error yield the analytical buckling load on the un-conservative side.

Table 6.1 S-Glass/Epoxy material properties [21].

| **Material** | $E_{11}$ | $E_{22}$ | $G_{12}$ | $\nu_{12}$ |
|---|---|---|---|---|
| **S-Glass/Epoxy** | 55.0 GPa | 16.0 GPa | 7.6 GPa | 0.28 |

Table 6.2 Comparison of analytical and numerical buckling load for different layup sequences.

| **Ply orientation** | **Analytical Results Eq. (19), N** | **Analytical Results Eq. (31), N** | **Numerical Results, N** | **% Error, Eq. (19)** | **% Error, Eq. (31)** | **Layup Type** |
|---|---|---|---|---|---|---|
| **0/0/0/0** | 1.18507 | 1.18507 | 1.1851 | 0.0026 | 0.0026 | Single Specially Orthotropic |
| **90/90/90/90** | 0.34475 | 0.34475 | 0.3448 | 0.0146 | 0.0146 | Single Specially Orthotropic |
| **30/-30/30/-30** | 0.84436 | 0.84436 | 0.803 | 4.8984 | 4.8984 | Antisymmetric Angle Ply |
| **45/-45/45/-45** | 0.59074 | 0.59074 | 0.5668 | 4.0526 | 4.0526 | Antisymmetric Angle Ply |
| **60/-60/60/-60** | 0.4242 | 0.4242 | 0.4173 | 1.6266 | 1.6266 | Antisymmetric Angle Ply |
| **30/-30/0/0** | 1.01471 | 0.99326 | 0.9796 | 3.4602 | 1.3753 | Anisotropic |
| **30/-30/0/90** | 0.64708 | 0.62754 | 0.6141 | 5.0968 | 2.1417 | Anisotropic |

| | | | | | | |
|---|---|---|---|---|---|---|
| **30/30/30/30** | 0.84436 | 0.84436 | 0.8465 | 0.2535 | 0.2535 | Single anisotropic layer |
| **30/-30/-30/30** | 0.84436 | 0.84436 | 0.8461 | 0.2061 | 0.2061 | Symmetric angle Ply |
| **0/90/90/0** | 1.08003 | 1.08003 | 1.0796 | 0.0399 | 0.0399 | Symmetric Cross Ply |
| **30/-60/-60/30** | 0.79184 | 0.79184 | 0.7928 | 0.1213 | 0.1213 | Symmetric Multiple Angle Ply |
| **0/90/0/90** | 0.76491 | 0.72164 | 0.7216 | 5.6622 | 0.0056 | Antisymmetric Cross Ply |
| **-45/30/-30/45** | 0.62244 | 0.62244 | 0.6024 | 3.2196 | 3.2196 | Antisymmetric Multiple Angle Ply |
| **90/0/0/90** | 0.44979 | 0.44979 | 0.4499 | 0.0245 | 0.0245 | Symmetric Cross Ply |
| **30/-30/45/-45** | 0.71755 | 0.70074 | 0.669 | 6.7661 | 4.5295 | Balanced Angle Ply |
| **60/-60/45/-45** | 0.50747 | 0.49722 | 0.48273 | 4.8752 | 2.9143 | Balanced Angle Ply |
| **60/-60/30/-30** | 0.63428 | 0.5821 | 0.56148 | 11.4776 | 3.5424 | Balanced Angle Ply |

Figure 6.4 presents load versus mid height deflection curve for two different stacking sequences obtained from the finite element nonlinear Riks analysis along with the analytical solution Eq. (31) for comparison. Results exhibits an excellent agreement between analytical and numerical (FE) solutions. Anisotropic layup (30/-30/0/0) exhibit higher buckling load with minimal error between the analytical and numerical results. Furthermore, (30/-30/0/90) layup shows lower buckling load value.

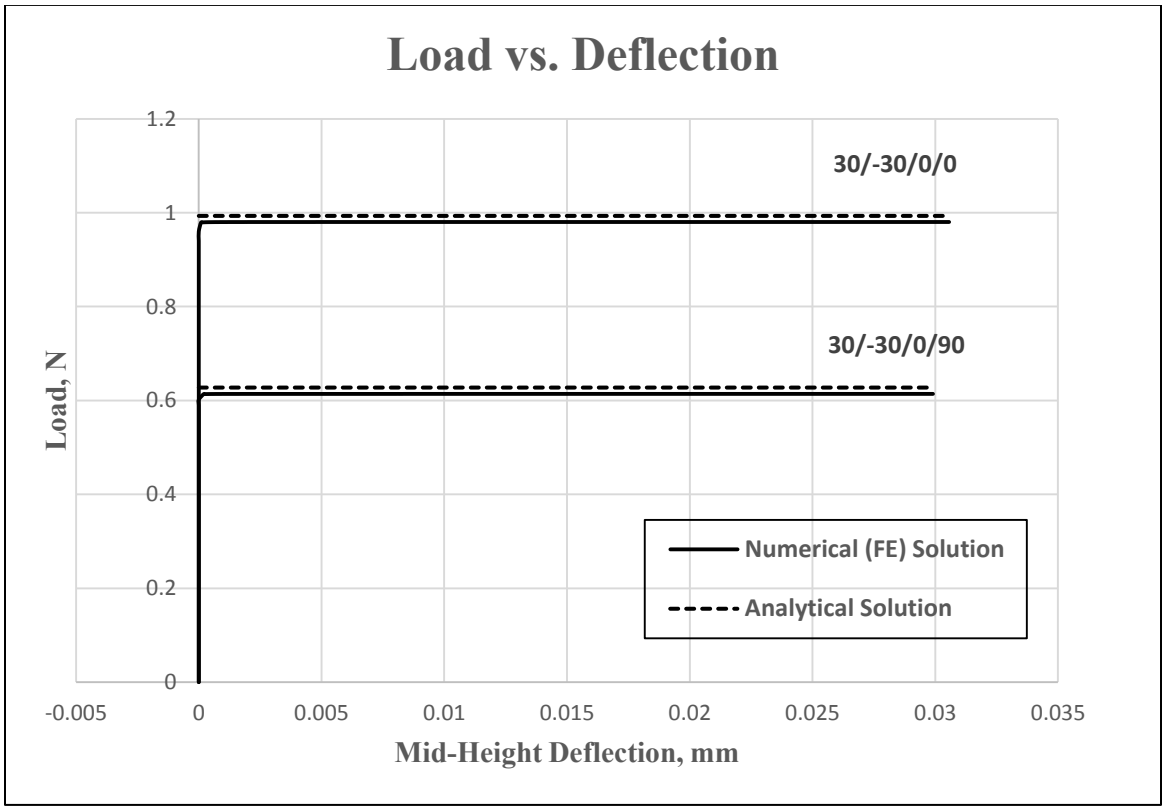


Figure 6.4 Analytical versus numerical solutions.

## 6.5.2 Parametric Study

### 6.5.2.1 Effect of Ply Orientation

Studying the effect of having different stacking sequences was conducted for plates with the following dimensions: 1000 mm x 100 mm x 0.4 mm for width, length, and thickness, respectively.

Table 6.2 reports buckling load values for different stacking sequences with values range between 0.3448 N and 1.1851 N. As observed in Figure 6.5, the buckling mode shape of the fixed-fixed anisotropic plate for symmetric cross ply layup (0/90/0/90) is uniform along the plate. On the other hand, some of the stacking sequences such as the balanced angle ply layup (30/-30/45/-45) exhibit an edge effect during buckling as shown in Figure 6.6 which may contribute to a slight difference between analytical and numerical results.

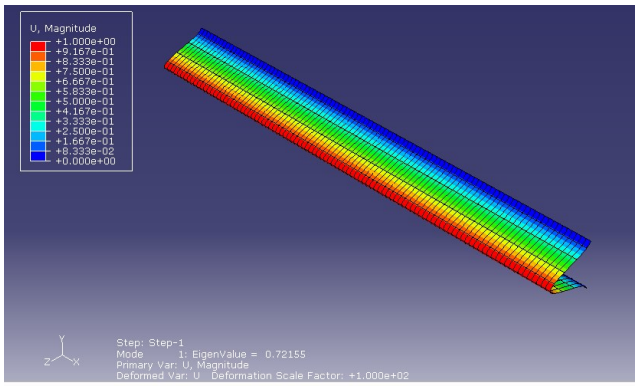


Figure 6.5 Buckling shape of the fixed-fixed plate for symmetric cross ply (0/90/0/90).

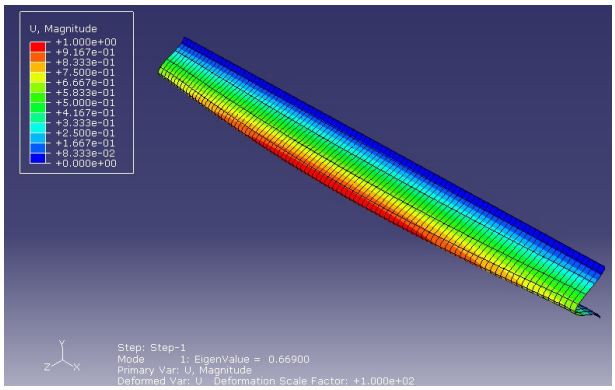


Figure 6.6 Buckling shape of the fixed-fixed plate for balanced angle ply (30/-30/45/-45).

### 6.5.2.2 Effect of Material Properties

To study the effect of changing material properties on the stability of the laminated composite plate, two types of material were used. S-Glass/Epoxy and High Strength Graphite/Epoxy were used to conduct this study and their properties; reported in an FRP textbook [21], are reported in Table 6.1and Table 6.3.

Table 6.3 High Strength Graphite/Epoxy Material Properties [21].

| **Material** | $E_{11}$ | $E_{22}$ | $G_{12}$ | $\nu_{12}$ |
|---|---|---|---|---|
| **High Strength Graphite/Epoxy** | 145.0 GPa | 10.0 GPa | 4.8 GPa | 0.25 |

Table 6.2 and Table 6.4 illustrates buckling load values for S-Glass/Epoxy and High Strength Graphite/Epoxy material with different stacking sequences. In general, S-Glass/Epoxy exhibits lower buckling load values than High Strength Graphite/Epoxy because of its lower stiffness values in the fiber direction. Additionally, the error value between analytical and numerical solution increases for High Strength Graphite/Epoxy since it has higher $E_{11}/E_{22}$ ratio compared with S-Glass/Epoxy. As mentioned earlier, Eq. (31) reduced down the error significantly since the coupling and extensional effect was taken into account compared with Eq. (19). Single specially-orthotropic layup (0/0/0/0) exhibited the maximum buckling load value which is equal to 3.06622 N since all fibers are aligned along the loading axis due to the vanish of the coupling term.

Table 6.4 Analytical and numerical results for different layup sequences for High Strength Graphite /Epoxy.

| **Ply orientation** | **Analytical Results Eq. (19), N** | **Analytical Results Eq. (31), N** | **Numerical Results, N** | **% Error, Eq. (19)** | **% Error, Eq. (31)** | **Layup Type** |
|---|---|---|---|---|---|---|
| **0/0/0/0** | 3.06622 | 3.06622 | 3.0617 | 0.1475 | 0.1475 | Single Specially Orthotropic |
| **90/90/90/90** | 0.21147 | 0.21147 | 0.2116 | 0.0615 | 0.0615 | Single Specially Orthotropic |
| **30/-30/30/-30** | 1.83359 | 1.83359 | 1.5798 | 13.8412 | 13.8412 | Antisymmetric Angle Ply |
| **45/-45/45/-45** | 0.94692 | 0.94692 | 0.8281 | 12.5481 | 12.5481 | Antisymmetric Angle Ply |
| **60/-60/60/-60** | 0.40621 | 0.40621 | 0.3766 | 7.2894 | 7.2894 | Antisymmetric Angle Ply |
| **30/-30/0/0** | 2.4499 | 2.33362 | 2.2216 | 9.3188 | 4.80027 | Anisotropic |
| **30/-30/0/90** | 1.20095 | 1.11183 | 1.0028 | 16.4995 | 9.80636 | Anisotropic |
| **30/30/30/30** | 1.83359 | 1.83359 | 1.8336 | 0.0006 | 0.0006 | Single anisotropic layer |
| **30/-30/-30/30** | 1.83359 | 1.83359 | 1.8279 | 0.3104 | 0.3104 | Symmetric angle Ply |
| **0/90/90/0** | 2.70938 | 2.70938 | 2.7043 | 0.1875 | 0.1875 | Symmetric Cross Ply |
| **30/-60/-60/30** | 1.65517 | 1.65517 | 1.6496 | 0.3366 | 0.3366 | Symmetric Multiple Angle Ply |

| | | | | | | |
|---|---|---|---|---|---|---|
| **0/90/0/90** | 1.63884 | 1.40574 | 1.4044 | 14.3053 | 0.09533 | Antisymmetric Cross Ply |
| **-45/30/-30/45** | 1.05776 | 1.05776 | 0.9601 | 9.2328 | 9.2328 | Antisymmetric Multiple Angle Ply |
| **90/0/0/90** | 0.56831 | 0.56831 | 0.5683 | 0.0018 | 0.0018 | Symmetric Cross Ply |
| **30/-30/45/-45** | 1.39026 | 1.28423 | 1.109 | 20.2308 | 13.6448 | Balanced Angle Ply |
| **60/-60/45/-45** | 0.67657 | 0.59554 | 0.5638 | 16.6679 | 5.3297 | Balanced Angle Ply |
| **60/-60/30/-30** | 1.1199 | 0.77879 | 0.66467 | 40.6492 | 14.6536 | Balanced Angle Ply |

#### 6.5.2.3 Effect of Element Type in FE Analysis

The effect of using different element types in finite element analysis of S-Glass/Epoxy was studied. Using quadratic shell element (S8R) and quadratic solid element (C3D20R) both with reduced integration schemes and mesh size equal to 10.0 mm x 10.0 mm. Table 6.5 presents comparison between analytical and numerical solution. An excellent agreement between analytical and shell element results is observed for all stacking sequences. Additionally, solid element results were off in most of the different stacking sequences. Accordingly, it might be argued that for this type of analysis the shell element (S8R) is more reliable than solid element (C3D20R).

Table 6.5 Analytical and numerical results with shell and solid element

| **Ply Orientation** | **Analytical Results, N** | **Shell Element S8R, N** | **Solid Element C3D20R, N** |
|---|---|---|---|
| **0/0/0/0** | 1.18507 | 1.1851 | 0.739497 |
| **90/90/90/90** | 0.34475 | 0.3448 | 0.2149 |
| **30/-30/30/-30** | 0.84436 | 0.803 | 0.521911 |
| **45/-45/45/-45** | 0.59074 | 0.5668 | 0.362858 |
| **60/-60/60/-60** | 0.4242 | 0.4173 | 0.261628 |
| **30/-30/0/0** | 0.99326 | 0.9796 | 0.630799 |
| **30/-30/0/90** | 0.62754 | 0.6141 | 0.498114 |
| **30/30/30/30** | 0.84436 | 0.8465 | 0.534503 |
| **30/-30/-30/30** | 0.84436 | 0.8461 | 0.522302 |
| **0/90/90/0** | 1.08003 | 1.0796 | 0.47738 |

| | | | |
|---|---|---|---|
| **30/-60/-60/30** | 0.79184 | 0.7928 | 0.401967 |
| **0/90/0/90** | 0.72164 | 0.7216 | 0.476869 |
| **-45/30/-30/45** | 0.62244 | 0.6024 | 0.44262 |
| **90/0/0/90** | 0.44979 | 0.4499 | 0.477378 |

## 6.6 Conclusion

Using Rayleigh-Ritz approximation, a generalized closed form buckling formula was derived for anisotropic laminated composite plates under axial compression with fixed-fixed conditions. The buckling load formula was expressed in terms of the composite material effective flexural stiffness coefficient as well as the plate geometry. A new formula was developed in terms of extensional, coupling, and flexural coefficients using the pre-buckling solution. The new analytical formula showed an excellent agreement with the numerical results. From the parametric study, it was shown that using composite material with high $E_{11}/E_{22}$ ratio the analytical solution yielded more deviation of the analytical solution from the numerical solution compared with low stiffness composite material. Moreover, some stacking sequences showed an edge effect during buckling therefore a slight difference between the analytical results and numerical results was observed. Additionally, the use of solid elements in the finite element analysis was found to be less reliable compared to the use of shell elements in the buckling predictions.

## 6.7 References

[1] Herencia, J.E., Weaver, P.M., and Friswell, M.I., "Closed-form solutions for buckling of long anisotropic plates with various boundary conditions under axial compression," *Journal of Engineering Mechanics*, vol. 136, no. 9, pp. 1105-1114, 2010.

[2] Weaver, P.M., "Approximate analysis for buckling of compression loaded long rectangular plates with flexural/twist anisotropy," Proc. R. Soc. London, vol. 462, no. 2065 pp. 59-73, 2006.

[3] Weaver, P.D., "Buckling of long clamped anisotropic plates under compression," in American Society of Composites, 22nd Technical Conf., Lancaster, 2007

[4] Qiao, P., and Shan, L., "Explicit local buckling analysis and design of fiber-reinforced plastic composite structural shapes," *Composite Structures*, vol. 70, no. 4, pp. 468-483, 2005.

[5] Mahesh, P.E., and Archibald, S.N., "Buckling od anisotropic composite plates under stress gradient," *Journal of Engineering Mechanics*, vol. 117, no. 2, pp. 260-275, 1991.

[6] Bellman, R.E., and Casti, J., "Differential quadrature and long-term integration," *J. Math. Anal. Appl.*, vol. 34, no. 2, pp. 235-238, 1971.

[7] Silva, N.M.F., Silvestre, N., and Camotim, D., "GBT formulation to analyse the buckling behaviour of FRP composite open-section thin-walled columns," *Composite Structures*, vol. 93, pp. 79-92, 2010.

[8] Silvestre, N., and Camotim, D., "Second-order generalised beam theory for arbitrary orthotropic materials," *Thin-Walled Structures*, vol. 40, pp. 791-820, 2002.

[9] Bauld, R.B., and Tzeng, L.A., "Vlasov theory for fiber-reinforced beams with thin-walled open cross-section," *Int. J. Solids Struct.*, vol. 20, no. 3, pp. 277-94, 1984.

[10] Ghaheri, A., Keshmiri, A., and Taheri-Behrooz, F., "Buckling and vibration of symmetrically laminated composite elliptical plates on an elastic foundation subjected to uniform in-plane force," *Journal of Engineering Mechanics*, vol. 140, no. 7, pp. 1-10, 2014.

[11] Weaver, P.M., Nemeth, M.P., and Taheri-Behrooz, F., "Bounds on flexural properties and buckling response for symmetrically laminated composite plates" J*ournal of Engineering Mechanics*, vol. 133, no. 11, pp. 1-10, 2007.

[12] Xu, D., Ganesan, R. and Hoa, S.V., "Buckling analysis of tri-axial woven fabric composite structures subjected to bi-axial loading," *Composite Structures*, vol. 21, pp. 140-152, 2007.

[13] Harik, I.E., and Salamoun, G.L., "The analytical strip method of solution for stiffened rectangular plates," *Computers & Structures*, vol. 29, no. 2, pp. 283-291, 1988.

[14] Sun, L., and Harik, I.E., "Buckling of stiffened antisymmetric laminated plates," *Journal of Engineering Mechanics*, vol. 139, no. 8, 2013.

[15] Shufrin, I., Rabinovitch, O., and Eisenberger M., "Buckling of laminated plates with general boundary conditions under combined compression, tension, and shear- A semi-analytical solution," *Thin-Walled Structures*, vol. 46, pp. 925-938, 2008.

[16] Kerr, A.D., "An extended Kantorovich method for solution of eigenvalue problem," *Int. J. Solid Struct*, vol. 5, no. 6, pp. 559-572, 1969.

[17] Thai, H.T., and Kim S.E., "Levy-type solution for buckling analysis of orthotropic plates based on two variable refined plate theory," *Composite Structures*, vol.93, no. 7, pp. 1738-1746, 2011.

[18] Jones, R.M, Mechanics of composite materials, New York: Hemisphere Publishing Corporation, 1975.

[19] Hernandez, V., Roman, J.E., Tomas, A., and Vidal, V., "Lanczos methods in SLEPc," Polytechnic University of Valencia, Province of Valencia, 2006.

[20] Memon, B.A., Su, X.S., "Arc-length technique for nonlinear finite element analysis," *Journal of Zhejiang University SCI*, vol. 5, no. 5, pp. 618-628, 2004.

[21] Rasheed, H.A., Strengthening Design of Reinforced Concrete with FRP, New York: CRC Press, 2015.

# Chapter 7 - Buckling Solution of Fixed-Free Anisotropic Laminated Composite Columns under Axial Compression using Rayleigh Ritz Formulation

**Hayder A. Rasheed[1] and Rund Al-Masri[2]**

## 7.1 Abstract

**A generalized analytical buckling formula for anisotropic laminated composite fixed-free columns under axial compression is presented on the basis of Rayleigh Ritz displacement field approximation. The effective axial, coupling and flexural stiffness coefficients of the anisotropic layup is determined from the generalized constitutive relationship using dimensional reduction by static condensation of the 3 dimensional composite stiffness matrix. The developed formula is expressed in terms of the generally anisotropic material properties as well as the column geometry. For isotropic and certain classes of laminated composites, the derived formula reduces down to Euler buckling formula. The analytical results are verified against finite element Eigen value solutions for a wide range of anisotropic laminated layups yielding high accuracy. A brief parametric study is then conducted to examine the effect of ply orientations, element thickness, finite element type, and material properties including hybrid carbon/glass fiber composites. Relevance of the numerical and analytical results is discussed for all these cases.**

Keywords: Buckling of Composite Columns, Clamped-free Boundary Conditions, Anisotropic Laminated Composites, Axial Compression.

[1] Professor, Department of Civil Engineering, Kansas State University, Manhattan, KS 66506

[2] Ph.D. Candidate, Department of Civil Engineering, Kansas State University, Manhattan, KS 66506

## 7.2 Introduction

The demand to understand the stability mechanism of laminated composite members has increased in the last few decades due to the growth of using composites in different industrial applications such as aerospace, marine, automotive, and civil engineering. Composite materials have many advantages such as high stiffness-to-weight ratio, high strength-to-weight ratio, as well as fatigue and corrosion resistance. Although limited amount of research has focused on the buckling of anisotropic laminated composite columns, significant amount of studies have been conducted on the stability of composite shells, plates, and cylinders [1-11]. Based on Hellinger-Reissner principal, Cortinez and Piovan [1] developed a theoretical model to study the stability of composite thin-walled beams with shear deformability using nonlinear displacement field. A finite element with fourteen degrees of freedom was used to solve the governing equations. Based on the results, shear flexibility had a significant effect on the stability of the composite beams. Depending on the unified three degrees of freedom shear deformable beam theory, Aydogdu [2] studied the buckling of cross-ply laminated beams with general boundary conditions using Ritz method. The use of the shape function satisfied the requirements for continuity conditions between symmetric cross-ply layers of the beam. The results were compared with previous work for various length-to-thickness ratios and various layups. Abramovich and Livshits [3] studied the free vibrations of non-symmetric cross ply laminated composite beams based on the first order shear deformation theory. Longitudinal, transverse displacement, rotary inertia, and shear deformation were considered in the analysis. The following equation of motion of cross ply laminated composite beams was solved for different boundary conditions:

$$[\mathbf{M}]\{\ddot{q}\}+[\mathbf{C}]\ \{q\} = \{0\} \tag{1}$$

Where [M] is the generalized mass matrix, [C] is the matrix differential operator; and $\{q\}$ is the vector of the generalized displacements. The new approach and Bernoulli-Euler theory were verified against numerical solutions. Abramovich et al. [4] studied the vibrations and buckling of cross-ply non-symmetric rectangular laminated composite beams using the exact method based on Timoshenko equation. A good agreement between analytical and numerical results was observed considering the effect of material properties, number of layers, and boundary conditions. Additionally, a coupling effect was observed between the axial and lateral motion of the non-symmetric layup in the beams. Based on the response surface method and Monte Carlo method, Schanbl [5] presented a model to study buckling of two-layer composite columns with interlayer slip, random material properties, and loading parameters. Using Rayleigh-Ritz method, Herencia et al. [6] presented closed-form solutions for buckling of long plates with flexural anisotropy of simply supported short edges and various boundary conditions for longitudinal edges under axial compression. The closed form solution was expressed with respect to minimum non-dimensional buckling coefficient and stiffness parameters. The results showed an excellent agreement with previous solution and finite element analysis. Ovesy et al. [7] studied the buckling of laminated composite plates with simply supported boundary conditions under uniaxial pure compression using higher order semi analytical finite strip method based on Reddy's higher order plate theory. Matsunga [8] investigated the free vibration and stability of angle-ply laminated composite and sandwich plates under thermal loading. Using two dimensional global higher order deformation theory, the following eigenvalue problem can be expressed as:

$$([\boldsymbol{K}] - \boldsymbol{\omega^2}[\boldsymbol{M}])\{\boldsymbol{U}\} = \{\boldsymbol{0}\} \quad \textbf{(2)}$$

Where [K] is the stiffness matrix which includes the initial thermal stresses term, [M] is the mass matrix, and {U} is the generalized displacement vector. Using energy method and orthogonal

polynomial sequences obtained by a Gram-Schmidt process, Pandey and Sherbourne [9] presented a general formulation for buckling of rectangular anisotropic symmetric angle ply composite plates under linearly varying uniaxial compression loading with clamped and simply supported boundary conditions. Based on the energy approach, Rasheed and Yousif [10] derived a closed form buckling solution to investigate the stability of thin laminated orthotropic composite rings/long cylinders under external pressure. Timarci and Aydogdu [11] studied the buckling of symmetric cross-ply square plates with various boundary conditions under uniaxial, biaxial compression, and compression-tension loading based on the unified five degree of freedom shear deformable plate theory. The results were verified with existing work for various length-to-thickness ratios.

In this study, a closed form buckling solution was derived of anisotropic laminated composite fixed-free columns under axial compression using Rayleigh-Ritz approximation field based on the energy approach. Three dimensional 6 x 6 composite stiffness matrix is converted to 1D axial, coupling, and flexural rigidities using static condensation method. Furthermore, the analytical results were verified against finite element analysis using commercial software Abaqus yielding an excellent agreement between the results.

## 7.3 Analytical Formulation

### 7.3.1 Assumptions and Kinematics

An analytical buckling formula is developed using Rayleigh-Ritz approximation field for fixed free anisotropic laminated composite columns under axial compression. Several assumptions are taken into consideration prior to deriving the analytical formula and can be illustrated in the following points:

- Buckling occurs in the x-y plane about the z-axis (weak axis).

- The y-axis runs through the thickness of the plate where the composite lamination takes place, Figure 7.1.
- The lamination angle ( α ) is measured with respect to the x-axis (i.e. 0° fibers run parallel to the x-axis and 90° fibers run parallel to the z-axis). Accordingly, the angle ( α ) is rotated about the y-axis.
- Plane sections before bending remain plane after bending and perpendicular to the mid surface (i.e. simple beam theory holds).
- Classical lamination theory is applicable with shear deformations ignored.

Figure 7.1 presents the Cartesian coordinates and the geometry of the fixed-free column. Bending takes place about the z-axis which is the weak axis of the column. Equation (3) presents the assumed displacement field based on the isotropic buckling mode:

$$\boldsymbol{u}\,(\boldsymbol{x}) = \boldsymbol{B_1 x}\,; \quad \boldsymbol{v}\,(\boldsymbol{x}) = \boldsymbol{C_1}(\mathbf{1} - \mathbf{cos}\frac{\boldsymbol{\pi x}}{\mathbf{2}\boldsymbol{L}}) \tag{3}$$

Where $u(x)$, v$(x)$ are the axial and lateral displacement, $B_1$ and $C_1$ are constants to be solved and x is the distance along the axis of the column as shown in Figure 7.1. The axial strain $\boldsymbol{\varepsilon_x}$ and curvature $\boldsymbol{\kappa_x}$ are presented in equation (4) depending on the intermediate class of deformation:

$$\boldsymbol{\varepsilon_x} = \frac{\boldsymbol{du}}{\boldsymbol{dx}} + \frac{\mathbf{1}}{\mathbf{2}}(\frac{\boldsymbol{dv}}{\boldsymbol{dx}})^{\mathbf{2}} = \boldsymbol{u'} + \frac{\mathbf{1}}{\mathbf{2}}\boldsymbol{v'^2}; \qquad \boldsymbol{\kappa_x} = \frac{\boldsymbol{d^2v}}{\boldsymbol{d^2x}} = \boldsymbol{v''} \tag{4}$$

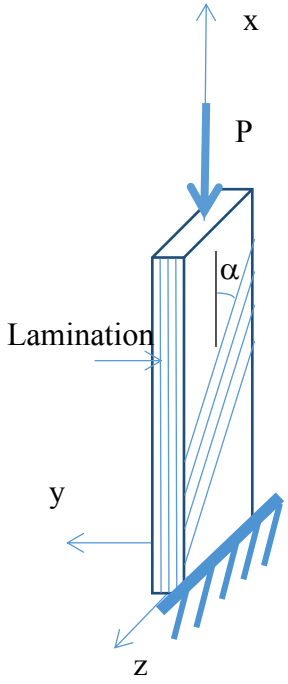


Figure 7.1 Column geometry

### 7.3.2 Constitutive equations

The stresses and strains are related by the transformed reduced stiffness matrix $\bar{Q}_{ij}$ presented in equation (5); as defined in standard composite textbook [12], in order to transform the principle material directions into the column coordinate system.

$$\begin{Bmatrix} \boldsymbol{\sigma_x} \\ \boldsymbol{\sigma_z} \\ \boldsymbol{\tau_{xz}} \end{Bmatrix} = \begin{bmatrix} \boldsymbol{\bar{Q}_{11}} & \boldsymbol{\bar{Q}_{12}} & \boldsymbol{\bar{Q}_{16}} \\ \boldsymbol{\bar{Q}_{12}} & \boldsymbol{\bar{Q}_{22}} & \boldsymbol{\bar{Q}_{26}} \\ \boldsymbol{\bar{Q}_{16}} & \boldsymbol{\bar{Q}_{26}} & \boldsymbol{\bar{Q}_{66}} \end{bmatrix} \begin{Bmatrix} \boldsymbol{\varepsilon_x} \\ \boldsymbol{\varepsilon_z} \\ \boldsymbol{\gamma_{xz}} \end{Bmatrix} \quad \textbf{(5)}$$

Accordingly, the coupled force-strain relationship is established as

$$\begin{Bmatrix} N_x \\ N_z \\ N_{xz} \\ M_x \\ M_z \\ M_{xz} \end{Bmatrix} = \begin{bmatrix} A_{11} & A_{12} & A_{16} & B_{11} & B_{12} & B_{16} \\ A_{12} & A_{22} & A_{26} & B_{12} & B_{22} & B_{26} \\ A_{16} & A_{26} & A_{66} & B_{16} & B_{26} & B_{66} \\ B_{11} & B_{12} & B_{16} & D_{11} & D_{12} & D_{16} \\ B_{12} & B_{22} & B_{26} & D_{12} & D_{22} & D_{26} \\ B_{16} & B_{26} & B_{66} & D_{16} & D_{26} & D_{66} \end{bmatrix} \begin{Bmatrix} \varepsilon_x \\ \varepsilon_z \\ \gamma_{xz} \\ \kappa_x \\ \kappa_z \\ \kappa_{xz} \end{Bmatrix} \quad (6)$$

Where

$$A_{ij} = \sum_{k=1}^{N} \bar{Q}_{ij} t_k$$

$$B_{ij} = \sum_{k=1}^{N} \bar{Q}_{ij} t_k \bar{y}_k$$

$$D_{ij} = \sum_{k=1}^{N} \bar{Q}_{ij} t_k \left(\bar{y}_k^2 + \frac{t_k^2}{12}\right) \quad (7)$$

$$t_k = y_k - y_{k-1}$$

$$\bar{y}_k = \frac{y_k + y_{k-1}}{2}$$

Where $A_{ij}$, $B_{ij}$, and $D_{ij}$ are the extensional, coupling, and flexural rigidity coefficients. $t_k$ = thickness of the k-th ply; and $N$ = number of different plies in the stacking sequence.

In order to generate the three dimensional (3D) constitutive matrix, material properties and the fiber orientations are used in equation (6). The 3D classical lamination matrix is reduced to 1D anisotropic extensional, coupling, and flexural stiffness coefficients using static condensation after applying the zero forces and moments.

$$\begin{Bmatrix} N_x \\ N_z = 0 \\ N_{xz} = 0 \\ M_x \\ M_z = 0 \\ M_{xz} = 0 \end{Bmatrix} = \begin{bmatrix} A_{11} & A_{12} & A_{16} & B_{11} & B_{12} & B_{16} \\ A_{12} & A_{22} & A_{26} & B_{12} & B_{22} & B_{26} \\ A_{16} & A_{26} & A_{66} & B_{16} & B_{26} & B_{66} \\ B_{11} & B_{12} & B_{16} & D_{11} & D_{12} & D_{16} \\ B_{12} & B_{22} & B_{26} & D_{12} & D_{22} & D_{26} \\ B_{16} & B_{26} & B_{66} & D_{16} & D_{26} & D_{66} \end{bmatrix} \begin{Bmatrix} \varepsilon_x \\ \varepsilon_z \\ \gamma_{xz} \\ \kappa_x \\ \kappa_z \\ \kappa_{xz} \end{Bmatrix} \quad (8)$$

Extracting the second, third, fifth, and sixth linear equations from matrix (8) to solve the axial strain and axial curvature ($\boldsymbol{\varepsilon_x}$ ,$\boldsymbol{\kappa_x}$) with respect to the other deformation components.

$$-\begin{bmatrix} \boldsymbol{A_{12}} & \boldsymbol{B_{12}} \\ \boldsymbol{A_{16}} & \boldsymbol{B_{16}} \\ \boldsymbol{B_{12}} & \boldsymbol{D_{12}} \\ \boldsymbol{B_{16}} & \boldsymbol{D_{16}} \end{bmatrix} \begin{Bmatrix} \boldsymbol{\varepsilon_x} \\ \boldsymbol{\kappa_x} \end{Bmatrix} = \begin{bmatrix} \boldsymbol{A_{22}} & \boldsymbol{A_{26}} & \boldsymbol{B_{22}} & \boldsymbol{B_{26}} \\ \boldsymbol{A_{26}} & \boldsymbol{A_{66}} & \boldsymbol{B_{26}} & \boldsymbol{B_{66}} \\ \boldsymbol{B_{22}} & \boldsymbol{B_{26}} & \boldsymbol{D_{22}} & \boldsymbol{D_{26}} \\ \boldsymbol{B_{26}} & \boldsymbol{B_{66}} & \boldsymbol{D_{26}} & \boldsymbol{D_{66}} \end{bmatrix} \begin{Bmatrix} \boldsymbol{\varepsilon_y} \\ \boldsymbol{\gamma_{xz}} \\ \boldsymbol{\kappa_{yz}} \\ \boldsymbol{\kappa_{xz}} \end{Bmatrix}$$

$$-\boldsymbol{R}\begin{Bmatrix} \boldsymbol{\varepsilon_x} \\ \boldsymbol{\kappa_x} \end{Bmatrix} = \boldsymbol{Q}\begin{Bmatrix} \boldsymbol{\varepsilon_z} \\ \boldsymbol{\gamma_{xz}} \\ \boldsymbol{\kappa_z} \\ \boldsymbol{\kappa_{xz}} \end{Bmatrix} \tag{9}$$

Inverting the matrix Q to the other side of Eq. (9), the condensed deformation components are obtained in terms of the axial strain and curvature:

$$\begin{Bmatrix} \boldsymbol{\varepsilon_z} \\ \boldsymbol{\gamma_{xz}} \\ \boldsymbol{\kappa_z} \\ \boldsymbol{\kappa_{xz}} \end{Bmatrix} = -[\boldsymbol{Q}]^{-1}[\boldsymbol{R}] \begin{Bmatrix} \boldsymbol{\varepsilon_x} \\ \boldsymbol{\kappa_x} \end{Bmatrix} \tag{10}$$

The axial force and in-plane moment versus the axial strain and in-plane curvature relationship is developed in terms of the generally anisotropic material properties by substituting Eq. (10) into the first and fourth linear equation of matrix (8)

$$\begin{bmatrix} \boldsymbol{N_x} \\ \boldsymbol{M_x} \end{bmatrix} = \begin{bmatrix} \boldsymbol{A_{ani}} & \boldsymbol{B_{ani}} \\ \boldsymbol{B_{ani}} & \boldsymbol{D_{ani}} \end{bmatrix} \begin{Bmatrix} \boldsymbol{\varepsilon_x} \\ \boldsymbol{\kappa_x} \end{Bmatrix} \tag{11}$$

Where

$$\begin{bmatrix} \boldsymbol{A_{ani}} & \boldsymbol{B_{ani}} \\ \boldsymbol{B_{ani}} & \boldsymbol{D_{ani}} \end{bmatrix} = \begin{bmatrix} \boldsymbol{A_{11}} & \boldsymbol{B_{11}} \\ \boldsymbol{B_{11}} & \boldsymbol{D_{11}} \end{bmatrix} - [\boldsymbol{R}]^{\boldsymbol{T}}[\boldsymbol{Q}]^{-1}[\boldsymbol{R}] \tag{12}$$

### 7.3.3 Energy Formulation

A generalized analytical buckling formula was developed using Rayleigh-Ritz approximation based on the energy approach. Strain energy can be expressed in terms of the integration of the applied loads multiplying the corresponding deformations.

$$U = \int_0^L \left(\frac{1}{2} N_x \varepsilon_x + \frac{1}{2} M_x \kappa_x\right) dx \tag{13}$$

$$= \int_0^L \frac{1}{2} (A_{ani} \varepsilon_x^2 + B_{ani} \varepsilon_x \kappa_x)\, dx + \int_0^L \frac{1}{2} (B_{ani} \varepsilon_x \kappa_x + D_{ani} \kappa_x^2)\, dx$$

The potential of external loads can be expressed as

$$W = -P\, u(L) \tag{14}$$

In view of Eq. (13) and (14), the total potential energy function is given by

$$\Pi = U - W = \int_0^L \frac{1}{2} (A_{ani} \varepsilon_x^2 + 2B_{ani} \varepsilon_x \kappa_x + D_{ani} \kappa_x^2)\, dx + P\, u(L) \tag{15}$$

$$\Pi = \frac{1}{2} A_{ani} B_1^2 L + \frac{1}{4} A_{ani} B_1 C_1^2 L \left(\frac{\pi}{2L}\right)^2 + \frac{3}{64} A_{ani} C_1^4 L \left(\frac{2\pi}{L}\right)^4 + \frac{2}{\pi} B_{ani} B_1 C_1 L \left(\frac{\pi}{2L}\right)^2 + \frac{1}{3\pi} B_{ani} C_1^3 L \left(\frac{\pi}{2L}\right)^4 + \frac{1}{4} D_{ani} C_1^2 L \left(\frac{\pi}{2L}\right)^4 + P B_1 L \tag{16}$$

Minimizing the total potential energy with respect to the unknown $B_1$ and $C_1$, setting the differential expressions to zero, performing integration by parts and manipulating the expressions, the following equations are developed

$$\frac{\partial \Pi}{\partial B_1} = A_{ani} B_1 L + \frac{A_{ani} C_1^2 L}{4} \left(\frac{\pi}{2L}\right)^2 + \frac{2B_{ani} C_1 L}{\pi} \left(\frac{\pi}{2L}\right)^2 + PL = 0 \tag{17}$$

$$\frac{\partial \Pi}{\partial C_1} = \frac{A_{ani} B_1 C_1 L}{2} \left(\frac{\pi}{2L}\right)^2 + \frac{3A_{ani} C_1^3 L}{16} \left(\frac{\pi}{2L}\right)^4 + \frac{2B_{ani} B_1 L}{\pi} \left(\frac{\pi}{2L}\right)^2 + \frac{B_{ani} C_1^2 L}{\pi} \left(\frac{\pi}{2L}\right)^4 + \frac{D_{ani} C_1 L}{2} \left(\frac{\pi}{2L}\right)^4 = 0 \tag{18}$$

Solving equation (17) for $B_1$ then substituting the resulting expression in equation (18), the following cubic equation is formulated in terms of $C_1$ value

$$B_1 = -\frac{C_1^2}{4}\left(\frac{\pi}{2L}\right)^2 - \frac{\pi}{2L}C_1\frac{B_{ani}}{A_{ani}L} - \frac{P}{A_{ani}} \quad (19)$$

$$q_1C_1^3 + q_2C_1^2 + q_3C_1 + q_4 = 0 \quad (20)$$

Where

$$q_1 = \frac{A_{ani}L}{16}\left(\frac{\pi}{2L}\right)^2,\ q_2 = -\frac{B_{ani}}{4}\left(\frac{\pi}{2L}\right),\ q_3 = \left[\frac{D_{ani}L}{2}\left(\frac{\pi}{2L}\right)^2 - \frac{B_{ani}^2}{A_{ani}L} - \frac{L}{2}P\right], q_4 = \frac{2B_{ani}}{A_{ani}}\frac{PL}{\pi}$$

Equation (20) does not lend itself to a closed form solution. Therefore, considering the critical stability matrix:

$$\begin{bmatrix} \frac{\partial^2\Pi}{\partial^2 B_1} & \frac{\partial^2\Pi}{\partial B_1 \partial C_1} \\ \frac{\partial^2\Pi}{\partial C_1 \partial B_1} & \frac{\partial^2\Pi}{\partial^2 C_1} \end{bmatrix} \quad (21)$$

Where

$$\frac{\partial^2\Pi}{\partial B_1^2} = A_{ani}L$$

$$\frac{\partial^2\Pi}{\partial B_1 \partial C_1} = A_{ani}C_1\left(\frac{\pi}{2L}\right)^2\frac{L}{2} + B_{ani}\frac{\pi}{2L}$$

$$\frac{\partial^2\Pi}{\partial C_1 \partial B_1} = A_{ani}C_1\left(\frac{\pi}{2L}\right)^2\frac{L}{2} + B_{ani}\frac{\pi}{2L} \quad (22)$$

$$\frac{\partial^2\Pi}{\partial C_1^2} = \frac{A_{ani}B_1L}{2}\left(\frac{\pi}{2L}\right)^2 + \frac{9A_{ani}C_1^2L}{16}\left(\frac{\pi}{2L}\right)^4 + B_{ani}C_1\left(\frac{\pi}{2L}\right)^3 + \frac{D_{ani}L}{2}\left(\frac{\pi}{2L}\right)^4$$

Setting the determinant of the matrix in Equation (21) to zero, substituting $B_1$ expression from equation (19) and solving for $C_1$ using the general solution of a quadratic equation:

$$C_1 = \frac{\frac{A_{ani}LB_{ani}}{2}(\frac{\pi}{2L}) \mp \sqrt{\frac{A_{ani}^2L^2B_{ani}^2}{4}(\frac{\pi}{2L})^2 - 4(\frac{3}{16})A_{ani}^2L^2\left(\frac{\pi}{2L}\right)^2[\frac{A_{ani}D_{ani}L^2}{2}\left(\frac{\pi}{2L}\right)^2 - B_{ani}^2 - \frac{A_{ani}^2L^2}{2}P}}{2(\frac{3}{16})A_{ani}^2L^2(\frac{\pi}{2L})^2} \quad (23)$$

In order for the $C_1$ value to be real, the discriminant must be at least zero. By setting the discriminant to zero and manipulating its expression, a closed form solution for the critical buckling load is derived:

$$P_{cr} = \frac{D_{ani}\pi^2}{4L^2} - \frac{32}{12}\frac{B_{ani}^2}{A_{ani}L^2} \quad (24)$$

The general critical buckling formula for columns with different width values other than unity is:

$$P_{cr} = \left(\frac{D_{ani}\pi^2}{4L^2} - \frac{32}{12}\frac{B_{ani}^2}{A_{ani}L^2}\right)w \quad (25)$$

Where w is the width of the column, equation (25) reduces down to Euler buckling formula of fixed free columns when the coupling term vanishes in case of isotropic or specially-orthotropic materials.

## 7.4 Numerical Formulation

In order to validate the analytical formula for laminated anisotropic fixed-free columns derived in the previous section, finite element analysis was conducted using commercial software package Abaqus. Column models were constructed with four layers of linear elastic laminated material. Moreover, fixed support and free end were provided at the bottom and top of the column, respectively. Axial compression load was applied at the top of the model as presented in Figure 7.2. Quadrilateral eight node doubly curved thick shell element (S8R) and 20-node quadratic solid

element (C3D20R) were used to model the anisotropic columns in 3D space. The mesh contains 0.5 x 0.5 mm element size in the analysis of a column size of 100 mm x 1.0 mm x 0.4 mm for length, width, and thickness, respectively.

To solve for eigenvalue and eigenvector numerically, buckling analysis was conducted using Lanczos solver. Based on the power method, Lanczos technique is used to simulate eigenvalue computation for complex Hermitian matrix in which a symmetric matrix is reduced to tridiagonal matrix using multidimensional array values (recurrence relations) [13].

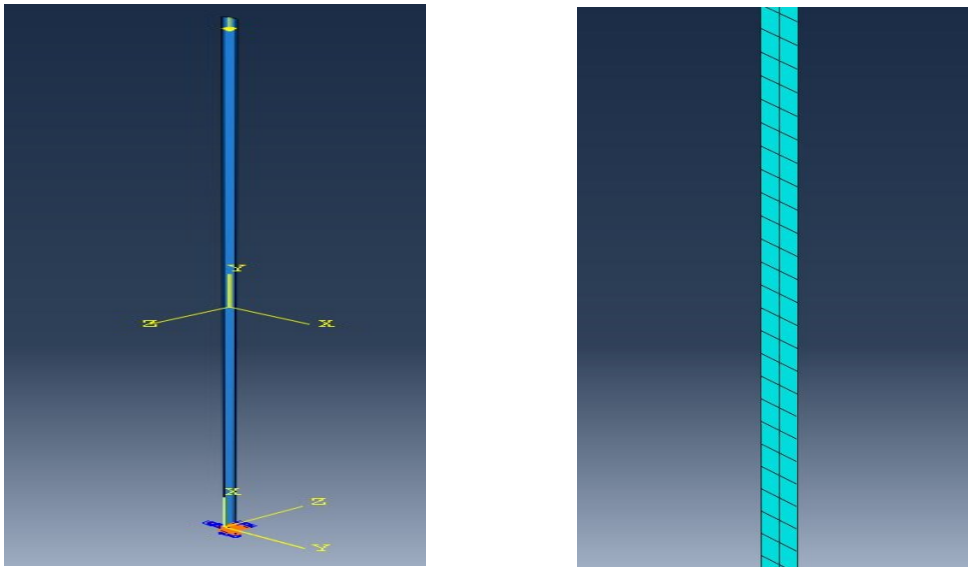

Figure 7.2 Left: Boundary conditions and applied load. Right: Meshed Model.

To indicate the existence of pre-buckling deformation in the transverse direction and predict the nonlinear stability response of the anisotropic columns, nonlinear geometry analysis using the modified Riks technique was performed. Based on the arc length method, Riks analysis follows the equilibrium path (bifurcation points or the limit points) while applying a load increment during the analysis. Equilibrium iterations converge along the arc length, forcing the constraint equation to be satisfied at every arc length increment [14].

## 7.5 Results and Applications:

### 7.5.1 Numerical Validation

High Strength Graphite/Epoxy material was mainly used to simulate the composite columns and its properties are illustrated in Table 7.1; obtained from typical values in an FRP textbook [15]. Table 7.2 presents the comparison between the analytical and numerical results for different stacking sequences of composite column with the following dimensions for length, width, and thickness: 100 mm x 1.0 mm x 0.4 mm, respectively. The analytical results showed an excellent agreement with the finite element results with a maximum error equal to 3.60 % for the balanced angle ply layup (30/-30/60/-60) and a minimum error equal to 0.00076% for single specially-orthotropic layup (90/90/90/90). It is important to note that the layup with maximum error yields the analytical load on the conservative side.

Table 7.1 High Strength Graphite/Epoxy Material Properties [15].

| **Material** | **$E_{11}$** | **$E_{22}$** | **$G_{12}$** | **$\nu_{12}$** |
|---|---|---|---|---|
| **High Strength Graphite/Epoxy** | 145.0 GPa | 10.0 GPa | 4.8 GPa | 0.25 |

Table 7.2 Comparison of analytical and numerical buckling load for various layup sequences of Graphite/Epoxy Composite Column (t = 0.4 mm).

| **Ply Orientation** | **Analytical Results, N** | **Numerical Results, N** | **% Error** | **Layup Type** |
|---|---|---|---|---|
| **0/0/0/0** | 0.19082 | 0.1908 | 0.01049 | Single Specially Orthotropic |
| **90/90/90/90** | 0.0131595 | 0.0131594 | 0.00076 | Single Specially Orthotropic |

| | | | | |
|---|---|---|---|---|
| **30/-30/30/-30** | 0.05979 | 0.05997 | 0.30106 | Antisymmetric Angle Ply |
| **45/-45/45/-45** | 0.02218 | 0.02226 | 0.36069 | Antisymmetric Angle Ply |
| **60/-60/60/-60** | 0.01423 | 0.01425 | 0.14055 | Antisymmetric Angle Ply |
| **60/-60/45/-45** | 0.01742 | 0.01752 | 0.57406 | Balanced Angle Ply |
| **30/-30/45/-45** | 0.03275 | 0.03337 | 1.89313 | Balanced Angle Ply |
| **30/-30/60/-60** | 0.02359 | 0.02444 | 3.60323 | Balanced Angle Ply |
| **30/-30/0/0** | 0.09127 | 0.09369 | 2.65148 | Anisotropic |
| **30/-30/0/90** | 0.04393 | 0.04401 | 0.18211 | Anisotropic |
| **30/30/30/30** | 0.02711 | 0.02726 | 0.55331 | Single Anisotropic Layer |
| **30/-30/-30/30** | 0.04814 | 0.04833 | 0.39469 | Symmetric Angle Ply |
| **0/90/90/0** | 0.16903 | 0.16901 | 0.01184 | Symmetric Cross Ply |
| **30/-60/-60/30** | 0.02893 | 0.02909 | 0.55306 | Symmetric Multiple Angle Layers |

| | | | | |
|---|---|---|---|---|
| **0/90/0/90** | 0.08658 | 0.08775 | 1.35136 | Antisymmetric Cross Ply |
| **-45/30/-30/45** | 0.02852 | 0.02863 | 0.3857 | Antisymmetric Angle Ply |
| **90/0/0/90** | 0.035455 | 0.03546 | 0.01411 | Symmetric Cross Ply |
| **30/30/-30/-30** | 0.04043 | 0.04046 | 0.07421 | Antisymmetric Angle Ply |

Load versus free end displacement curve is plotted for three different stacking sequences obtained from the nonlinear finite element Riks analysis along with the analytical solution as shown in Figure 7.3. The analytical results showed an excellent agreement with the Riks analysis where the anisotropic layup (30/-30/0/0) exhibit the highest buckling load with the maximum error value. The three stacking sequences indicate an existence of transverse deformation prior to buckling.

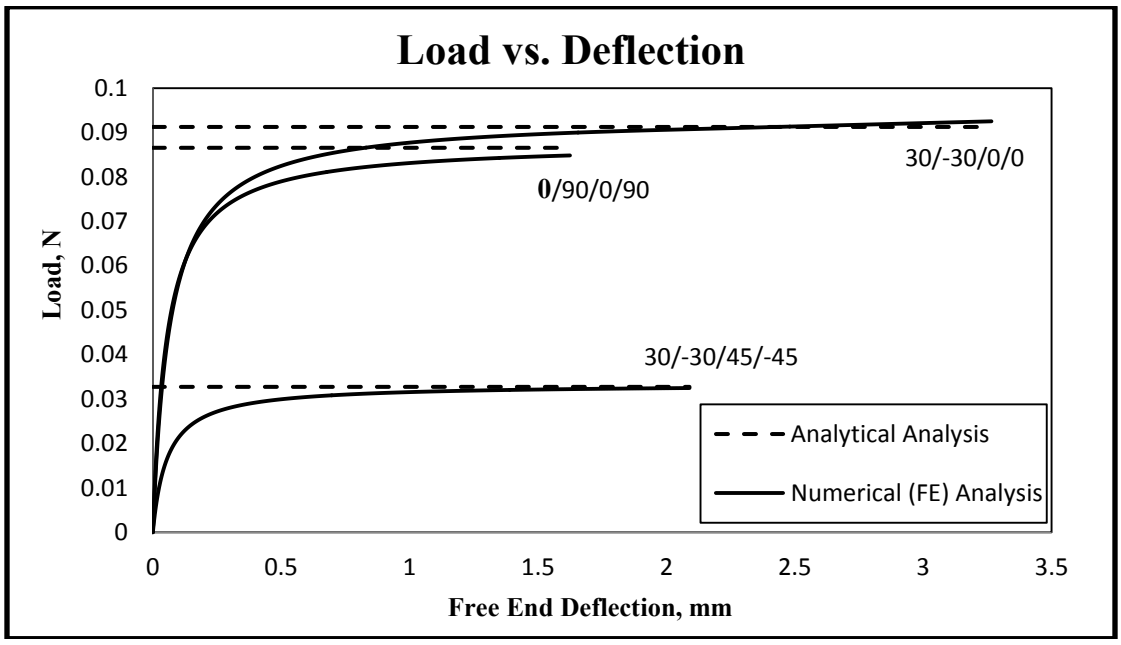


Figure 7.3 Analytical versus numerical solutions.

## 7.5.2 Parametric Study

### 7.5.2.1 Effect of Ply Orientation

Table **7.2** in the previous section presents the effect of having different stacking sequences of anisotropic column with the following dimensions for length, width, and thickness: 100 mm x 1.0 mm x 0.4 mm, respectively. The buckling load values vary between 0.19082 N and 0.0131595 N for different stacking sequences. Figure **7.4** presents the buckling mode shape of the composite fixed-free columns with stacking sequence (30/-30/0/90) obtained from the finite element analysis.

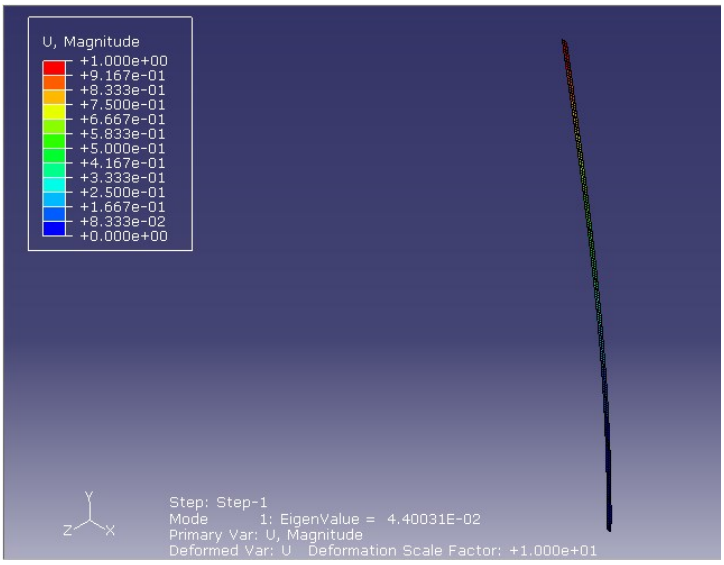


Figure 7.4 Buckling shape of fixed-free column.

### 7.5.2.2 Effect of Material Properties

The effect of having different material properties on the buckling load was performed in this paper. High Strength Graphite/Epoxy and S-Glass/Epoxy material properties were used and their properties are illustrated in Table 7.1 and Table 7.3; obtained from typical values in FRP textbook [15].

Table 7.3 S-Glass/Epoxy material properties [15].

| **Material** | **$E_{11}$** | **$E_{22}$** | **$G_{12}$** | **$\nu_{12}$** |
|---|---|---|---|---|
| **S-Glass/Epoxy** | 55.0 GPa | 16.0 GPa | 7.6 GPa | 0.28 |

High Strength Graphite/Epoxy and S-Glass/Epoxy results are presented in Table 7.2 and Table 7.4 for different stacking sequences. S-Glass/Epoxy showed lower buckling load values compared to High Strength Graphite/Epoxy since it has lower stiffness value along the fiber direction.

Table 7.4 Analytical and numerical results for various layup sequences for S-Glass/Epoxy (t = 0.4 mm).

| Ply Orientation | Analytical Results, N | Numerical Results, N | % Error | Layup Type |
|---|---|---|---|---|
| **0/0/0/0** | 0.072378 | 0.072384 | 0.00829 | Single Specially Orthotropic |
| **90/90/90/90** | 0.0210552 | 0.0210559 | 0.00333 | Single Specially Orthotropic |
| **30/-30/30/-30** | 0.04353 | 0.04356 | 0.06892 | Antisymmetric Angle Ply |
| **45/-45/45/-45** | 0.0287 | 0.02873 | 0.10453 | Antisymmetric Angle Ply |
| **60/-60/60/-60** | 0.02264 | 0.02265 | 0.04417 | Antisymmetric Angle Ply |
| **60/-60/45/-45** | 0.02527 | 0.02531 | 0.1583 | Balanced Angle Ply |
| **30/-30/45/-45** | 0.03472 | 0.03484 | 0.34563 | Balanced Angle Ply |
| **30/-30/60/-60** | 0.02989 | 0.0301 | 0.70258 | Balanced Angle Ply |
| **30/-30/0/0** | 0.05401 | 0.05426 | 0.46288 | Anisotropic |
| **30/-30/0/90** | 0.03441 | 0.03446 | 0.14531 | Anisotropic |
| **30/30/30/30** | 0.03567 | 0.03573 | 0.16821 | Single Anisotropic Layer |
| **30/-30/-30/30** | 0.04006 | 0.0401 | 0.09986 | Symmetric Angle Ply |

| | | | | |
|---|---|---|---|---|
| **0/90/90/0** | 0.066207 | 0.06621 | 0.00454 | Symmetric Cross Ply |
| **30/-60/-60/30** | 0.03535 | 0.0354 | 0.14145 | Symmetric Multiple Angle Layers |
| **0/90/0/90** | 0.04413 | 0.04435 | 0.49853 | Antisymmetric Cross Ply |
| **-45/30/-30/45** | 0.03102 | 0.03105 | 0.09672 | Antisymmetric Angle Ply |
| **90/0/0/90** | 0.0275724 | 0.0275734 | 0.00363 | Symmetric Cross Ply |
| **30/30/-30/-30** | 0.038219 | 0.038236 | 0.04449 | Antisymmetric Angle Ply |

Hybrid material composed of High Strength Graphite/Epoxy and S-Glass/Epoxy was used to study the effect of changing material properties on the stability of the composite columns. S-Glass/Epoxy material properties were used for layers with orientation equal to $90^{o}$ and $\pm 60^{o}$ and High Strength Graphite/Epoxy for the other orientations. Table 7.5 reports the analytical and numerical results for various layup sequences of hybrid material with a maximum error of 2.35% for the balanced angle ply layup (30/-30/60/-60) and a minimum error of 0.082% for symmetric cross ply layup (0/90/90/0).

Table 7.5 Analytical vs. numerical buckling loads for various layup sequences of hybrid Graphite and S-Glass/Epoxy composites.

| Ply Orientation | Analytical Results, N | Numerical Results, N | % Error |
|---|---|---|---|
| **30/-30/60/-60** | 0.03187 | 0.03262 | 2.35332 |
| **30/-30/0/90** | 0.0475 | 0.04736 | 0.29474 |
| **0/90/90/0** | 0.16986 | 0.16972 | 0.08243 |
| **0/90/0/90** | 0.0926 | 0.09331 | 0.76674 |
| **90/0/0/90** | 0.04227 | 0.04233 | 0.14195 |

#### 7.5.2.3 Effect of Element Type in FE Analysis

A parametric study was conducted to investigate the effect of changing the element type in the finite element analysis on the bucking load of the composite columns. Quadratic thick shell element (S8R) and quadratic solid element (C3D20R) both with reduced integration schemes were utilized with an element size equal to 0.5 mm x 0.5 mm, as illustrated earlier. Table **7.6** reports the comparison between the analytical and numerical results for shell and solid element. It was observed that the shell element results showed an excellent agreement with the analytical results for all stacking sequences. On the other hand, the solid element results were noticeably off for the cross-ply and anisotropic stacking sequences having the same mesh size as that of the shell element since solid elements have only translation degrees of freedom while shell elements have rotational degrees of freedom. Accordingly, shell element might be more reliable than solid element in buckling analysis of composite members.

Table 7.6 Analytical and numerical results with shell and solid elements.

| Ply Orientation | Analytical Results, N | Shell Element Results (S8R), N | Solid Element Results (C3D20R), N |
|---|---|---|---|
| **0/0/0/0** | 0.19082 | 0.1908 | 0.1908 |
| **90/90/90/90** | 0.0131595 | 0.01316 | 0.01317 |
| **30/-30/30/-30** | 0.05979 | 0.05997 | 0.0599 |
| **45/-45/45/-45** | 0.02218 | 0.02226 | 0.02266 |
| **60/-60/60/-60** | 0.01423 | 0.01425 | 0.01425 |
| **60/-60/45/-45** | 0.01742 | 0.01752 | 0.01854 |
| **30/-30/45/-45** | 0.03275 | 0.03337 | 0.04178 |
| **30/-30/60/-60** | 0.02359 | 0.02444 | 0.03831 |
| **30/-30/0/0** | 0.09127 | 0.09369 | 0.12587 |
| **30/-30/0/90** | 0.04393 | 0.04401 | 0.08151 |
| **30/30/30/30** | 0.02711 | 0.02726 | 0.02727 |
| **30/-30/-30/30** | 0.04814 | 0.04833 | 0.06453 |
| **0/90/90/0** | 0.16903 | 0.16901 | 0.10232 |
| **30/-60/-60/30** | 0.02893 | 0.02909 | 0.02817 |
| **0/90/0/90** | 0.08658 | 0.08775 | 0.10231 |
| **-45/30/-30/45** | 0.02852 | 0.02863 | 0.04528 |
| **90/0/0/90** | 0.035455 | 0.03546 | 0.10232 |
| **30/30/-30/-30** | 0.04043 | 0.04046 | 0.03952 |

#### 7.5.2.4 Effect of Element Thickness

The effect of having thin and thick columns was also studied. Comparison between the analytical and numerical results, were conducted, using columns with 0.4 mm and 1.6 mm thickness while maintaining the same width to thickness ratio equal to 2.5. Table 7.7 and Table 7.8 presents comparisons between the analytical and numerical buckling load results for Graphite/Epoxy and S-Glass/Epoxy composite columns with 1.6 mm thickness, respectively. The level of errors between the numerical solution, capable of capturing the behavior of thick shells, with the analytical solution for thick columns is similar to that of thin columns. This may suggest that the present formula can be successfully used to re-produce accurate results in cases of moderately thick shells.

Table 7.7 Comparison of analytical and numerical buckling load for various layup sequences of Graphite/Epoxy Composite Column (t = 1.6 mm).

| Ply Orientation | Analytical Results, N | Numerical Results, N | % Error |
|---|---|---|---|
| **0/0/0/0** | 48.84797 | 48.749 | 0.20261 |
| **90/90/90/90** | 3.368825 | 3.3681 | 0.02153 |
| **30/-30/30/-30** | 15.30558 | 15.451 | 0.95012 |
| **45/-45/45/-45** | 5.6772 | 5.7491 | 1.26647 |
| **60/-60/60/-60** | 3.6404 | 3.6592 | 0.51643 |
| **60/-60/45/-45** | 4.45936 | 4.5111 | 1.16026 |
| **30/-30/45/-45** | 8.38221 | 8.6099 | 2.71635 |
| **30/-30/60/-60** | 6.03803 | 6.2825 | 4.04884 |
| **30/-30/0/0** | 23.36326 | 24.106 | 3.1791 |
| **30/-30/0/90** | 11.2436 | 11.309 | 0.58167 |

| | | | |
|---|---|---|---|
| **30/30/30/30** | 6.93956 | 7.079 | 2.00935 |
| **30/-30/-30/30** | 12.3238 | 12.489 | 1.3405 |
| **0/90/90/0** | 43.27124 | 43.164 | 0.24784 |
| **30/-60/-60/30** | 7.40565 | 7.5477 | 1.91814 |
| **0/90/0/90** | 22.16371 | 22.431 | 1.20599 |
| **-45/30/-30/45** | 7.3007 | 7.3968 | 1.31632 |
| **90/0/0/90** | 9.076407 | 9.0713 | 0.05627 |
| **30/30/-30/-30** | 10.34909 | 10.334 | 0.14581 |

Table 7.8 Comparison of analytical and numerical buckling load for various layup sequences of S-Glass/Epoxy Composite Column (t = 1.6 mm).

| **Ply Orientation** | **Analytical Results, N** | **Numerical Results, N** | **% Error** |
|---|---|---|---|
| **0/0/0/0** | 18.52854 | 18.527 | 0.00832 |
| **90/90/90/90** | 5.39012 | 5.3893 | 0.01522 |
| **30/-30/30/-30** | 11.14204 | 11.166 | 0.21505 |
| **45/-45/45/-45** | 7.3457 | 7.3675 | 0.29678 |
| **60/-60/60/-60** | 5.79429 | 5.8028 | 0.14687 |
| **60/-60/45/-45** | 6.46851 | 6.4882 | 0.3044 |
| **30/-30/45/-45** | 8.88751 | 8.9346 | 0.52985 |
| **30/-30/60/-60** | 7.64932 | 7.7148 | 0.85603 |
| **30/-30/0/0** | 13.82426 | 13.906 | 0.59128 |
| **30/-30/0/90** | 8.80835 | 8.8274 | 0.21628 |
| **30/30/30/30** | 9.13073 | 9.1845 | 0.5889 |

| | | | |
|---|---|---|---|
| **30/-30/-30/30** | 10.25316 | 10.296 | 0.41783 |
| **0/90/90/0** | 16.9489 | 16.938 | 0.06432 |
| **30/-60/-60/30** | 9.04752 | 9.0906 | 0.47616 |
| **0/90/0/90** | 11.29621 | 11.347 | 0.44962 |
| **-45/30/-30/45** | 7.94057 | 7.964 | 0.29507 |
| **90/0/0/90** | 7.058518 | 7.0581 | 0.00593 |
| **30/30/-30/-30** | 9.784 | 9.792 | 0.08177 |

## 7.6 Conclusions

Based on Rayleigh-Ritz approximation, analytical buckling formula for anisotropic laminated composite columns with fixed free end conditions under axial compression was developed. The derived analytical buckling formula was expressed with respect to the effective extensional, coupling, and flexural rigidities along with the column geometry. The analytical results exhibited an excellent agreement with the finite element analysis results. The derived analytical formula was able to capture the complexity in the behavior of anisotropic columns for different stacking sequences, material properties, and hybrid columns yielding an excellent agreement with the numerical analysis results. Moreover, using shell elements yielded very accurate buckling load results for all stacking sequences compared to the use of solid elements. Furthermore, the derived analytical formula yielded accurate results for thin and moderately thick columns when compared to finite element predictions.

## 7.7 References

[1] Cortinez, H.V., and Piovan, M. T., "Stability of composite thin-walled beams with shear deformability," *Computers & Structures*, vol. 84, pp. 978-990, 2006.

[2] Aydogdu, M., "Buckling analysis of cross-ply laminated beams with general boundary conditions by Ritz method," *Composite Science & Technology*, vol. 66, pp. 1248-1255, 2006.

[3] Abramovich, H., and Livshits, A., "Free vibrations of non-symmetric cross-ply laminated composite beams", *Journal of Sound and Vibration* , vol. 176, pp. 597-612, 1994.

[4] Abramovich, H., Eisenberger, M., and Shulepov, O., "Vibrations and buckling of cross-ply non-symmetric laminated composite beams", *AIAA Journal* , vol. 34, pp. 1064-1069, 1996.

[5] Shnabl, S., Planinc, I., and Turk, G., "Buckling loads of two-layer composite columns with interlayer slip and stochastic material properties," *Journal of Enginnering Mechanics,* vol. 139, no. 8, pp. 961-966, 2013.

[6] Herencia, J. E., Weaver, P. M., and Friswell, M. I., "Closed-form solutions for buckling of long anisotropic plates with various boundary conditions under axial compression," *Journal of Engineering Mechanics*, vol. 136, no. 9, pp. 1105-1114, 2010.

[7] Ovesy, H. R., Ghannadpour, S.A.M., and Sherafat, M. H, "Buckling analysis of laminated composite plates using higer order semi-analytical finite strip method," *Appl Compos Mater*, vol. 17, pp. 69-80, 2010.

[8] Matsunaga, H., "Free vibration and stability of angle-ply laminated composite and sandwich plates under thermal laoding," *Composite Structures*, vol. 77, pp. 249-262, 2007.

[9] Pandey, M. D., and Sherbourne, A. N., "Buckling of anisotropic composite plates under stress gradient," *Journal of Engineering Mechanics*, vol. 117, no. 2, pp. 260-275, 1991.

[10] Rasheed, H.A., and Yousif, O.H., "Buckling of thin laminated orthotropic rings/long cylinders under external pressure," *International Journal of Structural Stability and Dynamics*, vol. 1, no. 4, pp. 485-507, 2002.

[11] Timarci, T., Aydogdu, M., "Buckling of symmetric cross-ply square plates with various boundary conditions," *Composite Structures*, vol. 68, pp. 381-389, 2005.

[12] Jones, R.M, Mechanics of composite materials, New York: Hemisphere Publishing Corporation, 1975.

[13] Hernandez, V., Roman, J.E., Tomas, A., and Vidal, V., "Lanczos methods in SLEPc," Polytechnic University of Valencia, Province of Valencia, 2006.

[14] Memon, B.A., Su, X.S., "Arc-length technique for nonlinear finite element analysis," J*ournal of Zhejiang University SCI*, vol. 5, no. 5, pp. 618-628, 2004.

[15] Rasheed, H.A., Strengthening Design of Reinforced Concrete with FRP, New York: CRC Press, 2015.

# Chapter 8 - Stability Solution for Clamped-Free Wide Plates under Compression Edge Loading

**Rund Al-Masri[1] and Hayder A. Rasheed[2]**

## 8.1 Abstract

**Buckling of anisotropic laminated composite clamped-free wide plate under compression edge loading is investigated. Using Rayleigh-Ritz approximation based on energy method, a generalized analytical critical buckling formula is developed. Based on the generalized constitutive relationship, the effective extensional, coupling and flexural stiffness coefficients of the anisotropic layup are determined using dimensional reduction of the three dimensional composite stiffness matrix. The developed formula is expressed in terms of the generally anisotropic material properties in the principal directions along with wide plate geometry. The formula reduces down to Euler buckling formula for certain types of layups. The analytical solution is confirmed against finite element analysis for wide range of anisotropic layups yielding high accuracy. A brief parametric study is then conducted to examine the effect of ply orientations, element thickness, and material properties including hybrid carbon/glass fiber composites. Relevance of the numerical and analytical results is discussed for all these cases.**

Keywords: Buckling of Composite Wide Plates, Clamped-free Boundary Conditions, Anisotropic Laminated Composites, Axial Compression.

[1] Ph.D. Candidate, Department of Civil Engineering, Kansas State University, Manhattan, KS 66506

[2] Professor, Department of Civil Engineering, Kansas State University, Manhattan, KS 66506

## 8.2 Introduction

In the past few decades, composites had captured the attention in various industrial applications such as aerospace, marine, and automotive due to their mechanical advantages. An increase in the demand to understand the mechanics of composite material has resulted. Stability analysis is a critical issue in the composite members. Although a limited amount of research has focused on the stability of anisotropic laminated composite wide plates, sufficient amount of studies has investigated the buckling of composite plates, beams, cylinders, and shells [1-10]. Haung et al. [1] presented an efficient finite element model to investigate buckling of grid stiffened laminated composite plates. Curved beam element was proposed to model the stiffeners. Moreover, the developed element was used to solve different numerical examples. Wang and Abdalla [2] studied the global and local buckling of grid stiffened composite panels based on Bloch wave theory. The presented method is confirmed for different composite configurations. Based on sets of trigonometric shape functions, Weber and Middendorf [3] studied the skin buckling of curved orthotropic grid-stiffened shells with a semi-analytical Ritz method. Depending on Principal of virtual work with linear kinematics, Grover et al. [4] proposed a new inverse hyperbolic shear deformation theory (IHSDT) to study static and buckling response of laminated composite and sandwich plate depending on the shear strain shape function to ensure a nonlinear distribution of transverse shear stresses and satisfies traction at free boundary conditions. Analytical solution was determined using Navier type approach of simply supported composite sandwich plate. Several numerical examples were solved for the presented theory. The developed theory accurately predicted the critical buckling load for simply supported thick plates with minimal numerical error and computational cost. Khayat et al. [5] analyzed the buckling of laminated composite cylindrical shell under lateral displacement-dependent pressure using semi-analytical finite strip method.

Based on the first shear deformation theory with Sanders type of kinematics nonlinearity, the governing equations were developed. The results showed a decrease in the buckling pressure when the pressure stiffness was taken into consideration. Baba and Baltaci [6] studied the buckling characteristics of symmetrical and anti-symmetrical E-glass/Epoxy laminated composite rectangular plates with central cutout experimentally and numerically. Different laminate configurations, cutout shape, boundary conditions, and length to thickness ratio were taken into account. The experimental results were confirmed against finite element analysis yielding a higher buckling load values than the numerical ones. Becheri et al. [7] developed an exact analytical solution to study the buckling of symmetrical cross-ply plates using nth-order shear deformation theory with curvature effects. The closed form solution was compared with previous work. Debski [8] presented numerical analysis of buckling and post-buckling of thin-walled simply supported laminated composite columns with channel section under axial compression. Eight symmetrical layered Carbon/Epoxy columns were modeled using the software Abaqus and Ansys and verified with analytical-numerical method [9]. Linear four node shell element with reduced integration schemes (S4R) and eight node shell element (Shell99) were attempted in Abaqus and Ansys, respectively. A good agreement was observed between the finite element results and results obtained from the analytical-numerical method. Cortinez and Piovan [10] proposed a theoretical model to study the buckling of composite thin-walled beams with shear deformability using nonlinear displacement field depending on Hellinger-Reissner principal. The governing equations were solved using finite element with fourteen degrees of freedom.

Based on Rayleigh-Ritz method, a generalized closed form critical buckling solution of anisotropic laminated composite clamped-free wide plates under uniaxial compression loading was developed in this work. Using fiber orientations and material properties, the three dimensional stiffness matrix

was constructed then reduced down to 1D axial, coupling, flexural stiffness coefficients by excluding zero strains and curvatures. Additionally, the analytical critical buckling formula was validated along with the finite element analysis yielding an excellent agreement.

## 8.3 Analytical Formulation

### 8.3.1 Assumptions

Rayleigh-Ritz method is invoked to develop a generalized closed-form buckling solution for clamped-free anisotropic laminated composite wide plates under uniaxial compression loading. The following several assumptions are considered prior to the formulation process:

- Buckling occurs by bending parallel to the x-y plane about the z-axis (weak axis).
- The y-axis is perpendicular to the composite lamination surface, Figure 8.1.
- The lamination angle ( $\alpha$ ) is measured with respect to the x-axis in which 0° fibers run parallel to the x-axis and 90° fibers run parallel to the z-axis. Accordingly, the angle ( $\alpha$ ) is rotated about the y-axis.
- Simple beam theory holds in which Plane sections before bending remain plane after bending and perpendicular to the mid surface.
- Classical lamination theory is applicable with shear deformations ignored.

### 8.3.2 Kinematics

Figure 8.1 presents the Cartesian coordinates and the geometry of the clamped-free wide plates. Bending takes place about the z-axis which is the weak axis of the plates. Equation (1) presents the assumed displacement field based on the isotropic buckling mode:

$$\boldsymbol{u}(\boldsymbol{x}) = \boldsymbol{B_1 x}\,; \quad \boldsymbol{v}(\boldsymbol{x}) = \boldsymbol{C_1}\left(\mathbf{1} - \cos\frac{\boldsymbol{\pi x}}{\boldsymbol{2L}}\right) \tag{1}$$

Where $u(x)$, v$(x)$ are the axial and lateral displacement, $B_1$ and $C_1$ are constants to be solved and x is the distance along the axis of the wide plates as shown in Figure 8.1.The axial strain $\boldsymbol{\varepsilon_x}$ and curvature $\boldsymbol{\kappa_x}$ are presented in equation (2) depending on the intermediate class of deformation:

$$\boldsymbol{\varepsilon_x = \frac{du}{dx} + \frac{1}{2}\left(\frac{dv}{dx}\right)^2 = u' + \frac{1}{2}v'^2; \qquad \kappa_x = \frac{d^2v}{d^2x} = v''} \tag{2}$$

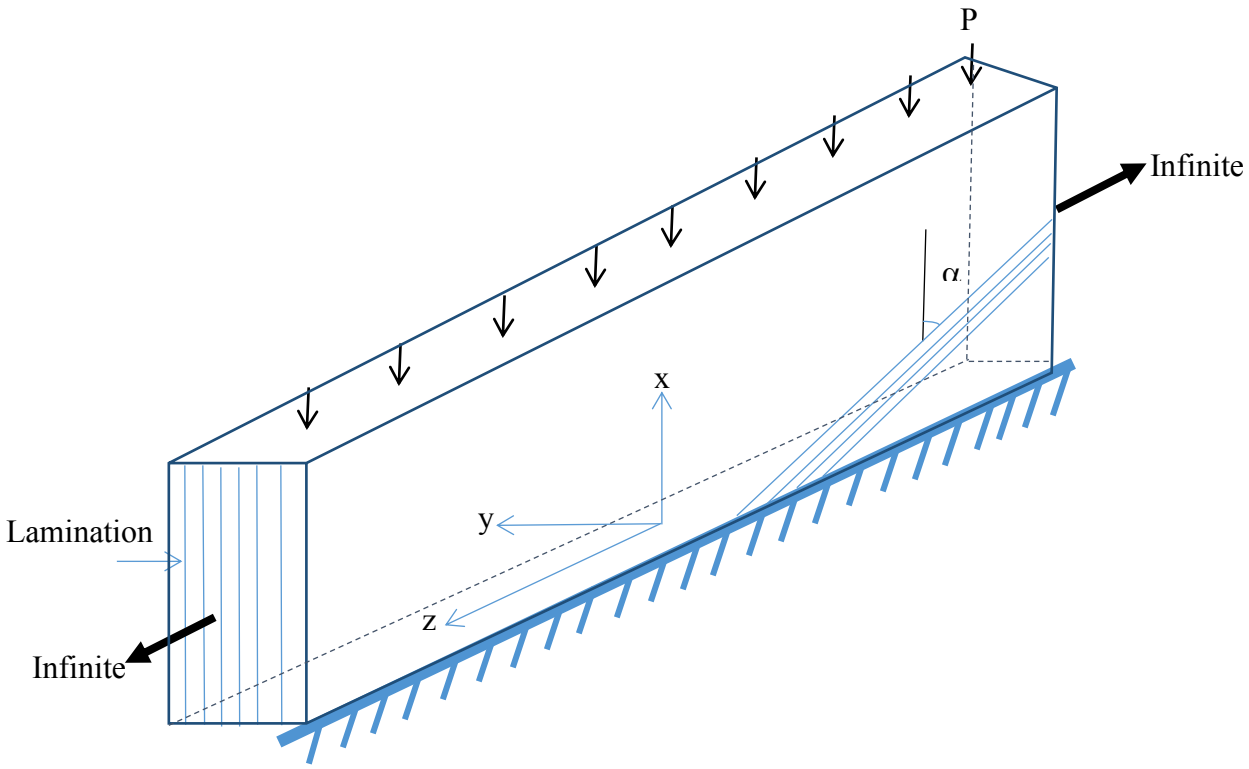


Figure 8.1Wide Plate geometry

### 8.3.3 Constitutive equations

The principle material directions are transformed into the wide plate coordinate system. The stresses and strains are then related by the transformed reduced stiffness matrix $\bar{Q}_{ij}$ presented in equation (3); as defined in standard composite textbook [11]

$$\begin{Bmatrix} \boldsymbol{\sigma_x} \\ \boldsymbol{\sigma_z} \\ \boldsymbol{\tau_{xz}} \end{Bmatrix} = \begin{bmatrix} \boldsymbol{\bar{Q}_{11}} & \boldsymbol{\bar{Q}_{12}} & \boldsymbol{\bar{Q}_{16}} \\ \boldsymbol{\bar{Q}_{12}} & \boldsymbol{\bar{Q}_{22}} & \boldsymbol{\bar{Q}_{26}} \\ \boldsymbol{\bar{Q}_{16}} & \boldsymbol{\bar{Q}_{26}} & \boldsymbol{\bar{Q}_{66}} \end{bmatrix} \begin{Bmatrix} \boldsymbol{\varepsilon_x} \\ \boldsymbol{\varepsilon_z} \\ \boldsymbol{\gamma_{xz}} \end{Bmatrix} \tag{3}$$

Accordingly, the coupled force-strain relationship is established as

$$\begin{Bmatrix} \boldsymbol{N_x} \\ \boldsymbol{N_z} \\ \boldsymbol{N_{xz}} \\ \boldsymbol{M_x} \\ \boldsymbol{M_z} \\ \boldsymbol{M_{xz}} \end{Bmatrix} = \begin{bmatrix} \boldsymbol{A_{11}} & \boldsymbol{A_{12}} & \boldsymbol{A_{16}} & \boldsymbol{B_{11}} & \boldsymbol{B_{12}} & \boldsymbol{B_{16}} \\ \boldsymbol{A_{12}} & \boldsymbol{A_{22}} & \boldsymbol{A_{26}} & \boldsymbol{B_{12}} & \boldsymbol{B_{22}} & \boldsymbol{B_{26}} \\ \boldsymbol{A_{16}} & \boldsymbol{A_{26}} & \boldsymbol{A_{66}} & \boldsymbol{B_{16}} & \boldsymbol{B_{26}} & \boldsymbol{B_{66}} \\ \boldsymbol{B_{11}} & \boldsymbol{B_{12}} & \boldsymbol{B_{16}} & \boldsymbol{D_{11}} & \boldsymbol{D_{12}} & \boldsymbol{D_{16}} \\ \boldsymbol{B_{12}} & \boldsymbol{B_{22}} & \boldsymbol{B_{26}} & \boldsymbol{D_{12}} & \boldsymbol{D_{22}} & \boldsymbol{D_{26}} \\ \boldsymbol{B_{16}} & \boldsymbol{B_{26}} & \boldsymbol{B_{66}} & \boldsymbol{D_{16}} & \boldsymbol{D_{26}} & \boldsymbol{D_{66}} \end{bmatrix} \begin{Bmatrix} \boldsymbol{\varepsilon_x} \\ \boldsymbol{\varepsilon_z} \\ \boldsymbol{\gamma_{xz}} \\ \boldsymbol{\kappa_x} \\ \boldsymbol{\kappa_z} \\ \boldsymbol{\kappa_{xz}} \end{Bmatrix} \tag{4}$$

**Where**

$$\boldsymbol{A_{ij}} = \sum_{\boldsymbol{k=1}}^{\boldsymbol{N}} \boldsymbol{\bar{Q}_{ij} t_k}$$

$$\boldsymbol{B_{ij}} = \sum_{\boldsymbol{k=1}}^{\boldsymbol{N}} \boldsymbol{\bar{Q}_{ij} t_k \bar{y}_k}$$

$$\boldsymbol{D_{ij}} = \textstyle\sum_{\boldsymbol{k=1}}^{\boldsymbol{N}} \boldsymbol{\bar{Q}_{ij} t_k} (\boldsymbol{\bar{y}_k^2} + \frac{\boldsymbol{t_k^2}}{\boldsymbol{12}}) \tag{5}$$

$$\boldsymbol{t_k} = \boldsymbol{y_k} - \boldsymbol{y_{k-1}}$$

$$\boldsymbol{\bar{y}_k} = \frac{\boldsymbol{y_k} + \boldsymbol{y_{k-1}}}{\boldsymbol{2}}$$

Where $A_{ij}$, $B_{ij}$, and $D_{ij}$ are the extensional, coupling, and flexural stiffness coefficients. $t_k$ = thickness of the k-th ply; and N = number of different plies in the stacking sequence.

Material properties and the fiber orientations are used in Eq. (4) to generate the three dimensional (3D) constitutive matrix. Using the static condensation approach, the 3D classical lamination matrix is then reduced to one dimensional (1D) anisotropic extensional, coupling, and flexural stiffness coefficients after applying the zero strain curvatures.

$$\begin{Bmatrix} N_x \\ N_z \\ N_{xz} \\ M_x \\ M_z \\ M_{xz} \end{Bmatrix} = \begin{bmatrix} A_{11} & A_{12} & A_{16} & B_{11} & B_{12} & B_{16} \\ A_{12} & A_{22} & A_{26} & B_{12} & B_{22} & B_{26} \\ A_{16} & A_{26} & A_{66} & B_{16} & B_{26} & B_{66} \\ B_{11} & B_{12} & B_{16} & D_{11} & D_{12} & D_{16} \\ B_{12} & B_{22} & B_{26} & D_{12} & D_{22} & D_{26} \\ B_{16} & B_{26} & B_{66} & D_{16} & D_{26} & D_{66} \end{bmatrix} \begin{Bmatrix} \varepsilon_x \\ \varepsilon_z = 0 \\ \gamma_{xz} = 0 \\ \kappa_x \\ \kappa_z = 0 \\ \kappa_{xz} = 0 \end{Bmatrix} \tag{6}$$

The axial force and in-plane moment versus the axial strain and in-plane curvature relationship are extracted to yield. The first and fourth linear equation of matrix (6)

$$\begin{bmatrix} N_x \\ M_x \end{bmatrix} = \begin{bmatrix} A_{11} & B_{11} \\ B_{11} & D_{11} \end{bmatrix} \begin{Bmatrix} \varepsilon_x \\ \kappa_x \end{Bmatrix} \tag{7}$$

Equation (7) expresses the material properties of wide plates with respect to the extensional, coupling, and flexural stiffness coefficients in the principal directions.

### 8.3.4 Energy Formulation

Rayleigh-Ritz approximation based on the energy approach was utilized in developing a generalized closed-form buckling solution of anisotropic laminated composite clamped-free wide plates under uniaxial compression loading. Strain energy can be expressed in terms of the integration of the applied loads multiplying the corresponding deformations.

$$U = \int_0^L \left( \frac{1}{2} N_x \varepsilon_x + \frac{1}{2} M_x \kappa_x \right) dx \tag{8}$$

$$= \int_0^L \frac{1}{2} (A_{11} \varepsilon_x^2 + B_{11} \varepsilon_x \kappa_x)\, dx + \int_0^L \frac{1}{2} (B_{11} \varepsilon_x \kappa_x + D_{11} \kappa_x^2)\, dx$$

The potential of external loads can be expressed as

$$W = -P\, u(L) \tag{9}$$

In view of Eq. (8) and (9), the total potential energy function is given by

$$\Pi = U - W = \int_0^L \frac{1}{2} (A_{11} \varepsilon_x^2 + 2B_{11} \varepsilon_x \kappa_x + D_{11} \kappa_x^2)\, dx + P\, u(L) \tag{10}$$

$$\Pi = \frac{1}{2}A_{11}B_1^2L + \frac{1}{4}A_{11}B_1C_1^2L\left(\frac{\pi}{2L}\right)^2 + \frac{3}{64}A_{11}C_1^4L\left(\frac{2\pi}{L}\right)^4 + \frac{2}{\pi}B_{11}B_1C_1L\left(\frac{\pi}{2L}\right)^2 +$$

$$\frac{1}{3\pi}B_{11}C_1^3L\left(\frac{\pi}{2L}\right)^4 + \frac{1}{4}D_{11}C_1^2L\left(\frac{\pi}{2L}\right)^4 + PB_1L \quad (11)$$

Minimizing the total potential energy with respect to the unknown $B_1$ and $C_1$, by setting the differential operators to zero, and manipulating the expressions, the following equations are developed

$$\frac{\partial \Pi}{\partial B_1} = A_{11}B_1L + \frac{A_{11}C_1^2L}{4}\left(\frac{\pi}{2L}\right)^2 + \frac{2B_{11}C_1L}{\pi}\left(\frac{\pi}{2L}\right)^2 + PL = 0 \quad (12)$$

$$\frac{\partial \Pi}{\partial C_1} = \frac{A_{11}B_1C_1L}{2}\left(\frac{\pi}{2L}\right)^2 + \frac{3A_{11}C_1^3L}{16}\left(\frac{\pi}{2L}\right)^4 + \frac{2B_{11}B_1L}{\pi}\left(\frac{\pi}{2L}\right)^2 + \frac{B_{11}C_1^2L}{\pi}\left(\frac{\pi}{2L}\right)^4 \quad (13)$$

$$+ \frac{D_{11}C_1L}{2}\left(\frac{\pi}{2L}\right)^4 = 0$$

Solving equation (12) for $B_1$ then substituting the resulting expression in equation (15), the following cubic equation is formulated in terms of $C_1$ value

$$B_1 = -\frac{C_1^2}{4}\left(\frac{\pi}{2L}\right)^2 - \frac{\pi}{2L}C_1\frac{B_{11}}{A_{11}L} - \frac{P}{A_{11}} \quad (14)$$

$$q_1C_1^3 + q_2C_1^2 + q_3C_1 + q_4 = 0 \quad (15)$$

**Where**

$$q_1 = \frac{A_{11}L}{16}\left(\frac{\pi}{2L}\right)^2,\ q_2 = -\frac{B_{11}}{4}\left(\frac{\pi}{2L}\right),\ q_3 = \left[\frac{D_{11}L}{2}\left(\frac{\pi}{2L}\right)^2 - \frac{B_{11}^2}{A_{11}L} - \frac{L}{2}P\right], q_4 = \frac{2B_{11}}{A_{11}}\frac{PL}{\pi}$$

Equation (15) does not lend itself to a closed form solution. Therefore, considering the critical stability matrix:

$$\begin{bmatrix} \frac{\partial^2\Pi}{\partial^2 B_1} & \frac{\partial^2\Pi}{\partial B_1 \partial C_1} \\ \frac{\partial^2\Pi}{\partial C_1 \partial B_1} & \frac{\partial^2\Pi}{\partial^2 C_1} \end{bmatrix} \quad (16)$$

Where

$$\frac{\partial^2 \Pi}{\partial B_1^2} = A_{11} L$$

$$\frac{\partial^2 \Pi}{\partial B_1 \partial C_1} = A_{11} C_1 \left(\frac{\pi}{2L}\right)^2 \frac{L}{2} + B_{11} \frac{\pi}{2L}$$

$$\frac{\partial^2 \Pi}{\partial C_1 \partial B_1} = A_{11} C_1 \left(\frac{\pi}{2L}\right)^2 \frac{L}{2} + B_{11} \frac{\pi}{2L} \quad \textbf{(17)}$$

$$\frac{\partial^2 \Pi}{\partial C_1^2} = \frac{A_{11} B_1 L}{2} \left(\frac{\pi}{2L}\right)^2 + \frac{9 A_{11} C_1^2 L}{16} \left(\frac{\pi}{2L}\right)^4 + B_{11} C_1 \left(\frac{\pi}{2L}\right)^3 + \frac{D_{11} L}{2} \left(\frac{\pi}{2L}\right)^4$$

Setting the determinant of the matrix in Equation (16) to zero, substituting $B_1$ expression from equation (14) and solving for $C_1$ using the general solution of a quadratic equation:

$$C_1 = \frac{\frac{A_{11} L B_{11}}{2} \left(\frac{\pi}{2L}\right) \mp \sqrt{\frac{A_{11}^2 L^2 B_{11}^2}{4} \left(\frac{\pi}{2L}\right)^2 - 4 \left(\frac{3}{16}\right) A_{11}^2 L^2 \left(\frac{\pi}{2L}\right)^2 \left[\frac{A_{11} D_{11} L^2}{2} \left(\frac{\pi}{2L}\right)^2 - B_{11}^2 - \frac{A_{11}^2 L^2}{2} P\right.}}{2 \left(\frac{3}{16}\right) A_{11}^2 L^2 \left(\frac{\pi}{2L}\right)^2} \quad \textbf{(18)}$$

In order for the $C_1$ value to be real, the discriminant must be at least zero. By setting the discriminant to zero and manipulating its expression, a closed form solution for the critical buckling load per unit width of the plate is derived:

$$P_{cr} = \frac{D_{11} \pi^2}{4L^2} - \frac{32}{12} \frac{B_{11}^2}{A_{11} L^2} \quad \textbf{(19)}$$

The general critical buckling formula for wide plates with any width values other than unity is:

$$P_{cr} = \left(\frac{D_{11} \pi^2}{4L^2} - \frac{32}{12} \frac{B_{11}^2}{A_{11} L^2}\right) w \quad \textbf{(20)}$$

Where w is the width of the wide plates, equation (22) reduces down to Euler buckling formula of clamped-free wide plates when the coupling term vanishes in case of isotropic or specially-orthotropic materials.

## Numerical Formulation

In order to validate the developed formula in the previous section, finite element analysis was performed using commercial software package Abaqus. Wide plates with the following dimensions for width, length, and thickness: 1000 mm x 100 mm x 0.4 mm were attempted, respectively. Linear elastic laminated material was assumed for both orthotropic and anisotropic layups where S-Glass/Epoxy material was used as main material. Fixed and free ends were illustrated at the bottom and top of the wide plate, respectively. Furthermore, the translation in the x-direction (z-direction in Figure 8.1) and the rotation about y-direction (about the x-direction in Figure 8.1) were prevented to mimic the infinitely wide plate, see Figure 8.2. Additionally, edge loading was applied at the top of wide plate as shown in Figure 8.2.

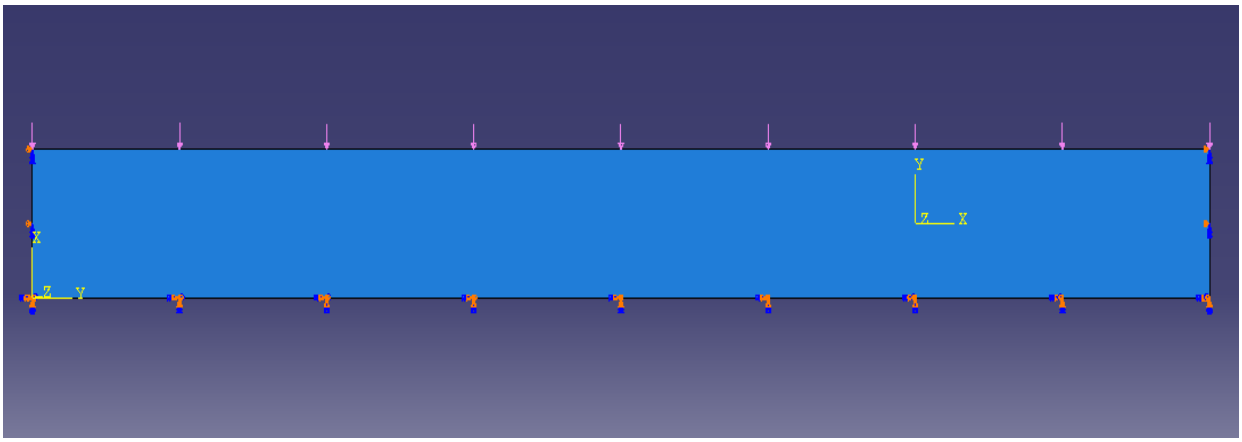


Figure 8.2 Boundary conditions and edge loading.

Quadrilateral eight node doubly curved thick shell element (S8R) with reduced integration having element size equal to 10.0 mm x 10.0 mm was used to model the anisotropic laminated composite

wide plates after performing a convergence study to select the appropriate mesh size. Figure 8.3 presents the meshed wide plate used in the numerical analysis.

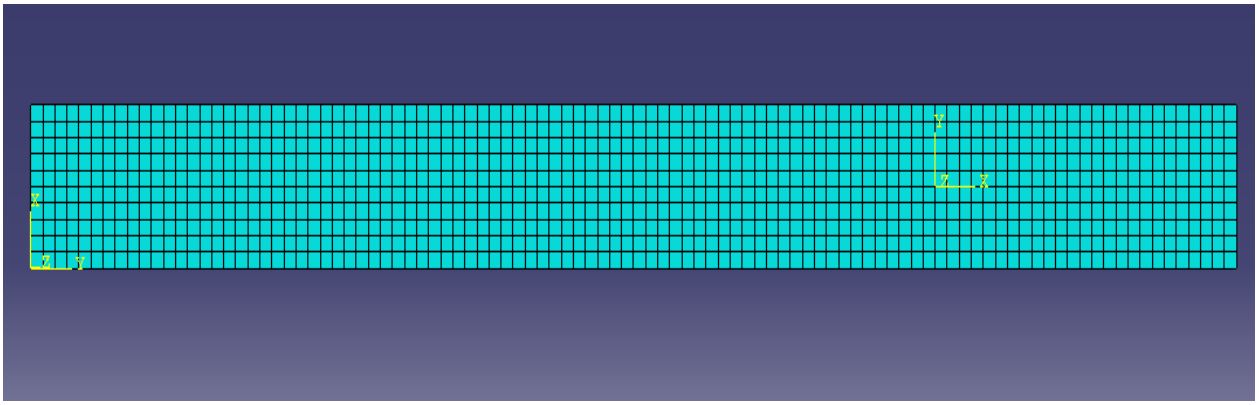

Figure 8.3 Meshed Model

Based on Lanczos solver, eigenvalue computation was conducted using buckling analysis. Lanczos technique extracts the eigenvalue and eigenvector values of a complex Hermitian matrix depending on the power method where a symmetric matrix is reduced to tridiagonal matrix using recurrence relations [12].

## 8.4 Results and Applications

### 8.4.1 Numerical Validation

The generalized closed form buckling solution of anisotropic wide plates was confirmed along with the finite element analysis. S-Glass/Epoxy material was attempted in the validation study and its properties are reported in Table 8.1; obtained from typical values in an FRP textbook [13].

Table 8.1 S-Glass/Epoxy material properties [13].

| **Material** | $E_{11}$ | $E_{22}$ | $G_{12}$ | $\nu_{12}$ |
|---|---|---|---|---|
| **S-Glass/Epoxy** | 55.0 GPa | 16.0 GPa | 7.6 GPa | 0.28 |

Table 8.2 illustrates the comparison between the analytical and numerical results for different stacking sequences of the anisotropic laminated composite wide plates with the following

dimensions for width, height, and thickness: 1000 mm x 100 mm x 0.4 mm, respectively. In general, an excellent agreement between the results is observed with maximum error around 4.51% for the Antisymmetric angle ply (30/-30/30/-30). It is observed that the stacking sequence with maximum error yields the analytical solution on the un-conservative side.

Table 8.2 Comparison between analytical and numerical results for S-Glass/Epoxy thin plates (h/t = 250 mm).

| **Ply Orientations** | **Analytical Results, N** | **Numerical Results, N** | **% Error** | **Layup Type** |
|---|---|---|---|---|
| **0/0/0/0** | 0.074067 | 0.074066 | 0.0014 | Single Specially Orthotropic |
| **90/90/90/90** | 0.0215466 | 0.021547 | 0.0019 | Single Specially Orthotropic |
| **30/-30/30/-30** | 0.052773 | 0.050391 | 4.5137 | Antisymmetric Angle Ply |
| **45/-45/45/-45** | 0.036921 | 0.035541 | 3.7378 | Antisymmetric Angle Ply |
| **60/-60/60/-60** | 0.026513 | 0.026124 | 1.4673 | Antisymmetric Angle Ply |
| **60/-60/45/-45** | 0.031025 | 0.030205 | 2.6431 | Balanced Angle Ply |
| **30/-30/45/-45** | 0.043712 | 0.04197 | 3.9852 | Balanced Angle Ply |
| **30/-30/60/-60** | 0.036118 | 0.035157 | 2.6608 | Balanced Angle Ply |
| **30/-30/0/0** | 0.061971 | 0.060086 | 3.0418 | Anisotropic |
| **30/-30/0/90** | 0.039123 | 0.037732 | 3.5555 | Anisotropic |

| | | | | |
|---|---|---|---|---|
| **30/30/30/30** | 0.052773 | 0.05462 | 3.4999 | Single Anisotropic Layer |
| **30/-30/-30/30** | 0.052773 | 0.054813 | 3.8657 | Symmetric Angle Ply |
| **0/90/90/0** | 0.067502 | 0.067498 | 0.006 | Symmetric Cross Ply |
| **30/-60/-60/30** | 0.04949 | 0.051363 | 3.7847 | Symmetric Multiple Angle Layers |
| **0/90/0/90** | 0.044884 | 0.045101 | 0.4835 | Antisymmetric Cross Ply |
| **-45/30/-30/45** | 0.038903 | 0.03774 | 2.9895 | Antisymmetric Angle Ply |
| **90/0/0/90** | 0.0281116 | 0.028112 | 0.0015 | Symmetric Cross Ply |

### 8.4.2 Effect of Ply Orientation

A parametric study was conducted to investigate the effect of different stacking sequences of the anisotropic laminated composite wide plates with the following dimensions: 1000 mm x 100 mm x 0.4 mm for width, height, and thickness, respectively, on the stability response. The critical buckling load varies between 0.074067 N and 0.021547 N for different ply orientations as shown in Table 8.2. Moreover, an edge effect was observed for some staking sequences such as the anisotropic layup (30/-60/-60/30) as shown in Figure 8.4. On the other hand, the other stacking sequences exhibited a uniform deformation along the plate, see Figure 8.5.

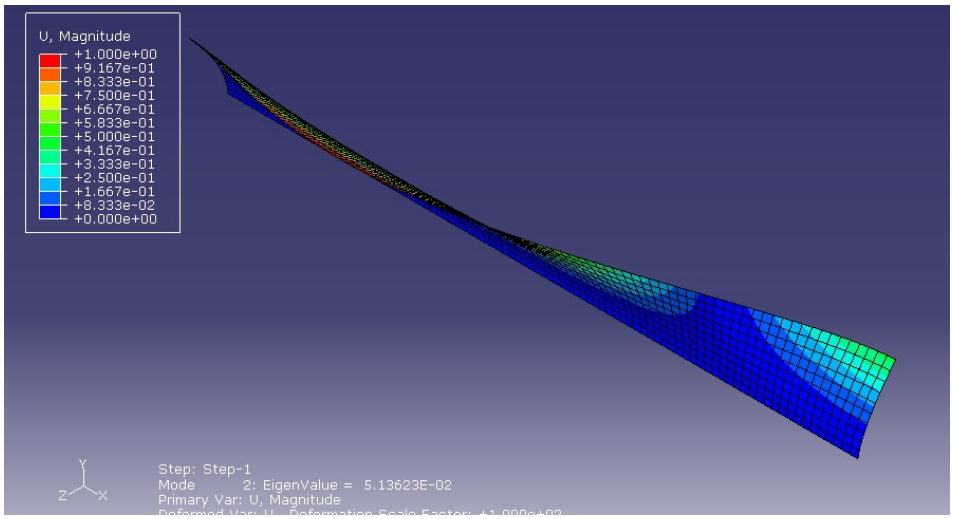

Figure 8.4 Buckling mode shape and edge effect of (30/-60/-60/30) layup.

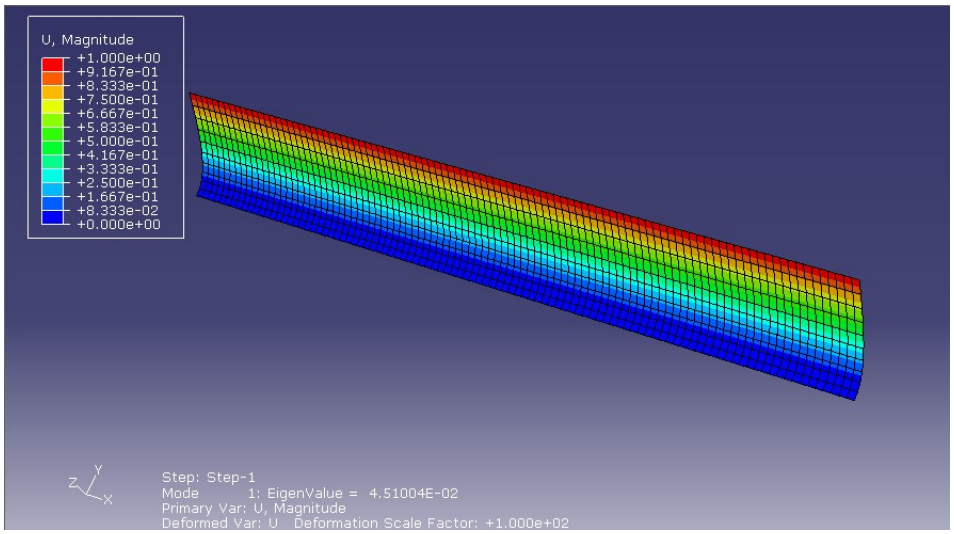

Figure 8.5 Bucking mode shape with uniform deformation.

### 8.4.3 Effect of Material Properties

Effect of Hybrid composite wide plates was investigated in this section. S-Glass/Epoxy and High Strength Graphite/Epoxy material were used and their properties are reported in Table 8.1 and Table 8.3; obtained from typical values in FRP textbook [13]. Layups with ply orientations equal to $90^o$ and $\pm 60^o$ were composed of S-Glass/Epoxy while High Strength Graphite/Epoxy was used for other orientations. Table 8.4 presents the analytical and numerical results of Hybrid wide plates

for various stacking sequences in which the balanced angle ply (30/-30/60/-60) and the symmetric cross ply (90/0/0/90) exhibited the maximum and minimum error value, respectively.

Table 8.3 High Strength Graphite/Epoxy Material Properties [13].

| **Material** | $E_{11}$ | $E_{22}$ | $G_{12}$ | $\nu_{12}$ |
|---|---|---|---|---|
| **High Strength Graphite/Epoxy** | 145.0 GPa | 10.0 GPa | 4.8 GPa | 0.25 |

Table 8.4 Comparison between analytical and numerical results of Hybrid plates (t = 0.4 mm).

| **Ply Orientations** | **Analytical Results, N** | **Numerical Results, N** | **% Error** |
|---|---|---|---|
| **30/-30/60/-60** | 0.04708 | 0.04308 | 8.4962 |
| **30/-30/0/90** | 0.07403 | 0.07021 | 5.1601 |
| **0/90/90/0** | 0.17038 | 0.17035 | 0.0177 |
| **0/90/0/90** | 0.09285 | 0.09387 | 1.0986 |
| **90/0/0/90** | 0.0428081 | 0.0428065 | 0.00374 |

### 8.4.4 Effect of Element Thickness

The effect of thin, moderately thick, and thick wide plate on the critical buckling load values was also reported herein. Comparison between the analytical and numerical (FE) results using S-Glass/Epoxy material were conducted for three different height to thickness ratios equal to 250, 62.5, and 10.0 to demonstrate thin, moderately thick, and thick wide plates, respectively. Table 8.2 illustrated the analytical and numerical solutions for thin anisotropic wide plates. Table 8.5 shows the results for moderately thick wide plates (h/t =62.5) in which a very good agreement was observed between the closed form solution and the finite element analysis with maximum error value around 7.4% for the symmetric angle ply (30/-30/-30/30). The analytical and numerical results for thick anisotropic wide plates are presented in Table 8.6.The generalized analytical

results were off from the finite element results. In general, it was observed the present formula was capable of capturing the behavior of moderate thick wide plates in similar manner to that of thin wide plates. This may suggest that the developed analytical formula herein can successfully re-produce accurate estimate of the buckling loads in moderately thick wide plates. On the other hand, the consideration of shear deformations is very important to estimate the buckling loads of thick wide plates.

Table 8.5 Comparison between analytical and numerical results for S-Glass/Epoxy moderately thick plates (h/t = 62.5)

| **Ply Orientations** | **Analytical Results, N** | **Numerical Results, N** | **% Error** | **Layup Type** |
|---|---|---|---|---|
| **0/0/0/0** | 4.740247 | 4.738 | 0.0475 | Single Specially Orthotropic |
| **90/90/90/90** | 1.378981 | 1.3785 | 0.0349 | Single Specially Orthotropic |
| **30/-30/30/-30** | 3.377426 | 3.2234 | 4.5605 | Antisymmetric Angle Ply |
| **60/-60/45/-45** | 1.985567 | 1.9323 | 2.6828 | Balanced Angle Ply |
| **30/-30/0/90** | 2.503835 | 2.4132 | 3.6199 | Anisotropic |
| **30/-30/-30/30** | 3.377426 | 3.1265 | 7.4296 | Symmetric Angle Ply |
| **0/90/90/0** | 4.320089 | 4.3163 | 0.0878 | Symmetric Cross Ply |
| **0/90/0/90** | 2.872542 | 2.885 | 0.4337 | Antisymmetric Cross Ply |

Table 8.6 Comparison between analytical and numerical results for S-Glass/Epoxy thick plates (h/t = 10.0)

| **Ply Orientations** | **Analytical Results, N** | **Numerical Results, N** | **% Error** | **Layup Type** |
|---|---|---|---|---|
| **0/0/0/0** | 2994.349676 | 1136.5 | 62.0452 | Single Specially Orthotropic |
| **90/90/90/90** | 206.506875 | 332.24 | 60.8857 | Single Specially Orthotropic |

| | | | | |
|---|---|---|---|---|
| **30/-30/30/-30** | 1790.61043 | 771.41 | 56.9192 | Antisymmetric Angle Ply |
| **60/-60/45/-45** | 575.19047 | 464.65 | 19.2181 | Balanced Angle Ply |
| **30/-30/0/90** | 1078.73674 | 616.48 | 42.8517 | Anisotropic |
| **30/-30/-30/30** | 1790.61043 | 833.47 | 53.4534 | Symmetric Angle Ply |
| **0/90/90/0** | 2645.86933 | 1019.8 | 61.457 | Symmetric Cross Ply |
| **0/90/0/90** | 1354.40817 | 690.05 | 49.0516 | Antisymmetric Cross Ply |

## 8.5 Conclusion

A generalized analytical buckling formula for clamped-free anisotropic laminated composite wide plates under uniaxial compression was presented in this work based on Rayleigh-Ritz approximation. The presented solution is expressed in terms of extensional, coupling, and flexural stiffness coefficients in the principal directions as well as infinitely wide plate geometry. In general, a very good agreement was observed between the analytical and numerical (FE) results. The proposed formula accurately predicted the critical buckling load values for hybrid carbon/glass composite fiber, and different ply orientations. Furthermore, the generalized close-form solution captured the complexity in the behavior of thin and moderately thick anisotropic wide plates.

## 8.6 References


[1] Huang, L. Sheikh, A. H., Ng, C-T., and Griffith, M. C., "An efficient finite element model for buckling analysis of grid stiffened laminated composite plates," Composite Structures, 122 (2015) 41-50.

[2] Wang, D., and Abdalla, M. M, "Global and local buckling analysis of grid-stiffened composite panels," Composite Structures , 119 (2015) 767-776.

[3] Weber, M. J., and Middendrof, P., "Semi-analytical skin buckling of curved orthotropic grid-stiffened shells," Composite Structures, 108 (2014) 616-624.

[4] Grover, N., Maiti, D. K., and Singh, B. N., "A new inverse hyperbolic shear deformation theory for static and buckling analysis of laminated composite and sandwich plates," Composite Structures, 95(2013) 667-675.

[5] Khayat, M., Poorveis, D., and Moradi, S., " Buckling analysis of laminated composite cylindrical shell subjected to lateral displacement-dependent pressure using semi-analytical finite strip method," Steel and Composite Structures, 22(2) (2016) 301-321.

[6] Baba, B. O., and Baltaci, A., "Buckling Characteristics of symmetrically and antisymmetrically laminated comosite plates with central cutout," Applied Composite Material, 14(4)(2007) 265-276.

[7] Becheri,T., Amara, K., Bouazza, M., Benseddiq, N.,"Buckling of symmetrically laminated plates using nth-order shear deformation theory with curvature effects," Steel and Composite Structures, 21(6) (2016) 1347-1368.

[8] Debski, H., "Numerical analysis of stability of thin-walled composite column with open cross-section," Mechanics and Mechanical Engineering, 17 (1)(2013) 29-35.

[9] Koiter, W.T., "Elastic stability and post-buckling behavior," In: Proceedings of the Symposium on Non-linear Problems, University of Wisconsin, Wisconsin (1963) 257-275.

[10] Cortinez, H.V., and Piovan, M. T., "Stability of composite thin-walled beams with shear deformability," Computers & Structures, 84(2006) 978-990.

[11] Jones, R.M, Mechanics of Composite Materials, New York: Hemisphere Publishing Corporation, 1975.

[12] Hernandez, V., Roman, J.E., Tomas, A., and Vidal, V., "Lanczos methods in SLEPc," Polytechnic University of Valencia, Province of Valencia, 2006.

[13] Rasheed, H.A., Strengthening Design of Reinforced Concrete with FRP, New York: CRC Press, 2015.

# Chapter 9 - Buckling Solutions of Clamped-Pinned Anisotropic Laminated Composite Columns under Axial Compression using Bifurcation Approach and Finite Elements

**Rund Al-Masri[1] and Hayder A. Rasheed[2]**

## 9.1 Abstract

**Following a bifurcation approach, a generalized closed form buckling solution for clamped-pinned anisotropic laminated composite columns under axial compression is developed using the energy method. The effective axial, coupling, and flexural rigidity coefficients of the anisotropic layups is determined following the generalized constitutive relationship using dimensional reduction by static condensation of 6x6 rigidity matrix. The presented analytical explicit formula reproduces Euler buckling expression in the case of isotropic or specially-orthotropic materials once the effective coupling term vanishes. On the other hand, the analytical formula furnishes two extra terms which are a function of the effective coupling, flexural and axial rigidity. The analytical buckling formula is confirmed against finite element Eigen value solutions for different anisotropic laminated layups yielding high accuracy for a wide range of stacking sequences. A parametric study is then conducted to examine the effect of ply orientations, material properties including hybrid carbon/glass fiber composites and FE element type. Relevance of the numerical and analytical results is discussed in comparison to previous results in literature.**

Keywords: Buckling of Composite Columns, Clamped-Pinned Boundary Conditions, Anisotropic Laminated Composites, Axial Compression.

[1] Ph.D. Candidate, Department of Civil Engineering, Kansas State University, Manhattan, KS 66506

[2] Professor, Department of Civil Engineering, Kansas State University, Manhattan, KS 66506

## 9.2 Introduction

The distinguished properties of laminated composite material such as high stiffness-to-weight ratio, high strength-to-weight ratio, as well as fatigue and corrosion resistance have captured the industry attention in the past few decades. Accordingly, the demand to understand the stability mechanics of laminated composite members has increased. Despite the fact that limited amount of research studies has addressed the buckling of anisotropic laminated composite columns, significant amount of studies has been conducted on the stability of composite shells, plates, beams, and cylinders [1-15]. Heidari-Rarani et al. [1] investigated the effect of angle-ply and cross-ply layups on the stability of E-glass/epoxy square composite laminated plates under axial compression with SFSF (S: simply supported, F: Free) boundary conditions analytically, numerically, and experimentally. A semi-analytical solution was developed using Rayleigh-Ritz approach. Analytical results were verified against finite element analysis yielding an excellent accuracy. Moreover, Hashin, Tsai-Wu, and Tsai-Hill failure criteria were attempted in the numerical analysis to study the layer failure of the laminated composites. Experimentally, E-glass/epoxy plates of four layers were made with angle-ply ($[\mp 30]_s$ and $[\mp 45]_s$) and cross-ply ($[0/90]_s$) stacking sequences using hand layup method. The test was conducted under displacement control with rate equal to 0.5 mm/min. On the other hand, the semi-analytical and numerical buckling load values were overestimated compared to the experimental results. Tsai-Wu and Tsai-Hill failure criteria had the same failure mode as the tested plates in which the failure started from the plate edge then developed along the plate. Abramovich and Livshits [2] studied the free vibrations of non-symmetric cross ply laminated composite beams based on the first order shear deformation theory. Longitudinal, transverse displacement, rotary inertia, and shear deformation

were considered in the analysis. The following equation of motion of cross ply laminated composite beams was solved for different boundary conditions:

$$\mathbf{[M]}\{\ddot{q}\}\mathbf{+[C]}\ \{q\}\ \mathbf{=}\ \{\mathbf{0}\} \qquad \mathbf{(1)}$$

Where [M] is the generalized mass matrix, [C] is the matrix differential operator; and $\{q\}$ is the vector of the generalized displacements. The new approach and Bernoulli-Euler theory were verified against numerical solutions. Based on the generalized Galerkin method, Lopatin and Morozov [3] proposed analytical formula to predict the buckling of composite cantilever circular cylindrical shell under uniform external lateral pressure. Finite element software COSMOS/M was used to perform the eigenvalue and eigenvector computations with SHELL4L element, which was confirmed against the analytical results yielding an accurate estimate of the buckling load values. Cortinez and Piovan [4] presented a theoretical model to study the stability of composite thin-walled beams with shear deformability using nonlinear displacement field depending on Hellinger-Reissner principal. A finite elements with fourteen degrees of freedoms were used to solve the governing equations. The results showed that shear flexibility had a significant effect on the stability of the composite beams. Using equivalent layer shell theory with six degrees of freedom and the first shear deformation theory, Rikards et al. [5] presented a triangular finite element to study the buckling and vibration of laminated composite stiffened plates and shells. The numerical results were confirmed with previous solutions developed by Jaunky et al. [6] yielding a good agreement. Kumar and Mukhopadhayay [7] developed a new finite element to investigate the buckling of laminated stiffened plate for different boundary conditions based on the first order shear deformation theory. The presented finite element predicted the critical buckling load without shear locking for thin and thick plates. Furthermore, the numerical results exhibited a good agreement with existing solutions (Loughlan [8]). Kidane et al. [9] introduced analytical model to

predict the stability of grid stiffened composite cylinders based on the smeared method. The equivalent material properties of the grid stiffened composite cylindrical shells were taking into account. Moreover, the results were confirmed against experimental and previous results [10]. Debski et al. [11] studied the buckling and post-buckling of simply supported thin-walled composite channel column under axial compression loading experimentally. Carbon/epoxy columns of eight symmetrical plies [0/-45/45/90]s were tested using Zwick Z100/SN3A universal testing machine. The experimental results were verified with numerical (FE) results and analytical-numerical method (ANM) [12-15].

A generalized analytical buckling formula was developed for anisotropic laminated composite clamped-pinned columns under axial compression loading using the bifurcation solution of pre-buckling deformation. Applying static condensation method, three dimensional 6 x 6 composite rigidity matrix is converted to one dimensional axial, coupling, and flexural rigidities. Moreover, the analytical results were confirmed against finite element analysis using commercial software Abaqus yielding an excellent agreement. Furthermore, comparison of the analytical results against previous finding for cross-ply laminates showed excellent correlations.

## 9.3 Analytical Formulation

### 9.3.1 Assumptions and Kinematics

Bifurcation solution is used to develop a generalized analytical critical buckling formula for clamped-pinned anisotropic laminated composite columns under axial compression. Prior to deriving the analytical solution, several assumptions are considered and presented in the following points:

- Buckling takes place in the x-y plane about the weak axis (z-axis).

- The y-axis runs through the thickness of the column where the composite lamination takes place, Figure 9.1
- The lamination angle ( α ) is measured with respect to the x-axis (i.e. 0° fibers run parallel to the x-axis and 90° fibers run parallel to the z-axis). Accordingly, the angle ( α ) is rotated about the y-axis.
- Plane sections before bending remain plane after bending and perpendicular to the mid surface (i.e. simple beam theory holds).
- Classical lamination theory is applicable with shear deformations ignored.

Cartesian coordinates and geometry of the clamped-pinned columns used are illustrated in Figure 9.1. The bending occurs about the z-axis (weak axis). The following displacement relations were assumed based on the isotopic Euler first buckling mode:

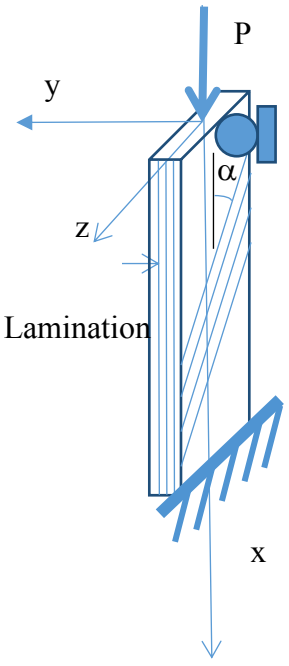


Figure 9.1 The column geometry.

$$\boldsymbol{u}\,(\boldsymbol{x}) = \boldsymbol{B_1}(\boldsymbol{L}-\boldsymbol{x})\,; \quad \boldsymbol{v}\,(\boldsymbol{x}) = \boldsymbol{C_1}\,(\frac{\boldsymbol{x}}{\boldsymbol{L}} + \mathbf{1.0245}\,\mathbf{sin}\,\frac{\mathbf{4.4934}\boldsymbol{x}}{\boldsymbol{L}}) \tag{2}$$

where $u(x)$, and $v(x)$ is the axial, and lateral displacements; $B_1$, and $C_1$ are constants to be solved for; and x is the distance along the axis of the column starting at the point load. For an intermediate class of deformation, the axial strain $\varepsilon_x$ and curvature $\kappa_x$are defined as follow.

$$\boldsymbol{\varepsilon_x} = \frac{\boldsymbol{du}}{\boldsymbol{dx}} + \frac{\mathbf{1}}{\mathbf{2}}(\frac{\boldsymbol{dv}}{\boldsymbol{dx}})^{\mathbf{2}} = \boldsymbol{u'} + \frac{\mathbf{1}}{\mathbf{2}}\boldsymbol{v'^2}; \qquad \boldsymbol{\kappa_x} = \frac{\boldsymbol{d^2v}}{\boldsymbol{d^2x}} = \boldsymbol{v''} \tag{3}$$

### 9.3.2 Constitutive equations

The principal material directions were transformed into the column coordinate system, the stresses and strains are then related in the following equation

$$\begin{Bmatrix} \boldsymbol{\sigma_x} \\ \boldsymbol{\sigma_z} \\ \boldsymbol{\tau_{xz}} \end{Bmatrix} = \begin{bmatrix} \boldsymbol{\bar{Q}_{11}} & \boldsymbol{\bar{Q}_{12}} & \boldsymbol{\bar{Q}_{16}} \\ \boldsymbol{\bar{Q}_{12}} & \boldsymbol{\bar{Q}_{22}} & \boldsymbol{\bar{Q}_{26}} \\ \boldsymbol{\bar{Q}_{16}} & \boldsymbol{\bar{Q}_{26}} & \boldsymbol{\bar{Q}_{66}} \end{bmatrix} \begin{Bmatrix} \boldsymbol{\varepsilon_x} \\ \boldsymbol{\varepsilon_z} \\ \boldsymbol{\gamma_{xz}} \end{Bmatrix} \tag{4}$$

Where $\bar{Q}_{ij}$ represent the transformed reduced stiffness matrix as defined in standard composite textbooks [16]. Accordingly, the coupled force-strain relationship is established as follows:

$$\begin{Bmatrix} \boldsymbol{N_x} \\ \boldsymbol{N_z} \\ \boldsymbol{N_{xz}} \\ \boldsymbol{M_x} \\ \boldsymbol{M_z} \\ \boldsymbol{M_{xz}} \end{Bmatrix} = \begin{bmatrix} \boldsymbol{A_{11}} & \boldsymbol{A_{12}} & \boldsymbol{A_{16}} & \boldsymbol{B_{11}} & \boldsymbol{B_{12}} & \boldsymbol{B_{16}} \\ \boldsymbol{A_{12}} & \boldsymbol{A_{22}} & \boldsymbol{A_{26}} & \boldsymbol{B_{12}} & \boldsymbol{B_{22}} & \boldsymbol{B_{26}} \\ \boldsymbol{A_{16}} & \boldsymbol{A_{26}} & \boldsymbol{A_{66}} & \boldsymbol{B_{16}} & \boldsymbol{B_{26}} & \boldsymbol{B_{66}} \\ \boldsymbol{B_{11}} & \boldsymbol{B_{12}} & \boldsymbol{B_{16}} & \boldsymbol{D_{11}} & \boldsymbol{D_{12}} & \boldsymbol{D_{16}} \\ \boldsymbol{B_{12}} & \boldsymbol{B_{22}} & \boldsymbol{B_{26}} & \boldsymbol{D_{12}} & \boldsymbol{D_{22}} & \boldsymbol{D_{26}} \\ \boldsymbol{B_{16}} & \boldsymbol{B_{26}} & \boldsymbol{B_{66}} & \boldsymbol{D_{16}} & \boldsymbol{D_{26}} & \boldsymbol{D_{66}} \end{bmatrix} \begin{Bmatrix} \boldsymbol{\varepsilon_x} \\ \boldsymbol{\varepsilon_z} \\ \boldsymbol{\gamma_{xz}} \\ \boldsymbol{\kappa_x} \\ \boldsymbol{\kappa_z} \\ \boldsymbol{\kappa_{xz}} \end{Bmatrix} \tag{5}$$

Where:

$$\boldsymbol{A_{ij}} = \sum_{\boldsymbol{k=1}}^{\boldsymbol{N}} \boldsymbol{\bar{Q}_{ij}} \boldsymbol{t_k}$$

$$\boldsymbol{B_{ij}} = \sum_{\boldsymbol{k=1}}^{\boldsymbol{N}} \boldsymbol{\bar{Q}_{ij}} \boldsymbol{t_k}\, \boldsymbol{\bar{y}_k}$$

$$\boldsymbol{D_{ij}} = \sum_{k=1}^{N} \bar{\boldsymbol{Q}}_{ij} \boldsymbol{t_k} (\bar{\boldsymbol{y}}_k^2 + \frac{\boldsymbol{t_k^2}}{12}) \tag{6}$$

$$\boldsymbol{t_k} = \boldsymbol{y_k} - \boldsymbol{y_{k-1}}$$

$$\bar{\boldsymbol{y}}_k = \frac{\boldsymbol{y_k} + \boldsymbol{y_{k-1}}}{2}$$

In which $A_{ij}$,$B_{ij}$ and $D_{ij}$ are the axial, coupling, and flexural rigidity coefficients. $t_k$ is the thickness of the k-th ply; and N is the number of different plies in the stacking sequence.

Using material properties and fiber orientations into equation (5), the three dimensional (3D) rigidity matrix is established. Accordingly, this matrix is reduced to 1D anisotropic axial, coupling and flexural rigidities using static condensation approach after applying the zero forces and moments.

$$\begin{Bmatrix} \boldsymbol{N_x} \\ \boldsymbol{N_z = 0} \\ \boldsymbol{N_{xz} = 0} \\ \boldsymbol{M_x} \\ \boldsymbol{M_z = 0} \\ \boldsymbol{M_{xz} = 0} \end{Bmatrix} = \begin{bmatrix} \boldsymbol{A_{11}} & \boldsymbol{A_{12}} & \boldsymbol{A_{16}} & \boldsymbol{B_{11}} & \boldsymbol{B_{12}} & \boldsymbol{B_{16}} \\ \boldsymbol{A_{12}} & \boldsymbol{A_{22}} & \boldsymbol{A_{26}} & \boldsymbol{B_{12}} & \boldsymbol{B_{22}} & \boldsymbol{B_{26}} \\ \boldsymbol{A_{16}} & \boldsymbol{A_{26}} & \boldsymbol{A_{66}} & \boldsymbol{B_{16}} & \boldsymbol{B_{26}} & \boldsymbol{B_{66}} \\ \boldsymbol{B_{11}} & \boldsymbol{B_{12}} & \boldsymbol{B_{16}} & \boldsymbol{D_{11}} & \boldsymbol{D_{12}} & \boldsymbol{D_{16}} \\ \boldsymbol{B_{12}} & \boldsymbol{B_{22}} & \boldsymbol{B_{26}} & \boldsymbol{D_{12}} & \boldsymbol{D_{22}} & \boldsymbol{D_{26}} \\ \boldsymbol{B_{16}} & \boldsymbol{B_{26}} & \boldsymbol{B_{66}} & \boldsymbol{D_{16}} & \boldsymbol{D_{26}} & \boldsymbol{D_{66}} \end{bmatrix} \begin{Bmatrix} \boldsymbol{\varepsilon_x} \\ \boldsymbol{\varepsilon_z} \\ \boldsymbol{\gamma_{xz}} \\ \boldsymbol{\kappa_x} \\ \boldsymbol{\kappa_z} \\ \boldsymbol{\kappa_{xz}} \end{Bmatrix} \tag{7}$$

Equation (7) is solved first for the axial strain and axial curvature ($\boldsymbol{\varepsilon_x}$ ,$\boldsymbol{\kappa_x}$) in terms of the rest of the deformation components by extracting the second, third, fifth and sixth linear equations from the matrix.

$$-\begin{bmatrix} \boldsymbol{A_{12}} & \boldsymbol{B_{12}} \\ \boldsymbol{A_{16}} & \boldsymbol{B_{16}} \\ \boldsymbol{B_{12}} & \boldsymbol{D_{12}} \\ \boldsymbol{B_{16}} & \boldsymbol{D_{16}} \end{bmatrix} \begin{Bmatrix} \boldsymbol{\varepsilon_x} \\ \boldsymbol{\kappa_x} \end{Bmatrix} = \begin{bmatrix} \boldsymbol{A_{22}} & \boldsymbol{A_{26}} & \boldsymbol{B_{22}} & \boldsymbol{B_{26}} \\ \boldsymbol{A_{26}} & \boldsymbol{A_{66}} & \boldsymbol{B_{26}} & \boldsymbol{B_{66}} \\ \boldsymbol{B_{22}} & \boldsymbol{B_{26}} & \boldsymbol{D_{22}} & \boldsymbol{D_{26}} \\ \boldsymbol{B_{26}} & \boldsymbol{B_{66}} & \boldsymbol{D_{26}} & \boldsymbol{D_{66}} \end{bmatrix} \begin{Bmatrix} \boldsymbol{\varepsilon_z} \\ \boldsymbol{\gamma_{xz}} \\ \boldsymbol{\kappa_{yz}} \\ \boldsymbol{\kappa_{xz}} \end{Bmatrix}$$

$$-\boldsymbol{R} \begin{Bmatrix} \boldsymbol{\varepsilon_x} \\ \boldsymbol{\kappa_x} \end{Bmatrix} = \boldsymbol{Q} \begin{Bmatrix} \boldsymbol{\varepsilon_z} \\ \boldsymbol{\gamma_{xz}} \\ \boldsymbol{\kappa_z} \\ \boldsymbol{\kappa_{xz}} \end{Bmatrix} \tag{8}$$

Inverting the matrix Q to the other side of equation (8), the condensed deformation components are obtained in terms of the axial strain and curvature:

$$\begin{Bmatrix} \boldsymbol{\varepsilon_z} \\ \boldsymbol{\gamma_{xz}} \\ \boldsymbol{\kappa_z} \\ \boldsymbol{\kappa_{xz}} \end{Bmatrix} = -[\boldsymbol{Q}]^{-1}[\boldsymbol{R}] \begin{Bmatrix} \boldsymbol{\varepsilon_x} \\ \boldsymbol{\kappa_x} \end{Bmatrix} \tag{9}$$

Substituting equation (9) into the first and fourth linear equation of the matrix (7); the axial force and in-plane moment vs. the axial strain and in-plane curvature relationship can be expressed in terms of the generally anisotropic material properties

$$\begin{bmatrix} \boldsymbol{N_x} \\ \boldsymbol{M_x} \end{bmatrix} = \begin{bmatrix} \boldsymbol{A_{ani}} & \boldsymbol{B_{ani}} \\ \boldsymbol{B_{ani}} & \boldsymbol{D_{ani}} \end{bmatrix} \begin{Bmatrix} \boldsymbol{\varepsilon_x} \\ \boldsymbol{\kappa_x} \end{Bmatrix} \tag{10}$$

Where

$$\begin{bmatrix} \boldsymbol{A_{ani}} & \boldsymbol{B_{ani}} \\ \boldsymbol{B_{ani}} & \boldsymbol{D_{ani}} \end{bmatrix} = \begin{bmatrix} \boldsymbol{A_{11}} & \boldsymbol{B_{11}} \\ \boldsymbol{B_{11}} & \boldsymbol{D_{11}} \end{bmatrix} - [\boldsymbol{R}]^{\boldsymbol{T}}[\boldsymbol{Q}]^{-1}[\boldsymbol{R}] \tag{11}$$

### 9.3.3 Pre-buckling Solution

Based on the mode shape of clamped-pinned column, pre-buckling solution is considered to derive the buckling formula. The in-plane moment ($M_x$) is set to zero during pre-buckling and before reaching the buckling load assuming a bifurcation response.

$$\boldsymbol{M_x} = \boldsymbol{B_{ani}\epsilon_x} + \boldsymbol{D_{ani}\kappa_x} \tag{12}$$

$$\boldsymbol{0} = \boldsymbol{B_{ani}\epsilon_x} + \boldsymbol{D_{ani}\kappa_x}$$

$$\boldsymbol{\kappa_x} = -\frac{\boldsymbol{B_{ani}}}{\boldsymbol{D_{ani}}}\boldsymbol{\epsilon_x} \tag{13}$$

By substituting Eq. (13) into the axial force equation, the axial force versus the axial strain can be expressed in terms of the generally anisotropic material properties

$$\boldsymbol{P_x} = \boldsymbol{A_{ani}\epsilon_x} + \boldsymbol{B_{ani}\kappa_x} \tag{14}$$

$$\boldsymbol{P_x} = \boldsymbol{A_{ani}\epsilon_x} - \frac{\boldsymbol{B_{ani}^2}}{\boldsymbol{D_{ani}}}\boldsymbol{\epsilon_x}$$

$$\boldsymbol{P_x = A_{eff}\epsilon_x} \tag{15}$$

Where

$$\boldsymbol{A_{eff} = A_{ani} - \frac{B_{ani}^2}{D_{ani}}} \tag{16}$$

The axial force ($P_x$) is positive and in compression based on the assumed sign convention. However, the axial strain ($\epsilon_x$) is negative while it is also in compression. Accordingly a negative sign is inserted into equation (2) as follow:

$$\boldsymbol{u = -B_1(L - x)} \tag{17}$$

Using the axial strain in Eq. (3), setting the lateral displacement term to zero, and substituting equation (17), the axial strain can be expressed as

$$\boldsymbol{\epsilon_x = B_1} \tag{18}$$

By substituting Eq. (18) into Eq. (15), a relationship between the axial force and the unknown constant ($B_1$) is obtained, i.e.

$$\boldsymbol{B_1 = \frac{P_x}{A_{eff}}} \tag{19}$$

### 9.3.4 Bifurcation Solution in terms of Pre-buckling Deformation

Energy approach is attempted in the bifurcation solution in which the strain energy can be expressed in terms of the integration of the applied loads multiplying the corresponding deformations.

$$\boldsymbol{U = \int_0^L \left(\frac{1}{2}N_x\varepsilon_x + \frac{1}{2}M_x\kappa_x\right) dx}$$

$$\boldsymbol{= \int_0^L \frac{1}{2}(A_{ani}\varepsilon_x^2 + B_{ani}\varepsilon_x\kappa_x)\, dx + \int_0^L \frac{1}{2}(B_{ani}\varepsilon_x\kappa_x + D_{ani}\kappa_x^2)\, dx} \tag{20}$$

The potential of external loads can be expressed as

$$W = -P\,u(L) \tag{21}$$

In view of equations (20) and (21), the total potential energy function is given by

$$\Pi = U - W = \int_0^L \frac{1}{2}\left(A_{ani}\varepsilon_x^2 + 2B_{ani}\varepsilon_x\kappa_x + D_{ani}\kappa_x^2\right) dx + P\,u(L) \tag{22}$$

$$\Pi = A_{ani}\left[\frac{1}{2}B_1^2 L - 5.048\,B_1\frac{C_1^2}{L} + 22.7975\frac{C_1^4}{L^3}\right] + B_{ani}\left[5.6036\,B_1\frac{C_1}{L} - 29.3124\,\frac{C_1^3}{L^3}\right] +$$

$$101.9215\,D_{ani}\frac{C_1^2}{L^3} - PB_1L \tag{23}$$

By substituting Eq. (19) into the total potential energy function given by Eq. (23), one obtains

$$\Pi = A_{ani}\left[\frac{1}{2}\frac{P^2}{A_{eff}}L - 5.048\,\frac{P}{A_{eff}}\frac{C_1^2}{L} + 22.7975\frac{C_1^4}{L^3}\right] + B_{ani}\left[5.6036\,\frac{P}{A_{eff}}\frac{C_1}{L} - 29.3124\,\frac{C_1^3}{L^3}\right] +$$

$$101.9215\,D_{ani}\frac{C_1^2}{L^3} - \frac{P^2}{A_{eff}}L \tag{24}$$

Minimizing the total potential energy with respect to the unknown $C_1$, setting the resulting expression to zero, and manipulating the equation, one gets

$$\frac{\partial\Pi}{\partial C_1} = A_{ani}\left[-10.096\frac{P}{A_{eff}}\frac{C_1}{L} + 91.19\frac{C_1^3}{L^3}\right] + B_{ani}\left[5.6036\,\frac{P}{A_{eff}}\frac{1}{L} - 87.9372\,\frac{C_1^2}{L^3}\right] +$$

$$203.843\,D_{ani}\frac{C_1}{L^3} = 0 \tag{25}$$

The cubic equation (25) with respect to $C_1$ does not lend itself to a close form solution of the buckling load. Therefore, the second derivative of Eq. (25) with respect to $C_1$ is considered

$$\frac{\partial^2\Pi}{\partial C_1^2} = A_{ani}\left[-10.096\frac{P}{A_{eff}}\frac{1}{L} + 273.57\frac{C_1^2}{L^3}\right] - 175.8744\,B_{ani}\frac{C_1}{L^3} + 203.843\,\frac{D_{ani}}{L^3} = 0 \tag{26}$$

By solving Eq. (26), one gets

$$C_1 = \frac{175.8744\frac{B_{ani}}{L^3} \mp \sqrt{175.8744^2\frac{B_{ani}^2}{L^6} - 4(273.57)\frac{A_{ani}}{L^3}\left(203.843\frac{D_{ani}}{L^3} - 10.096\frac{PA_{ani}}{A_{eff}L}\right)}}{2A_{ani}\frac{273.57}{L^3}} \tag{27}$$

In order for the $C_1$ value to be real, the discriminant must be at least zero. By setting the discriminant to zero, a closed form solution for the critical buckling load is developed in terms of the generally anisotropic material properties as well as the column geometry:

$$\boldsymbol{P_{cr} = 20.19\frac{D_{ani}}{L^2} - 22.9898\frac{B_{ani}^2}{A_{ani}L^2} + 2.7998\ \frac{B_{ani}^4}{A_{ani}^2 D_{ani} L^2}} \quad \textbf{(28)}$$

It is observed that Eq. (28) reduces down to Euler buckling formula of the clamped-pinned isotropic column in the case of isotropic or specially-orthotropic materials.

## 9.4 Numerical Formulation

The developed analytical formula in the previous section was confirmed against numerical analysis (FE) using the commercial software package Abaqus. Columns were assembled with fixed support and pin support at the bottom and top of the column, respectively. Furthermore, axial loading was applied at the top of the column. Quadrilateral eight node doubly curved thick shell element (S8R) was attempted in the modeling process in three dimensional space with element size 0.5 x 0.5 mm after performing a convergence study to select the appropriate mesh size. Linear elastic laminated material was assumed for orthotropic and anisotropic layups. The model's boundary conditions and meshed model are presented in Figure 9.2.

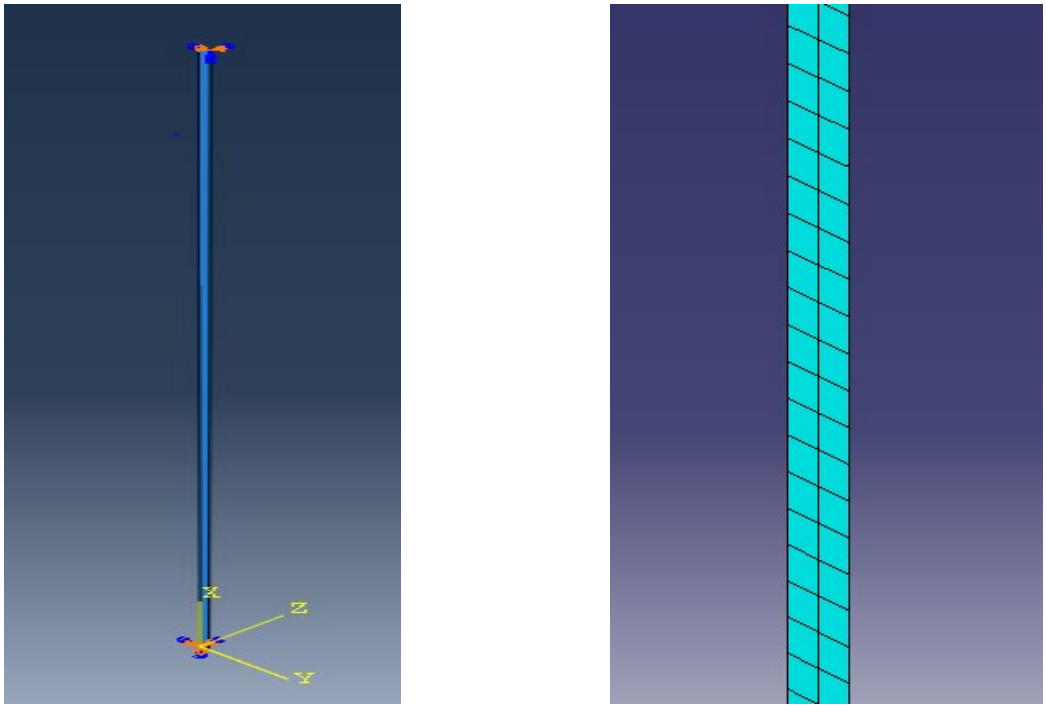


Figure 9.2. Left: Boundary conditions and applied load. Right: Meshed Model.

Using Lanczos solver, buckling analysis was attempted to simulate eigenvalue computation. Lanczos method solves eigenvalue and eigenvectors of complex Hermitian matrix based on the power method in which $m\,x\,m$ symmetric matrix is reduced to a tridiagonal matrix using multidimensional array values (recurrence relations) [17]. Nonlinear geometry analysis using the modified Riks formulation was performed to predict the stability response (pre-buckling and buckling) of the laminated composite columns. The modified Riks analysis is based on the Arc-length method in which it follows the equilibrium path, representing either the bifurcation points or the limit loads. During the analysis process, load increments are applied where equilibrium iterations converge along the arc length, forcing the constraint equation to be satisfied at every arc length increment [18].

## 9.5 Results and Applications

### 9.5.1 Numerical Validation

The analytical formula developed in section 2.4 was verified with the numerical (FE) analysis. Table 9.1 presents the material properties of S-Glass/Epoxy; obtained from typical values in FRP textbook [19], which was mainly used to simulate composite columns buckling behavior. The comparison between the analytical and numerical results for different stacking sequences is presented in Table 9.2 for composite columns with dimensions equal to: 100 mm x 1.0 mm x 0.4 mm for length, width, and thickness, respectively. The analytical results exhibited an excellent agreement with the numerical results having a maximum error value around 2.7 % for the single anisotropic layup (30/30/30/30). Single specially-orthotropic layer (0/0/0/0) exhibits the highest buckling load due to having all fibers aligned with the loading axis while the coupling coefficient $\boldsymbol{B_{ani}}$ vanishes. It is important to note that the layup with the maximum error yields the numerical buckling load on the conservative side.

Table 9.1 S-Glass/Epoxy material properties [19].

| **Material** | $\mathbf{E_{11}}$ | $\mathbf{E_{22}}$ | $\mathbf{G_{12}}$ | $\mathbf{\nu_{12}}$ |
|---|---|---|---|---|
| **S-Glass/Epoxy** | 55.0 GPa | 16.0 GPa | 7.6 GPa | 0.28 |

Table 9.2 Comparison of analytical and numerical results of S-Glass/Epoxy material.

| **Ply Orientations** | **Analytical Results, N** | **Numerical Results, N** | **% Error** | **Layup Type** |
|---|---|---|---|---|
| **0/0/0/0** | 0.59224 | 0.59218 | 0.01014 | Single Specially Orthotropic |
| **90/90/90/90** | 0.17229 | 0.17227 | 0.01161 | Single Specially Orthotropic |

| | | | | |
|---|---|---|---|---|
| **30/-30/30/-30** | 0.35615 | 0.35632 | 0.04774 | Antisymmetric Angle Ply |
| **45/-45/45/-45** | 0.2348 | 0.23498 | 0.07667 | Antisymmetric Angle Ply |
| **60/-60/60/-60** | 0.18521 | 0.18528 | 0.0378 | Antisymmetric Angle Ply |
| **60/-60/45/-45** | 0.20664 | 0.20719 | 0.26617 | Balanced Angle Ply |
| **30/-30/45/-45** | 0.28358 | 0.28512 | 0.54306 | Balanced Angle Ply |
| **30/-30/60/-60** | 0.24356 | 0.2467 | 1.28922 | Balanced Angle Ply |
| **30/-30/0/0** | 0.44074 | 0.44535 | 1.04597 | Anisotropic |
| **30/-30/0/90** | 0.28139 | 0.28289 | 0.53307 | Anisotropic |
| **30/30/30/30** | 0.29186 | 0.29967 | 2.67595 | Single Anisotropic Layer |
| **30/-30/-30/30** | 0.32773 | 0.33201 | 1.30596 | Symmetric Angle Ply |
| **0/90/90/0** | 0.54175 | 0.54155 | 0.03692 | Symmetric Cross Ply |

| | | | | |
|---|---|---|---|---|
| **30/-60/-60/30** | 0.2892 | 0.29458 | 1.86031 | Symmetric Multiple Angle Layers |
| **0/90/0/90** | 0.35998 | 0.36275 | 0.76949 | Antisymmetric Cross Ply |
| **-45/30/-30/45** | 0.25381 | 0.25401 | 0.0788 | Antisymmetric Angle Ply |
| **90/0/0/90** | 0.22562 | 0.22561 | 0.00444 | Symmetric Cross Ply |
| **30/30/-30/-30** | 0.31274 | 0.31277 | 0.0096 | Antisymmetric Angle Ply |

Moreover, the effect of having different stacking sequences of the simulated anisotropic columns is reported in Table 9.2 where the buckling load values varies between 0.59218 N and 0.17227 N. Furthermore, the buckling mode shape of the clamped-pinned composite columns is illustrated in Figure 9.3 for the anisotropic stacking sequence (30/-30/0/90) obtained from finite element analysis.

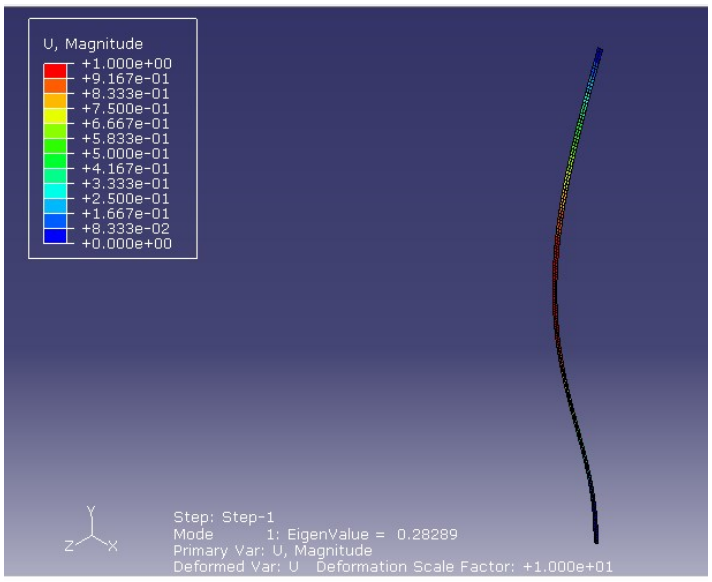

Figure 9.3 Buckling mode shape of clamped-pinned anisotropic column.

### 9.5.2 Nonlinear Geometry Analysis

Modified Riks analysis based on arc length method was conducted to indicate the existence of pre-buckling deformation in the transverse direction. Load versus maximum displacement curve is plotted for three different stacking sequences obtained from finite element against the analytical solution, see Figure 9.4. An excellent agreement is observed between the analytical and numerical results in which the Antisymmetric cross-ply (0/90/0/90) showed the highest buckling load compared to the other stacking sequences. On the other hand, the balanced angle ply (30/-30/60/-60) exhibited the lowest buckling load value. While the selected stacking sequences all show pre-buckling lateral displacement, the bifurcation formula predicted their buckling load very accurately.

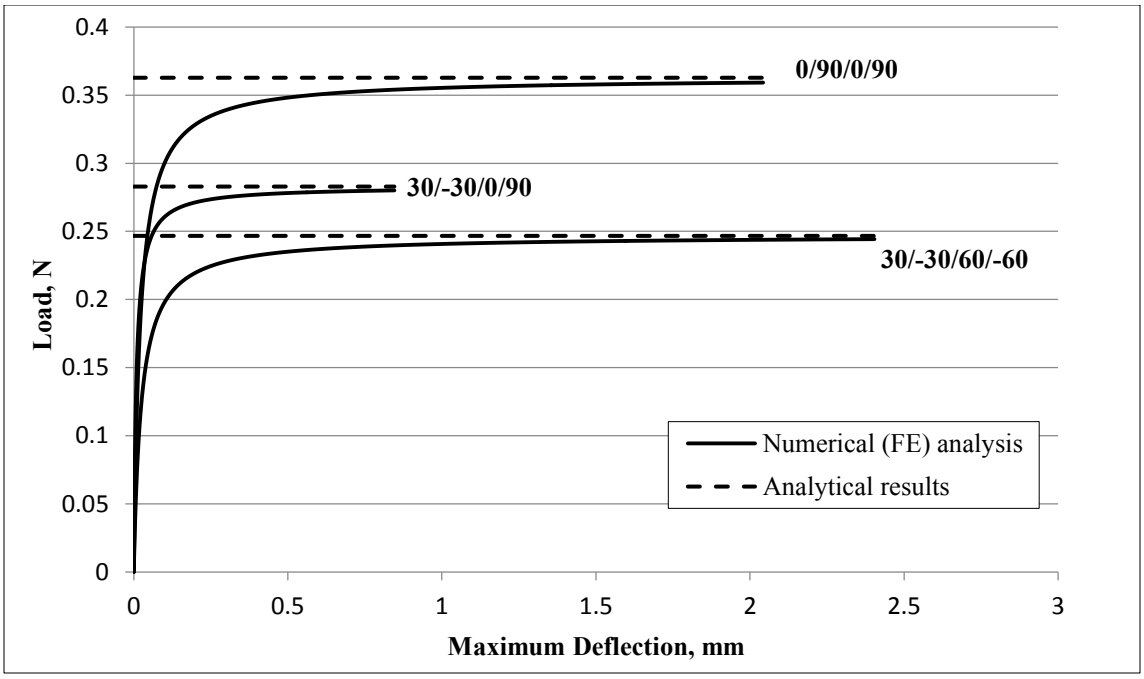


Figure 9.4 Load vs. deflection curve for analytical and numerical results.

### 9.5.3 Effect of Material Properties

A parametric study was performed to investigate the effect of having different material properties in which S-Glass/Epoxy and High Strength Graphite/Epoxy were assumed and their properties are illustrated in Table 9.1 and Table 9.3, respectively, obtained from typical values in FRP textbook [19].

Table 9.3 High Strength Graphite/Epoxy Material Properties [19].

| **Material** | $E_{11}$ | $E_{22}$ | $G_{12}$ | $\nu_{12}$ |
|---|---|---|---|---|
| **High Strength Graphite/Epoxy** | 145.0 GPa | 10.0 GPa | 4.8 GPa | 0.25 |

Critical buckling load values for S-Glass/Epoxy and High Strength Graphite/Epoxy are presented in Table 9.2 and Table 9.4, respectively. In general, High Strength Graphite/Epoxy columns showed a higher buckling load values compared to S-Glass/Epoxy ones due to the higher stiffness values along the fiber directions. The analytical results showed a good agreement against the

numerical (FE) results with maximum error and minimum error around 10.35%, 0.0093% for the single anisotropic layer layup (30/30/30/30) and single specially orthotropic layup (90/90/90/90), respectively.

Table 9.4 Comparison of analytical and numerical results of S-Glass/Epoxy material.

| **Ply Orientations** | **Analytical Results, N** | **Numerical Results, N** | **% Error** | **Layup Type** |
|---|---|---|---|---|
| **0/0/0/0** | 1.56136 | 1.5598 | 0.09992 | Single Specially Orthotropic |
| **90/90/90/90** | 0.10768 | 0.10767 | 0.00929 | Single Specially Orthotropic |
| **30/-30/30/-30** | 0.48923 | 0.4904 | 0.23916 | Antisymmetric Angle Ply |
| **45/-45/45/-45** | 0.18147 | 0.18212 | 0.35819 | Antisymmetric Angle Ply |
| **60/-60/60/-60** | 0.11637 | 0.11654 | 0.14609 | Antisymmetric Angle Ply |
| **60/-60/45/-45** | 0.14226 | 0.14386 | 1.12471 | Balanced Angle Ply |
| **30/-30/45/-45** | 0.26608 | 0.27358 | 2.81871 | Balanced Angle Ply |
| **30/-30/60/-60** | 0.19156 | 0.20152 | 5.19942 | Balanced Angle Ply |
| **30/-30/0/0** | 0.74085 | 0.77331 | 4.38146 | Anisotropic |
| **30/-30/0/90** | 0.35939 | 0.36327 | 1.07961 | Anisotropic |
| **30/30/30/30** | 0.22182 | 0.24478 | 10.35074 | Single Anisotropic Layer |

| | | | | |
|---|---|---|---|---|
| **30/-30/-30/30** | 0.39392 | 0.40376 | 2.49797 | Symmetric Angle Ply |
| **0/90/90/0** | 1.38311 | 1.3814 | 0.12364 | Symmetric Cross Ply |
| **30/-60/-60/30** | 0.23672 | 0.25552 | 7.94188 | Symmetric Multiple Angle Layers |
| **0/90/0/90** | 0.70389 | 0.71751 | 1.93497 | Antisymmetric Cross Ply |
| **-45/30/-30/45** | 0.23336 | 0.23424 | 0.3771 | Antisymmetric Angle Ply |
| **90/0/0/90** | 0.29012 | 0.29004 | 0.02758 | Symmetric Cross Ply |
| **30/30/-30/-30** | 0.3308 | 0.33021 | 0.17836 | Antisymmetric Angle Ply |

Hybrid composite columns were simulated to study the effect of combining two material on the stability response. S-Glass/Epoxy material was used for layups with orientations equal to $90^o$ and $\pm 60^o$ while the High Strength Graphite/Epoxy was attempted for the other orientations. In general, an excellent agreement was observed between the proposed analytical formula and the finite element analysis with maximum error around 3.6% for the balanced angle ply (30/-30/60/-60), see Table 9.5.

Table 9.5 Analytical and numerical results of the hybrid composite columns.

| **Ply Orientations** | **Analytical Results, N** | **Numerical Results, N** | **% Error** |
|---|---|---|---|
| **30/-30/60/-60** | 0.259 | 0.26829 | 3.5869 |
| **30/-30/0/90** | 0.38864 | 0.39015 | 0.3886 |
| **0/90/90/0** | 1.38986 | 1.3872 | 0.1914 |

| | | | |
|---|---|---|---|
| **0/90/0/90** | 0.75337 | 0.76297 | 1.2743 |
| **90/0/0/90** | 0.34581 | 0.34621 | 0.1157 |

### 9.5.4 Effect of Element Type in FE Analysis

The element type in finite element analysis was changed to study its on the buckling load values of composite columns compared to the analytical solution. Quadratic thick shell element (S8R) and quadratic solid element (C3D20R) both with reduced integration schemes were assumed with a mesh size equal to 0.5 mm, as mentioned earlier. The comparison between the analytical and numerical results for shell and solid element is presented in Table 9.6. Regarding the shell element results, an excellent agreement is exhibited between the results for all stacking sequences. However, the solid element results were noticeably off for the cross-ply and anisotropic stacking sequences having the same mesh size as that of the shell element since solid elements have only translation degrees of freedom while shell elements have rotational degrees of freedom. Accordingly, solid element might be less reliable than shell element in buckling analysis of composite members.

Table 9.6 Comparison of shell and solid element results

| **Ply Orientations** | **Analytical Results, N** | **Shell Element S8R, N** | **Solid Element C3D20R, N** |
|---|---|---|---|
| **0/0/0/0** | 1.56136 | 1.5598 | 1.5598 |
| **90/90/90/90** | 0.1077 | 0.1077 | 0.1077 |
| **30/-30/30/-30** | 0.4893 | 0.4904 | 0.48998 |
| **45/-45/45/-45** | 0.1815 | 0.1822 | 0.1822 |
| **60/-60/60/-60** | 0.1164 | 0.1166 | 0.1166 |

| | | | |
|---|---|---|---|
| **60/-60/45/-45** | 0.1423 | 0.1439 | 0.152 |
| **30/-30/45/-45** | 0.2661 | 0.2736 | 0.3419 |
| **30/-30/60/-60** | 0.1916 | 0.2016 | 0.3144 |
| **30/-30/0/0** | 0.7409 | 0.7734 | 1.0309 |
| **30/-30/0/90** | 0.3594 | 0.3633 | 0.6683 |
| **30/30/30/30** | 0.2219 | 0.2448 | 0.2447 |
| **30/-30/-30/30** | 0.394 | 0.4038 | 0.5279 |
| **0/90/90/0** | 1.3832 | 1.3814 | 0.8368 |
| **30/-60/-60/30** | 0.2368 | 0.2556 | 0.2423 |
| **0/90/0/90** | 0.7039 | 0.7176 | 0.8367 |
| **-45/30/-30/45** | 0.2334 | 0.2343 | 0.3705 |
| **90/0/0/90** | 0.2902 | 0.2901 | 0.8368 |
| **30/30/-30/-30** | 0.3308 | 0.3303 | 0.3233 |

### 9.5.5 Comparison to Previous Work

The presented analytical solution is compared to previous work conducted by Abramovich et al. [20] for non-symmetric cross ply rectangular laminated composite beams. Table **9.7** presents the results of Ref. [20] and the proposed analytical solution compared with numerical solution using S8R elements for three different material properties (Glass-Epoxy, Carbon Epoxy, and Kevlar-Epoxy). It was observed that the present analytical formula yields generally more accurate results when compared to finite element results for different material properties and number of layers.

Table 9.7 Comparison of the analytical formula with previous work.

| **Kevlar-epoxy** | | | | | | | |
|---|---|---|---|---|---|---|---|
| | **D11, Mpa** | **Non-dimensional buckling parameter, λ, Table 2, Ref. (20)** | **Ref. (20), N** | **Analytical solution, N** | **Numerical solution, N** | **%Error, Ref. (20)** | **%Error, Analytical solution** |
| **0/90/0/90** | 15.856 | 17.688 | 0.0842 | 0.0805 | 0.082 | 2.6129 | 1.86336 |
| **0/90/90/0** | 26.2565 | 20.093 | 0.158272 | 0.158528 | 0.15829 | 0.0114 | 0.15014 |
| **0/90** | 1.982 | 10.129 | 0.0241 | 0.0188 | 0.0204 | 15.3527 | 8.51064 |
| **0/90/0** | 12.1062 | 20.084 | 0.1297 | 0.1297 | 0.1294 | 0.2314 | 0.23131 |
| **Glass-epoxy** | | | | | | | |
| | **D11, Mpa** | **Non-dimensional buckling parameter, λ, Table 2, Ref. (20)** | **Ref. (20), N** | **Analytical solution, N** | **Numerical solution, N** | **%Error, Ref. (20)** | **%Error, Analytical solution** |
| **0/90/0/90** | 19.9433 | 19.381 | 0.116 | 0.1126 | 0.1133 | 2.3276 | 0.62167 |
| **0/90/90/0** | 27.4251 | 20.18 | 0.166032 | 0.163096 | 0.16308 | 1.778 | 0.00982 |
| **0/90** | 2.493 | 16.965 | 0.0508 | 0.0469 | 0.0482 | 5.1182 | 2.77186 |
| **0/90/0** | 12.3104 | 20.179 | 0.1325 | 0.129931 | 0.12992 | 1.9472 | 0.00847 |
| **Carbon-epoxy** | | | | | | | |
| | **D11, Mpa** | **Non-dimensional buckling parameter, λ, Table 2, Ref. (20)** | **Ref. (20), N** | **Analytical solution, N** | **Numerical solution, N** | **%Error, Ref. (20)** | **%Error, Analytical solution** |
| **0/90/0/90** | 36.4888 | 17.484 | 0.1914 | 0.1824 | 0.1862 | 2.7436 | 2.07 |
| **0/90/90/0** | 61.4403 | 20.113 | 0.3708 | 0.3717 | 0.3711 | 0.0985 | 0.1393 |

| | | | | | | | |
|---|---|---|---|---|---|---|---|
| **0/90** | 4.5611 | 9.207 | 0.0504 | 0.038 | 0.0415 | 17.6933 | 9.3397 |
| **0/90/0** | 28.3893 | 20.106 | 0.3045 | 0.3049 | 0.3042 | 0.0828 | 0.2319 |

L/r = 500, k = 5/6, c = 1 mm.

## 9.6 Conclusions

A generalized analytical buckling load formula for anisotropic laminated composite clamped-pinned columns under axial compression using bifurcation solution was developed herein. The presented analytical buckling solution was expressed in terms of column geometry as well as the effective composite extensional, coupling and flexural rigidities. An excellent agreement was observed between the analytical and numerical (FE) results. The derived formula predicted the complex stability response accurately of the anisotropic columns for different stacking sequences, material properties including hybrid material. In general, shell element results yielded accurate buckling load values compared to element predictions for all stacking sequences. Furthermore, the developed analytical formula showed an excellent correspondence to former buckling solutions of cross-ply laminated columns.

## 9.7 References


[1] Heidari-Rarani, M., Khalkhali-Sharifi, S.S., and Shokrieh, M.M., "Effect of ply stacking sequences on buckling behavior of E-glass/epoxy lamianted composites," *Computational Materials Science*, 89 (2014) 89-96.

[2] Abramovich, H., and Livshits, A., "Free vibrations of non-symmetric cross-ply laminated composite beams", *Journal of Sound and Vibration* , 176 (1994) 597-612.

[3] Lopatin, A. V., and Morozov, E. V., "Buckling of a composite cantilver circular cylindrical shell subjected to uniform external lateral pressure," *Composite Structures*, 94 (2012) 553-562.

[4] Cortinez, H.V., and Piovan, M. T., "Stability of composite thin-walled beams with shear deformability," *Computers & Structures*, 84(2006) 978-990.

[5] Rikards, R., Chate, A., and Ozolinsh, O., "Analysis for buckling and vibrations of composite stiffened shells and plates," *Composite Structures*, 51(2001) 361-370.

[6] Jaunky, N., Knight Jr., N. F., and Ambur, D. R., "Buckling aanlysis of anisotropic varaible-curvuture panels and shells," *Composite Structures*, 43(4) (1998) 321-329.

[7] Kumar, Y.V. S., and Mukhopadhyay, M., "A new finite element for buckling analysis of laminated stiffenend plates," *Composite Structures*, 46 (1999) 321-331.

[8] Loughlan, J., "A finite strip analysis of the buckling characteristics of some composite stiffenend shear panels," *Composite Structures*, 27(3) (1994) 283-294.

[9] Kidane, S., Li, G., Helms, J., Pang, S., and Woldesenbet, E., "Buckling load analysis of grid stiffened composite cylinders," *Composite: Part B*, 34(2003)1-9

[10] Whitney, J. M., Structural Analysis of Laminated Anisotropic Plates, Lancaster: Technomic, 1987.

[11] Debski, H., Kubiak, T., and Teter, A., "Buckling and postbuckling behaviour of thin-walled composite channel section column," *Composite Structures*, 100(2013) 195-204.

[12] Kolakowski, Z., and Kowal-Michalska, K., Selected Problems of Instabilities in Composite Stuctures, Lodz: Technical University of Lodz Press, A Series of Monographes, 1999.

[13] Kubiak, T., "Postbuckling behavior of thin-walled girders with orthotropy varying widthwise," *International Journal of Solid Structure*, 38(28-29) (2001) 4839-4855.

[14] Teter, A., "Static and dynamic interactive buckling of isotropic thin-walled closed columns with variable thickness," *Thin-Walled Stuctures*, 45(10-11) (2007) 936-940.

[15] Teter, A., and Kolakowski, Z., "Lower bound estimation of load-carrying capacity of thin-walled structures with intermediate stiffeners," *Thin-Walled Stuctures*, 39(8) (2001) 649-669.

[16] Jones, R.M, Mechanics of composite materials, New York: Hemisphere Publishing Corporation, 1975.

[17] Hernandez, V., Roman, J.E., Tomas, A., and Vidal, V., "Lanczos methods in SLEPc," Polytechnic University of Valencia, Province of Valencia, 2006.

[18] Memon, B.A., Su, X.S., "Arc-length technique for nonlinear finite element analysis," *Journal of Zhejiang University SCI*, vol. 5, no. 5, pp. 618-628, 2004.

[19] Rasheed, H.A., Strengthening Design of Reinforced Concrete with FRP, New York: CRC Press, 2015.

[20] Abramovich, H., Eisenberger, M., and Shulepov, O., "Vibrations and buckling of cross-ply non-symmetric laminated composite beams", *AIAA Journal* , vol. 34, 1064-1069, 1996.

# Chapter 10 - Stability Analysis of Pinned-Fixed Wide Plate Subjected to Uniaxial Compression

**Hayder A. Rasheed[1] and Rund Al-Masri[2]**

## 10.1 Abstract

**Stability analysis of pinned-fixed anisotropic laminated composite wide plates subjected to uniaxial compression is studied in this work. A generalized closed-form buckling solution is derived based on the bifurcation approach of the energy formulation. The three dimensional matrix was established in terms of extensional, coupling, and flexural rigidity coefficients then reduced to 1D using dimensional reduction. The proposed formula is expressed in terms of extensional, coupling, and flexural coefficients in the principal directions as well as the infinitely wide plate geometry. The analytical solution reduces down to Euler buckling formula for isotropic and certain types of layups. Finite element analysis is used to validate the presented analytical formula for a wide range of stacking sequences yielding high accuracy. A brief parametric study is then conducted to examine the effect of ply orientations, plate thickness, and material properties including hybrid carbon/glass fiber composites. Nonlinear Riks analysis showed that transverse pre-buckling deformation takes place prior to buckling. Relevance of the numerical and analytical results is discussed for all these cases.**

Keywords: Buckling of Composite Wide Plates, Pinned-Fixed Boundary Conditions, Anisotropic Laminated Composites, Axial Compression.

[1] Professor, Department of Civil Engineering, Kansas State University, Manhattan, KS 66506

[2] Ph.D. Candidate, Department of Civil Engineering, Kansas State University, Manhattan, KS 66506

## 10.2 Introduction

A growth of using composites in various industrial applications such as aerospace, marine, and automotive has been noticed in the past few decades due to their distinguished properties. An increase in the demand to understand the mechanics of composite material has resulted. Limited amount of research has focused on the stability of anisotropic laminated composite wide plates. Stability of composite plates, beams, cylinders, and shells has been investigated [1-10]. Silva et al. [1] proposed a formulation of a generalized beam theory (GBT) to investigate the local and global buckling behavior of fiber reinforced polymer (FRP) composite open-section thin-walled columns. The solution for buckling using GBT included solving the following eigenvalue problem:

$$(\boldsymbol{K} + \boldsymbol{\gamma G})\boldsymbol{d} = \boldsymbol{0} \quad \textbf{(1)}$$

Where K is the global linear stiffness matrix; G is the geometric stiffness matrix; and d is the eigenvector. Haung et al. [2] studied the stability of grid stiffened laminated composite plates by presenting an efficient finite element model. Curved beam element was presented to model the stiffeners. Additionally, various numerical examples were solved using the developed element. Wang and Abdalla [3] studied the global and local buckling of grid stiffened composite panels based on Bloch wave theory. The presented method is confirmed for different composite configurations. Weber and Middendorf [4] studied the skin buckling of curved orthotropic grid-stiffened shells with a semi-analytical Ritz method depending on sets of trigonometric shape functions. Khayat et al. [5] investigated the buckling of laminated composite cylindrical shell under lateral displacement-dependent pressure using semi-analytical finite strip method. The governing equations were developed based on the first shear deformation theory with Sanders type of kinematics nonlinearity. The results showed a decrease in the buckling pressure when the pressure stiffness was taken into consideration. Baseri et al. [6] studied the buckling of embedded

laminated composite plates based on higher order shear deformation theory by developing analytical solution. The analytical solution was solved using Navier method.

Becheri et al. [7] proposed an exact analytical solution to investigate the buckling of symmetrically cross-ply plates using $n^{th}$-order shear deformation theory with curvature effects. The closed form solution was compared with previous work. Debski [8] presented numerical analysis of buckling and post-buckling of thin-walled simply supported laminated composite columns with channel section under axial compression. Eight symmetrical layered Carbon/Epoxy columns were modeled using finite element software Abaqus and Ansys and verified with analytical-numerical method [9]. A good agreement was observed between the finite element results and results obtained from the analytical-numerical method. Cortinez and Piovan [10] investigated the buckling of composite thin-walled beams with shear deformability using nonlinear displacement field depending on Hellinger-Reissner principal by presenting a theoretical model. The governing equations were solved using a finite element with fourteen degrees of freedom.

Based on bifurcation approach, a generalized analytical critical buckling formula of anisotropic laminated composite pinned-fixed wide plates under uniaxial edge compression loading was derived. The three dimensional laminated stiffness matrix was constructed using fiber orientations and material properties and reduced down to 1D axial, coupling, flexural rigidities by applying zero strains and curvatures. Additionally, the analytical critical buckling formula was confirmed against the numerical (FE) analysis yielding an excellent agreement.

## 10.3 Analytical Formulation

### 10.3.1 Assumptions and Kinematics

A generalized closed form critical buckling solution of pinned-fixed anisotropic laminated composite wide plates under axial compression is derived by using the bifurcation approach.

Several assumptions are taken into consideration before the deriving procedure and presented in the following points:

- Buckling takes place in the x-y plane about the weak axis (z-axis).

The y-axis runs through the thickness of the column where the composite lamination takes place,

- Figure 10.1.
- The lamination angle ( $\alpha$ ) is measured with respect to the x-axis in which 0° fibers run parallel to the x-axis and 90° fibers run parallel to the z-axis. Accordingly, the angle ( $\alpha$ ) is rotated about the y-axis.
- Plane sections before bending remain plane after bending and perpendicular to the mid surface (i.e. simple beam theory holds).

  Classical lamination theory is applicable with shear deformations ignored.

Figure 10.1 illustrates Cartesian coordinates and geometry of the pinned-fixed wide plates used. The bending occurs about the weak axis (z-axis). The following displacement relations were assumed based on the isotopic Euler first buckling mode:

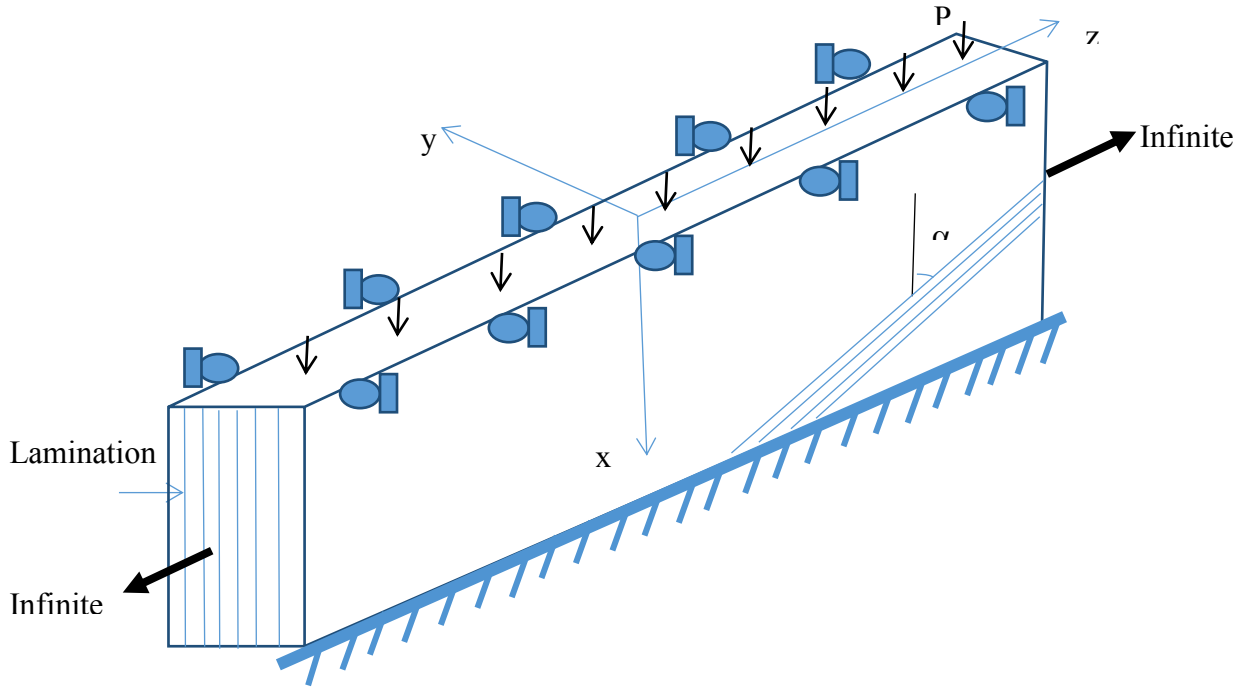


Figure 10.1Wide Plate geometry

$$\boldsymbol{u}\,(\boldsymbol{x}) = \boldsymbol{B_1}(\boldsymbol{L}-\boldsymbol{x})\,; \quad \boldsymbol{v}\,(\boldsymbol{x}) = \boldsymbol{C_1}\,(\frac{\boldsymbol{x}}{\boldsymbol{L}} + \mathbf{1.0245}\,\sin\frac{\mathbf{4.4934}\boldsymbol{x}}{\boldsymbol{L}}) \tag{2}$$

where $u(x)$, and $v(x)$ is the axial, and lateral displacements; $B_1$, and $C_1$ are constants to be solved; and x is the distance along the axis of the wide plate. For an intermediate class of deformation, the axial strain $\varepsilon_x$ and curvature $\kappa_x$are defined as follow.

$$\boldsymbol{\varepsilon_x} = \frac{\boldsymbol{du}}{\boldsymbol{dx}} + \frac{\mathbf{1}}{\mathbf{2}}(\frac{\boldsymbol{dv}}{\boldsymbol{dx}})^{\mathbf{2}} = \boldsymbol{u'} + \frac{\mathbf{1}}{\mathbf{2}}\boldsymbol{v'^2}; \qquad \boldsymbol{\kappa_x} = \frac{\boldsymbol{d^2v}}{\boldsymbol{d^2x}} = \boldsymbol{v''} \tag{3}$$

### 10.3.2 Constitutive equations

The principal material directions were transformed into the wide plate coordinate system, the stresses and strains are then related in the following equation

$$\begin{Bmatrix}\boldsymbol{\sigma_x}\\ \boldsymbol{\sigma_z}\\ \boldsymbol{\tau_{xz}}\end{Bmatrix} = \begin{bmatrix}\boldsymbol{\bar{Q}_{11}} & \boldsymbol{\bar{Q}_{12}} & \boldsymbol{\bar{Q}_{16}}\\ \boldsymbol{\bar{Q}_{12}} & \boldsymbol{\bar{Q}_{22}} & \boldsymbol{\bar{Q}_{26}}\\ \boldsymbol{\bar{Q}_{16}} & \boldsymbol{\bar{Q}_{26}} & \boldsymbol{\bar{Q}_{66}}\end{bmatrix}\begin{Bmatrix}\boldsymbol{\varepsilon_x}\\ \boldsymbol{\varepsilon_z}\\ \boldsymbol{\gamma_{xz}}\end{Bmatrix} \tag{4}$$

Where $\bar{Q}_{ij}$ matrix represents the transformed reduced stiffness matrix as defined in standard composite textbooks [11]. Accordingly, the coupled force-strain relationship is established as follows:

$$\begin{Bmatrix} N_x \\ N_z \\ N_{xz} \\ M_x \\ M_z \\ M_{xz} \end{Bmatrix} = \begin{bmatrix} A_{11} & A_{12} & A_{16} & B_{11} & B_{12} & B_{16} \\ A_{12} & A_{22} & A_{26} & B_{12} & B_{22} & B_{26} \\ A_{16} & A_{26} & A_{66} & B_{16} & B_{26} & B_{66} \\ B_{11} & B_{12} & B_{16} & D_{11} & D_{12} & D_{16} \\ B_{12} & B_{22} & B_{26} & D_{12} & D_{22} & D_{26} \\ B_{16} & B_{26} & B_{66} & D_{16} & D_{26} & D_{66} \end{bmatrix} \begin{Bmatrix} \varepsilon_x \\ \varepsilon_z \\ \gamma_{xz} \\ \kappa_x \\ \kappa_z \\ \kappa_{xz} \end{Bmatrix} \quad \textbf{(5)}$$

Where:

$$A_{ij} = \sum_{k=1}^{N} \bar{Q}_{ij} t_k$$

$$B_{ij} = \sum_{k=1}^{N} \bar{Q}_{ij} t_k \bar{y}_k$$

$$D_{ij} = \sum_{k=1}^{N} \bar{Q}_{ij} t_k \left( \bar{y}_k^2 + \frac{t_k^2}{12} \right) \quad \textbf{(6)}$$

$$t_k = y_k - y_{k-1}$$

$$\bar{y}_k = \frac{y_k + y_{k-1}}{2}$$

In which $A_{ij}, B_{ij}$ and $D_{ij}$ are the axial, coupling, and flexural rigidity coefficients. $t_k$ is the thickness of the k-th ply; and N is the number of different plies in the stacking sequence.

Using material properties and fiber orientations into equation (5), the three dimensional (3D) rigidity matrix is established. Accordingly, the 3D stiffness matrix is reduced to 1D anisotropic axial, coupling and flexural rigidities using static condensation approach after applying the zero forces and moments.

$$\begin{Bmatrix} N_x \\ N_z \\ N_{xz} \\ M_x \\ M_z \\ M_{xz} \end{Bmatrix} = \begin{bmatrix} A_{11} & A_{12} & A_{16} & B_{11} & B_{12} & B_{16} \\ A_{12} & A_{22} & A_{26} & B_{12} & B_{22} & B_{26} \\ A_{16} & A_{26} & A_{66} & B_{16} & B_{26} & B_{66} \\ B_{11} & B_{12} & B_{16} & D_{11} & D_{12} & D_{16} \\ B_{12} & B_{22} & B_{26} & D_{12} & D_{22} & D_{26} \\ B_{16} & B_{26} & B_{66} & D_{16} & D_{26} & D_{66} \end{bmatrix} \begin{Bmatrix} \varepsilon_x \\ \varepsilon_z = 0 \\ \gamma_{xz} = 0 \\ \kappa_x \\ \kappa_z = 0 \\ \kappa_{xz} = 0 \end{Bmatrix} \tag{7}$$

The axial force and in-plane moment vs. the axial strain and in-plane curvature relationship can be expressed in terms of the generally anisotropic material properties in the principal directions as follow

$$\begin{bmatrix} N_x \\ M_x \end{bmatrix} = \begin{bmatrix} A_{11} & B_{11} \\ B_{11} & D_{11} \end{bmatrix} \begin{Bmatrix} \varepsilon_x \\ \kappa_x \end{Bmatrix} \tag{8}$$

### 10.3.3 Pre-buckling Solution

Pre-buckling deformation is taken into account to derive the buckling formula depending on the pinned-fixed mode shape. The in-plane moment ($M_x$) is set to zero during pre-buckling and before reaching the buckling load.

$$M_x = B_{11}\epsilon_x + D_{11}\kappa_x \tag{9}$$

$$0 = B_{11}\epsilon_x + D_{11}\kappa_x$$

$$\kappa_x = -\frac{B_{11}}{D_{11}}\epsilon_x \tag{10}$$

By substituting Eq. (10) into the axial force equation, the axial force versus the axial strain can be expressed in terms of the generally anisotropic material properties

$$P_x = A_{11}\epsilon_x + B_{11}\kappa_x \tag{11}$$

$$P_x = A_{11}\epsilon_x - \frac{B_{11}^2}{D_{11}}\epsilon_x$$

$$P_x = A_{eff}\epsilon_x \tag{12}$$

Where

$$A_{eff} = A_{11} - \frac{B_{11}^2}{D_{11}} \tag{13}$$

The axial force ($P_x$) is positive and in compression based on the assumed sign convention. However, the axial strain ($\epsilon_x$) is negative although it is in compression. Accordingly, a negative sign is inserted in equation (2) as follow:

$$u = -B_1(L - x) \tag{14}$$

Using the axial strain in Eq. (3), setting the lateral displacement term to zero, and substituting equation (14), the axial strain can be expressed as

$$\epsilon_x = B_1 \tag{15}$$

By substituting Eq. (15) into Eq. (12), a relationship between the axial force and the unknown constant ($B_1$) is obtained, i.e.

$$B_1 = \frac{P_x}{A_{eff}} \tag{16}$$

### 10.3.4 Bifurcation Solution in terms of Pre-buckling Deformation

Energy approach is assumed in the bifurcation solution in which the strain energy can be expressed in terms of the integration of the applied loads multiplying the corresponding deformations.

$$U = \int_0^L \left(\frac{1}{2} N_x \varepsilon_x + \frac{1}{2} M_x \kappa_x\right) dx$$

$$= \int_0^L \frac{1}{2} (A_{11}\varepsilon_x^2 + B_{11}\varepsilon_x\kappa_x)\, dx + \int_0^L \frac{1}{2} (B_{11}\varepsilon_x\kappa_x + D_{11}\kappa_x^2)\, dx \tag{17}$$

The potential of external loads can be expressed as

$$W = -P\, u(L) \tag{18}$$

In view of equations (17) and (18), the total potential energy function is given by

$$\boldsymbol{\Pi = U - W = \int_0^L \frac{1}{2}(A_{11}\varepsilon_x^2 + 2B_{11}\varepsilon_x\kappa_x + D_{11}\kappa_x^2)\,dx + P\,u(L)} \quad \textbf{(19)}$$

$$\boldsymbol{\Pi = A_{11}\left[\frac{1}{2}B_1^2 L - 5.048\,B_1\frac{C_1^2}{L} + 22.7975\frac{C_1^4}{L^3}\right] + B_{11}\left[5.6036\,B_1\frac{C_1}{L} - 29.3124\,\frac{C_1^3}{L^3}\right] +}$$

$$\boldsymbol{101.9215\,D_{11}\frac{C_1^2}{L^3} - PB_1L} \quad \textbf{(20)}$$

By substituting Eq. (16) into the total potential energy function given by Eq. (20), one obtains

$$\boldsymbol{\Pi = A_{11}\left[\frac{1}{2}\frac{P^2}{A_{eff}}L - 5.048\,\frac{P}{A_{eff}}\frac{C_1^2}{L} + 22.7975\frac{C_1^4}{L^3}\right] + B_{11}\left[5.6036\,\frac{P}{A_{eff}}\frac{C_1}{L} - 29.3124\,\frac{C_1^3}{L^3}\right] +}$$

$$\boldsymbol{101.9215\,D_{11}\frac{C_1^2}{L^3} - \frac{P^2}{A_{eff}}L} \quad \textbf{(21)}$$

Minimizing the total potential energy with respect to the unknown $C_1$, setting the resulting expression to zero, and manipulating the equation, one gets

$$\boldsymbol{\frac{\partial\Pi}{\partial C_1} = A_{11}\left[-10.096\frac{P}{A_{eff}}\frac{C_1}{L} + 91.19\frac{C_1^3}{L^3}\right] + B_{11}\left[5.6036\,\frac{P}{A_{eff}}\frac{1}{L} - 87.9372\,\frac{C_1^2}{L^3}\right] +}$$

$$\boldsymbol{203.843\,D_{11}\frac{C_1}{L^3} = 0} \quad \textbf{(22)}$$

The cubic equation (22) with respect to $C_1$ does not lend itself to a close form solution. Therefore, the second derivative of Eq. (22) with respect to $C_1$ is considered

$$\boldsymbol{\frac{\partial^2\Pi}{\partial C_1^2} = A_{11}\left[-10.096\frac{P}{A_{eff}}\frac{1}{L} + 273.57\frac{C_1^2}{L^3}\right] - 175.8744\,B_{11}\frac{C_1}{L^3} + 203.843\,\frac{D_{11}}{L^3} = 0} \quad \textbf{(23)}$$

By solving Eq. (23), one gets

$$\boldsymbol{C_1 = \frac{175.8744\frac{B_{11}}{L^3} \mp \sqrt{175.8744^2\frac{B_{11}^2}{L^6} - 4(273.57)\frac{A_{11}}{L^3}\left(203.843\frac{D_{11}}{L^3} - 10.096\frac{PA_{11}}{A_{eff}L}\right)}}{2A_{11}\frac{273.57}{L^3}}} \quad \textbf{(24)}$$

In order for the $C_1$ value to be real, the discriminant must be at least zero. By setting the discriminant to zero, a closed form solution for the critical buckling load is developed in terms of the generally anisotropic material properties as well as the column geometry:

$$P_{cr} = 20.19\frac{D_{11}}{L^2} - 22.9898\frac{B_{11}^2}{A_{11}L^2} + 2.7998\ \frac{B_{11}^4}{A_{11}^2 D_{11}L^2} \quad (25)$$

The general analytical critical buckling formula for different wide plate width's values is:

$$P_{cr} = \left(20.19\frac{D_{11}}{L^2} - 22.9898\frac{B_{11}^2}{A_{11}L^2} + 2.7998\ \frac{B_{11}^4}{A_{11}^2 D_{11}L^2}\right) w \quad (26)$$

Where w is the width of the wide plate. It is observed that Eq. (26) reduces down to Euler buckling formula of the pinned-fixed isotropic wide plates in the case of isotropic or specially-orthotropic materials.

## 10.4 Numerical Formulation

Finite element analysis was conducted to validate the closed form solution developed earlier using commercial software package Abaqus. Wide plates with the following dimensions: 1000 mm x 100 mm x 0.4 mm were assumed for width, height, and thickness, respectively. Linear elastic laminated material was attempted for both orthotropic and anisotropic layups where S-Glass/Epoxy material was used as main material. Fixed support and pinned support were utilized at the bottom and top of the wide plate, respectively. Additionally, the translation in the x-direction (z-direction in

Figure 10.1) and the rotation about y-direction (about the x-direction in

Figure 10.1) were prevented to mimic the infinitely wide plate, see Figure 10.2. Furthermore, uniaxial edge loading was applied at the top of wide plate as shown in Figure 10.2

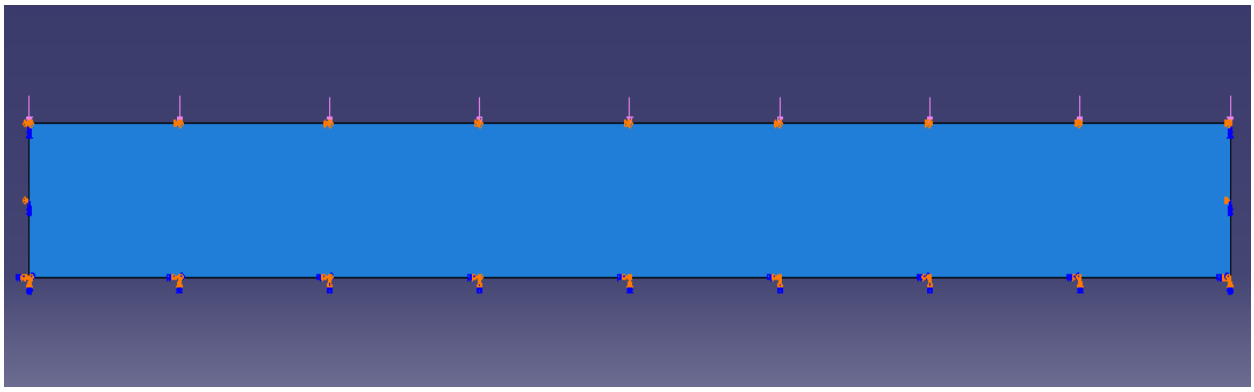

Figure 10.2 Boundary conditions and edge loading.

Quadrilateral eight node doubly curved thick shell element (S8R) with reduced integration having mesh size equal to 10.0 mm was used to model the anisotropic laminated composite wide plates in 3D space after conducting a convergence study to select the appropriate element size. Figure 10.3 presents the meshed wide plate used in the numerical analysis.

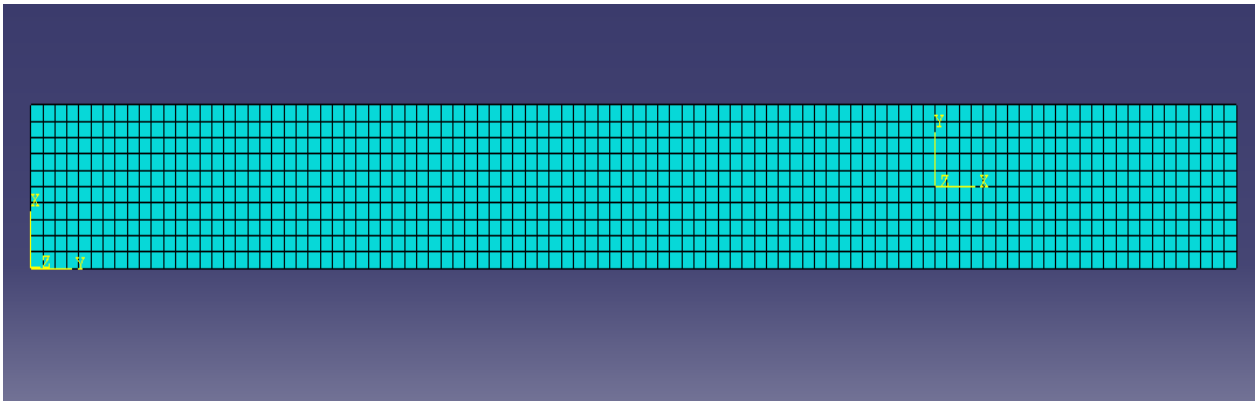

Figure 10.3 Meshed Model

Eigenvalue computation was conducted using buckling analysis depending on Lanczos solver. Lanczos technique simulates the eigenvalue and eigenvector computation for a complex Hermitian matrix based on the power method in which a symmetric matrix is reduced to tridiagonal matrix using multidimensional arrays [12]. Based on the modified Riks approach, nonlinear geometry analysis was performed to indicate the existence of pre-buckling deformation in the transverse direction and predict the stability response of the anisotropic laminated composite wide plates. Modified Riks analysis uses the arc length method in which the equilibrium path (i.e. bifurcation

or limit points) is followed during the load increment application. Equilibrium iterations converge along the arc length forcing the constraint equation to be satisfied at each arc length increment [13].

## 10.5 Results and Applications

### 10.5.1 Numerical Validation

S-Glass/Epoxy four-layer wide plate's analytical results were validated against finite element results using Abaqus. Table 10.1 presents S-Glass/Epoxy material properties used in the validation process; obtained from typical values in an FRP textbook [14]. The comparison between the analytical and numerical results are reported in Table 10.2 for various stacking sequences of the anisotropic laminated composite wide plates with the following dimensions: 1000 mm x 100 mm x 0.4 mm for width, height, thickness, respectively. The analytical results exhibited an excellent agreement with finite element results with maximum error around 4.1% for the antisymmetric angle ply layup (30/-30/30/-30) and minimum error around 0.0007% for symmetric cross ply layup (90/0/0/90).

Table 10.1 S-Glass/Epoxy material properties [14].

| Material | $E_{11}$ | $E_{22}$ | $G_{12}$ | $\nu_{12}$ |
|---|---|---|---|---|
| **S-Glass/Epoxy** | 55.0 GPa | 16.0 GPa | 7.6 GPa | 0.28 |

Table 10.2 Comparison between analytical and numerical results for S-Glass/Epoxy thin plates (h/t = 250 mm).

| Ply Orientations | Analytical Results, N | Numerical Results, N | % Error | Layup Type |
|---|---|---|---|---|
| **0/0/0/0** | 0.60607 | 0.606 | 0.01155 | Single Specially Orthotropic |

| | | | | |
|---|---|---|---|---|
| **90/90/90/90** | 0.17631 | 0.1763 | 0.00568 | Single Specially Orthotropic |
| **30/-30/30/-30** | 0.43182 | 0.41405 | 4.11515 | Antisymmetric Angle Ply |
| **45/-45/45/-45** | 0.30212 | 0.29182 | 3.40925 | Antisymmetric Angle Ply |
| **60/-60/60/-60** | 0.21695 | 0.21394 | 1.38742 | Antisymmetric Angle Ply |
| **60/-60/45/-45** | 0.25358 | 0.248 | 2.20049 | Balanced Angle Ply |
| **30/-30/45/-45** | 0.35721 | 0.34473 | 3.49375 | Balanced Angle Ply |
| **30/-30/60/-60** | 0.2943 | 0.28874 | 1.88923 | Balanced Angle Ply |
| **30/-30/0/0** | 0.50649 | 0.49973 | 1.33468 | Anisotropic |
| **30/-30/0/90** | 0.3196 | 0.31412 | 1.71465 | Anisotropic |
| **30/30/30/30** | 0.43182 | 0.43439 | 0.59516 | Single Anisotropic Layer |
| **30/-30/-30/30** | 0.43182 | 0.43371 | 0.43769 | Symmetric Angle Ply |
| **0/90/90/0** | 0.55235 | 0.55216 | 0.0344 | Symmetric Cross Ply |

| | | | | |
|---|---|---|---|---|
| **30/-60/-60/30** | 0.40497 | 0.40708 | 0.52103 | Symmetric Multiple Angle Layers |
| **0/90/0/90** | 0.36616 | 0.369 | 0.77562 | Antisymmetric Cross Ply |
| **-45/30/-30/45** | 0.31833 | 0.30968 | 2.71731 | Antisymmetric Angle Ply |
| **90/0/0/90** | 0.2300284 | 0.23003 | 0.0007 | Symmetric Cross Ply |

### 10.5.2 Modified Riks Analysis

Figure 10.4 presents load versus maximum displacement curve is plotted for three different stacking sequences obtained from the nonlinear Riks analysis along with the analytical solution. An excellent agreement was observed between the results in which the anisotropic layup (30/-30/0/90) showed the lowest buckling load. The results indicate an existence of pre-buckling deformation in the transverse direction for the drawn layups.

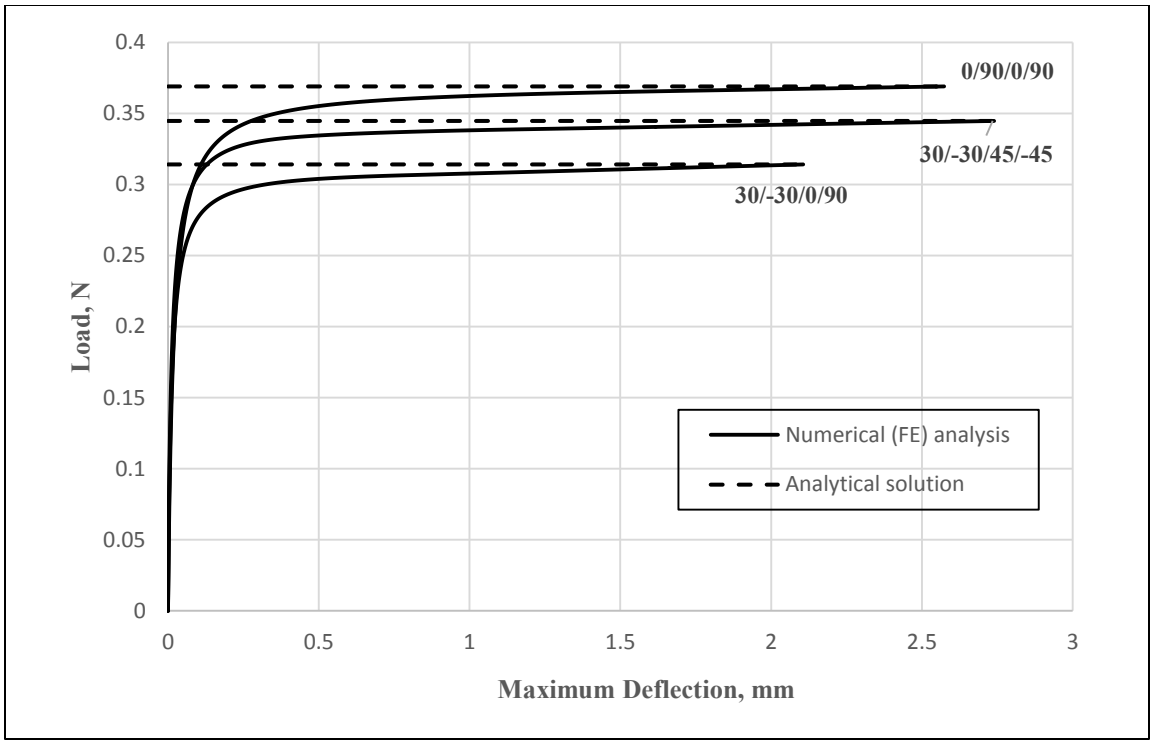

Figure 10.4 Load versus maximum deflection.

## 10.5.3 Parametric Study

### 10.5.3.1 Effect of Ply Orientation

The effect of stacking sequences on the stability response of the anisotropic laminated composite wide plates was addressed in this study. As reported in Table 10.2, critical buckling load values vary between 0.606 N and 0.1763 N for different stacking sequences. For specific stacking sequences such as balanced angle ply and anisotropic layups, an edge effect was noticed in which the deformation along the plate was not uniform as illustrated in Figure 10.5. However, a uniform deformation along the plate was observed for the other stacking sequences, see Figure 10.6.

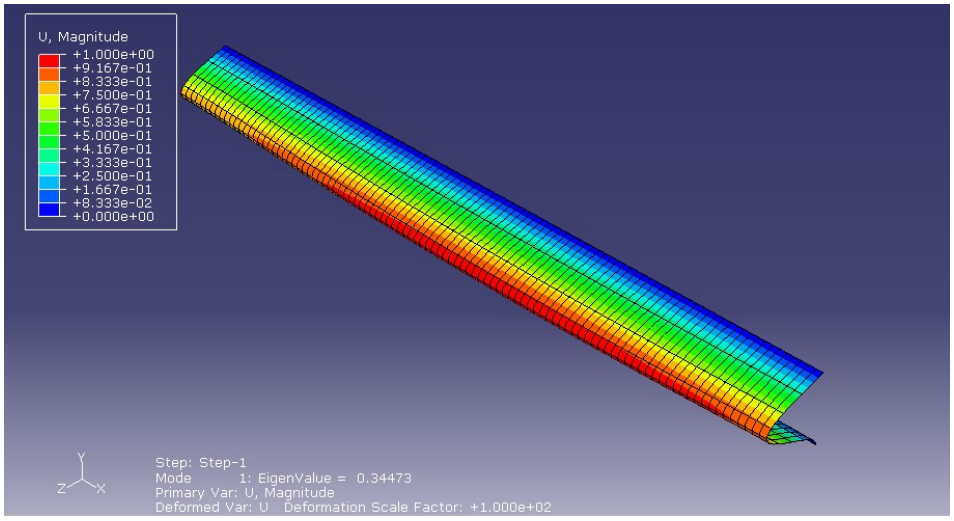

Figure 10.5 Buckling mode shape and edge effect of (30/-30/45/-45) layup.

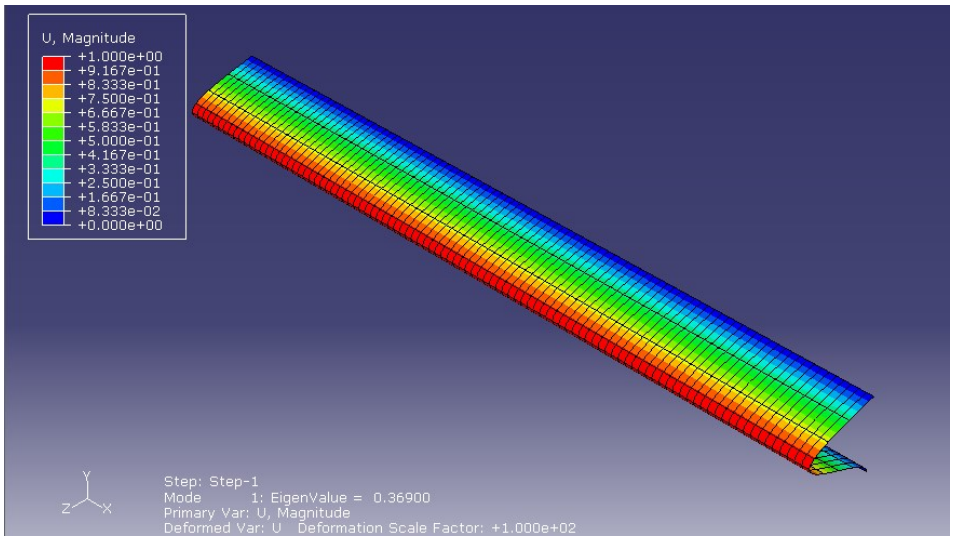

Figure 10.6 Bucking mode shape with uniform deformation

### 10.5.3.2 Effect of Material Properties

A parametric study was addressed herein to assess the effect of Hybrid carbon/glass fiber composites on the critical buckling load values. High Strength Graphite/Epoxy and S-Glass/Epoxy material was used for Hybrid wide plates, moreover, their properties are reported in Table 10.1 and Table 10.3; obtained from typical values in FRP textbook [14]. Layups with ply orientations equal to $0^o$ and $\pm 30^o$ were composed of High Strength Graphite/Epoxy and S-Glass/Epoxy was attempted for the other orientations. A good agreement was observed between the analytical and

finite element results as presented in Table 10.4 with maximum error around 6.4% for the anisotropic (30/-30/0/90) due to edge effect for the mentioned layup.

Table 10.3 High Strength Graphite/Epoxy Material Properties [14].

| Material | $E_{11}$ | $E_{22}$ | $G_{12}$ | $\nu_{12}$ |
|---|---|---|---|---|
| **High Strength Graphite/Epoxy** | 145.0 GPa | 10.0 GPa | 4.8 GPa | 0.25 |

Table 10.4 Comparison between analytical and numerical results of Hybrid plates (t = 0.4 mm).

| Ply Orientations | Analytical Results, N | Numerical Results, N | % Error |
|---|---|---|---|
| **30/-30/60/-60** | 0.38242 | 0.36252 | 5.2038 |
| **30/-30/0/90** | 0.60395 | 0.56509 | 6.4344 |
| **0/90/90/0** | 1.39415 | 1.3925 | 0.1184 |
| **0/90/0/90** | 0.7554 | 0.7676 | 1.6151 |
| **90/0/0/90** | 0.350286 | 0.35022 | 0.0189 |

#### 10.5.3.3 Effect of Element Thickness

A comparison between results was conducted to investigate the effect of different height to thickness ratio on the buckling values. S-Glass/Epoxy thin, moderately thick, and thick wide plates were taken into consideration with the following height to thickness ratios: 250, 62.5, and 10.0, respectively. Table 10.2 showed the comparison between the analytical and numerical results for thin (h/t = 250) laminated composite wide plates yielding an excellent agreement. Table 10.5 and

Table 10.6 illustrates the analytical and numerical results for moderately thick (h/t = 62.5) and thick (h/t = 10.0) anisotropic laminated composite wide plates, respectively. In general, an excellent agreement was observed between results of moderately thick plates (h/t = 62.5) in which the antisymmetric cross ply (0/90/0/90) exhibited the maximum error. However, the closed-form

solution was not capable of predict an accurate estimate for the buckling load values in case of thick wide plates with height to thickness ratio equal to 10.0 as shown in Table 10.6

Table 10.6. The proposed formula was able to accurately predict the stability behavior in a similar way for moderately thick wide plates. On the other hand, the consideration of shear deformations is very important to estimate the buckling loads of thick wide plates.

Table 10.5 Comparison between analytical and numerical results for S-Glass/Epoxy moderately thick plates (h/t = 62.5)

| **Ply Orientations** | **Analytical Results, N** | **Numerical Results, N** | **% Error** | **Layup Type** |
|---|---|---|---|---|
| **0/0/0/0** | 38.788009 | 38.631 | 0.4048 | Single Specially Orthotropic |
| **90/90/90/90** | 11.283785 | 11.251 | 0.2906 | Single Specially Orthotropic |
| **30/-30/30/-30** | 27.63646 | 26.381 | 4.5428 | Antisymmetric Angle Ply |
| **60/-60/45/-45** | 16.60598 | 15.819 | 4.7392 | Balanced Angle Ply |
| **30/-30/0/90** | 21.17189 | 20.24 | 4.4016 | Anisotropic |
| **30/-30/-30/30** | 27.63646 | 27.621 | 0.056 | Symmetric Angle Ply |
| **0/90/90/0** | 35.34999 | 35.079 | 0.7666 | Symmetric Cross Ply |
| **0/90/0/90** | 25.01988 | 23.509 | 6.0388 | Antisymmetric Cross Ply |

Table 10.6 Comparison between analytical and numerical results for S-Glass/Epoxy thick plates (h/t = 10.0)

| Ply Orientations | Analytical Results, N | Numerical Results, N | % Error | Layup Type |
|---|---|---|---|---|
| **0/0/0/0** | 9469.728685 | 8134.6 | 14.099 | Single Specially Orthotropic |
| **90/90/90/90** | 2754.830163 | 2460.3 | 10.6915 | Single Specially Orthotropic |
| **30/-30/30/-30** | 6747.18144 | 5459.3 | 19.0877 | Antisymmetric Angle Ply |
| **60/-60/45/-45** | 3962.11149 | 3403 | 14.1115 | Balanced Angle Ply |
| **30/-30/0/90** | 4993.59686 | 4307.9 | 13.7316 | Anisotropic |
| **30/-30/-30/30** | 6747.18144 | 5662.2 | 16.0806 | Symmetric Angle Ply |
| **0/90/90/0** | 8630.36637 | 6602.6 | 23.4958 | Symmetric Cross Ply |
| **0/90/0/90** | 5721.24652 | 4846.7 | 15.286 | Antisymmetric Cross Ply |

## 10.6 Conclusion

Based on the bifurcation approach, a generalized closed form buckling solution for pinned-fixed anisotropic laminated composite wide plates subjected to uniaxial compression loading was developed herein. The presented solution is expressed in terms of extensional, coupling, and

flexural rigidities in the principal directions as well as infinitely wide plate geometry. An excellent agreement was observed between the analytical and numerical (FE) results for different stacking sequences. The derived formula accurately estimated the critical buckling load values for hybrid carbon/glass composite fiber, and different ply orientations. Additionally, the generalized analytical buckling formula successfully re-produce accurate prediction in the buckling behavior for thin and moderately thick anisotropic laminated composite wide plates.

## 10.7 References


[1] Silva, N.M.F., Silvestre, N., and Camotim, D., "GBT formulation to analyse the buckling behaviour of FRP composite open-section thin-walled columns," *Composite Structures,* 93(1) (2010) 79-92.

[2] Huang, L. Sheikh, A. H., Ng, C-T., and Griffith, M. C., "An efficient finite element model for buckling analysis of grid stiffened laminated composite plates," *Composite Structures,* 122 (2015) 41-50.

[3] Wang, D., and Abdalla, M. M, "Global and local buckling analysis of grid-stiffened composite panels," *Composite Structures ,* 119 (2015) 767-776.

[4] Weber, M. J., and Middendrof, P., "Semi-analytical skin buckling of curved orthotropic grid-stiffened shells," *Composite Structures,* 108 (2014) 616-624.

[5] Khayat, M., Poorveis, D., and Moradi, S., " Buckling analysis of laminated composite cylindrical shell subjected to lateral displacement-dependent pressure using semi-analytical finite strip method," *Steel and Composite Structures,* 22(2) (2016) 301-321.

[6] Baseri, V., Jafari, G.S., and Kolahchi, A., " Analytical solution for buckling of embedded laminated plates based on higher order shear deformation plate theory," *Steel and Composite Structures,* 21(4) (2016) 883-919.

[7] Becheri,T., Amara, K., Bouazza, M., Benseddiq, N.,"Buckling of symmetrically laminated plates using nth-order shear deformation theory with curvature effects," *Steel and Composite Structures,* 21(6) (2016) 1347-1368.

[8] Debski, H., "Numerical analysis of stability of thin-walled composite column with open cross-section," *Mechanics and Mechanical Engineering,* 17 (1)(2013) 29-35.

[9] Koiter, W.T., "Elastic stability and post-buckling behavior," *In: Proceedings of the Symposium on Non-linear Problems,* University of Wisconsin, Wisconsin (1963) 257-275.

[10] Cortinez, H.V., and Piovan, M. T., "Stability of composite thin-walled beams with shear deformability," *Computers & Structures,* 84(2006) 978-990.

[11] Jones, R.M, *Mechanics of Composite Materials*, New York: Hemisphere Publishing Corporation, 1975.

[12] Hernandez, V., Roman, J.E., Tomas, A., and Vidal, V., "Lanczos methods in SLEPc," Polytechnic University of Valencia, Province of Valencia, 2006.

[13] Memon, B.A., Su, X.S., "Arc-length technique for nonlinear finite element analysis," Journal of Zhejiang University SCI, 5(5) (2004) 618-628.

[14] Rasheed, H.A., *Strengthening Design of Reinforced Concrete with FRP*, New York: CRC Press, 2015.

# Chapter 11 - Buckling of Simply Supported Anisotropic Steel-FRP Hybrid Columns Using Rayleigh-Ritz Formulation with Numerical and Experimental Verification

**Rund Al-Masri[1], Hayder A. Rasheed[2]* and Yu-Szu Chen[3]**

## 11.1 Abstract

**Limited number of research studies has addressed the topic of buckling of steel-fiber reinforced polymer (FRP) members. A generalized analytical buckling formula for simply supported anisotropic steel-FRP (hybrid) thin columns under axial compression is developed herein using the Rayleigh-Ritz approximation. Following the generalized constitutive relationship, the effective axial, coupling, and flexural stiffness coefficients of the anisotropic steel-FRP layup is determined using dimensional reduction by static condensation of 6x6 hybrid stiffness matrix. The analytical explicit formula reproduces Euler buckling expression while it furnishes an extra term which is a function of the effective coupling and axial stiffness. For certain types of steel-laminated composites, the analytical formula reduced down to Euler buckling formula once the effective coupling term vanishes. The analytical buckling formula is verified against finite element Eigen value solutions for different anisotropic laminated layups yielding high accuracy. Comparison with experimental work is conducted for two categories of anisotropic steel-glass fiber reinforced polymer (GFRP) columns in which category A has steel in-between the composite layup and category B has steel on the side of the composite layup. Verification of the analytical solution against some of the experimental results yielded excellent comparison. Moreover, curing methods, roughness of steel and type of epoxy used have a direct influence on the bonding conditions and buckling loads.**

Keywords: Buckling of Steel-FRP Columns, Simply Supported Columns, Anisotropic Laminated Material, Rayleigh-Ritz Formulation.

[1] Ph.D. Candidate, Department of Civil Engineering, Kansas State University, Manhattan, KS 66506

[2] Professor, Department of Civil Engineering, Kansas State University, Manhattan, KS 66506

[3] Ph.D. Student, Department of Civil Engineering, Kansas State University, Manhattan, KS 66506

## 11.2 Introduction

The use of fiber reinforced polymer (FRP) is ever growing in different industrial applications such as aerospace, marine, automotive, and civil engineering because of their distinguished properties (High stiffness-to-weight ratio, high strength-to-weight ratio, ease of application in construction sites, corrosion and fatigue resistance). This growth increased the demand for better understanding the mechanics of fiber reinforced polymer (FRP). Fiber reinforced polymer (FRP) is used with different types of materials such as steel and concrete making the so called hybrid structures. Hybrid columns, like any traditional members subjected to axial compression, undergo stability issues prior to failure. Limited amount of researches have focused on the buckling of hybrid columns if any, however, a significant amount of research has been performed to study the buckling behavior of composite members like plates and shells in the recent years [1-20]. Herenica et al. [1] derived a closed form solution for buckling of long anisotropic plates under axial compression ($N_x$) with various boundary conditions. The closed form solution can be expressed as:

$$N_x^{cr} = \kappa_x \frac{\pi^2}{b^2} \sqrt{D_{11} D_{22}} \quad (1)$$

Where $D_{ij}$ is the bending stiffness; b is the width of the plate; and $\kappa_x$ is the non-dimensional buckling coefficient related to the boundary conditions. The results showed an excellent agreement when validated with existing solutions (Weaver [2] [3], Qiao and Shan [4]), and finite element solutions. Mahesh et al. [5] developed a general buckling formulation for plates under linearly varying uniaxial compressive load with general out-of-plane boundary conditions using Rayleigh-Ritz method based on the energy approach along with orthogonal polynomials generated by a Gram-Schmidt process. Results showed a good agreement with differential quadrature (DQ) models [6]. Silva et al. [7] presented a formulation of a generalized beam theory (GBT) to study

local and global buckling behavior of fiber reinforced polymer composite open section thin-walled columns. The solution for buckling using GBT included solving the following eigenvalue problem:

$$(\boldsymbol{K} + \boldsymbol{\gamma G})\boldsymbol{d} = \boldsymbol{0} \quad \textbf{(2)}$$

Where K is the global linear stiffness matrix; G is the geometric stiffness matrix; and d is the eigenvector.

Silvestre and Camotim [8] developed a second order generalized beam theory (GBT) to predict buckling behavior for thin walled arbitrary orthotropic members and compared it with Bauld and Lih-Shyng theory [9]. The results showed that the critical load exists for all isotropic or cross-ply orthotropic members. On the other hand, non-linear primary path is exhibited and no specific bifurcation is detected for asymmetric orthotropic lay-ups. Rasheed and Yousif [10], derived a closed form solution for buckling of anisotropic laminated composite rings and long cylinders subjected to external hydrostatic pressure. The analytical results were confirmed against finite element solutions and also concluded that the buckling modes are symmetric with respect to rotated axes of the twisted section of the pre-buckling solution in case of anisotropy. Xu et al. [11] presented an approximate analytical solution to predict buckling of a tri-axial woven fabric composite structure under bi-axial loading based on the equivalent anisotropic plate method. Results showed that the analytical solution gives an upper bound buckling load and it can be used to predict buckling behavior for real world problems subjected to bi-axial loading. Using first order shear deformation and von-Karman type nonlinearity, Shukla et al. [12] predicted the critical buckling loads for laminated composite plates with various boundary conditions under in-plane uniaxial and biaxial loading. Span to thickness ratio, plate aspect ratio, lamination scheme, number of layers and modulus ratio effects were considered in estimating the buckling behavior. Sun and Harik [13] developed analytical buckling solution of stiffened antisymmetric laminated composite

plates with bending-extension coupling using analytical strip method (ASM) which was first developed by Harik and Salamoun [14] to analyze bending of thin orthotropic and stiffened rectangular plates. The results showed that plates with free boundary conditions contribute the weakest stiffening effect. Moreover, the number of layers of ply orientations equal to 0 and 90 had no effect on the critical buckling load since the coupling stiffness matrix vanishes.

Debski et al. [15] studied buckling and post-buckling behavior of thin-walled composite channel column sections experimentally. The results were compared with numerical solutions obtained from finite element models (Abaqus and ANSYS) and analytical-numerical method (ANM). The results showed that the stability of angle-ply laminated plates improved under biaxial compression/tension and shear. Moreover, additional in-plane forces were created due to the in-plane restrains. Haung et al. [16] addressed the stability of grid stiffened laminated composite plates by presenting an efficient finite element model. Curved beam element was presented to model the stiffeners. Furthermore, different numerical examples were solved using the developed element. Wang and Abdalla [17] presented a method to study the global and local buckling of grid stiffened composite panels based on Bloch wave theory and confirmed for different composite configurations. Khayat et al. [18] studied the stability of laminated composite cylindrical shell under lateral displacement-dependent pressure using semi-analytical finite strip method. The governing equations were developed based on the first shear deformation theory with Sanders type of kinematics nonlinearity. Baseri et al. [19] proposed analytical solution to investigate the buckling of embedded laminated composite plates based on higher order shear deformation theory. The analytical solution was solved using Navier method. Becheri et al. [20] presented an exact analytical solution to study the buckling of symmetrically cross-ply plates using $n^{th}$-order shear

deformation theory with curvature effects. The analytical solution was compared with previous work.

In this work, a generalized analytical buckling formula for simply supported anisotropic steel-FRP hybrid columns under axial compression is developed using Rayleigh-Ritz approximation. Axial, coupling and flexural rigidities in 1D are determined using dimensional reduction by the static condensation approach starting with the 3D rigidity matrix. The analytical buckling formula is verified against finite element Eigen value solutions for different anisotropic laminated layups yielding high accuracy. Comparison with experimental work is conducted for two categories of anisotropic steel-glass fiber reinforced polymer (GFRP) columns in which category A has steel sandwiched in-between the composite layers and category B has steel on the side of the composite layup. Verification of the analytical solution against some of the experimental results yielded excellent comparison. Moreover, curing methods, roughness of steel and type of epoxy used have a direct influence on the bonding conditions and the buckling loads.

## 11.3 Analytical Formulation

Using Rayleigh-Ritz approximation, a generalized closed form buckling formula for simply supported anisotropic steel-FRP columns under axial compression is realized.

### 11.3.1 Assumptions:

- Buckling takes place in the x-y plane about the z-axis (weak axis).
- The y-axis runs through the thickness of the column and perpendicular to the lamination composite surface.
- The lamination angle ( $\alpha$ ) is measured with respect to the x-axis (i.e. 0° fibers run parallel to the x-axis and 90° fibers run parallel to the z-axis). Accordingly, the angle ( $\alpha$ ) is rotated about the y-axis.

- Plane sections before bending remain plane after bending and perpendicular to the mid surface (i.e. simple beam theory holds).
- Classical lamination theory is applicable with shear deformations ignored.

Geometry and the Cartesian coordinates of the simply supported column used are illustrated in Figure 11.1. The z-axis is the weak axis of the column about which bending takes place. The following displacement relations were assumed based on the isotopic Euler first buckling mode:

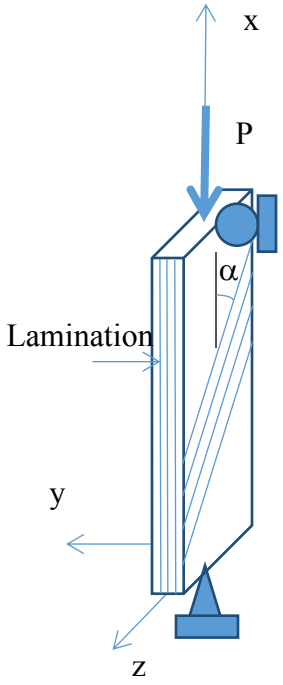


Figure 11.1 The column geometry.

$$\boldsymbol{u}\,(\boldsymbol{x}) = \boldsymbol{B_1 x}\,; \quad \boldsymbol{v}\,(\boldsymbol{x}) = \boldsymbol{C_1}\sin\frac{\boldsymbol{\pi x}}{\boldsymbol{L}} \tag{3}$$

Where $u(x)$, and $v(x)$ is the axial, and lateral displacements; $B_1$, and $C_1$ are constants to be solved; and x is the distance along the axis of the column. For an intermediate class of deformation, the axial strain $\varepsilon_x$ and curvature $\kappa_x$are defined as follow.

$$\boldsymbol{\varepsilon_x} = \frac{\boldsymbol{du}}{\boldsymbol{dx}} + \frac{\boldsymbol{1}}{\boldsymbol{2}}\left(\frac{\boldsymbol{dv}}{\boldsymbol{dx}}\right)^{\boldsymbol{2}} = \boldsymbol{u'} + \frac{\boldsymbol{1}}{\boldsymbol{2}}\boldsymbol{v'^2}; \qquad \boldsymbol{\kappa_x} = \frac{\boldsymbol{d^2v}}{\boldsymbol{dx^2}} = \boldsymbol{v''} \tag{4}$$

### 11.3.2 Constitutive equations

The principal material directions were transformed into the column coordinate system, the stresses and strains are then related in the following equation

$$\begin{Bmatrix} \boldsymbol{\sigma_x} \\ \boldsymbol{\sigma_z} \\ \boldsymbol{\tau_{xz}} \end{Bmatrix} = \begin{bmatrix} \boldsymbol{\bar{Q}_{11}} & \boldsymbol{\bar{Q}_{12}} & \boldsymbol{\bar{Q}_{16}} \\ \boldsymbol{\bar{Q}_{12}} & \boldsymbol{\bar{Q}_{22}} & \boldsymbol{\bar{Q}_{26}} \\ \boldsymbol{\bar{Q}_{16}} & \boldsymbol{\bar{Q}_{26}} & \boldsymbol{\bar{Q}_{66}} \end{bmatrix} \begin{Bmatrix} \boldsymbol{\varepsilon_x} \\ \boldsymbol{\varepsilon_z} \\ \boldsymbol{\gamma_{xz}} \end{Bmatrix} \quad \textbf{(5)}$$

Where $\bar{Q}_{ij}$ matrix represents the transformed reduced constitutive matrix defined in standard composite textbooks [21]. The reduced constitutive matrix is simplified to the expression in Equation (6) for the steel sheet.

$$\begin{Bmatrix} \boldsymbol{\sigma_x} \\ \boldsymbol{\sigma_z} \\ \boldsymbol{\tau_{xz}} \end{Bmatrix} = \begin{bmatrix} \frac{\boldsymbol{E}}{\boldsymbol{1-\nu^2}} & \frac{\boldsymbol{\nu E}}{\boldsymbol{1-\nu^2}} & \boldsymbol{0} \\ \frac{\boldsymbol{\nu E}}{\boldsymbol{1-\nu^2}} & \frac{\boldsymbol{E}}{\boldsymbol{1-\nu^2}} & \boldsymbol{0} \\ \boldsymbol{0} & \boldsymbol{0} & \boldsymbol{G} \end{bmatrix} \begin{Bmatrix} \boldsymbol{\varepsilon_x} \\ \boldsymbol{\varepsilon_z} \\ \boldsymbol{\gamma_{xz}} \end{Bmatrix} \quad \textbf{(6)}$$

Accordingly, the coupled force-strain relationship is established as follows:

$$\begin{Bmatrix} \boldsymbol{N_x} \\ \boldsymbol{N_z} \\ \boldsymbol{N_{xz}} \\ \boldsymbol{M_x} \\ \boldsymbol{M_z} \\ \boldsymbol{M_{xz}} \end{Bmatrix} = \begin{bmatrix} \boldsymbol{A_{11}} & \boldsymbol{A_{12}} & \boldsymbol{A_{16}} & \boldsymbol{B_{11}} & \boldsymbol{B_{12}} & \boldsymbol{B_{16}} \\ \boldsymbol{A_{12}} & \boldsymbol{A_{22}} & \boldsymbol{A_{26}} & \boldsymbol{B_{12}} & \boldsymbol{B_{22}} & \boldsymbol{B_{26}} \\ \boldsymbol{A_{16}} & \boldsymbol{A_{26}} & \boldsymbol{A_{66}} & \boldsymbol{B_{16}} & \boldsymbol{B_{26}} & \boldsymbol{B_{66}} \\ \boldsymbol{B_{11}} & \boldsymbol{B_{12}} & \boldsymbol{B_{16}} & \boldsymbol{D_{11}} & \boldsymbol{D_{12}} & \boldsymbol{D_{16}} \\ \boldsymbol{B_{12}} & \boldsymbol{B_{22}} & \boldsymbol{B_{26}} & \boldsymbol{D_{12}} & \boldsymbol{D_{22}} & \boldsymbol{D_{26}} \\ \boldsymbol{B_{16}} & \boldsymbol{B_{26}} & \boldsymbol{B_{66}} & \boldsymbol{D_{16}} & \boldsymbol{D_{26}} & \boldsymbol{D_{66}} \end{bmatrix} \begin{Bmatrix} \boldsymbol{\varepsilon_x} \\ \boldsymbol{\varepsilon_z} \\ \boldsymbol{\gamma_{xz}} \\ \boldsymbol{\kappa_x} \\ \boldsymbol{\kappa_z} \\ \boldsymbol{\kappa_{xz}} \end{Bmatrix} \quad \textbf{(7)}$$

Where:

$$\boldsymbol{A_{ij}} = \sum_{\boldsymbol{k=1}}^{\boldsymbol{N}} \boldsymbol{\bar{Q}_{ij} t_k}$$

$$\boldsymbol{B_{ij}} = \sum_{\boldsymbol{k=1}}^{\boldsymbol{N}} \boldsymbol{\bar{Q}_{ij} t_k \bar{y}_k}$$

$$\boldsymbol{D_{ij}} = \sum_{\boldsymbol{k=1}}^{\boldsymbol{N}} \boldsymbol{\bar{Q}_{ij} t_k} \left( \boldsymbol{\bar{y}_k^2} + \frac{\boldsymbol{t_k^2}}{\boldsymbol{12}} \right) \quad \textbf{(8)}$$

$$\boldsymbol{t_k} = \boldsymbol{y_k - y_{k-1}} \ , \quad \boldsymbol{\bar{y}_k} = \frac{\boldsymbol{y_k + y_{k-1}}}{\boldsymbol{2}}$$

In which $A_{ij}$, $B_{ij}$, and $D_{ij}$ are the axial, coupling, and flexural rigidity coefficients. $t_k$ = thickness of the k-th ply; and N = number of different plies in the stacking sequence.

The three dimensional (3D) rigidity matrix is established first using the material properties and the fiber orientations into equation (7). Then the dimension is reduced to 1D anisotropic axial, coupling and flexural rigidities using static condensation approach after applying the zero forces and moments.

$$\begin{Bmatrix} \boldsymbol{N_x} \\ \boldsymbol{N_z = 0} \\ \boldsymbol{N_{xz} = 0} \\ \boldsymbol{M_x} \\ \boldsymbol{M_z = 0} \\ \boldsymbol{M_{xz} = 0} \end{Bmatrix} = \begin{bmatrix} \boldsymbol{A_{11}} & \boldsymbol{A_{12}} & \boldsymbol{A_{16}} & \boldsymbol{B_{11}} & \boldsymbol{B_{12}} & \boldsymbol{B_{16}} \\ \boldsymbol{A_{12}} & \boldsymbol{A_{22}} & \boldsymbol{A_{26}} & \boldsymbol{B_{12}} & \boldsymbol{B_{22}} & \boldsymbol{B_{26}} \\ \boldsymbol{A_{16}} & \boldsymbol{A_{26}} & \boldsymbol{A_{66}} & \boldsymbol{B_{16}} & \boldsymbol{B_{26}} & \boldsymbol{B_{66}} \\ \boldsymbol{B_{11}} & \boldsymbol{B_{12}} & \boldsymbol{B_{16}} & \boldsymbol{D_{11}} & \boldsymbol{D_{12}} & \boldsymbol{D_{16}} \\ \boldsymbol{B_{12}} & \boldsymbol{B_{22}} & \boldsymbol{B_{26}} & \boldsymbol{D_{12}} & \boldsymbol{D_{22}} & \boldsymbol{D_{26}} \\ \boldsymbol{B_{16}} & \boldsymbol{B_{26}} & \boldsymbol{B_{66}} & \boldsymbol{D_{16}} & \boldsymbol{D_{26}} & \boldsymbol{D_{66}} \end{bmatrix} \begin{Bmatrix} \boldsymbol{\varepsilon_x} \\ \boldsymbol{\varepsilon_z} \\ \boldsymbol{\gamma_{xz}} \\ \boldsymbol{\kappa_x} \\ \boldsymbol{\kappa_z} \\ \boldsymbol{\kappa_{xz}} \end{Bmatrix} \tag{9}$$

Equation (9) is solved first for the axial strain and axial curvature ($\boldsymbol{\varepsilon_x}$ ,$\boldsymbol{\kappa_x}$) in terms of the rest of the deformation components by extracting the second, third, fifth and sixth linear equations from the matrix.

$$-\begin{bmatrix} \boldsymbol{A_{12}} & \boldsymbol{B_{12}} \\ \boldsymbol{A_{16}} & \boldsymbol{B_{16}} \\ \boldsymbol{B_{12}} & \boldsymbol{D_{12}} \\ \boldsymbol{B_{16}} & \boldsymbol{D_{16}} \end{bmatrix} \begin{Bmatrix} \boldsymbol{\varepsilon_x} \\ \boldsymbol{\kappa_x} \end{Bmatrix} = \begin{bmatrix} \boldsymbol{A_{22}} & \boldsymbol{A_{26}} & \boldsymbol{B_{22}} & \boldsymbol{B_{26}} \\ \boldsymbol{A_{26}} & \boldsymbol{A_{66}} & \boldsymbol{B_{26}} & \boldsymbol{B_{66}} \\ \boldsymbol{B_{22}} & \boldsymbol{B_{26}} & \boldsymbol{D_{22}} & \boldsymbol{D_{26}} \\ \boldsymbol{B_{26}} & \boldsymbol{B_{66}} & \boldsymbol{D_{26}} & \boldsymbol{D_{66}} \end{bmatrix} \begin{Bmatrix} \boldsymbol{\varepsilon_y} \\ \boldsymbol{\gamma_{xz}} \\ \boldsymbol{\kappa_{yz}} \\ \boldsymbol{\kappa_{xz}} \end{Bmatrix}$$

$$-\boldsymbol{R}\begin{Bmatrix} \boldsymbol{\varepsilon_x} \\ \boldsymbol{\kappa_x} \end{Bmatrix} = \boldsymbol{Q}\begin{Bmatrix} \boldsymbol{\varepsilon_z} \\ \boldsymbol{\gamma_{xz}} \\ \boldsymbol{\kappa_z} \\ \boldsymbol{\kappa_{xz}} \end{Bmatrix} \tag{10}$$

Inverting the matrix Q to the other side of equation (10), the condensed deformation components are obtained in terms of the axial strain and curvature:

$$\begin{Bmatrix} \varepsilon_z \\ \gamma_{xz} \\ \kappa_z \\ \kappa_{xz} \end{Bmatrix} = -[Q]^{-1}[R] \begin{Bmatrix} \varepsilon_x \\ \kappa_x \end{Bmatrix} \tag{11}$$

Substituting equation (11) into the first and fourth linear equation of the matrix (9); the axial force and in-plane moment vs. the axial strain and in-plane curvature relationship can be expressed in terms of the generally anisotropic material properties

$$\begin{bmatrix} N_x \\ M_x \end{bmatrix} = \begin{bmatrix} A_H & B_H \\ B_H & D_H \end{bmatrix} \begin{Bmatrix} \varepsilon_x \\ \kappa_x \end{Bmatrix} \tag{12}$$

Where

$$\begin{bmatrix} A_H & B_H \\ B_H & D_{aH} \end{bmatrix} = \begin{bmatrix} A_{11} & B_{11} \\ B_{11} & D_{11} \end{bmatrix} - [R]^T[Q]^{-1}[R] \tag{13}$$

### 11.3.3 Energy Formulation

A generalized buckling formula was derived using Rayleigh-Ritz approximation based on the energy approach. Strain energy can be expressed in terms of the integration of the applied loads multiplying the corresponding deformations.

$$U = \int_0^L \left(\frac{1}{2} N_x \varepsilon_x + \frac{1}{2} M_x \kappa_x\right) dx$$

$$= \int_0^L \frac{1}{2} (A_H \varepsilon_x^2 + B_H \varepsilon_x \kappa_x)\, dx + \int_0^L \frac{1}{2} (B_H \varepsilon_x \kappa_x + D_H \kappa_x^2)\, dx \tag{14}$$

The potential of external loads can be expressed as shown in equation (15)

$$W = -P\, u(L) \tag{15}$$

Taking the total potential energy function and substituting equations (14) and (15) into equation (16)

$$\Pi = U - W = \int_0^L \frac{1}{2} (A_H \varepsilon_x^2 + 2B_H \varepsilon_x \kappa_x + D_H \kappa_x^2)\, dx + P\, u(L) \tag{16}$$

$$\Pi = \frac{1}{2}A_{ani}B_1^2L + \frac{1}{4}A_{ani}B_1C_1^2L\left(\frac{\pi}{L}\right)^2 + \frac{3}{64}A_{ani}C_1^4L\left(\frac{\pi}{L}\right)^4 - \frac{2}{\pi}B_{ani}B_1C_1L\left(\frac{\pi}{L}\right)^2 - \frac{1}{3\pi}B_{ani}C_1^3L\left(\frac{\pi}{L}\right)^4 + \frac{1}{4}D_{ani}C_1^2L\left(\frac{\pi}{L}\right)^4 + PB_1L \quad (17)$$

Minimizing the total potential energy function with respect to $B_1$ and $C_1$ and setting the resulting expressions to zero, performing the integrations and manipulating the equations to give:

$$\frac{\partial \Pi}{\partial B_1} = A_HB_1L + \frac{A_HC_1^2L}{4}\left(\frac{\pi}{L}\right)^2 - 2B_HC_1\left(\frac{\pi}{L}\right) + PL = 0 \quad (18)$$

$$\frac{\partial \Pi}{\partial C_1} = \frac{A_HB_1C_1L}{2}\left(\frac{\pi}{L}\right)^2 + \frac{3A_HC_1^3L}{16}\left(\frac{\pi}{L}\right)^4 - 2B_HB_1\left(\frac{\pi}{L}\right) - B_HC_1^2\left(\frac{\pi}{L}\right)^3 + \frac{D_HC_1L}{2}\left(\frac{\pi}{L}\right)^4 = 0 \quad (19)$$

Solving equation (18) for $B_1$ then substituting the resulting expression in equation (19), the following cubic equation is formulated in terms of $C_1$ value

$$B_1 = \frac{2B_HC_1}{A_HL}\frac{\pi}{L} - \frac{C_1^2}{4}\left(\frac{\pi}{L}\right)^2 - \frac{P}{A_H} \quad (20)$$

$$q_1C_1^3 + q_2C_1^2 + q_3C_1 + q_4 = 0 \quad (21)$$

Where

$$q_1 = \frac{A_HL}{16}\left(\frac{\pi}{L}\right)^2,\ q_2 = \frac{B_H}{2}\frac{\pi}{L},\ q_3 = \left[\frac{D_HL}{2}\left(\frac{\pi}{L}\right)^2 - \frac{4B_H^2}{A_HL} - \frac{L}{2}P\right], q_4 = \frac{2B_H}{A_H}\frac{PL}{\pi}$$

Equation (21) does not lend itself to a closed form solution. Therefore, considering the critical stability matrix:

$$\begin{bmatrix} \frac{\partial^2\Pi}{\partial {B_1}^2} & \frac{\partial^2\Pi}{\partial B_1 \partial C_1} \\ \frac{\partial^2\Pi}{\partial C_1 \partial B_1} & \frac{\partial^2\Pi}{\partial {C_1}^2} \end{bmatrix} \quad (22)$$

Where

$$\frac{\partial^2 \Pi}{\partial B_1^2} = A_H L$$

$$\frac{\partial^2 \Pi}{\partial B_1 \partial C_1} = A_H C_1 \left(\frac{\pi}{L}\right)^2 \frac{L}{2} - 2B_H \frac{\pi}{L}$$

$$\frac{\partial^2 \Pi}{\partial C_1 \partial B_1} = A_H C_1 \left(\frac{\pi}{L}\right)^2 \frac{L}{2} - 2B_H \frac{\pi}{L} \quad \textbf{(23)}$$

$$\frac{\partial^2 \Pi}{\partial C_1^2} = \frac{A_H B_1 L}{2}\left(\frac{\pi}{L}\right)^2 + \frac{9A_H C_1^2 L}{16}\left(\frac{\pi}{L}\right)^4 - 2B_H C_1 \left(\frac{\pi}{L}\right)^3 + \frac{D_H L}{2}\left(\frac{\pi}{L}\right)^4$$

Setting the determinant of the matrix in Equation (22) to zero, substituting $B_1$ expression from equation (20) and solving for $C_1$ using the general solution of a quadratic equation:

$$C_1 = \frac{-A_H L B_H (\frac{\pi}{L}) \mp \sqrt{A_H^2 L^2 B_H^2 (\frac{\pi}{L})^2 - 4(\frac{3}{16}) A_H^2 L^2 \left(\frac{\pi}{L}\right)^2 [\frac{A_H D_H L^2}{2}\left(\frac{\pi}{L}\right)^2 - 4B_H^2 - \frac{A_H^2 L^2}{2} P]}}{2(\frac{3}{16}) A_H^2 L^2 (\frac{\pi}{L})^2} \quad \textbf{(24)}$$

In order for the $C_1$ value to be real, the discriminant must be at least zero. By setting the discriminant to zero and manipulating its expression, a closed form solution for the critical buckling load is derived:

$$P_{cr} = \frac{D_H \pi^2}{L^2} - \frac{32}{3}\frac{B_H^2}{A_H L^2} \quad \textbf{(25)}$$

In the case of isotropic or specially-orthotropic materials, the coupling term vanishes reducing the equation to that of Euler buckling.

## 11.4 Numerical Formulation

Finite element buckling analysis was used to verify the analytical solution using the commercial software package Abaqus for hybrid columns. Columns were constructed with simply supported ends, in which roller and pin supports were introduced on the top and bottom of the column, respectively. Moreover, a concentrated load was applied at the top of the column. Linear elastic laminated material was used for orthotropic and anisotropic layups, respectively. Quadrilateral eight-node doubly curved thick shell element (S8R) was used for modeling the columns in 3D-space. Element size of 2.5 x 2.5 mm was used with total number of elements equal to 300 for hybrid columns after conducting a convergence study to select the appropriate mesh size. Figure 11.2 illustrates the model's boundary conditions and mesh for the shell elements.

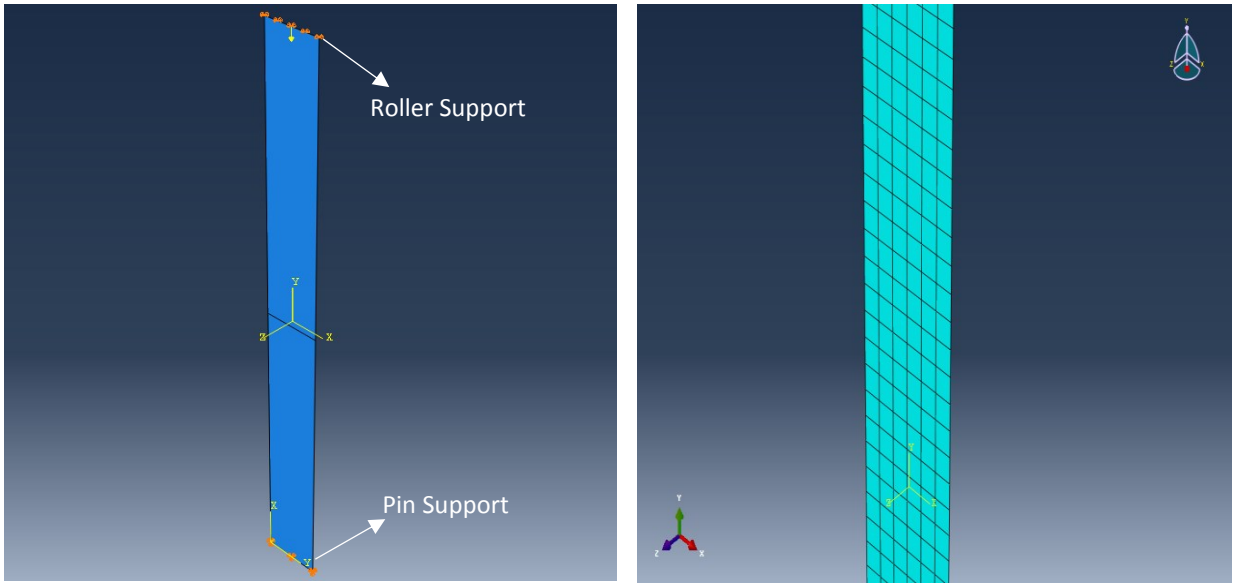


Figure 11.2 Left: Boundary conditions and applied load. Right: Meshed Model.

Two types of analyses were performed in this study. Buckling analysis to simulate eigenvalue computation was attempted using Lanczos solver. Lanczos method is one of the methods used to solve for eigenvalues and eigenvectors for complex Hermitian matrix using power methods. Lanczos method reduces $m \times m$ symmetric matrix using recurrence relations (multidimensional

array values) to a tridiagonal matrix [22]. To predict the stability response (pre-buckling and buckling), nonlinear geometry analysis using the modified Riks formulation was conducted. The modified Riks analysis is based on the Arc length method in which it follows the equilibrium path, representing either the bifurcation points or the limit points. Load increments are applied during the analysis in which equilibrium iterations converge along the arc length, forcing the constraint equation to be satisfied at every arc length increment [23].

## 11.5 Experimental Program

### 11.5.1 Specimen Preparation

Twenty four hybrid columns were designed and prepared in the laboratory with two categories of anisotropic steel-glass fiber reinforced polymer (GFRP) columns in which category A has steel sandwiched in-between the composite layers and category B has steel on the side of the composite layup. Steel plate; of 14.73 mm thickness, surface was roughed to insure a good bond with the composite layups, see Figure 11.3.

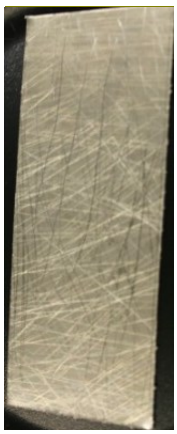

Figure 11.3 Roughened surface of steel plate.

V-Wrap EG50 unidirectional fabric was cut at different angles (-30, 0, 30, and 90 degree) as shown in Figure 11.4. Properties of V-Wrap EG50 fabric are shown in Table 11.1 [24].

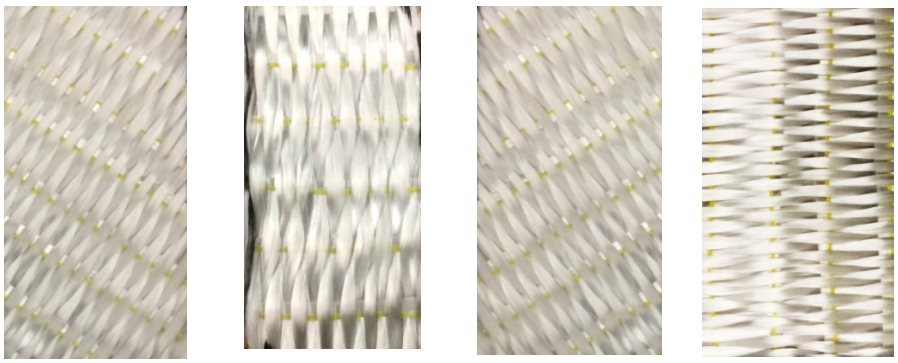

-30 0 30 90

Figure 11.4 Glass fiber orientations

Table 11.1 Dry fiber properties [21].

| | |
|---|---|
| **Tensile Strength** | 3240 MPa (470,000 psi) |
| **Tensile Modulus** | 72,400 MPa (10.5 x $10^6$ psi) |
| **Elongation** | 4.5 % |
| **Density** | 2.55 g/$cm^3$ (0.092 lbs/$in^3$) |

Epoxy resin and hardener were mixed together to make the matrix material with 100 to 34.5 ratio by volume, respectively, using a mechanical rotary mixer as shown in Figure 11.5. The epoxy resin was first applied to the non-stick preparation sheet then a ply of fiber is laid by a paint roller against the resin. A second layer of resin was applied with the roller on top of the fiber ply and the process is repeated as many times as the number of fiber plies in the stacking sequence. Pressure was implemented to remove excess epoxy and insure steel plate was bonded to the fibers, Figure 11.6.

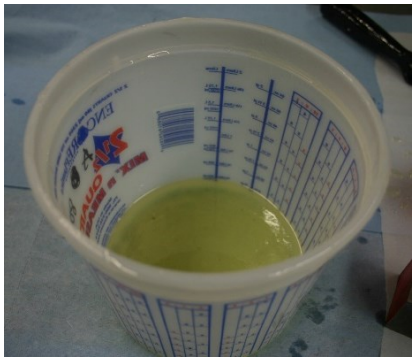

Figure 11.5 Matrix material.

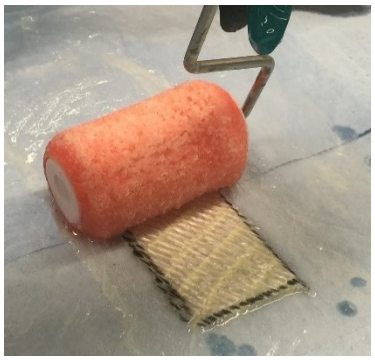

Figure 11.6 Specimen preparation

Figure 11.7 shows the composite strips before the cutting process and uniform load applied to ensure a strong bond between the layers. Four different stacking sequences were constructed by the wet layup process. The strips were then left to harden for one week at room temperature under uniform load then were cut to column final sizes using a band-saw.

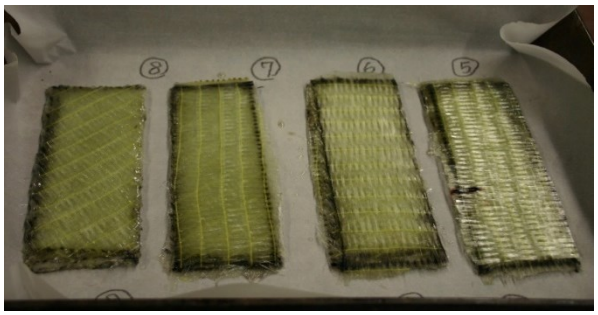



Figure 11.7 Composite strip after the wet layup process and uniform load.

Thickness and width of the hardened specimens were measured using a digital caliper at three locations to take the average. Layer thickness ($t_i$) is assumed equal to one quarter of the average specimen's thickness since each laminate was composed of four plies. Fiber and matrix volume fractions ($V_f$ and $V_m$) were calculated using equation (26). Using rule of mixtures and the Halpin-Tsai equation, elastic properties in the fiber, transverse and in-plane shear directions were obtained.

$$V_f = \frac{thickness\ of\ uncured\ fiber\ (t_f)}{thickness\ of\ cured\ layer\ (t_i)}$$

$$V_m = 1 - V_f \quad \textbf{(26)}$$

Where the thickness $t_f$ *was* measured to be 0.305 mm, the thickness $t_i$ varied based on the different laminates as shown in Table 2 below.

$$Rule\ of\ mixtures:$$

$$E_1 = E_f V_f + E_m V_m \quad \textbf{(27)}$$

$$\nu_{12} = \nu_f V_f + \nu_m V_m$$

$$Halpin - Tsai\ equation:\ \frac{E_2}{E_m} = \frac{1 + \xi\eta V_f}{1 - \eta V_f}$$

$$\eta = \frac{{E_f}/{E_m} - 1}{{E_f}/{E_m} + \xi} \quad \textbf{(28)}$$

$$\frac{G_{12}}{G_m} = \frac{1 + \xi\eta V_f}{1 - \eta V_f}$$

$$\eta = \frac{{G_f}/{G_m} - 1}{{G_f}/{G_m} + \xi}$$

In which $E_f$, and $E_m$ are fiber and matrix modulus, $G_f$, and $G_m$ are fiber and matrix shear modulus, $\xi$ value was taken equal to one to provide more accurate results [25]. Equation (29) determines the minor Poisson's ratio:

$$\frac{\nu_{12}}{E_1} = \frac{\nu_{21}}{E_2} \tag{29}$$

### 11.5.2 Test Setup

After one week of curing, the four different stacking sequences, shown in Table 11.2, were tested. Columns were tested under axial compression using the Shimadzu AG-IC 50 kN testing machine, operating with Trapezium X software following a displacement control protocol with a displacement rate of 1 mm/minute.

Table 11.2 Samples of the four different stacking sequences

| **Specimen Number** | **Category A** | **Specimen Number** | **Category B** |
|---|---|---|---|
| **1** | 30/-30/S/0/90 | **5** | 90/0/-30/30/S |
| **2** | 30/90/S/-30/0 | **6** | 0/-30/90/30/S |
| **3** | 0/30/S/-30/90 | **7** | 90/-30/30/0/S |
| **4** | 30/-30/S/30/-30 | **8** | -30/30/-30/30/S |

Simply supported boundary conditions were utilized at the ends of the composite columns, see Figure 11.8. Columns were aligned horizontally and vertically and loaded in axial compressive displacement until the load dropped indicating the attainment of a limit load.

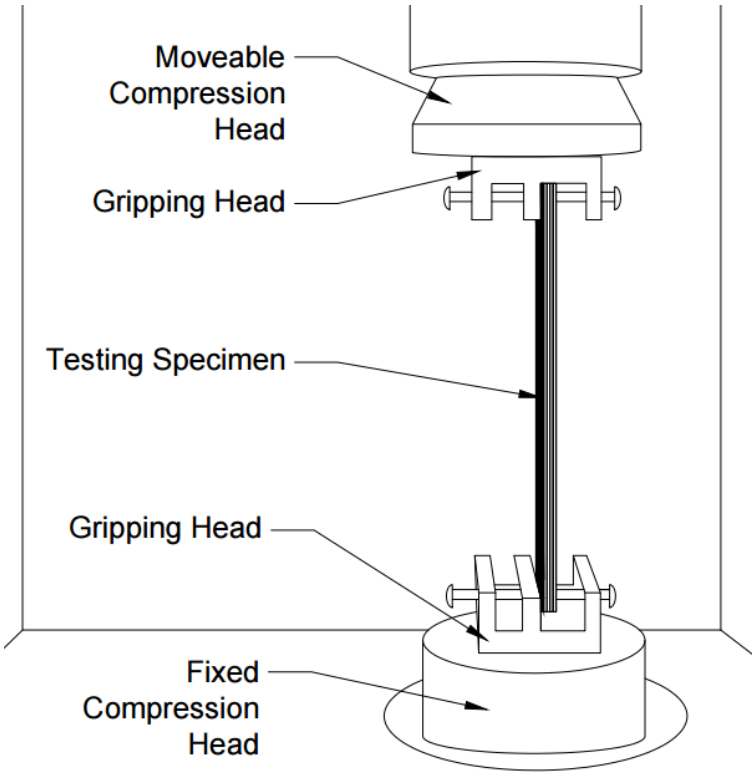


Figure 11.8 Axial Compression Test Setup for Category B.

## 11.6 Results and Discussion

The average thickness, and width of the tested specimen for category A and B with length equal to 128 mm is presented in Table 11.3 where the difference in column sizes is due to wet layup procedure that has a limited control over the amount of epoxy applied at each layer and personal error in the cutting process. Table 11.4 presents mechanical properties of composite.

Table 11.3 Geometry of column specimen.

| **Category A** | | | **Category B** | | |
|---|---|---|---|---|---|
| **Specimen #** | **Thickness** | **Width** | **Specimen #** | **Thickness** | **Width** |
| | ***mm*** | ***mm*** | | ***mm*** | ***mm*** |
| **1-1** | 5.64 | 12.45 | **5-1** | 6.07 | 14.91 |
| **1-2** | 5.66 | 12.50 | **5-2** | N.A. | N.A. |
| **1-3** | 5.54 | 12.78 | **5-3** | N.A. | N.A. |
| **2-1** | 5.97 | 12.95 | **6-1** | 5.54 | 15.14 |
| **2-2** | 5.82 | 12.50 | **6-2** | 5.61 | 14.86 |

| | | | | | |
|---|---|---|---|---|---|
| **2-3** | 5.66 | 12.40 | **6-3** | 5.56 | 15.11 |
| **3-1** | 5.77 | 12.40 | **7-1** | 5.64 | 14.83 |
| **3-2** | 5.82 | 12.70 | **7-2** | 5.64 | 14.10 |
| **3-3** | 5.79 | 12.19 | **7-3** | 5.84 | 13.79 |
| **4-1** | 5.64 | 12.78 | **8-1** | 5.21 | 14.61 |
| **4-2** | 5.26 | 12.55 | **8-2** | 5.79 | 15.47 |
| **4-3** | 5.61 | 12.88 | **8-3** | 5.59 | 15.34 |

Table 11.4 Composite properties of E-glass/epoxy used in experiments.

| | Vf | Vm | E1 | E2 | G12 | v12 | v21 |
|---|---|---|---|---|---|---|---|
| **1_1** | 0.549055 | 0.450946 | 41555.356 | 11734.4728 | 4323.5068 | 0.320586 | 0.09053 |
| **1_2** | 0.548233 | 0.451768 | 41499.101 | 11711.7193 | 4315.0226 | 0.32066 | 0.0905 |
| **1_3** | 0.560405 | 0.439596 | 42331.649 | 12055.3317 | 4443.1837 | 0.319564 | 0.09101 |
| **2_1** | 0.519444 | 0.480557 | 39529.946 | 10954.7148 | 4032.9595 | 0.323251 | 0.08958 |
| **2_2** | 0.532674 | 0.467327 | 40434.871 | 11293.3324 | 4159.0814 | 0.32206 | 0.08995 |
| **2_3** | 0.547823 | 0.452178 | 41471.037 | 11700.3926 | 4310.7994 | 0.320697 | 0.09048 |
| **3_1** | 0.537761 | 0.46224 | 40782.839 | 11427.6576 | 4209.134 | 0.321602 | 0.09012 |
| **3_2** | 0.533839 | 0.466162 | 40514.586 | 11323.8975 | 4170.4695 | 0.321955 | 0.08999 |
| **3_3** | 0.535401 | 0.4646 | 40621.416 | 11365.0517 | 4185.8041 | 0.321814 | 0.09004 |
| **4_1** | 0.550708 | 0.449293 | 41668.372 | 11780.38494 | 4340.627192 | 0.320437 | 0.090594 |
| **4_2** | 0.589278 | 0.410723 | 44306.5529 | 12933.82176 | 4771.213083 | 0.316966 | 0.092528 |
| **4_3** | 0.553205 | 0.446796 | 41839.1778 | 11850.28442 | 4366.695138 | 0.320212 | 0.090695 |
| **5_1** | 0.510034 | 0.489967 | 38886.2876 | 10722.84614 | 3946.642788 | 0.324097 | 0.08937 |
| **6_1** | 0.560834 | 0.439167 | 42361.0175 | 12067.72735 | 4447.808611 | 0.319525 | 0.091026 |
| **6_2** | 0.55237 | 0.447631 | 41782.0706 | 11826.84546 | 4357.953561 | 0.320287 | 0.090661 |
| **6_3** | 0.55657 | 0.443431 | 42069.3431 | 11945.46112 | 4402.195233 | 0.319909 | 0.090838 |
| **7_1** | 0.549055 | 0.450946 | 41555.3555 | 11734.47276 | 4323.506764 | 0.320586 | 0.090528 |
| **7_2** | 0.549385 | 0.450616 | 41577.9045 | 11743.61179 | 4326.914551 | 0.320556 | 0.090541 |
| **7_3** | 0.530743 | 0.469258 | 40302.7842 | 11242.95361 | 4140.312262 | 0.322234 | 0.089891 |
| **8_1** | 0.595026 | 0.404975 | 44699.7236 | 13120.31564 | 4840.918443 | 0.316448 | 0.092885 |
| **8_2** | 0.534619 | 0.465382 | 40567.9229 | 11344.41697 | 4178.11519 | 0.321885 | 0.090012 |
| **8_3** | 0.555303 | 0.444698 | 41982.7037 | 11909.50063 | 4388.781548 | 0.320023 | 0.090783 |

Two out of twenty one specimen was excluded from testing due to imperfection after the cutting process in which the steel plate observed partial de-bonding from glass fiber as shown in Figure 11.9.

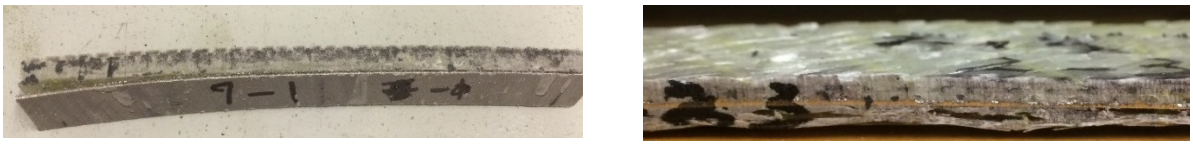

Figure 11.9 Imperfections in specimens before test.

Table 11.5 presents columns limit loads comparison between analytical, numerical, and experimental results for category A. an excellent agreement between analytical and numerical results was observed. Moreover, stacking sequences 1 and 4 showed a good agreement between analytical and experimental results. On the other hand, stacking sequence 2 and 3 experimental results were off from analytical and numerical due to initial imperfection and weak bond between steel and glass fiber.

Table 11.5 Comparisons of results for category A

| **Results** | **Analytical, N (1)** | **Numerical, N (2)** | **Experimental, N (3)** | **Error % [(1) & (3)]** | **Error % [(1) & (2)]** |
|---|---|---|---|---|---|
| **1_1** | 2858.823 | 2898.1 | 2375 | 16.924 | 1.374 |
| **1_2** | 2924.716 | 2964.6 | 2315.63 | 20.826 | 1.364 |
| **1_3** | 2801.257 | 2842 | 2185.94 | 21.966 | 1.455 |
| **2_1** | 5536.154 | 5602.5 | 2431.25 | 56.085 | 1.199 |
| **2_2** | 5023.719 | 5085.4 | 1864.06 | 62.895 | 1.228 |
| **2_3** | 4672.077 | 4733 | 1743.75 | 62.678 | 1.304 |
| **3_1** | 3490.341 | 3469.5 | 1925 | 44.848 | 0.598 |
| **3_2** | 3595.326 | 3573.8 | 1732.81 | 51.804 | 0.599 |

| | | | | | |
|---|---|---|---|---|---|
| **3_3** | 3436.664 | 3416.1 | 1521.88 | 55.717 | 0.599 |
| **4_1** | 3465.665 | 3428 | 3229.69 | 6.809 | 1.087 |
| **4_2** | 3055.181 | 3026.2 | 2553.13 | 16.433 | 0.949 |
| **4_3** | 3518.552 | 3480.2 | 3010.94 | 14.427 | 1.09 |

Comparison between results for category B is presented in Table 11.6. Analytical and numerical results showed an excellent agreement with maximum error equal to 4.427% for stacking sequence 7_1. The experimental results were off for all stacking sequence in category B because of partial or entire de-bonding of steel plate from composite. Curing method, and amount of epoxy applied in the wet layup process may have contributed to the de-bonding failure in the tested specimens.

Table 11.6 Comparisons of results for category B

| **Results** | **Analytical, N (1)** | **Numerical, N (2)** | **Experimental, N (3)** | **Error % [(1) & (3)]** | **Error % [(1) & (2)]** |
|---|---|---|---|---|---|
| 5_1 | 7264.572 | 7310.9 | 1009.38 | 86.106 | 0.638 |
| 6_1 | 9129.856 | 8973.2 | 4542.19 | 50.25 | 1.716 |
| 6_2 | 9162.398 | 9000 | 3139.06 | 65.74 | 1.773 |
| 6_3 | 9118.312 | 8962.6 | 3512.5 | 61.479 | 1.708 |
| 7_1 | 5369.325 | 5607 | 1934.38 | 63.974 | 4.427 |
| 7_2 | 5170.103 | 5395.8 | 3070.56 | 40.61 | 4.366 |
| 7_3 | 5337.616 | 5569.1 | 1521.88 | 71.488 | 4.337 |
| 8_1 | 6152.170 | 6248.3 | 4265.63 | 30.665 | 1.563 |
| 8_2 | 7949.617 | 8050.7 | 5128.13 | 35.493 | 1.272 |
| 8_3 | 7187.544 | 7291.9 | 4479.69 | 37.675 | 1.452 |

Load versus mid-height deflection from the numerical Riks analysis was plotted in Figure 11.10 along with the analytical solution for the antisymmetric angle ply sequence in category A and B for comparison. An excellent agreement between the results is observed.

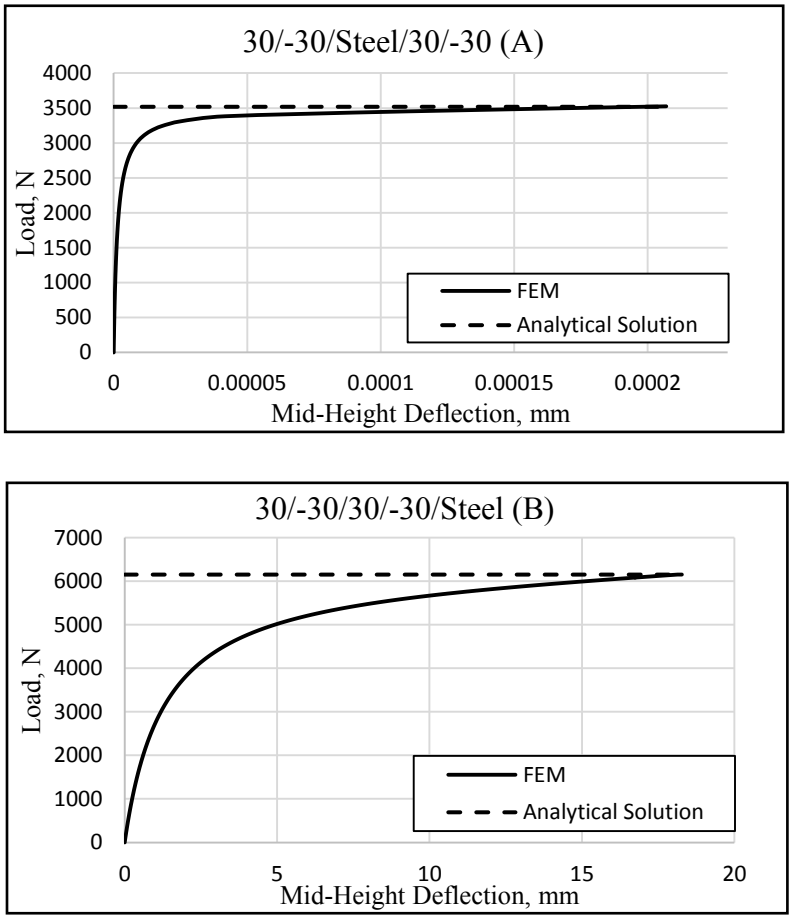


Figure 11.10 Analytical vs. Numerical (FEM) solution.

Buckling shape of the tested specimen, and de-bonding of columns after testing in category A and B is illustrated in Figure 11.11. The first three critical buckling mode shape obtained from numerical (FEM) analysis is presented in Figure 11.12. This confirms the applicability of the lowest mode shape from isotropic columns used to formulate the present analytical solution.

Buckling Shape

Failure Mode: De-bonding, Category A

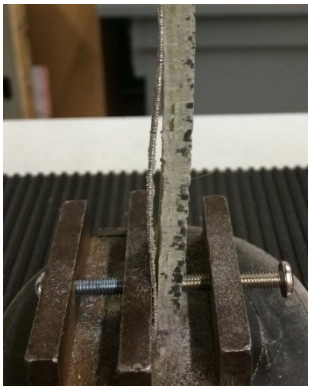

Failure Mode: De-bonding, Category B

Figure 11.11 Failure modes.

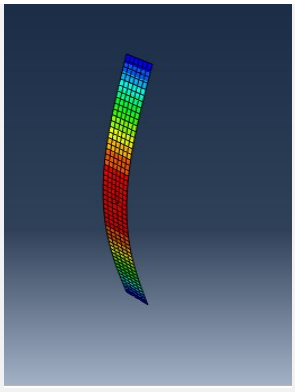

Buckling Shape I

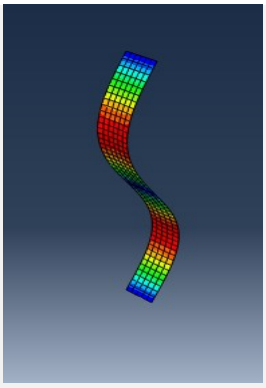

Buckling Shape II

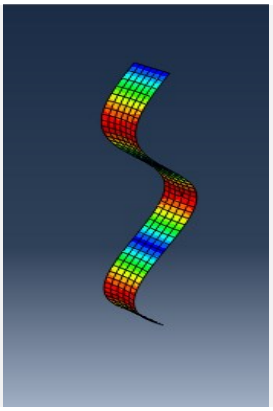

Buckling Shape III

Figure 11.12 Buckling Mode Shapes I, II and III

## 11.7 Conclusion

A generalized analytical buckling formula of simply supported anisotropic steel-FRP hybrid columns using Rayleigh-Ritz approximation was developed under axial compression. The explicit formula is an extension to Euler buckling formula with extra term expressed with respect to effective coupling and axial stiffness. An excellent agreement between the analytical formula and the finite element results is observed. Two of the stacking sequences in category A showed a good agreement between analytical and experimental results. On the other hand, results of category B

were off due to initial imperfection and entire or partial de-bonding of steel plate from composite. Moreover, steel provide more buckling load in category B than category A since the overall flexural stiffness is higher for category B. Different curing method should be considered in order to achieve the appropriate bond between composites and steel plate.

## 11.8 References


[1] Herencia, J.E., Weaver, P.M., and Friswell, M.I., "Closed-form solutions for buckling of long anisotropic plates with various boundary conditions under axial compression," Journal of Engineering Mechanics, vol. 136, no. 9, pp. 1105-1114, 2010.

[2] Weaver, P.M., "Approximate analysis for buckling of compression loaded long rectangular plates with flexural/twist anisotropy," Proc. R. Soc. London, vol. 462, no. 2065 pp. 59-73, 2006.

[3] Weaver, P.D., "Buckling of long clamped anisotropic plates under compression," in American Society of Composites, 22nd Technical Conf., Lancaster, 2007

[4] Qiao, P., and Shan, L., "Explicit local buckling analysis and design of fiber-reinforced plastic composite structural shapes," Composite Structures, vol. 70, no. 4, pp. 468-483, 2005.

[5] Mahesh, P.E., and Archibald, S.N., "Buckling od anisotropic composite plates under stress gradient," Journal of Engineering Mechanics, vol. 117, no. 2, pp. 260-275, 1991.

[6] Bellman, R.E., and Casti, J., "Differential quadrature and long-term integration," J. Math. Anal. Appl., vol. 34, no. 2, pp. 235-238, 1971.

[7] Silva, N.M.F., Silvestre, N., and Camotim, D., "GBT formulation to analyse the buckling behaviour of FRP composite open-section thin-walled columns," Composite Structures, pp. 79-92, 2010.

[8] Silvestre, N., and Camotim, D., "Second-order generalised beam theory for arbitrary orthotropic materials," Thin-Walled Structures, pp. 791-820, 2002.

[9] Bauld, R.B., and Tzeng, L.A., "Vlasov theory for fiber-reinforced beams with thin-walled open cross-section," Int. J. Solids Struct., vol. 20, no. 3, pp. 277-94, 1984.

[10] Rasheed, H.A., and Yousif, O.H., "Stability of anisotropic laminated rings and long cylinders subjected to external hydrostatic pressure," Journal of Aerospace Engineering , vol. 18, no. 3, pp. 129-138, 2005.

[11] Xu, D., Ganesan, R. and Hoa, S.V., "Buckling analysis of tri-axial woven fabric composite structures subjected to bi-axial loading," Composite Structures, pp. 140-152, 2007.

[12] Shukla, K.K., Nath, Y., Kreuzer, E., and Kumar, K.V.S., "Buckling of laminated composite rectangular plates," Journal of Aerospace Engineering, vol. 18, no. 4, pp. 215-223, 2005.

[13] Sun, L., and Harik, I.E., "Buckling of stiffened antisymmetric laminated plates," Journal of Engineering Mechanics, vol. 139, no. 8, 2013.

[14] Harik, I.E., and Salamoun, G.L., "The analytical strip method of solution for stiffened rectangular plates," Computers & Structures, vol. 29, no. 2, pp. 283-291, 1988.

[15] Debski, H., Kubiak, T., and Teter, A., "Buckling and postbuckling behaviour of thin-walled composite channel section column," Composite Structures, vol. 100, pp. 195-204, 2013.

[16] Huang, L. Sheikh, A. H., Ng, C-T., and Griffith, M. C., "An efficient finite element model for buckling analysis of grid stiffened laminated composite plates," Composite Structures, vol. 122, 41-50, 2015.

[17] Wang, D., and Abdalla, M. M, "Global and local buckling analysis of grid-stiffened composite panels," Composite Structures , vol. 119, 767-776, 2015.

[18] Khayat, M., Poorveis, D., and Moradi, S., " Buckling analysis of laminated composite cylindrical shell subjected to lateral displacement-dependent pressure using semi-analytical finite strip method," Steel and Composite Structures, vol. 22, no.2, 301-321, 2016.

[19] Baseri, V., Jafari, G.S., and Kolahchi, A., " Analytical solution for buckling of embedded laminated plates based on higher order shear deformation plate theory," Steel and Composite Structures, vol.21, no.4, 883-919, 2016.

[20] Becheri,T., Amara, K., Bouazza, M., Benseddiq, N.,"Buckling of symmetrically laminated plates using nth-order shear deformation theory with curvature effects," Steel and Composite Structures, vol.21, no.6, 1347-1368, 2016.

[21] Jones, R.M, Mechanics of composite materials, New York: Hemisphere Publishing Corporation, 1975.

[22] Hernandez, V., Roman, J.E., Tomas, A., and Vidal, V., "Lanczos methods in SLEPc," Polytechnic University of Valencia, Province of Valencia, 2006.

[23] Memon, B.A., Su, X.S., "Arc-length technique for nonlinear finite element analysis," Journal of Zhejiang University SCI, vol. 5, no. 5, pp. 618-628, 2004.

[24] Structural Technologies, "Strengthening Solutions, V-WrapTM EG50, High Strength Glass Fiber Fabric". structuraltechnologies.com. 2011.

[25] Rasheed, H.A., Strengthening Design of Reinforced Concrete with FRP, New York: CRC Press, 2015.

# Chapter 12 - Conclusions and Recommendations

## 12.1 Conclusions

Generalized analytical buckling formulas of anisotropic laminated composite columns and infinitely wide plates subjected to axial compression with various boundary conditions are developed in this work based on Rayleigh-Ritz approximation. The presented formulas may be considered as an extension to the buckling formulas of the isotropic cases and the first of their kind since Euler solutions. The buckling load formulas are expressed in terms of the generally anisotropic material properties along with the member geometry. Motivated by reducing some of the discrepancy with the numerical analysis, the bifurcation approach was attempted in the case of fixed-fixed anisotropic laminated composite columns and plates. Furthermore, the bifurcation method was substituted in the pre-buckling deformation for the pinned-fixed anisotropic laminated composite columns and plates since the Rayleigh-Ritz approximation was not able to accurately predict the closed-form stability solution. Finite element analysis was performed using commercial software ABAQUS to validate the developed formulas. Moreover, quadrilateral eight node doubly curved thick shell elements (S8R) were utilized in the numerical analysis process. The new analytical formulas exhibited excellent agreements with the numerical (FE) analysis results for a wide range of stacking sequences. In addition, Modified Riks analysis was performed to investigate the nonlinear stability response and indicate the existence of pre-buckling deformation. The effects on the stability response of different aspects of the studied problems were addressed in this work and the conclusions are illustrated in the corresponding sections.

### 12.1.1 Effect of Material Properties

In general, composite materials with high stiffness ratio ($E_{11}/E_{22}$) where $E_{11}$ is the modulus along the fiber direction and $E_{22}$ is the modulus in the transverse direction has yielded higher error values compared to one with lower stiffness ratio. Additionally, the results demonstrate that using a single composite material type per column or plate yielded less deviation of the analytical solution from the finite element solution compared to using a two-material hybrid composite (carbon/glass fibers composite) for a limited and specific number of layups.

### 12.1.2 Effect of Element Type in Finite Element Analysis

It is observed that quadrilateral eight-node doubly curved thick shell element (S8R) and quadratic triangular thin shell element (STRI65) both with reduced integration schemes accurately estimate the buckling load values for various stacking sequences. Moreover, quadratic solid element (C3D20R) with reduced integration schemes has yielded an excellent agreement with the analytical solution for the single specially-orthotropic layups and Antisymmetric angle ply layups. However, solid element (C3D20R) was not capable of capturing the complexity of behavior of the anisotropic and Antisymmetric cross ply when benchmarked against the present analytical solutions.

### 12.1.3 Effect of Element Thickness

The developed formulas successfully predicted accurate buckling loads in cases of moderately thick shells in which the level of errors between the numerical and the analytical solution is comparable to that of thin shells. In some boundary conditions, the use of the developed formulas to predict buckling loads for thick shells was reasonably accurate compared to the errors obtained for thin shells.

## 12.2 Recommendations

Recommendations relevant to the results and observations obtained from this work are described in this section. The use of the presented solutions is highly recommended in predicting the stability response of the anisotropic laminated composite members since the generalized analytical formulas developed herein were capable of accurately estimating the buckling values for different boundary conditions and structural members as well as capturing the complexity of behavior in case of hybrid composites, thin, and moderately thick shells. Furthermore, the 3D quadratic 20-nodes solid element with reduced integration schemes (C3D20R) was not reliable in reproducing the analytical or other numerical buckling results.

## 12.3 Future Work

This work provides a foundation for future work in the following several areas.

- Developing a computer program to estimate the buckling load values for various boundary conditions, material properties, structural members, and number of layers using the developed formals and Excel-based Visual Basic computer language.
- Establishing analytical buckling solutions for thin-walled columns with sections different from rectangular and verifying the experimental buckling results conducted by Debski et al. [43] for simply supported thin-walled composite channel section columns.
- Implementing the bifurcation approach in the case of simply supported and clamped-free members.

# Bibliography for Chapter Two


[1] Rasheed, H.A., and Yousif, O.H., "Buckling of thin laminated orthotropic rings/long cylinders under external pressure," *International Journal of Structural Stability and Dynamics,* 1(4) (2002) 485-507.

[2] Rasheed, H.A., and Yousif, O.H., "Stability of anisotropic laminated rings and long cylinders subjected to external hydrostatic pressure," *Journal of Aerospace Engineering ,* 18(3) (2005) 129-138.

[3] Silva, N.M.F., Silvestre, N., and Camotim, D., "GBT formulation to analyse the buckling behaviour of FRP composite open-section thin-walled columns," *Composite Structures,* 93(1) (2010) 79-92.

[4] Silvestre, N., and Camotim, D., "Second-order generalised beam theory for arbitrary orthotropic materials," *Thin-Walled Structures,* 40(9) (2002) 791-820.

[5] Bauld, R.B., and Lih-Shyng, L.A., "Vlasov theory for fiber-reinforced beams with thin-walled open cross-section," *Int. J. Solids Struct.,* 20(3) (1984) 277-294.

[6] Xu, D., Ganesan, R. and Hoa, S.V., "Buckling analysis of tri-axial woven fabric composite structures subjected to bi-axial loading," *Composite Structures*, 21(3) (2007) 140-152.

[7] Shukla, K.K., Nath, Y., Kreuzer, E., and Kumar, K.V.S., "Buckling of laminated composite rectangular plates," *Journal of Aerospace Engineering,* 18(4) (2005) 215-223.

[8] Herencia, J.E., Weaver, P.M., and Friswell, M.I., "Closed-form solutions for buckling of long anisotropic plates with various boundary conditions under axial compression," *Journal of Engineering Mechanics,* vol. 136, no. 9, pp. 1105-1114, 2010.

[9] Weaver, P.M., "Approximate analysis for buckling of compression loaded long rectangular plates with flexural/twist anisotropy," *Proc. R. Soc. London,* vol. 462, no. 2065 pp. 59-73, 2006.

[10] Weaver, P.D., "Buckling of long clamped anisotropic plates under compression," in *American Society of Composites, 22nd Technical Conf.*, Lancaster, 2007

[11] Qiao, P., and Shan, L., "Explicit local buckling analysis and design of fiber-reinforced plastic composite structural shapes," *Composite Structures,* vol. 70, no. 4, pp. 468-483, 2005.

[12] Sun, L., and Harik, I.E., "Buckling of stiffened antisymmetric laminated plates," *Journal of Engineering Mechanics*, 139(8) (2013) 1110-1123.

[13] Harik, I.E., and Salamoun, G.L., "The analytical strip method of solution for stiffened rectangular plates," *Computers & Structures*, 29(2) (1988) 283-291.

[14] Shufrin, I., Rabinovitch, O., and Eisenberger M., "Buckling of laminated plates with general boundary conditions under combined compression, tension, and shear- A semi-analytical solution," *Thin-Walled Structures,* 46 (2008) 925-938.

[15] Kerr, A.D., "An extended Kantorovich method for solution of eigenvalue problem," *Int. J. Solid Struct,* 5(6) (1969) 559-572.

[16] Weaver, P.L., and Nemeth, M.P., "Bounds on flexural properties and buckling response for symmetrically laminated composite plates," *Journal of Engineering Mechanics*, 133(11) (2007) 1178-1191.

[17] Kazemi, M., "A new exact semi-analytical solution for buckling aanlysis of laminated plates under biaxial compression," *Archive of Applied Mechanics*, 85(11) (2015) 1667-1677.

[18] Thai, H.T., and Kim, S.E., "Levy-type solution for buckling analysis of orthotropic plates based on two variable refined plate theory," *Composite Structures,* 93(7) (2011) 1738-1746.

[19] Ovesy, H. R., Ghannadpour, S.A.M., and Sherafat, M. H, "Buckling analysis of laminated composite plates using higer order semi-analytical finite strip method," *Appl Compos Mater,* 77(2010) 69-80.

[20] Abramovich, H., and Livshits, A., "Free vibrations of non-symmetric cross-ply laminated composite beams", *Journal of Sound and Vibration* , 176 (1994) 597-612.

[21] Abramovich, H., Eisenberger, M., and Shulepov, O., "Vibrations and buckling of cross-ply non-symmetric laminated composite beams", *AIAA Journal* , (34) (1996) 1064-1069.

[22] Cortinez, H.V., and Piovan, M. T., "Stability of composite thin-walled beams with shear deformability," *Computers & Structures,* 84(2006) 978-990.

[23] Aydogdu, M., "Buckling analysis of cross-ply laminated beams with general boundary conditions by Ritz method," *Composite Science & Technology,* 66(2006) 1248-1255.

[24] Pandey, M. D., and Sherbourne, A. N., "Buckling of anisotropic composite plates under stress gradient," *Journal of Engineering Mechanics,* 117(2)(1991) 260-275.

[25] Ghaheri, A., Keshmiri, A., and Taheri-Behrooz, F., "Buckling and vibration of symmetrically laminated composite elliptical plates on an elastic foundation subjected to uniform in-plane force," *Journal of Engineering Mechanics,* 140(7)(2014) 1-10.

[26] Heidari-Rarani, M., Khalkhali-Sharifi, S.S., and Shokrieh, M.M., "Effect of ply stacking sequences on buckling behavior of E-glass/epoxy lamianted composites," *Computational Materials Science,* 89 (2014) 89-96.

[27] Lopatin, A. V., and Morozov, E. V., "Buckling of a composite cantilver circular cylindrical shell subjected to uniform external lateral pressure," *Composite Structures,* 94 (2012) 553-562.

[28] Debski, H., "Numerical analysis of stability of thin-walled composite column with open cross-section," *Mechanics and Mechanical Engineering,* 17 (1)(2013) 29-35.

[29] Koiter, W.T., "Elastic stability and post-buckling behavior," *In: Proceedings of the Symposium on Non-linear Problems,* University of Wisconsin, Wisconsin (1963) 257-275.

[30] Kumar, Y.V. S., and Mukhopadhyay, M., "A new finite element for buckling analysis of laminated stiffenend plates," *Composite Structures,* 46 (1999) 321-331.

[31] Loughlan, J., "A finite strip analysis of the buckling characteristics of some composite stiffenend shear panels," *Composite Structures,* 27(3) (1994) 283-294.

[32] Rikards, R., Chate, A., and Ozolinsh, O., "Analysis for buckling and vibrations of composite stiffened shells and plates," *Composite Structures,* 51(2001) 361-370.

[33] Jaunky, N., Knight Jr., N. F., and Ambur, D. R., "Buckling aanlysis of anisotropic varaible-curvuture panels and shells," *Composite Structures,* 43(4) (1998) 321-329.

[34] Setoodeh, A. R., and Karami, G., "Static, free vibration, and buckling analysis of anisotropic thick laminated composite plates on distributed and point elastic supports using a 3-D layer-wise FEM," *Engineering Structures,* 26(2) (2004) 211-221.

[35] Nayak, A. K., Moy, S. S. J., and Shenoi, R. A., "A higher order finite element theory for buckling and vibration analysis of initially stressed composite sandwich plates," *Journal of Sound and Vibration,* 286(4-5) (2005) 763-780.

[36] Noor, A. K., "Stability of multilayered composite plates," *Fiber Science and Technology ,* 8(1975) 81-89.

[37] Noor, A. K., Peters, J. M., and Burton, W. S., "Three dimensional solutions for initially stressed structural sandwiches," *Journal of Engineering Mechanics,* 120(1994) 284-303.

[38] Grover, N., Maiti, D. K., and Singh, B. N., "A new inverse hyperbolic shear deformation theory for static and buckling analysis of laminated composite and sandwich plates," *Composite Structures,* 95(2013) 667-675.

[39] Kidane, S., Li, G., Helms, J., Pang, S., and Woldesenbet, E., "Buckling load analysis of grid stiffened composite cylinders," *Composite: Part B,* 34(2003)1-9.

[40] Whitney, J. M., Structural Analysis of Laminated Anisotropic Plates, Lancaster: Technomic, 1987.

[41] Jianqiao, Y., and Soldatos, K. P., "Three dimensional buckling analysis of laminated composite hollow cylinders and cylinderical panels," *International Journal of Solids and Structures,* 32(13) (1995) 1949-1962.

[42] Noor, A. K., and Peters, J. M., "Stress, vibration, and buckling of multilayered cylinders," *Journal of Structural Engineering,* 115(1) (1989) 69-88.

[43] Dbski, H., Kubiak, T., and Teter, A., "Buckling and postbuckling behaviour of thin-walled composite channel section column," *Composite Structures,* 100(2013) 195-204.

[44] Kolakowski, Z., and Kowal-Michalska, K., Selected Problems of Instabilities in Composite Stuctures, Lodz: Technical University of Lodz Press, A Series of Monographes, 1999.

[45] Kubiak, T., "Postbuckling behavior of thin-walled girders with orthotropy varying widthwise," *International Journal of Solid Structure,* 38(28-29) (2001) 4839-4855.

[46] Teter, A., "Static and dynamic interactive buckling of isotropic thin-walled closed columns with variable thickness," *Thin-Walled Stuctures,* 45(10-11) (2007) 936-940.

[47] Teter, A., and Kolakowski, Z., "Lower bound estimation of load-carrying capacity of thin-walled structures with intermediate stiffeners," *Thin-Walled Stuctures,* 39(8) (2001) 649-669.

[48] Meyer-Piening, H.R., Farshad, M., Geier, B., and Zimmermann, R., "Buckling loads of CFRP composite cylinder under combined axial and torsion loading-experiments and computations," *Composite Structures,* 53(2001) 427-435.

[49] Geier, B., and Singh, G., "Some simple solutions for buckling loads of thin and moderately thick cylindrical shells and panels made of laminated composite material," *Aerospace Science and Technology,* 1(1)(1997) 47-63.

[50] Aslan, Z., and Şahin, M., "Buckling behavior and compressive failure of composite laminates containing multiple large delaminations," *Composite Stuctures,* 89(2009) 382-390.

[51] Baba, B. O., and Baltaci, A., "Buckling Characteristics of symmetrically and antisymmetrically laminated comosite plates with central cutout," *Applied Composite Material,* 14(4)(2007) 265-276.